

Report

Loads, design and operation of floaters in the Arctic

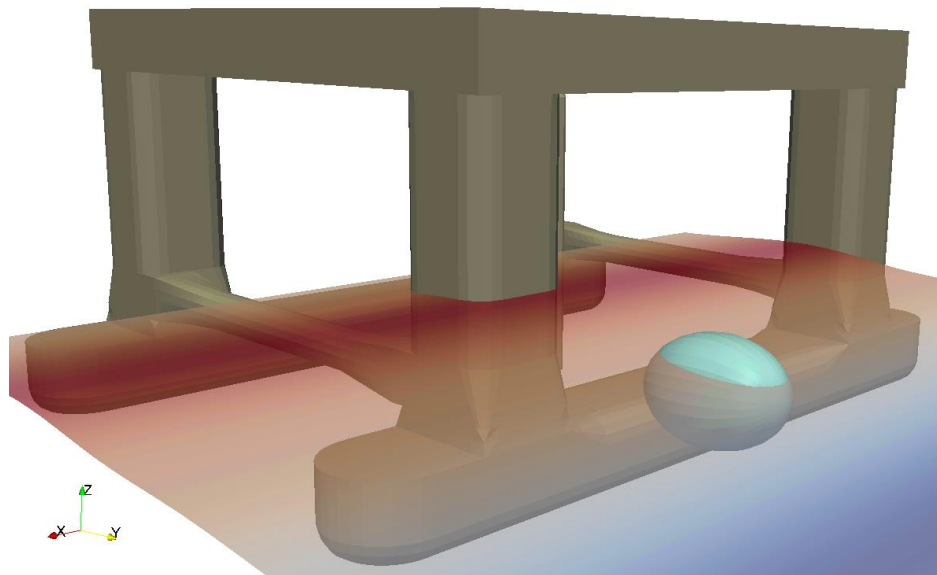
Ptil – NORD ST20

Author(s)

Babak Ommani

Petter Andreas Berthelsen

Reza Firoozkoohi



Report

Loads, design and operation of floaters in the Arctic

Ptil – NORD ST20

REPORT NO	PROJECT NUMBER	VERSION	DATE
OCE2018 A-116	302004333	1	2018-12-11

KEYWORDS:

Arctic

Hydrodynamics

Glacial Ice Impact

AUTHOR(S)

Babak Ommani,
Petter Andreas Berthelsen
Reza Firoozkoohi

CLIENT(S)

Petroleumstilsynet

CLIENT'S REF.	NUMBER OF PAGES/APPENDICES:
NORD ST20	164

CLASSIFICATION	CLASSIFICATION THIS PAGE	ISBN
Unrestricted	Unrestricted	978-82-7174-344-4

ABSTRACT

This report presents results from hydrodynamic analysis of interaction between glacial ice and semisubmersible drilling units, as part of the Petroleum Safety Authority's project "NORD ST20 Loads, design and operation of floaters in the northern area".

The overall objective of the study has been to study the hydrodynamic behaviour of smaller masses of glacial ice (growlers or bergy bits) exposed to environmental loads, and to assess the hydrodynamic interaction and possibility of collision with a semisubmersible drilling unit. Comprehensive numerical analysis of ice mass response in waves have been performed, with focus on nonlinear Froude-Krylov forces and hydrodynamic interactions due to the near presence of a larger semisubmersible. Position of impact, impact velocity and impact energy have been estimated in cases when collision between the ice mass and semisubmersible occurred.



PREPARED BY

Petter Andreas Berthelsen

CHECKED BY

Halvor Lie

APPROVED BY

Vegard Øgård Aksnes

Document history

VERSION	DATE	VERSION DESCRIPTION
1	2018-12-11	Final report

Table of contents

1	Summary and conclusion	5
2	Introduction	8
2.1	Objectives	8
2.2	Background	8
2.3	Scope of work	9
2.3.1	Description of simulation tools	9
3	Summary of glacial ice hydrodynamic interactions with offshore structures	10
4	System description	12
4.1	Semisubmersible particulars.....	12
4.2	Ice geometry and mass	12
4.3	Coordinate systems	13
4.3.1	Global (earth-fixed) coordinate system.....	13
4.3.2	Local (body-fixed) coordinate system	13
5	Linear hydrodynamic frequency domain analysis	15
5.1	Hydrodynamic interaction between glacial ice and semisubmersible	16
5.1.1	Motion response in the frequency domain.....	16
5.1.2	Sensitivity due to distance from platform column – asymptotic properties. ..	20
6	Glacial Ice Motions in Waves	23
6.1	Modelling	23
6.1.1	Nonlinear Froude-Krylov Forces	24
6.2	Validation Studies	26
6.2.1	Free-surface elevation	26
6.2.2	Comparing with CFD	27
6.2.2.1	Simulation set-up.....	27
6.2.2.2	Fixed ice cube	28
6.2.2.3	Moving ice cube.....	30
6.2.3	Existing model test data	30
7	Simulations.....	33
7.1	Methodology.....	33
7.1.1	Impact.....	34
7.1.2	Hydrodynamic interactions	35
7.2	Improvements comparing to previous study.....	42
7.3	Selected Cases.....	42
7.4	Results and conclusions	45

7.4.1	Height and location of impact	45
7.4.2	Velocity at the time of impact	47
7.4.2.1	The influence of NLFK_A0 model on relative collision velocity on column.....	50
7.4.2.2	Relative collision velocity at the pontoon	51
7.4.3	Kinetic energy at the time of impact	54
8	Proposal of simplified model test for verification and illustration of the numerical results	56
9	References.....	58

APPENDICES

Appendix A

1 Summary and conclusion

This report has been worked out by SINTEF Ocean as part of the project:

- NORD ST20 Loads, design and operation of floaters in the northern area. initiated by the Petroleum Safety Authority.

The overall objective of this project has been to study the behaviour of smaller masses of glacial ice (less than 15 meters at the waterline, classified as growlers or bergy bits) in waves, current and wind, and to assess the possibility of interaction and collision with a semisubmersible drilling unit.

The objectives have been:

- Obtain new and better understanding of the hydrodynamic interaction between glacial ice masses and semisubmersible drilling units.
- Assess the collision energy, the point of impact and the probability of collision at different locations of the drilling unit (e.g. columns, pontoons, drilling string) in a generic way.
- Suggest simple tank model experiments to evaluate the results from the analysis.

Earlier studies (e.g. ST5 [1]) show that:

- Multibody analysis in frequency domain showed that the wave frequency response of glacial ice masses was affected by the presence of a drilling unit, but not vice versa.
- There are uncertainties related to damping in heave, roll and pitch.
- The nonlinear time domain analysis showed substantially larger pitch motion than the linear frequency domain analysis.

In this project, the response of ice in waves is further investigated using time-domain simulations and by partly introducing important nonlinear effects. This includes:

- Adopting a 6-degree of freedom simulation in time-domain, which better accounts for the role of stochastic variability of waves on impact and allows for introducing quadratic forces.
- Introducing viscous drag forces using Morison-type elements.
- Accounting for nonlinear Froude-Krylov and buoyancy forces.
- Investigating the hydrodynamic interaction between ice and platform.
- Perform sensitivity study on impact scenario to ice initial location and wave realization
- Briefly studying the repellent force introduced by variation of zero-frequency added mass as the ice gets closer to the platform.

The numerical analyses are divided into three parts, and the main findings are summarized below:

Linear frequency domain analysis in WAMIT

The purpose of the linear frequency domain diffraction-radiation analysis has been to establish hydrodynamic coefficients such as added mass, wave radiation damping, wave force and drift force coefficients for the semisubmersible and the glacial ice. WAMIT has further been used to investigate the hydrodynamic interaction between the platform and the glacial ice, i.e. how the hydrodynamic pressure acting on one body is influenced by the presence of the other body. The multibody analysis has been performed for various positions of the glacial ice relative to the semisubmersible.

Main findings from the linear frequency domain analysis include:

- The hydrodynamic influence from the ice mass on the platform motion response is negligible, but the motion response of the glacial ice was highly influenced by the presence of semisubmersible, noting the linear nature of considered restoring and excitation forces.

- Hydrodynamic influence due to the near presence of the semisubmersible was evident both in the wave diffraction forces acting on the ice as well as the added mass coefficients for the ice mass.
- It is not clear from the results what hydrodynamic interaction effects (radiation or diffraction) dominates, and a general conclusion that one effect is more important than the other cannot be made as that will be highly frequency dependent.
- There is a noticeable variation in the zero-frequency and infinity-frequency added mass coefficients as the ice mass is moved closer to the semisubmersible.
- For the cases investigated, the increase in added mass due to the motion of the ice in near proximity to the platform is more significant for sway direction than heave direction with an increase of 47% and 14%, respectively. The closer the ice is to the semisubmersible hull, the greater is the added mass. The ice need to be relatively close to the platform before there is any significant influence on the added mass, approximately within one length (L) of the ice mass.
- Hydrodynamic interactions due to the motion of the platform influence the ice's of-diagonal coupled added mass in a larger distance from the platform, i.e. in a length scale equivalent to 1.5-3 pontoon lengths.
- The changes in the of-diagonal coupling added mass terms due to the platform motion is most prominent when the platform oscillates towards the ice.

Nonlinear Froude-Krylov force model:

- It was shown that the nonlinear restoring and Froude-Krylov excitation forces are important due to large variation in the ice's water-plain area as it moves vertically, and the fact that it can get completely submerged as it moves in waves.
- The adopted nonlinear Froude-Krylov model is validated against CFD, and previously existing model test data with reasonable accuracy.
- The CFD simulations is further used to validate a quadratic drag model for the ice cube implemented using Morison drag forces.
- A clear improvement in the prediction of the vertical forces on the ice cube in regular waves was obtained using the developed model, in comparison to linear predictions.

Ice-platform impact studies:

- A selection of irregular wave conditions, corresponding to 1-year return period, are considered.
- Ten different initial locations and orientations of ice are investigated.
- The dependency of the results to selected realization of waves is investigated through seed variation.
- In total 23 different cases, 19 cases with 20 seeds, 3 with 40 seeds, and one with 120 seeds are studied.
- The simulations are processed until the first impact. Impact locations, ice and platform's velocities, collision vector, relative collision velocities, and estimated impact energies are presented.
- Brief sensitivity study to the repellent/attractive force due to variation of zero-frequency added mass as the ice gets closer to the platform is presented.

- Strong dependency of the impact velocity and location to the ice initial location and selected wave realization is observed.
- Super imposing the collision locations for all considered realizations, it was clear that ice could impact the pontoons as well as the risers between the columns.
- Due to the large scatter of data it was not possible to conclude on any clear trend in the dependency of the impact results to the sea-state, initial ice location, or ice shape.
- To calculate ice impact energy, suitable ice added mass is selected based on the collision vector and location. Moreover, most probable, expected and P90 fractal values for the magnitude of relative collision velocity are obtained by fitting a Gumbel distribution and presented, in addition to the recorded samples mean and absolute maximum. The expected impact energy is calculated using

each of the statistical values of collision velocity; and presented for impact on column, pontoon, brace, and riser separately. The dissipation of energy due to crushing of ice during impact is not considered in calculating the impact energy. The results for a selection of cases with the highest most probable collision velocities are presented in the Table below for different collision locations. More details could be found in Chapter 7.

Case ID	Collision Location	Hs[m], Tp[s], WD[deg]	Sample Mean[MJ]	Sample Max[MJ]	MP[MJ]	Exp[MJ]	P90[MJ]
10	Column	8.6, 12.0, 270	7.0	37.0	4.0	5.8	20.8
15	Pontoon	9.8, 14.8, 270	1.7	5.4	0.9	1.4	4.9
22	Pontoon	9.8, 14.8, 270	1.2	13.6	0.6	0.9	4.3
13	Brace	9.8, 14.8, 180	2.6	11.0	1.5	2.1	7.5
22	Riser	9.8, 14.8, 270	2.6	14.0	1.6	2.2	6.8

- It was shown that the added mass at the time of impact varies based on the location of the ice. Moreover, the speed and collision and how fast the ice is stopped after collision determines which added mass, i.e. zero or infinite frequency, is applicable. As a conservative measure the larger of the two, i.e. zero-frequency added mass, is considered here. In addition, variation of added mass as the ice approaches the column introduce a repelling force which is briefly studied for two of the cases.

Recommendations for further work:

- A more detailed study of nonlinearities in forces due to ice oscillations and its effect on the ice motion. Examples are added mass and damping of ice when it is going in and out of water. This can be studied numerically in combination to performing new model test or looking into existing model test data.
- The influence of platform on the excitation and radiation forces on the ice could be added in the next step. The adopted methodology (see Chapter 6) has the ability to take these effects into account by adding the diffracted and radiated pressures due to presence of the platform to the incoming waves when calculating nonlinear Froude-Krylov forces on the ice.
- The repelling or attraction forces due to variation of zero-frequency added mass, as ice approaches the platform, are studied briefly here, only for translational motions of ice. A more detailed investigation and validation of the implemented model is needed, in particular since these forces may play an important role on determining the velocity of ice at the time of impact.
- The variability of the results with sea-state, wave realization, and ice location must be further studied through extensive sensitivity and seed variation investigations in an attempt to clarify the statistical behaviour of the impact. Investigating existing, and novel, statistical model to represent this highly nonlinear process is of interest.
- Near-field description of ice mass collision with a steel hull needs to be further investigated in order to get a better understating of the impact energy. Such a study should include modelling of ice mechanics (crushing), deformation of hull, and the resulted variation of contact point and plane. In addition comes the hydrodynamic interaction between the bodies during the collision.
- Wave tank model experiments including both the ice mass and platform should be carried out to validate the numerical analysis results. Hydrodynamic tests should be carried out on the glacial ice with and without the platform present.

2 Introduction

2.1 Objectives

This report has been worked out by SINTEF Ocean to meet the request by the Petroleum Safety Authority in project:

- NORD ST20 Loads, design and operation of floaters in the northern area.

The overall objective of this project is to study the behaviour of smaller masses of glacial ice (less than 15 meters at the waterline, classified as growlers or bergy bits) in waves, current and wind, and to assess the possibility of interaction and collision with a semisubmersible drilling unit.

The project shall:

- Obtain new and better understanding of the hydrodynamic interaction between glacial ice masses and semisubmersible drilling units.
- Assess the collision energy, the point of impact and the probability of collision at different locations of the drilling unit (e.g. columns, pontoons, drilling string) in a generic way.
- Suggest simple tank model experiments to evaluate the results from the analysis.

2.2 Background

Smaller ice masses caused by breaking of ice chunks from the edge of a glacier pose a potentially risk to drilling in the arctic regions. These so-called growlers and bergy bits are difficult to detect visually or by radar in order to timely take proper measures to avoid interactions with stationary floating units. Thus, drilling units must be designed to withstand a possible impact with smaller ice masses.

The Petroleum Safety Authority has identified knowledge gaps for safe operations in the arctic area related to impact with smaller glacier ice masses. An earlier study (ST5) performed by DNVGL [1] showed that semisubmersible drilling units may not withstand impacts from smaller ice masses, even if they are reinforced to withstand ship collisions. The study shows that the ice can hit both above and below areas reinforced for ship collisions. Furthermore, ice of this size can pass through the columns and potentially hit the drilling riser.

The ST5 project used two different modelling approaches to quantify the hydrodynamic characteristics of ice masses. The main part of the study is based on linearized frequency domain analysis applied to calculate the wave frequency relative motion between the ice and the drilling unit. Impact area and energy was estimated from the extreme value statistics assuming the impact to be a narrow banded stochastic process. The second method applied was a nonlinear time domain analysis, where the objective was to investigate nonlinear hydrodynamic effects on a single ice piece (without the interaction of the drilling unit). Findings from the ST5 study include:

- Multibody analysis in frequency domain showed that the wave frequency response of glacial ice masses was affected by the presence of a drilling unit, but not vice versa.
- There are uncertainties related to damping in heave, roll and pitch.
- The nonlinear time domain analysis showed substantially larger pitch motion than the linear frequency domain analysis.

In this project, new methodology to study the above hydrodynamic challenges will be proposed.

2.3 Scope of work

The scope of work is outlined below:

- Review relevant literature on current state-of-the-art methodology to investigate hydrodynamic interaction between glacial ice and floating units.
- Establish numerical simulation model of a generic drilling unit.
- Establish numerical models of glacial ice:
 - to study hydrodynamic characteristics of ice masses.
 - for simulation of impact with drilling units.
- Establish a contact- and collision model to model ice impact on the drilling unit.
- Establish a coupled simulation model for ice mass and drilling unit.
- Carry out coupled ice-drilling unit time domain analysis to estimate the following for various sea states:
 - Relative motion between ice and drilling unit.
 - Collision points.
 - Collision energies.
- Provide recommendation for further studies.

2.3.1 Description of simulation tools

The following simulations tools are used in this study:

SIMA

SIMA is a workbench that offers a complete solution for simulation and analysis of marine operations and floating systems. It supports the entire process from the definition of the simulation and its execution to the interpretation and documentation of the results. SIMA uses software such as SIMO and WAMIT as the underlying analysis tools. SIMA is developed and owned by SINTEF Ocean and are commercially available from DNV GL Digital Solutions. See www.sintef.no/en/software/sima for more information.

SIMO

SIMO is a time domain simulation program for study of motions and station keeping of multibody systems. Flexible modelling of station keeping forces and connecting force mechanisms (e.g. anchor lines, ropes, thrusters, fenders, bumpers) is included. The results from the program are presented as time traces, statistics and spectral analysis of all forces and motions of all bodies in the analysed system. SIMO is developed and owned by SINTEF Ocean and are commercially available from DNV GL Digital Solutions. See www.sintef.no/globalassets/project/oilandgas/pdf/simo.pdf for more information.

WAMIT

WAMIT is a three-dimensional frequency domain panel based on linear and second order potential theory for diffraction-radiation analysis of floating and submerged bodies in waves. WAMIT is a commercial engineering tool developed by WAMIT Inc. See www.wamit.com for more information.

3 Summary of glacial ice hydrodynamic interactions with offshore structures

The paper by Sayeed et al. [2] contains a comprehensive review on the literature related to hydrodynamic interaction between drifting ice and offshore structures for the past 30–40 years. In their review, they categorize the problem of drifting ice trajectory and impact with structures into three phases: far field, near field and contact phases. Here follows a short summary of the main findings with focus on the hydrodynamics in the far field and near field phases.

In the far field region, the objective has been to accurately predict the trajectory of drifting ice. Drift models in open water have been studied, where the simplest models include effects from wind, current and Coriolis forces. Statistical models that rely on the past trajectories to predict future paths have also been applied. Most of the work has focused on the larger icebergs, and some of the discussions have been related to the importance of including wave forces for better predictions of the drift trajectories. For smaller bergy bits, the drift trajectories will be more affected by waves, surface current and wind than deep current. Furthermore, the drift models assumed a constant added mass which is not valid for ice masses close to large offshore structures [3].

In iceberg impact analysis, models including only mean drift speed underestimated impact velocity. This is even more pronounced for smaller icebergs, and several studies were conducted related to wave induced motions on smaller ice fragments. E.g. in [4, 5] the authors applied linear potential theory to calculate wave induced surge and heave motion. It was also demonstrated by [5] that smaller icebergs showed fluid particle motion behaviour for wave length to iceberg ratios greater than 10–15. This was later matched with experimental results [6] where the ratio was found to be 13. Many of the studies demonstrated the increasing importance of wave-induced motions as the size of the ice mass decreased. The shape of the iceberg was also shown to be important for the total surge velocities [7].

Wave tank experiments were conducted to validate results from linear diffraction analysis, e.g. [8, 9]. Linear potential theory was found to predict the motion with a slightly underestimated surge and overestimated heave response. A probable explanation for the discrepancy was identified as due to the lack of including viscous damping and the nonlinear wetted surface [9].

With the aim to provide more certainty in the impact and risk analysis, the effect of the presence of a large offshore structure got more attention in the near field analysis. Several studies were conducted where the flow field around the ice mass was influenced by the offshore structure, e.g. [10, 11]. The study in [11] showed that the zero-frequency added mass increased prior to impact, but exclusion of complete viscous effect as well as coarse discretization of numerical model deemed the results unreliable.

The work by [12, 13] showed an increase in added mass as two circular cylinders (one with twice the diameter as the other) approach each other. The results were based on a potential flow code, and the added mass increased by 60% at contact compared to the far-field solution. This effect was found to be more pronounced as the relative difference in size increased. They also found that using the contact point added mass yields a higher impact force than the far-field value.

Isaacson and McTaggart [14] found that the added mass varies with impact duration. It was suggested to use infinite-frequency added mass for short duration and zero-frequency added mass for longer impact durations. Furthermore, the presence of the structure can result in velocity reduction. Wave induced motion is important for smaller ice masses but are little affected by the presence of a structure. For relatively small icebergs (diameter ratio of less than 0.5 compared to structure), the negative drift forces may lead to significant reduction of impact velocity and in some cases no collision. Similarly, the

hydrodynamic interaction was concluded to reduce the approaching velocity in [15, 16]. LS-DYNA was used to investigate effect of sea water in a fluid-structure calculation in [17] for iceberg approaching a LNGC. It was found that the pressure increased drastically due to the confined water layer entrapped between the two bodies as the ice mass approached the hull. However, for slowly approaching icebergs the water between the two bodies will have time to flow away without resistance and the same pressure increase will not be present. For a constant approaching velocity, the increase in pressure due to the confinement showed a slower rise time. The squeezing pressure effect of the entrapped water reduces the collision velocity.

The near field problem has been investigated through various physical model tests [6, 18, 19] in order to assess effects of iceberg size and shape. The ratio between wave length (λ) and the characteristic length (L) of the iceberg decides if the iceberg shows particle-like motion or not. For long waves, with λ/L larger than 13, [6] found the iceberg to behave like particles, while diffraction and viscous effects were important when λ/L was less 10. For ratios between 10 and 13, the iceberg motion was dependant on shape. For ice floes, studies by [20] showed that particle motion was shown for ratios between 3.3 and 5. Iceberg size relative to structure size was investigated by [18, 21] and no collisions were found to occur if the iceberg was small enough, that is, the characteristic length of the iceberg was less than 0.2-0.5 times the structure size (diameter in case of a column or cylinder). For medium sized icebergs, [18] found eccentric collisions and sometimes repetitive collisions. Large icebergs always led to impact. Similarly, tests with FPSOs [19] showed more collisions in head sea, than in beam sea.

The contact phase is usually modelled separately from the near field phase. There are several challenges related to the contact phase, but only the hydrodynamic ones are highlighted here. Added mass of the ice object, the structure and associated coupling terms are needed for computation of impact energy. A common assumption is to use a constant added mass of 0.5 times the ice mass for the ice [22, 23, 24, 25], although several studies [26, 25] show that the impact load is sensitive to this uncertain added mass value.

Clearly, the estimation of impact loads is highly depended on the impact velocity, which again depends strongly on the hydrodynamic forces acting prior to the impact. Important hydrodynamic effects that influence the impact velocity that has been highlighted in the literature include:

- The changes of added mass as the ice gets closer to the platform.
- Inclusion of incident wave forces, not only mean drift forces.
- Wave reflection and radiated waves from the platform.
- Viscous effects.
- Size and shape of the ice mass.
- Nonlinear vs linear methods.

Knowledge of these effects are thus important in order to provide good and reliable predictions of impact energy and collision force.

4 System description

4.1 Semisubmersible particulars

The semisubmersible used in this study is an existing model from the EXWAVE JIP [27]. It is a modern drilling rig with four columns and two pontoons. The platform is designed for extreme environmental condition and is considered representative for drilling rigs in the Arctic. Hydrodynamic properties of the semisubmersible are obtained from a WAMIT analysis that is further imported into the time-domain simulation tool SIMA. In the analysis, the draft of the semisubmersible is put in survival condition. Figure 1 shows the WAMIT model of the submerged part of the semisubmersible. The main properties of the platform in survival draft are summarized in Table 1.

Table 1 Main properties of the semisubmersible

Description	Unit	Value
Length of pontoons	m	107.50
Breadth outside pontoons	m	81.25
Survival draft	m	23.00
Displacement	t	39206

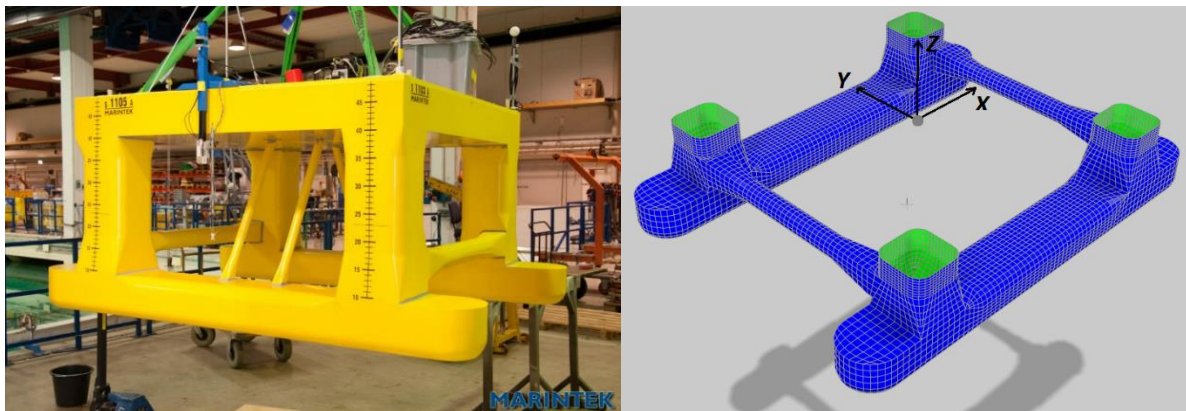


Figure 1 The semisubmersible drilling unit from the EXWAVE JIP [27]. Picture of the scale model (left) and illustration of the WAMIT panel model (right).

4.2 Ice geometry and mass

Two different ice shapes are considered in the study: a prolate spheroid and a cuboid. Dimensions and mass for both shapes are presented in Table 2. They are defined to be the same shape and size as the largest bergy bit used in the ST5 study [1]. The shapes are selected to have two different types of representative shapes: A round-shaped spheroid with a highly non-linear waterline, and a cuboid with sharp corners that will be more affected by viscous damping.

The shapes are illustrated in Figure 2. The spheroid is characterised by the following equation:

$$\frac{X^2}{c^2} + \frac{Y^2 + Z^2}{a^2} = 1,$$

where c is the distance from centre to the pole along the y -axis. The semi axis a is the equatorial radius and the relationship [1] to c is given as $a = 0.7c \cdot \exp(-0.00124c)$.

The cuboid is defined with its length L , height H and breadth B , and the relations [1] are defined as $H=B$ and $H = 0.7L \cdot \exp(-0.00124L)$.

Table 2 Shape, dimensions and mass of glacial ice

Case				
Spheroid	2c [m]	2a [m]	Mass [t]	Draft [m]
	15.0	10.4	765	8.1
Cuboid	L [m]	H [m]	Mass [t]	Draft [m]
	15.0	10.3	1432	9.0

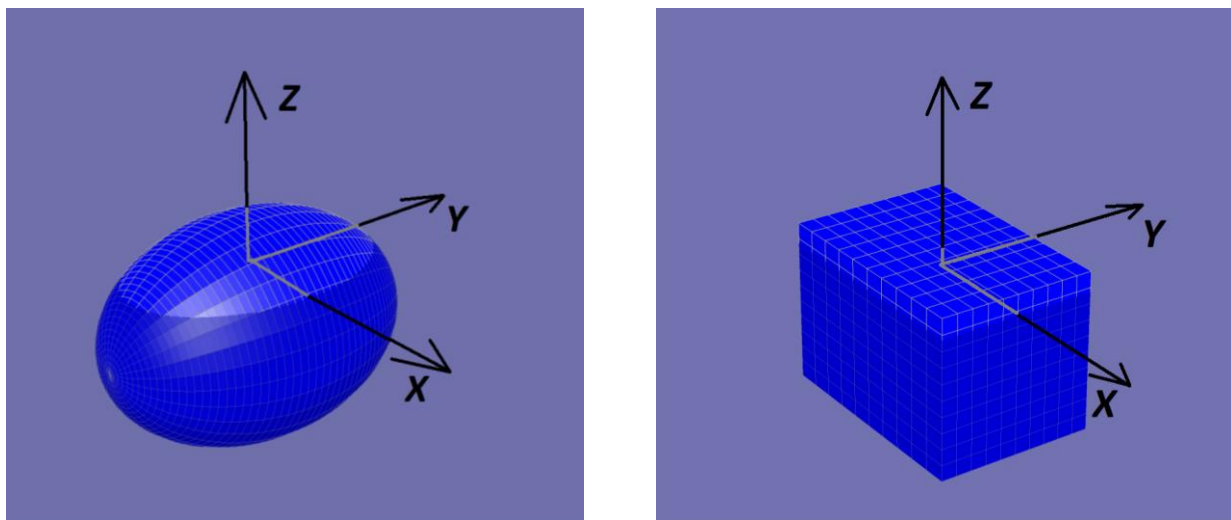


Figure 2 WAMIT panel models of the ice shapes including definition of the local body coordinate systems: Spheroid (left) and cuboid (right).

4.3 Coordinate systems

4.3.1 Global (earth-fixed) coordinate system

The global coordinate system is a right-handed earth fixed coordinate system to which the positions of all the local (body) systems are referred. The XY -plane coincides with the still water, and the Z -axis is positive upwards.

The propagation direction of the environment is referring to this system, i.e. for 0-degree wave direction the waves are propagating along the positive X -axis and for 90-degree wave direction the waves propagate along the positive Y -axis.

4.3.2 Local (body-fixed) coordinate system

Each body (i.e. platform and glacial ice) have their own local coordinate systems. This system is fixed to the body and translates and rotates along with the body. Load and motion response calculations refer to the local coordinate system. The definitions of the local coordinate systems are shown in Figure 1 and

Figure 2 for the semisubmersible and glacial ice, respectively. The origin of the local coordinate system is in the body's centre of floatation.

The global coordinate system coincides with the semisubmersible's local coordinate system in calm water.

5 Linear hydrodynamic frequency domain analysis

The linear hydrodynamic frequency domain analysis has been performed with WAMIT. The purpose of the linear diffraction-radiation analysis is to establish hydrodynamic coefficients such as added mass, wave damping, wave force and drift force coefficients for the semisubmersible and the glacial ice.

WAMIT is further used to investigate the hydrodynamic interaction between the platform and the glacial ice, i.e. how the hydrodynamic pressure acting on one body is influenced by the presence of the other body. This multibody analysis is performed for various positions of the glacial ice relative to the platform. A sensitivity study is also carried out, to study the variations of the hydrodynamic interactions as the glacial ice is approaching the platform (from a far distance to close proximity).

It should be noted that WAMIT is based on inviscid potential flow, i.e. viscous forces are not accounted for. A linear damping matrix can be included in the calculation of the motion response resembling viscous damping. In the current frequency domain study, viscous damping is included for the glacial ice as percentage of the critical damping. The critical damping for a single degree is defined as

$$C_{crit} = 2\sqrt{mk}$$

where m is the system mass and k is the stiffness coefficient. The percentage of critical damping for the glacial ice is 7% for heave and 11% for both roll and pitch [1]. The linear damping of the platform is tuned to model test data [27].

Also, WAMIT assumes that the hydrostatic restoring forces are linear around the mean waterline, i.e. it does not include the effect of changes in the waterline area. This causes an unrealistically large restoring force for bodies with nonconstant waterline area undergoing large vertical motions.

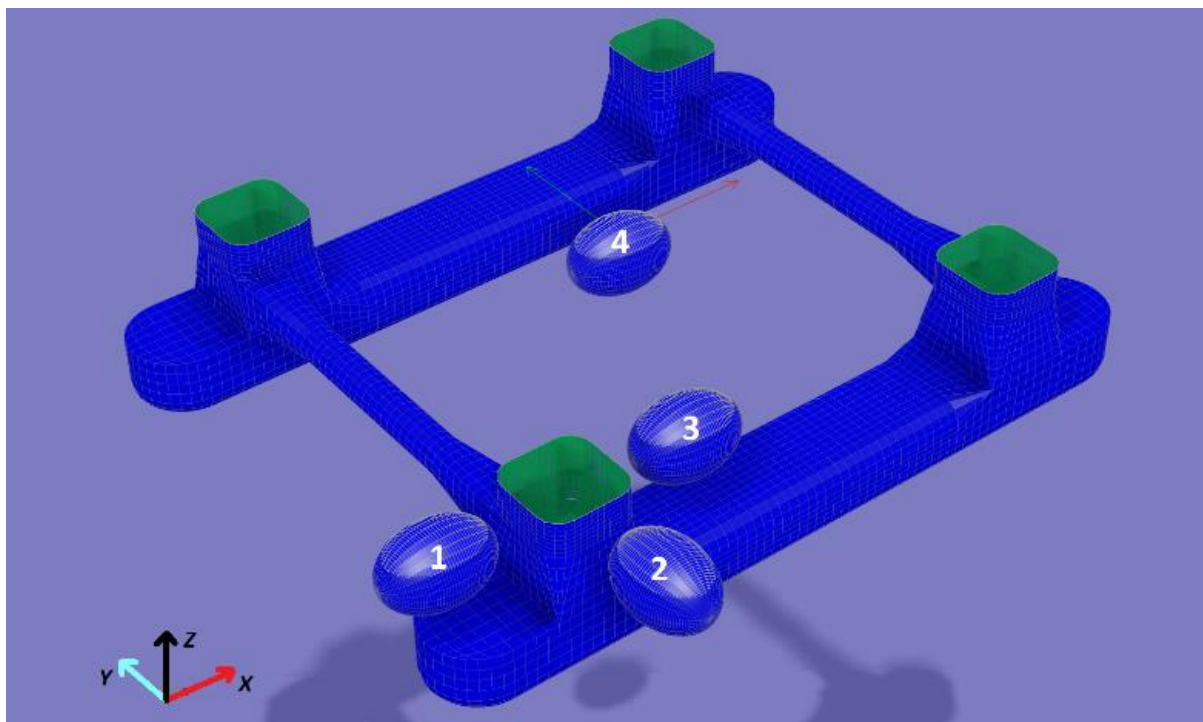


Figure 3 Illustration of the relative positions of the glacial ice and semisubmersible for the WAMIT multibody analysis. The three-coloured axis-system defines the directions of the global coordinate system.

5.1 Hydrodynamic interaction between glacial ice and semisubmersible

The multibody WAMIT analysis is limited to study the platform-ice hydrodynamic interaction only for the largest spheroid glacial ice shape. Four different cases are considered, as illustrated in Figure 3, where the glacial ice is moved to different positions relative to the platform.

In Case 1 to 3, the glacial ice is positioned in the proximity of one of the columns. The distance from the tip of the ice to the column wall is $0.25L$ for these three cases, where $L=2c$ is the longitudinal length of the spheroid. In Case 4, the glacial ice is placed in the horizontal centre of the platform.

In addition, Case 2 is extended to also study the effect on varying the distance between the column wall and the ice tip along the longitudinal direction.

5.1.1 Motion response in the frequency domain

The response amplitude operators (RAOs) show the motion response amplitude per unit wave amplitude. The RAOs are given in the local body coordinates system. Wave propagation directions are defined in the global system.

Figure 4 shows the RAOs for the semisubmersible. The plots compare the single body motion response (no glacial ice present) with the multibody motion response due to the presence of glacial ice (Case 1-4). The results are shown for the motion modes surge, sway, heave, roll and pitch, and for wave periods between 1-30 seconds. The wave propagation direction in Figure 4 is 0 degrees for surge, heave and pitch, and 90 degrees for sway. In general, the results show that the motion responses of the semisubmersible are not significantly influenced by the near presence of the glacial ice, which is in line with the findings of ST5 [1].

The motion response of the glacial ice is shown in Figure 5 together with the wave force transfer function. For the four cases (Case 1-4) the wave directions are selected to ensure movement of the ice towards the platform. The RAOs and the forces are given in the local body-fixed coordinate system. As expected, due to the relatively large difference in size and mass compared to the semisubmersible, the motion of the glacial ice is to a great extent influenced by the presence of the platform. Furthermore, the added-mass coefficients for sway and heave are shown in Figure 6, including the added mass coupling due to the platforms motion in surge, sway and heave. Both the diffraction forces (Figure 5 - right) and the radiation forces (represented by the added mass in Figure 6) show large changes due to the presence of the semisubmersible. Thus, a general conclusion that one interaction effect is more important than the other cannot be made, as that will depend highly on the wave period.

However, from the diffraction force in Figure 5 it is possible to see if the platform provides a sheltering effect (e.g. heave force for Case 4 for wave periods around 7-10 seconds) or amplifies the wave loads (e.g. heave force for Case 3). For Case 4 the heave resonance response is reduced by approximately 40% due to the sheltering effect, while for Case 3 the resonance response is amplified by about 50%. Furthermore, the influence on the glacial ice due to the platform motion is demonstrated by the coupled added mass coefficients in Figure 6, e.g. platform surge motion has relatively smaller effect on Case 2 than for the other cases, while influence due to platform sway motion is more pronounced for Case 2. Also, the hydrodynamic interaction due to the semisubmersible heave motion is clearly visible in the ice RAOs near the platform's heave resonance period at 23 seconds, especially for the sway and roll response (see Figure 5).

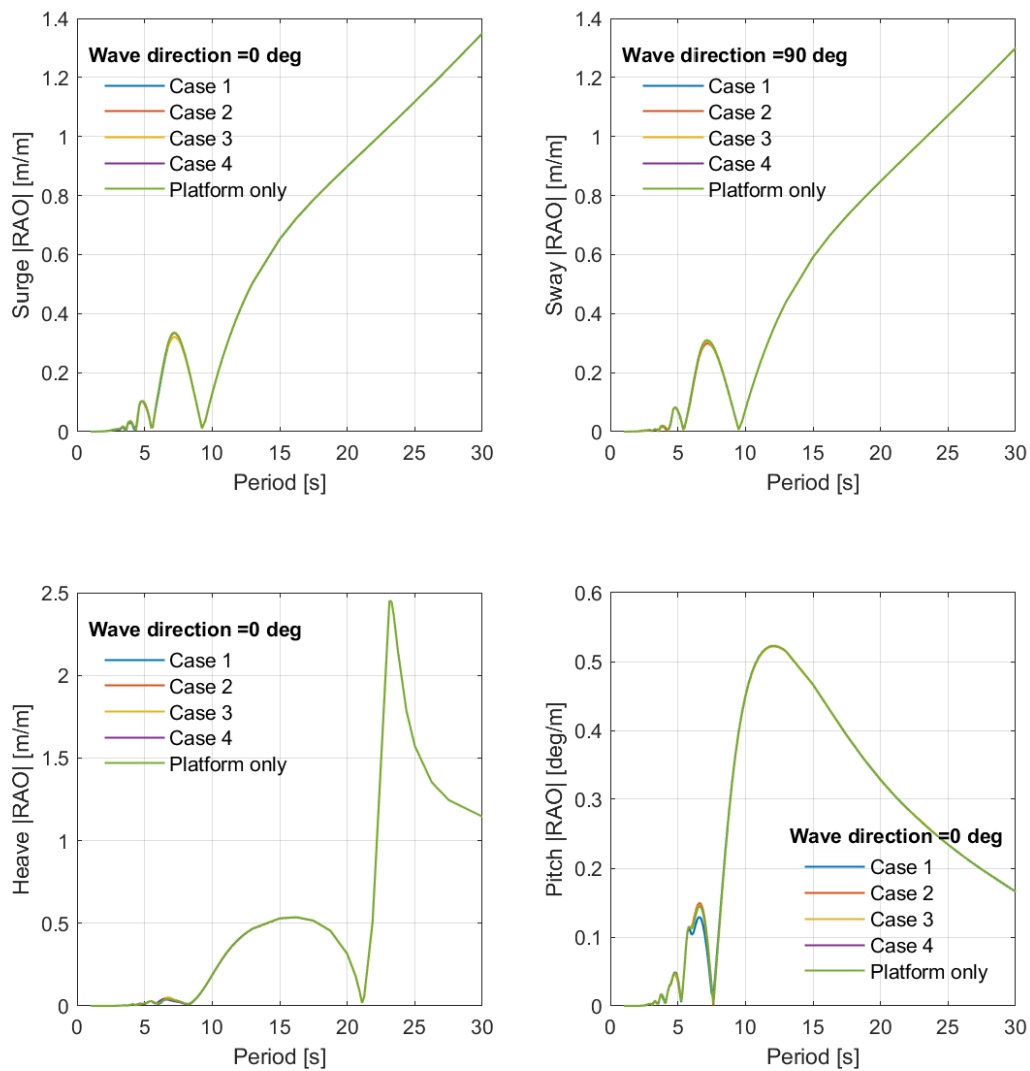


Figure 4 The response amplitude operators (RAOs) for the semisubmersible in surge, sway, heave and pitch. The motions response is shown for platform only (no hydrodynamic interaction) and for the four cases with the glacial ice present.

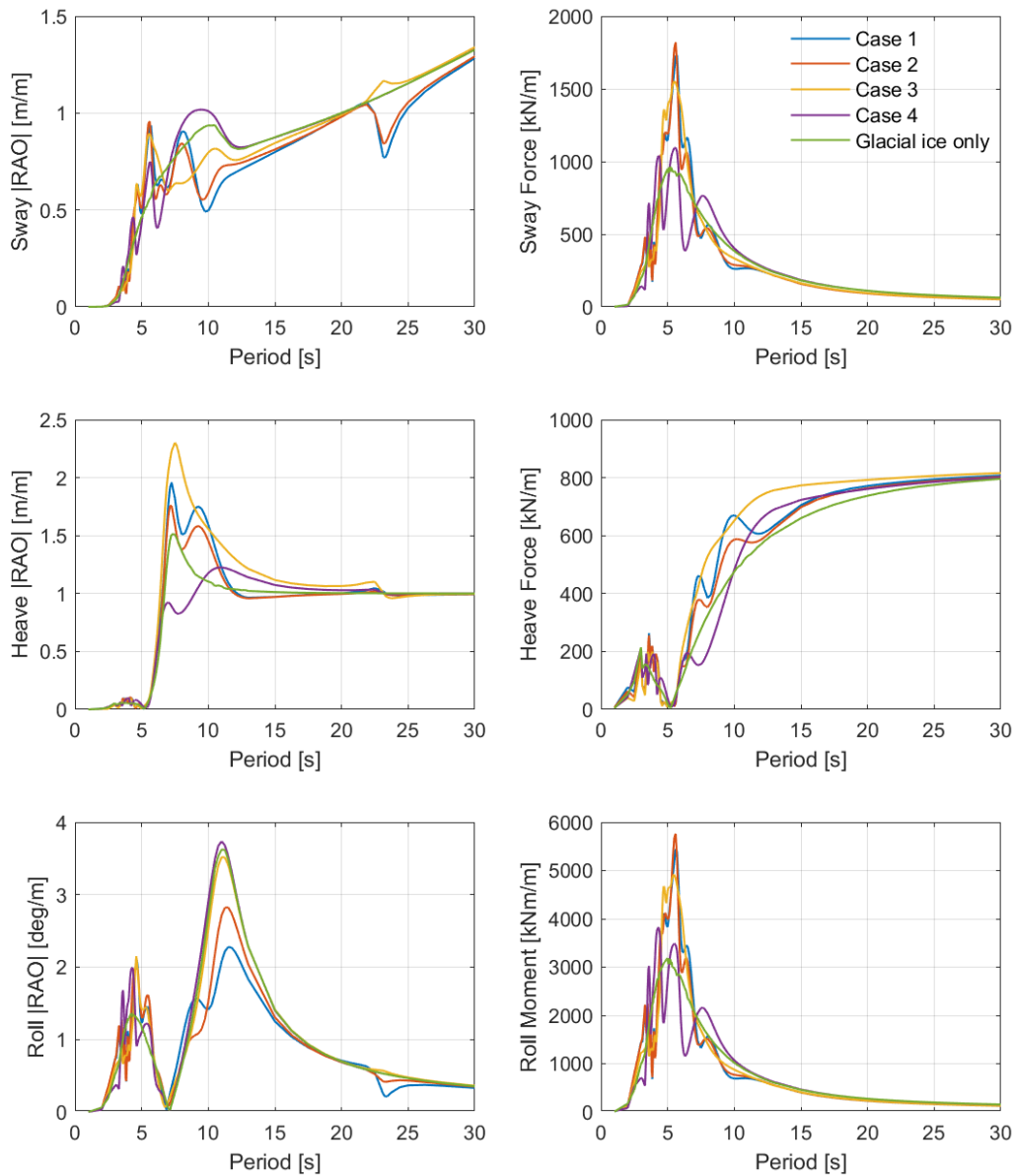


Figure 5 The response amplitude operators (Left) and the wave force transfer functions (Right) for the spheroid in sway, heave and roll. The transfer functions are shown for glacial ice only (no hydrodynamic interaction) and for the four cases with the semisubmersible present. The wave directions are selected to ensure a movement of the glacial ice towards the platform: Case 1 – 0 deg; Case 2 – 90 deg; Case 3 – 180 deg; Case 4 – 0 deg.

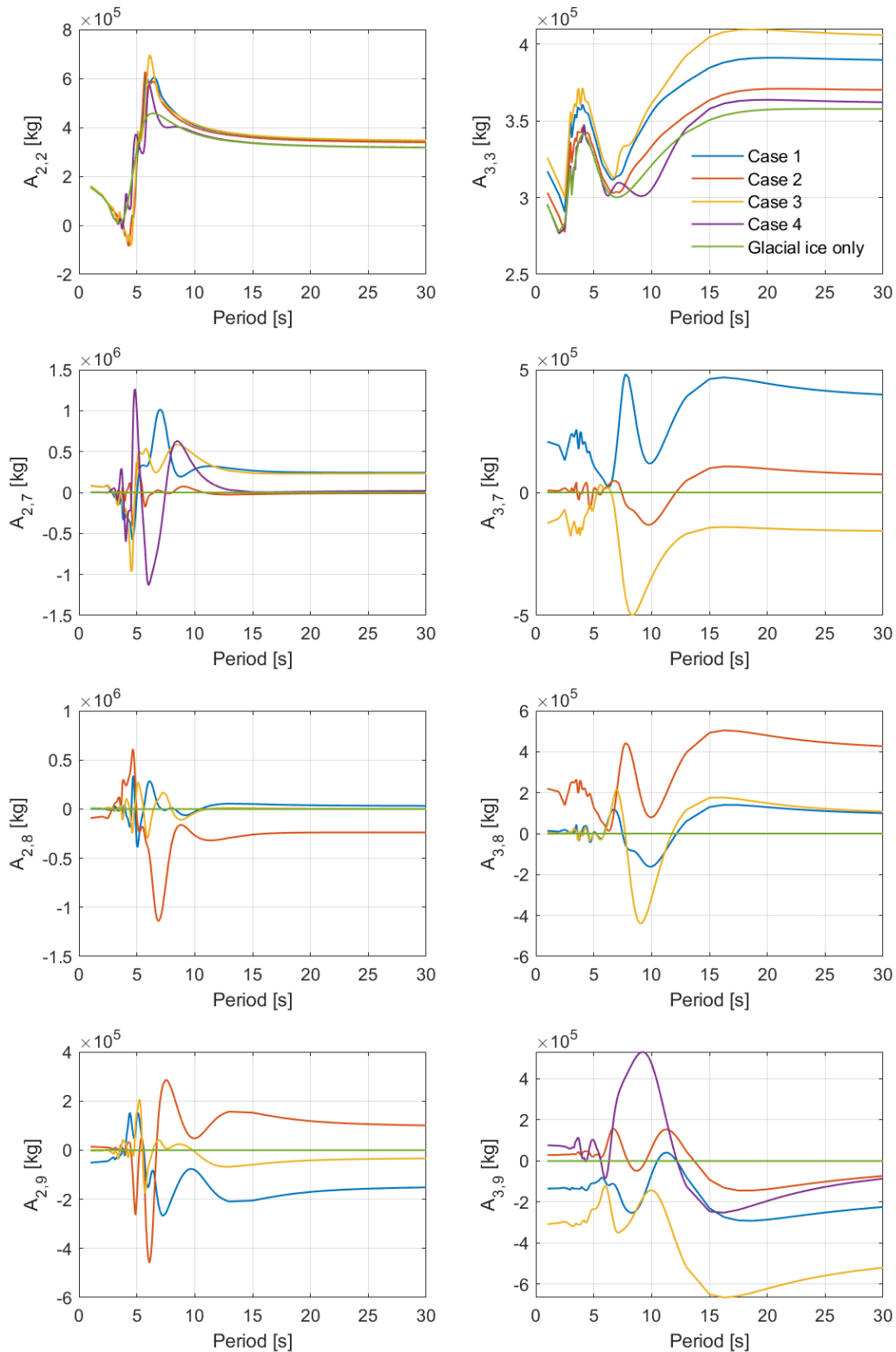


Figure 6 Frequency dependent added mass coefficients for spheroid sway-sway and heave-heave, and added mass due to coupling with platform motion in surge, sway and heave (i.e. A_{ij} for $i=2,3$ and $j=7,8,9$).

5.1.2 Sensitivity due to distance from platform column – asymptotic properties.

Case 2 has been further investigated, where the distance from the ice tip to the column wall has been varied along the longitudinal direction (global Y -axis). The purpose of this sensitivity analysis is to investigate numerically the asymptotic behaviour of the added mass coefficients as the gap between the ice and the platform column gets smaller.

The asymptotic behaviour of the zero- and infinite-frequency added mass as function of the distance to the platform are shown in Figure 7 and Figure 8, respectively. The plots show the diagonal elements of added mass in sway and heave ($A_{2,2}$ and $A_{3,3}$), and their coupling due to the semisubmersible motion in surge, sway and heave ($A_{i,j}$, for $i=2,3$ and $j=7,8,9$).

The diagonal elements are only influenced by the presence of the platform in the very near proximity to the column ($\Delta < 2c = L$). The added mass increase is more significant for sway motion than heave, and the changes are approximately 47% and 14%, respectively, as the ice mass is moved very close to the column. Moreover, as presented in Faltinsen [28] with reference to Greenshaw & Yanbao [29], the asymptotic solution for a cylinder moving towards a fixed boundary shows a zero-frequency added mass equal to $(\pi^2/3-1)$ at the wall, or 2.29 times the far distance added mass. This increase is only significant very close to the boundary, e.g. at $H/R=1.0$ the increase is only 20% where H is the distance to the wall and R is the radius of the cylinder. In the present study with the spheroid accelerating towards the platform column the water is allowed to flow around the column; thus, the pressure increase will be less compared to the case when the cylinder moves towards an infinite wall. Consequently, the increase in added mass for the spheroid is less extreme in the present study than what was found for the cylinder in [29]. The increase in added mass as the ice mass moves closer to the platform will cause a repellent force [30].

The hydrodynamic interactions due to the motion of the platform acts in a larger distance from the platform, i.e. in a length scale of $5-10L$ (equivalent 1.5-3 pontoon lengths). This is because the displaced volume of the platform is much larger than the ice, and the pressure field generated by the platform motion must be considered in the length scale of the platform. The changes in sway and heave added mass due to the platform motion is most prominent when the platform oscillates in the direction towards the ice (i.e. in sway direction). The magnitude of the added masses due to platform sway motion, $A_{2,8}$ and $A_{3,8}$, are comparable to the diagonal elements $A_{2,2}$ and $A_{3,3}$ when the ice is very close to the platform.

Note that the accuracy of the asymptotic results is highly dependent on the panel size when the two bodies are close to each other. To quantify the accuracy of the asymptotic results, a panel size sensitivity study is needed. However, due to scope limitation, such grid dependency study has not been carried out.

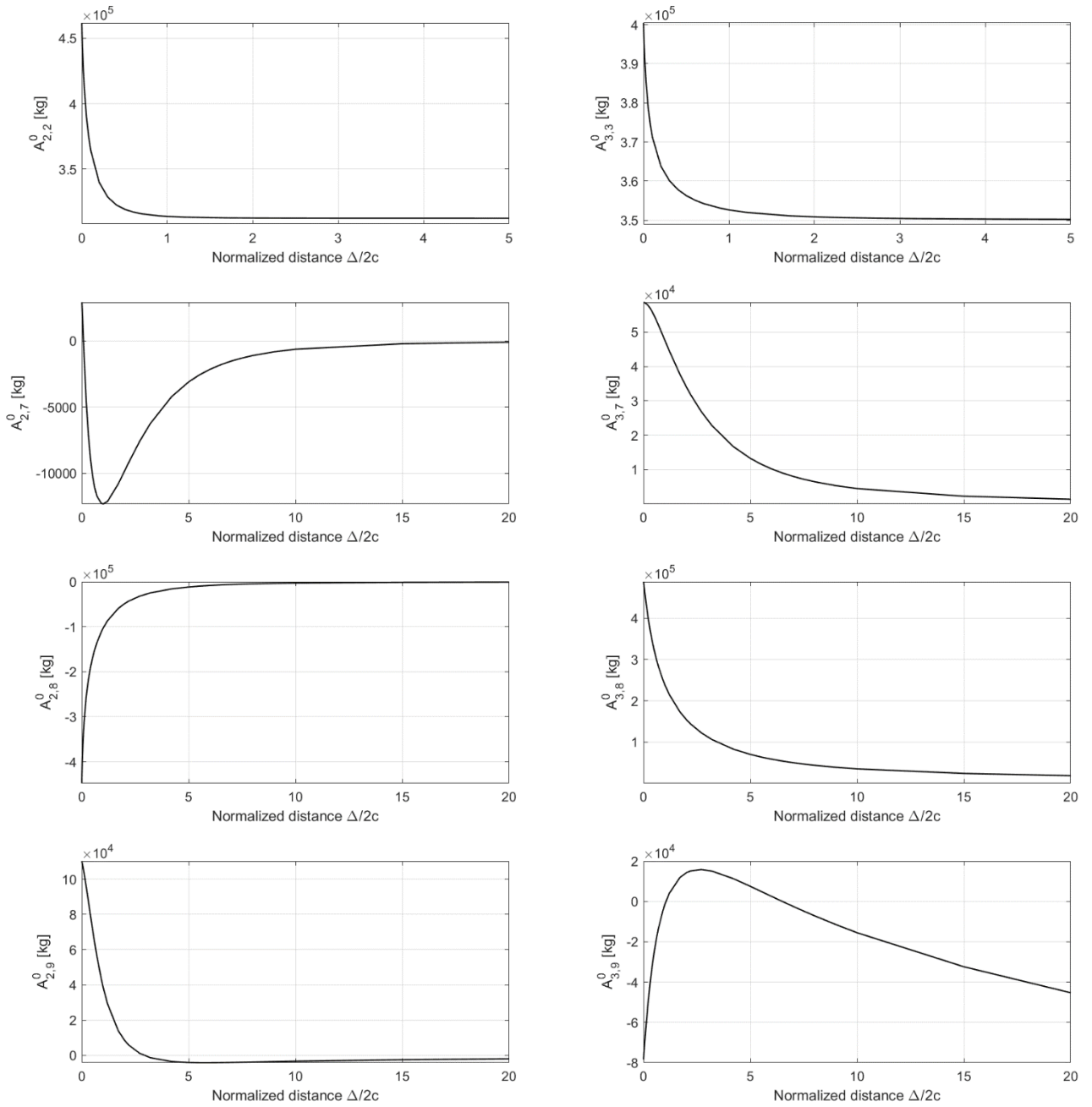


Figure 7 The zero-frequency added mass coefficient as function of distance to the platform's column wall.

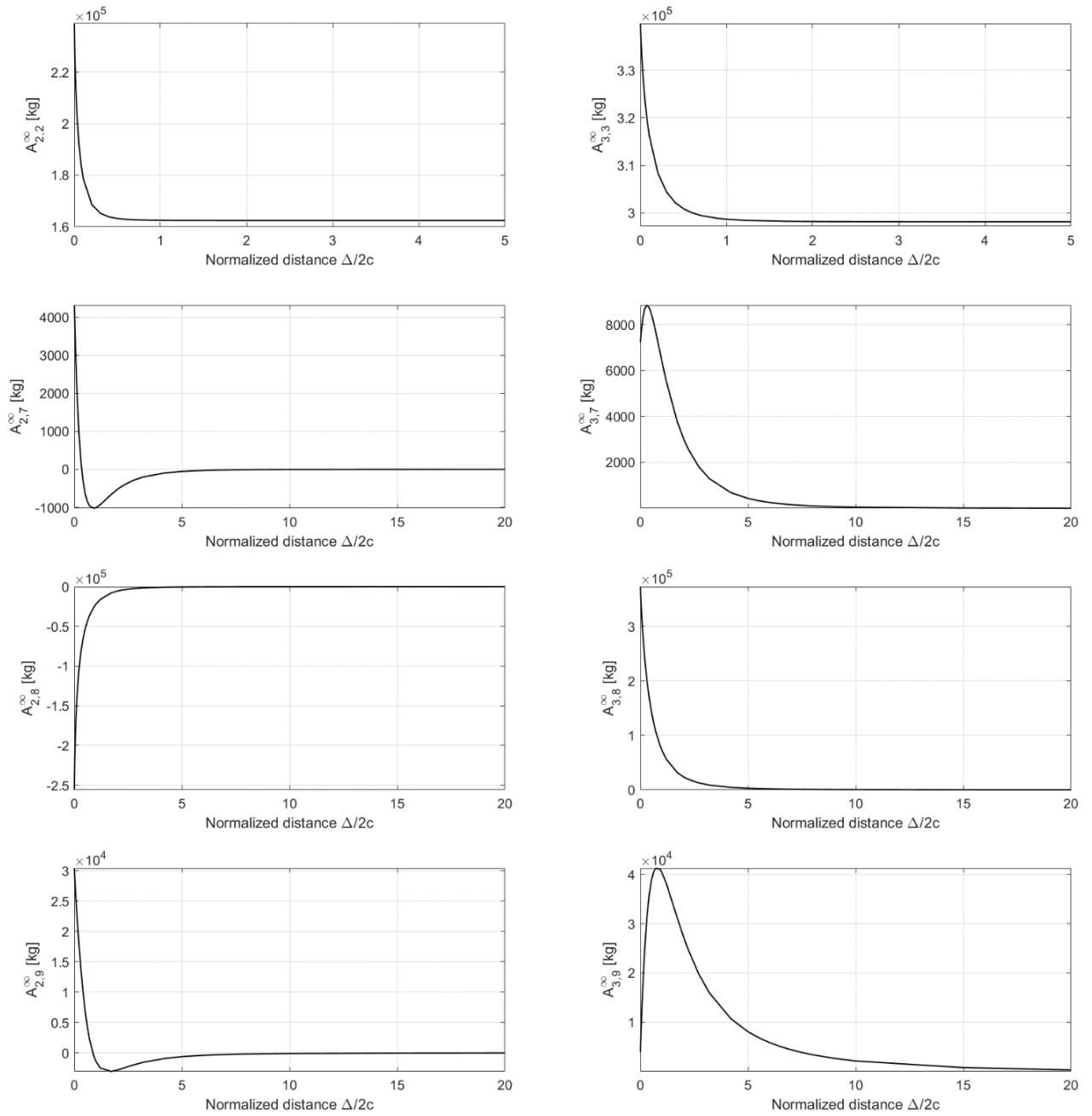


Figure 8 The infinite-frequency added mass coefficient as function of distance from the platform's column.

6 Glacial Ice Motions in Waves

In order to predict the velocity and location of time just before the impact, ice motions in waves must be solved. The traditional solution methods for this purpose are based on linear assumptions. Several of these assumptions are not applicable to ice shapes. In Particular linear restoring, which is based on assumption that the change in the ice water plane area during oscillation is negligible, is not valid. Adopting such model may result in unrealistically large restoring forces especially when ice is submerged.

A nonlinear Froude-Krylov model is adopted together with traditional linear model for radiation and scattering forces in the present study. The model is validated against existing model test data and CFD calculations in and outside the range of linear theory's validity. This model is then adopted in the next chapter to study several sleeted impact scenarios.

6.1 Modelling

The dynamics of semi-submersible platform and ice are solved using the SINTEF Ocean's time domain simulator SIMO and the simulation platform SIMA.

The dynamics of semi-submersible are presented using state-of-the-art models and validated against model tests during the first phase of EXWAVE JIP [27]. The description of the model could be found in the referenced reported and is not repeated here.

The dynamic model of ice is constructed based on decomposition of forces, rooted in linear assumption. The following components are considered with this respect

- Mass forces
 - A mass matrix is calculated for the selected ice geometries, assuming uniform density of ice.
- Hydrostatic forces
 - Linear hydrostatic stiffness matrix, obtained from WAMIT, is used in the **linear** calculations. This effect is directly included when nonlinear Froude-Krylov model is used, therefore the stiffness matrix is removed in those cases.
- Potential flow radiation forces
 - Radiation problem is solved using WAMIT to calculate added mass and damping coefficients for the mean position of the ice. The results are transformed into retardation functions which is used by SIMO to calculate radiation memory effects through convolution integrals.
- Potential flow diffraction forces
 - The forces acting on the ice due to diffracting the waves are calculated using WAMIT. The Froude-Krylov component of the force is extracted, since it will be calculated separately.
- Potential flow second order mean drift forces
 - WAMIT is also used to calculated drift coefficients for the mean position of the ice.
- Potential flow, nonlinear, Froude-Krylov forces
 - A model is developed and adopted to calculate underwater portion of the ice and the corresponding total hydrostatic and hydrodynamic pressure at each time step. Forces, which included buoyancy and Froude-Krylov excitations are obtained by integrating pressure on instantaneous surface on the body. The model is described in more details in the following texts.
- Viscous forces

- In order to model viscous forces a set of current coefficients, and slender elements with content drag coefficients are adopted. The assumed net viscous drag forces, obtained from empirical drag coefficients found in [31], is decomposed into current coefficients, Morison-type element forces, and additional linear and quadratic damping coefficients in an attempt to represent a realistic approximation of viscous forces. Due to nonlinearities involved, this decomposition is not entirely consistent. However, based on previous experience with tuning viscous forces on floating platforms, acceptable results are expected from this type of decomposition. In lack of model test data, this approach is considered to be the best available option for modelling the viscous forces.

Six-degree-of-freedom model is used to solve the motions of the ice. Only wave interaction with ice is considered in the present study. Meaning current and wind forces are neglected. The stochastic waves are modelled using 3-parameter Jonswap spectrum. The wave realization is obtained through Fourier analysis by selecting a seed number to present a random selection of phases for wave components.

During the simulation, the ice drift in domain is considerable comparing to its length. Moreover, the correct phasing between the platform and ice motions is important to obtain to point of impact. Therefore, the waves have to be calculated for the position of the ice, as it moves in the domain. The Fourier wave components are transformed in time domain in order to include the phase shift in waves due to ice horizontal motions. This model is known as cos-series in SIMO.

6.1.1 Nonlinear Froude-Krylov Forces

The ice has a density close to water. Therefore, it floats with small free-board and it can get fully submerged as it moves in waves. Moreover, the surface of the ice around the waterline is not necessarily vertical. A linear hydrostatic restoring, and Froude-Krylov excitation, model assumes that the ice surface is vertical around the water line, i.e. a constant waterplane area. This results in unrealistically large restoring forces when ice shapes with nonconstant waterplane area become submerged (e.g. see Figure 9).

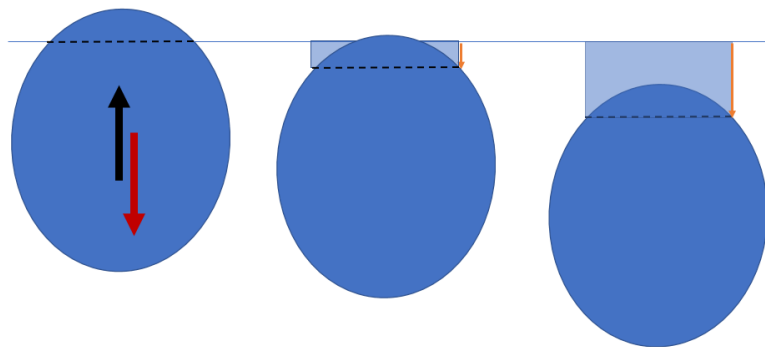


Figure 9: Schematic view of linear buoyancy force, represented by the volume of the transparent rectangle.

In the present study, the nonlinear Froude-Krylov force is calculated by obtaining the instantaneous underwater surface of the ice and integrating the incoming wave pressure on that. The free-surface elevation around the ice is reconstructed for a patch around the ice as shown in Figure 10. The ice surface is represented by triangles in a STL, stereolithography, format (Figure 10). The dynamic pressure due to incoming waves are constructed on a volume grid, starting from the mean free surface and extending downward, while horizontally it extends to the boundaries of the free-surface patch. The linear dynamic pressure is assumed constant above the mean water level. After cutting the ice geometry with instantaneous free surface to obtain the underwater surface, the hydro-static and dynamic pressures

are calculated using the distance of the points from mean water surface, and interpolation of calculated dynamic pressures on the nodes of the volume grid (Figure 11).

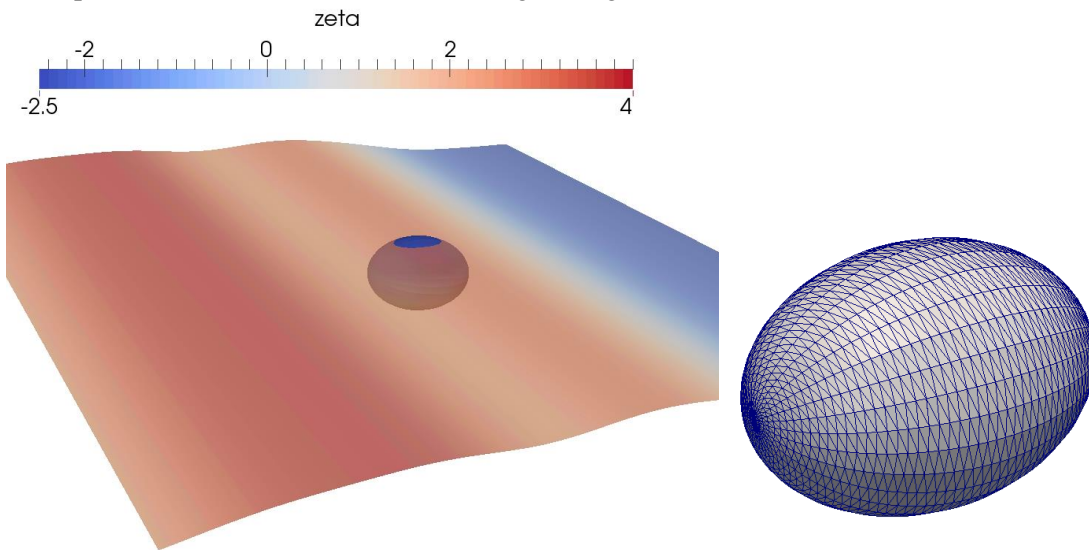


Figure 10: A snapshot of reconstructed free-surface elevation around ice, and the STL file for the spheroid ice

The horizontal extent of the free-surface patch and the dynamic pressure interpolation box are decided based on sensitivity studies. The surface patch and dynamic pressure box needs to be relocated and recomputed when the ice has drifted to the boundaries. On the other hand, selecting a too large domain put pressure on memory and slows down interpolation process at each time step. It is possible to optimize these number to achieve the best computation performance. Number of cells in these domains dictates the minimum resolvable wave length. This means prior to computations a cut off frequency for the wave energy must be assumed. For most computations presented here, the elements sizes are chosen to be between 2 to 4 meters. This makes the shortest resolvable wave to be around 2 seconds.

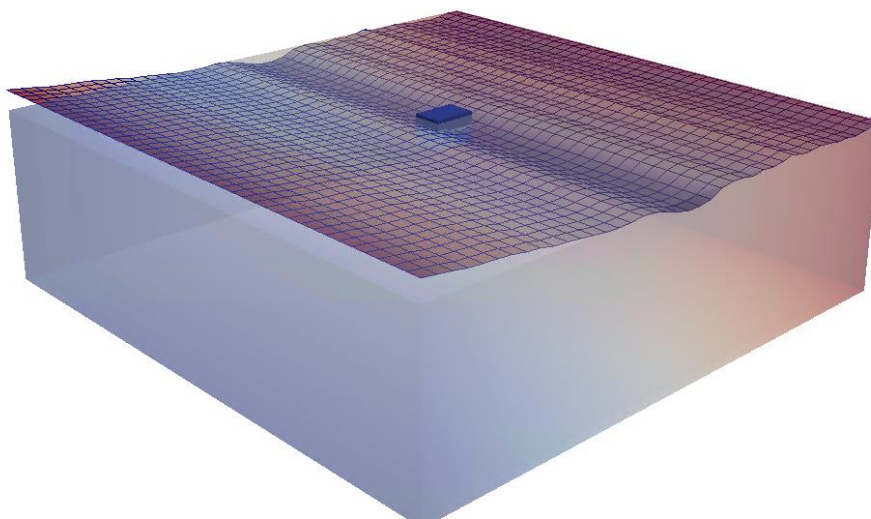


Figure 11: A view of the free surface patch and dynamic pressure box, with the ice in the centre.

6.2 Validation Studies

A series of verification and validation studies are presented here for the implemented and adopted nonlinear Froude-Krylov force model.

6.2.1 Free-surface elevation

A comparison between the calculated free-surface elevation at the centre of the body by interpolating the elevation on free-surface patch, and the internal cos-series method in SIMO is presented in Figure 12 for a regular wave. The free-surface elevation at the initial location of the ice is also included. A shift between the elevation at origin and what ice experiences appear as it drifts away. Figure 13 shows a similar comparison for irregular waves. The elevation at the instantaneous location of the ice obtained from two methods is identical. This means the interpolation method is accurate and the number of panels per wave length is sufficient to capture the energy from important wave lengths.

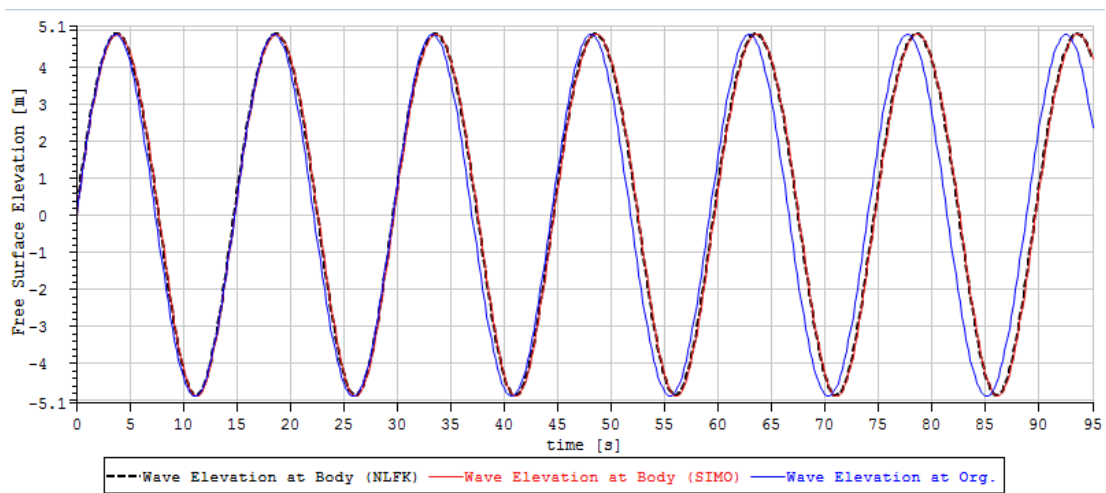


Figure 12: comparison of wave elevation at origin and centre of body, regular wave, $H=9.8$ [m], $T=14.8$ [s]

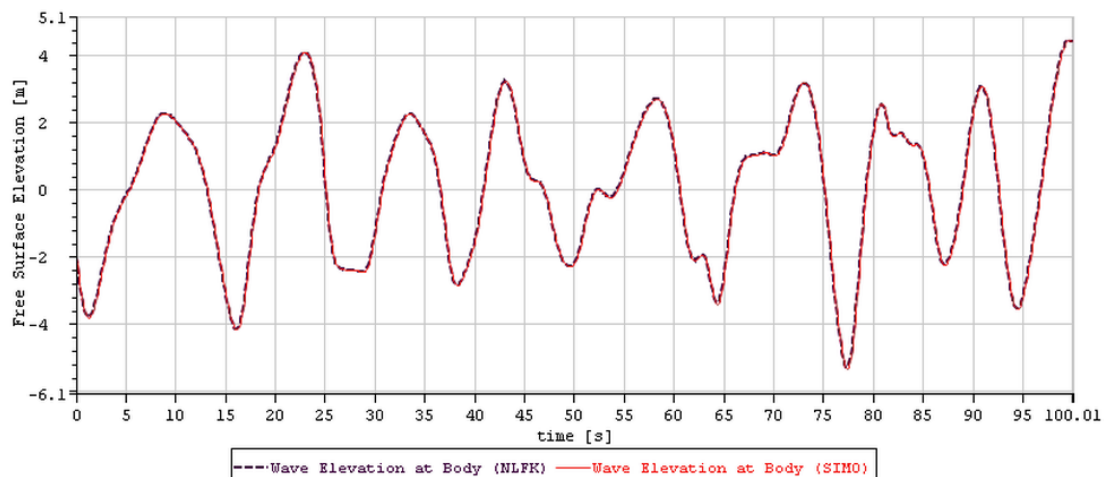


Figure 13: comparison of wave elevation at centre of body, irregular wave, $H_s=9.8$ [m], $T_p=14.8$ [s]

6.2.2 Comparing with CFD

A selection of cases in regular waves are studied with CFD in order to compare with the nonlinear Froude-Krylov model.

6.2.2.1 Simulation set-up

Simulations were performed in OpenFOAM by treating the floating ice in an overset mesh within a background mesh. The domain size and the mesh are shown in Figure 14 and Figure 15. The ice cube dimensions are $L_x \times B \times H = 15.0 \text{ m} \times 10.3 \text{ m} \times 10.3 \text{ m}$. The draft is 9 m providing a density of 0.896 kg/m^3 . The simulations were set for deep water. The origin of the global coordinate system is on the mean free surface at the centre of the ice in horizontal plane.

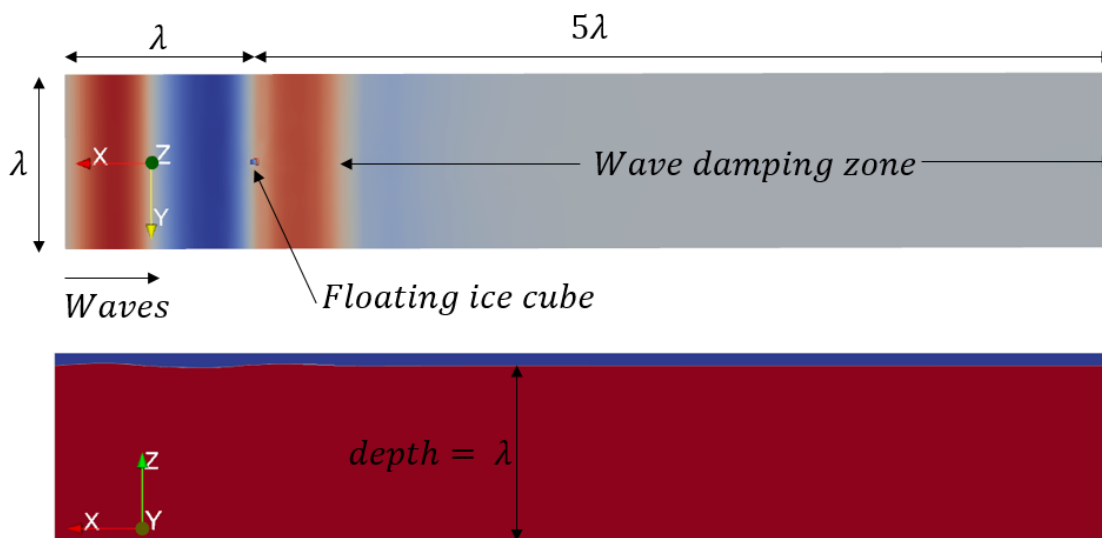


Figure 14. Simulation domain in CFD, λ is the wavelength corresponding a selected wave period

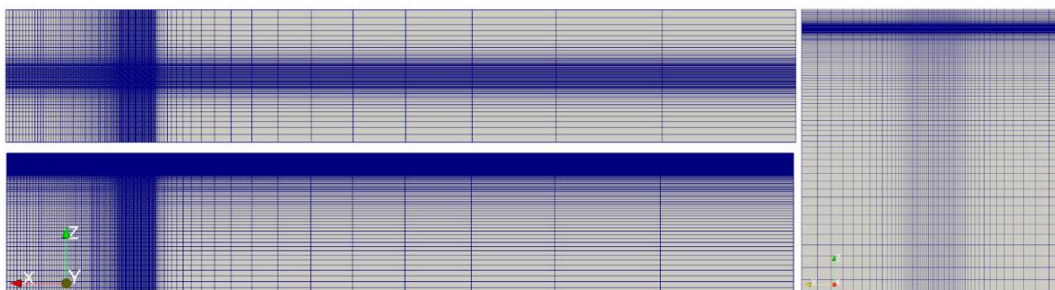


Figure 15. A mesh of 970000 cells was used. Top(XZ plane), side(XY plane) and front(YZ plane) are shown.

Both fixed and floating conditions are investigated. In the floating case the ice is restrained using a horizontal mooring system consisting of weightless lines with a stiffness of 4000 N/m on each line. The lines have a pretension of 165kN to avoid getting slack. The mooring lines setup for 0 and 20 degrees heading angles are shown in Figure 16.

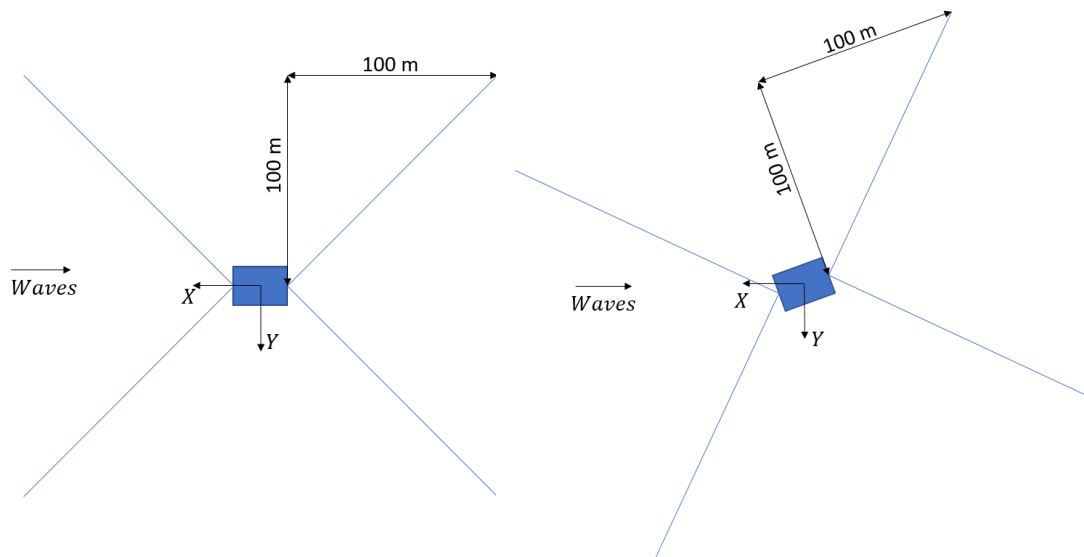


Figure 16. Horizontal mooring lines at 0 and 20 degrees heading angles. The lines and the vertical centre of gravity of the body are in a same horizontal plane.

6.2.2.2 Fixed ice cube

A fixed ice cube in regular waves of 9.8[m] height and 14.8[s] period, traveling towards positive x-axis along the cube, is considered. The goal is to compare the obtained vertical and horizontal force from different method, i.e. linear, nonlinear Froude-Krylov (NLFK), and CFD, to see if the implemented model improves the linear predictions comparing to CFD. In addition, it would be possible to verify the selected drag coefficients and the obtained viscous forces.

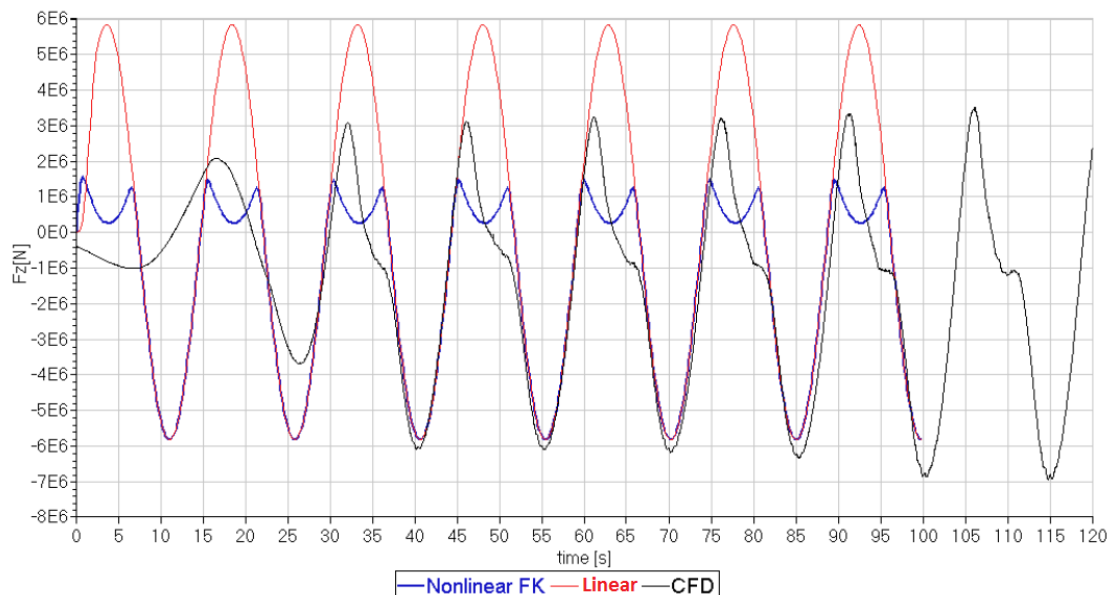


Figure 17: Vertical force acting on the fix ice cube in regular waves of 9.8[m] height and 14.8[s] period from three different methods.

Figure 17 shows the comparison between vertical forces acting on the ice from linear, NLFK, and CFD calculations. The linear model predicts a sinusoidal force as expected, while the NLFK model shows a very different behaviour when the ice cube becomes submerged. The resulted force in this case is close to CFD but still missing the higher harmonic components, and viscous effects.

Figure 18 shows a similar comparison when the viscous forces are included using a Morison-type elements forces and a constant drag coefficient. The viscous force is only included in the NLFK model. The obtained improvement comparing to CFD calculations is clear. The introduced viscous drag model here is further used in simulations of ice-platform impact.

The comparison for horizontal forces is presented in Figure 19 when viscous forces are introduced in the NLFK model. The differences between linear and NLFK predictions are smaller in this case between, and do not include the higher order forces present in the CFD results.

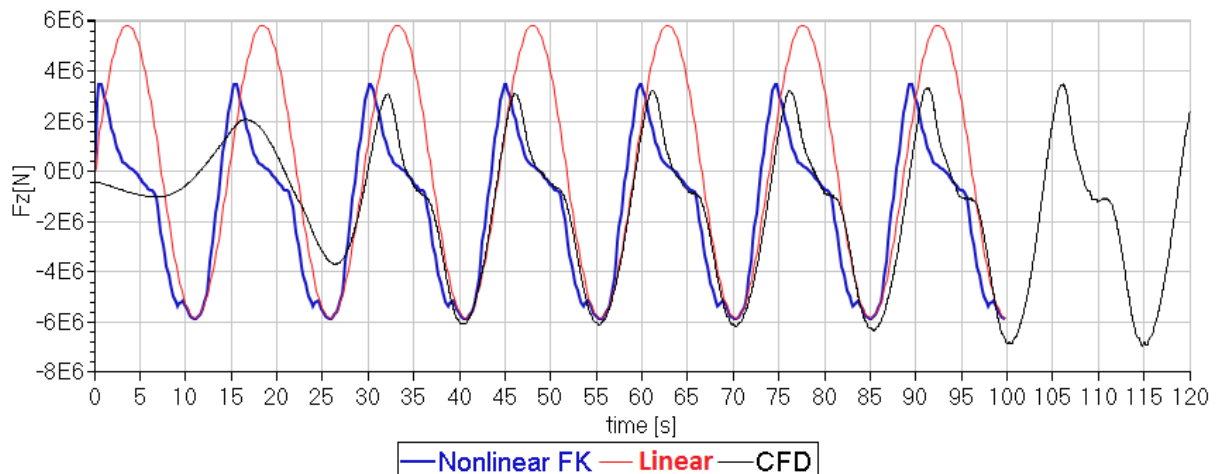


Figure 18: Vertical force acting on the fix ice cube in regular waves of 9.8[m] height and 14.8[s] period from three different methods. Nonlinear FK model includes Morison-type viscous forces introduced through a slender element with constant drag coefficient.

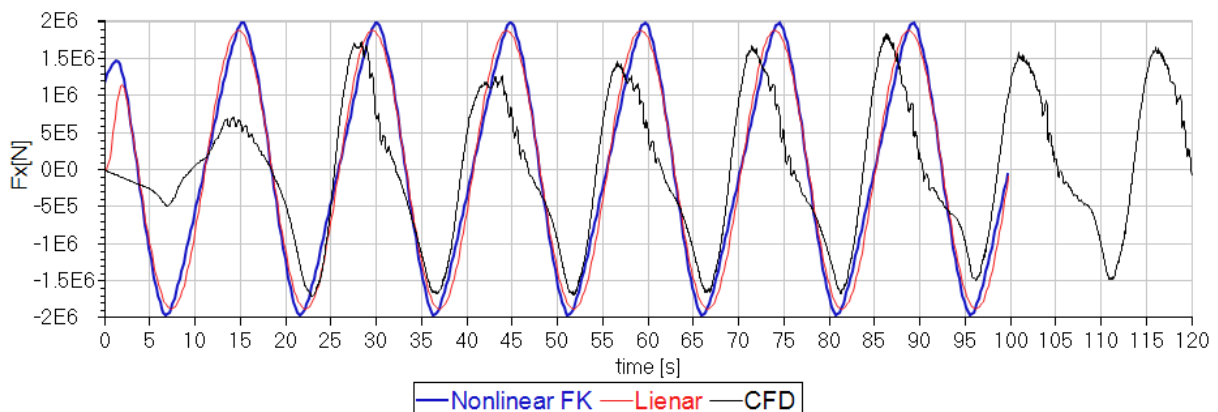


Figure 19: Horizontal force acting on the fix ice cube in regular waves of 9.8[m] height and 14.8[s] period from three different methods. Nonlinear FK model includes Morison-type viscous forces introduced through a slender element with constant drag coefficient.

6.2.2.3 Moving ice cube

A brief comparison of the freely floating ice cube is presented here. Only the case with zero heading and 9.8[m] wave height and 14.8[s] period is considered. A similar mooring system, as selected in CFD calculations is modelled in SIMO using linear springs. Figure 20 shows the motions of ice cube in horizontal (X) and vertical (Z) directions, from three different method. The difference between linear and NLFK models here is small since the regular wave is long and linear theory is still applicable. The comparisons for vertical motions are better than horizontal motions. CFD predicts 10 times larger mean drift force comparing to two other methods. The reason for this discrepancy is unclear. Possible viscous effects in the splash zone steepening the waves in the CFD domain could be among the reasons. Nevertheless, a relatively good comparison between the horizontal motions are obtained simply by adjusting the mean forces in the SIMO simulations according to CFD.

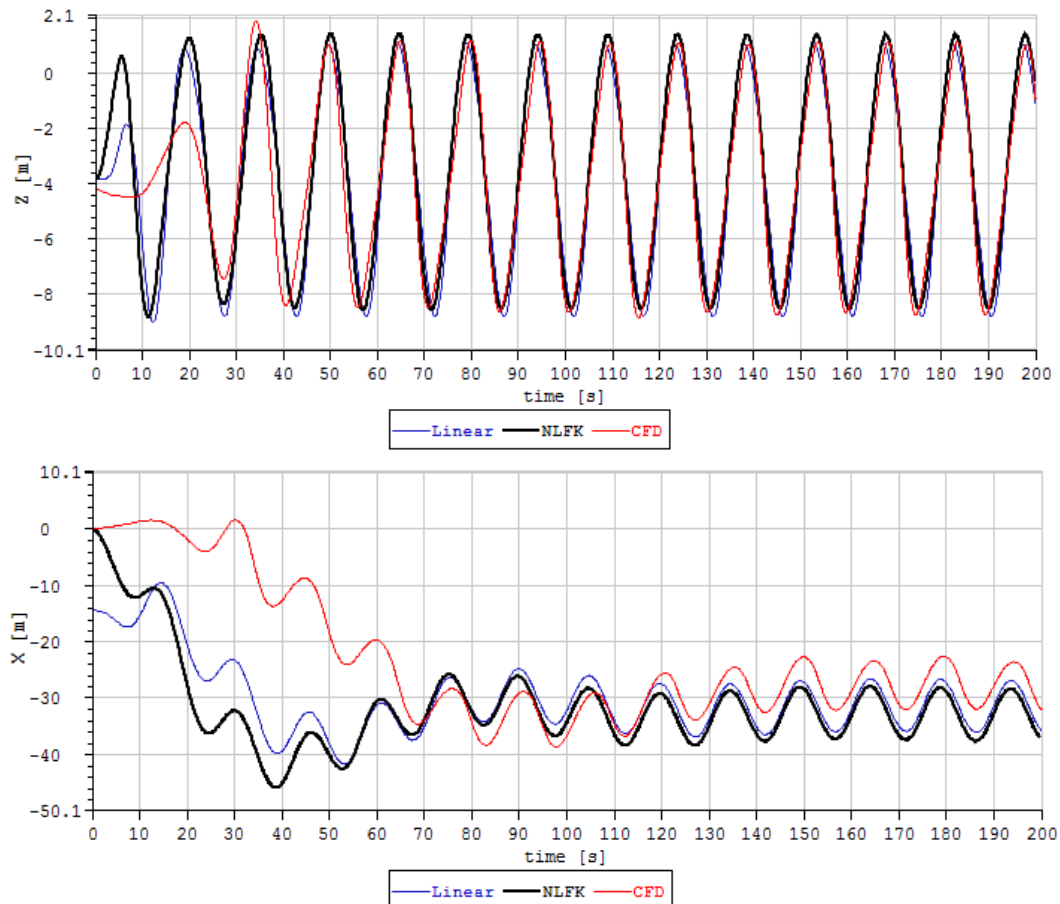


Figure 20: Motions of a freely floating ice cube in regular waves of 9.8[m] height and 14.8[s] period from three different methods.

6.2.3 Existing model test data

Existing model test data from a previous project carried out at SINTEF Ocean is used for a brief validation of the present method. Currently it is not possible to disclose the geometry and details of the model test due to confidentiality issues, but a comparison between motions for several regular wave conditions are included here just to show the applicability of the model. The comparison includes previously developed models for similar purpose but based on completely different formulations. The geometry surface has an angle of about 30 degrees at the water line which makes linear model of restoring questionable.

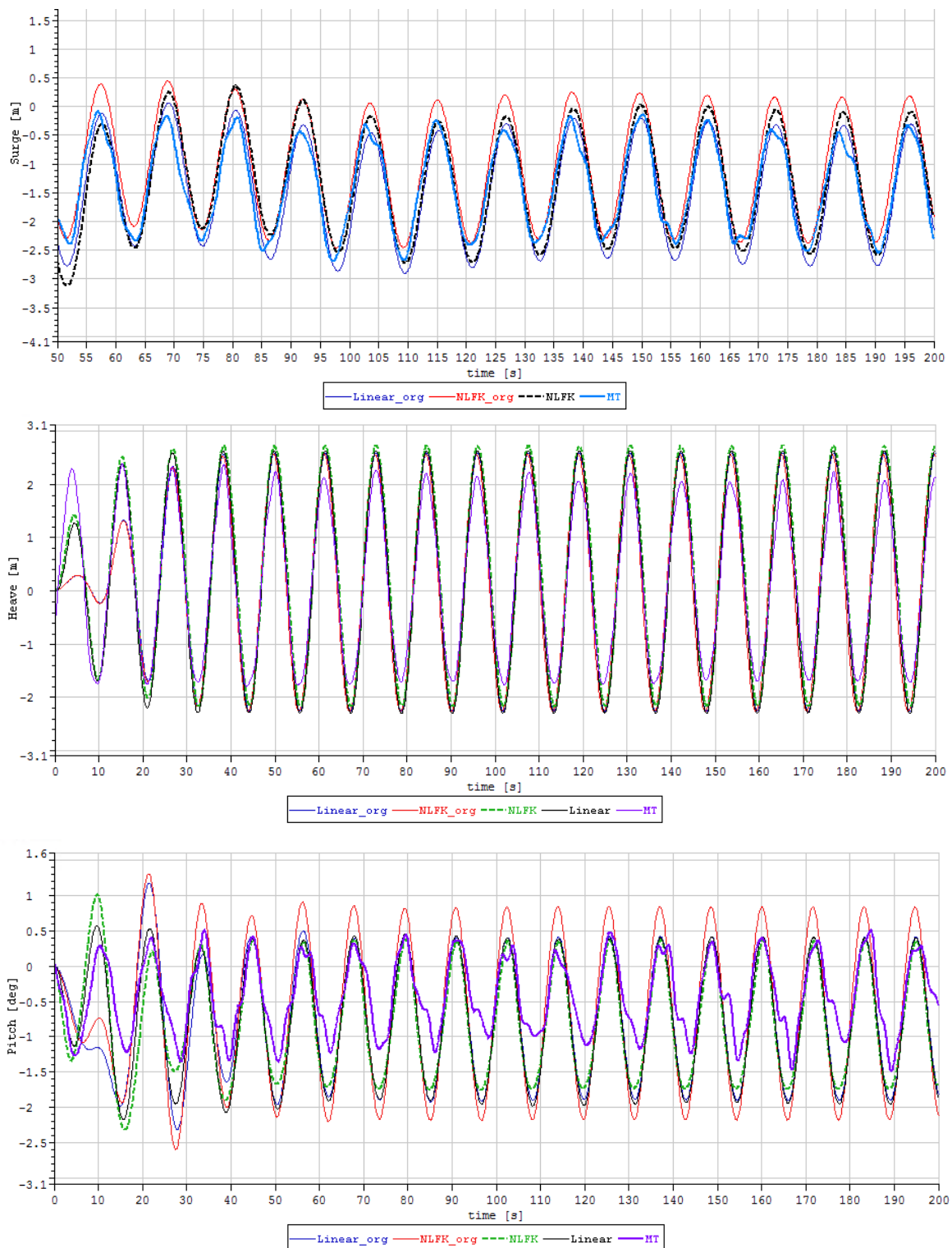


Figure 21: Responses on a model with nonlinear geometry at water-line calculated from different methods. Linear: linear model, NLFK: nonlinear Froude-Krylov model, MT: model test, _org: original calculations using a different implantation and formulation of nonlinear Froude-Krylov forces. Wave condition: regular, $H=5[m]$, $T=11.55[s]$.

Figure 21 shows a comparison between the motions for a regular wave. The present and previous linear calculations, denoted by "_org" in the figure, are exact match as expected. Over all the newly developed

nonlinear Froude-Krylov model behaves consistently and improves the response predictions in occasions. It is important to note that this object will never become submerged. Therefore, the NLFK is expected to be less important in this situation in comparison to calculating ice motions. The model test includes nonlinear and higher order effects which cannot be represented only by NLFK. The comparison, however, shows general validity of the adopted model.

7 Simulations

The described models of the ice and platform are simulated in irregular waves to investigate possible impact scenarios. Several initial locations for the ice and environmental condition are considered. The simulation loop has been constructed to accommodate sensitivity studies by varying ice initial location, environment and random seeds. The simulations methodology, description of selected cases, and results are presented in this chapter.

7.1 Methodology

The development of the models is carried on using an iterative approach to increase the complexity and completeness of each component step by step. These components include, the dynamic model of the drilling rig, hydrodynamic of ice, modelling of contact, coupled dynamics of ice and platform, and simulation procedures. Figure 22 presents a graphical view of these components. Here the focus will be on contact, doubled dynamic and simulation procedures.

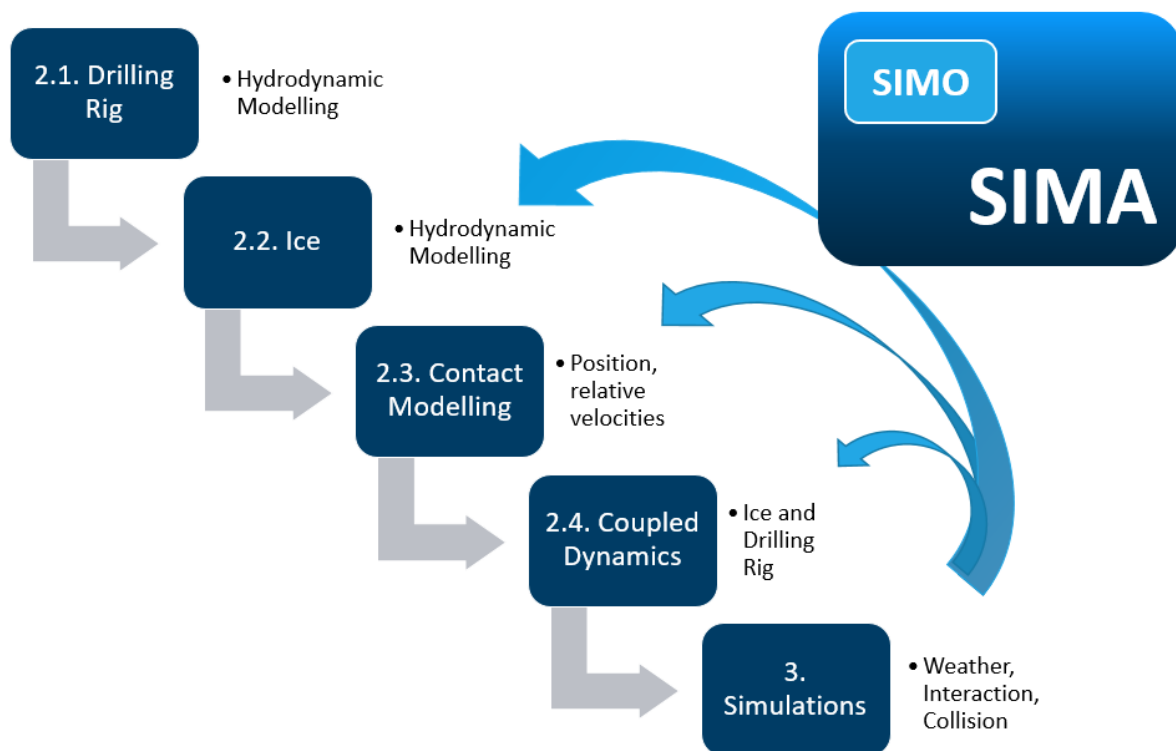


Figure 22: Schematic view of different components in the development chain the studies problem.

The hydrodynamic modelling of platform and ice are presented in previous sections. The dynamic model of the platform and ice are included in SINTEF Ocean's time domain simulator, SIMO, using the simulation platform SIMA. Irregular wave conditions are selected to be the focus of the present study. Therefore, the simulation loop has been constructed to accommodate several irregular wave conditions and random seed variation. Simulation platform SIMA is used to establish the simulation loops and post-processing procedures.

The ice's initial location and orientation are included in the simulations for sensitivity study, as well as simulation length. Simulations are run for a fixed amount of time regardless of occurrence of impact,

with the time step of 0.1[s]. The time step is selected based on experience with previous simulations and seems to be sufficiently small up to the point of impact.

7.1.1 Impact

The dynamics of collision, e.g. crushing of ice during impact, are considered out of scope of the present study and not modelled. Therefore, the responses only up to the time of impact are considered and the rest neglected. The occurrence of impact between ice and platform is detected using bumper models in SIMO. The platform and ice are covered with cylindrical bumpers with spherical ends as shown in Figure 23. This will give the approximate boundaries of the selected platform and ice. Looking at the recorded bumper forces, the collision time is assumed to be the instance the bumper force becomes non-zero.

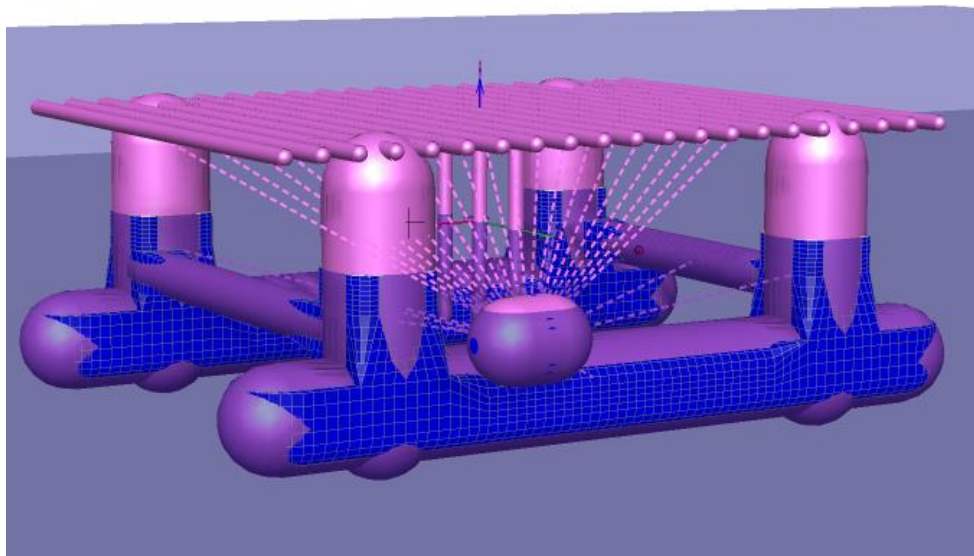


Figure 23: Schematic view of the bumper arrangement on the platform and ice. The dashed line connect the centre point of all interacting bumpers.

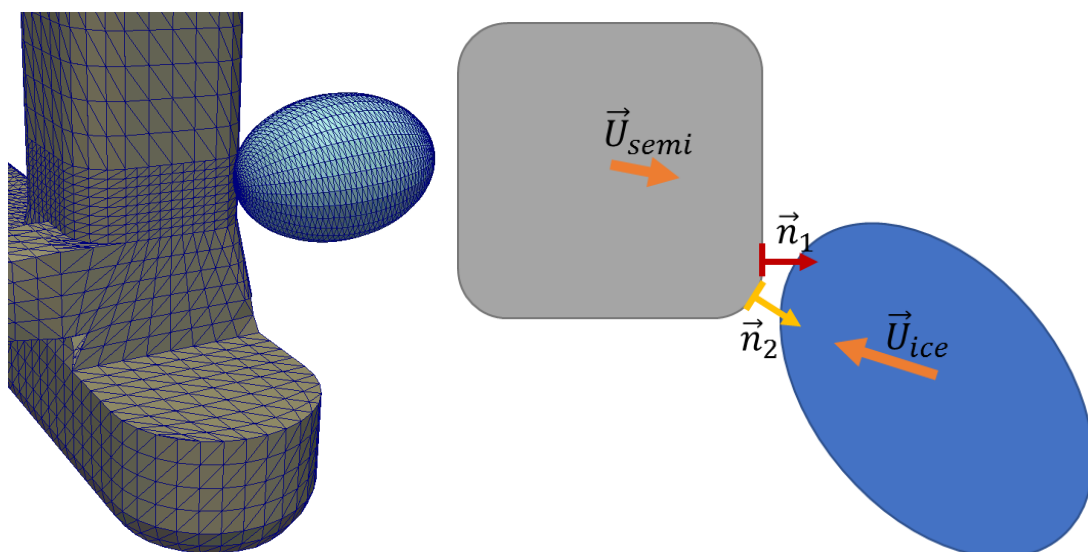


Figure 24: Detection of point of contact using STL geometries of platform and ice.

After determining the time of collision, the location and orientation of platform and ice are analysed to determine the point of contact, and normal to the plane of contact. The ice and platform's STL geometries as well as the recorded response time series are used in the calculations (Figure 24). These calculations are done as a post-processing on the results after simulation.

Determining the normal of the contact plain, here referred to as *collision vector*, is particularly important for estimating the available kinetic energy during impact. The contact plain is defined as the plane in which the two bodies meet and transfer energy. Here it is assumed that this plain, and the collision vector, are constant during the impact. Moreover, the normal to the semi surface at the point of contact is assumed to be the collision vector (\vec{n}_1 in Figure 24). In addition, it is assumed that the available kinetic energy during impact can be calculated using the magnitude of relative velocity of semi and ice in the direction of the collision vector (u_{col}^2) as:

$$E = \frac{1}{2}(m_{ice} + A_{ice})u_{col}^2$$

where m_{ice} and A_{ice} are the ice mass and added mass in the direction of collision vector respectively. This implies that both ice and semi stay intact during collision, and the ice velocity in the direction of collision vector will be equal to semi velocity in the same direction after the impact, which means that the ice will stick to platform after impact, and any changes in the platform velocity due to ice impact is neglected. The model also disregards the energy dissipation due to crushing of ice.

A conservative estimation of impact energy is expected to be obtained using this method. However, considering the crushing of ice can cause this estimation to be non-conservative due to change in the contact point and collision vector. This is particularly important when the impact happens around the corners, where the normal to semi surface is varying with location. Figure 24 shows a scenario where the contact point and collision vector can be changed from \vec{n}_1 to \vec{n}_2 when ice crushes. In this scenario, the magnitude of the relative collision velocity is larger in \vec{n}_2 direction, and hence a larger portion of the total kinetic energy of ice will be transferred to semi during impact. A model for crushing of ice is needed to assess the relative importance of above-mentioned increase in the impact energy and the energy loss due to crushing of ice.

Both zero, or infinite frequency added mass at the time of impact could be used to calculate impact energy depending on the impact process. If upon impact ice comes to abrupt stop then the infinite frequency added mass is an appropriate value. The infinite frequency implies that the water on free-surface can move upward, but has no time to propagate in form of waves. This condition is mainly used in slamming models when the acceleration due to impact is dominant over the gravitation. On the other hand, if ice quickly crushes during impact, and slowly stops after the impact, the zero-frequency condition, i.e. rigid free-surface, could be valid. Then the zero-frequency added mass is considered to give a better estimation of the kinetic energy at the time of impact.

7.1.2 Hydrodynamic interactions

As described in previous chapters, hydrodynamic interactions between ice and platform can change the response of the ice. These interactions are extensively studied in frequency domain in Section 5.1. Although the methodology developed here is designed to include these interactions, due to lack of time, detailed investigations of these effects are left for future studies.

Besides the motion of the ice, the interaction can change the ice added mass at the time of impact. This will influence the kinetic energy of the ice. The variation of a selection of zero and infinite frequency added mass values for the spheroid ice as it gets closer to the platform is presented in Section 5.1. Figure 25 and Figure 26 present the same values for the ice cube in more detail.

The centre of the ice cube, aligned with x-axis, is positioned at different locations around the platform and the zero and infinite frequency added masses are calculated. Assuming rigid free-surface condition, i.e. slow motions of ice, the zero-frequency added mass is a representation of the ice added mass as it moves towards the platform. Let us assume the cube is simply drifting in x-axis towards the platform without any restoring. Then the motion can be formulated as,

$$(m + A_0)\ddot{\eta} + \dot{A}_0\dot{\eta} + B\dot{\eta} = F$$

Where, η is the ice's surge motion, m is the cube mass, A_0 is the zero-frequency added mass in surge, B is the damping coefficient in surge, F is the excitation force in surge, and upper dot represents time derivative. The term, $\dot{A}_0\dot{\eta}$, is introduced due to variation of added mass with time as ice approaches the platform. If \dot{A}_0 is positive, meaning the added mass is increasing, this would create a repellent force. Similarly, an attraction force can be expected when the ice moving away from the platform. The issue described here is studied extensively in the scope of manoeuvring of two interacting ships in [30]. To what extent this effect influence the motions of the ice, and how to include it for an object which oscillates in waves, needs further investigations. Here we make a brief attempt to partly include this effect in the present calculations.

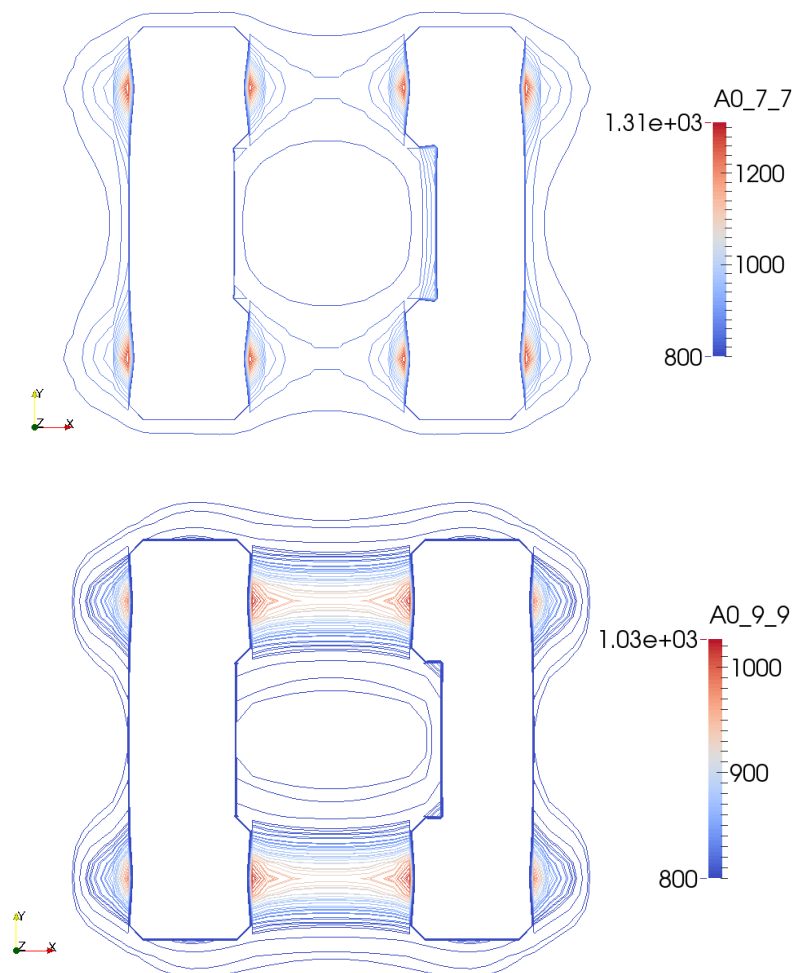


Figure 25: Zero frequency added mass [tons] of ice cube at different location around the platform. A0_7_7: ice added mass in surge, A0_9_9: ice added mass in heave. Platform pontoons are along x-axis. Ice cube length is along x-axis.

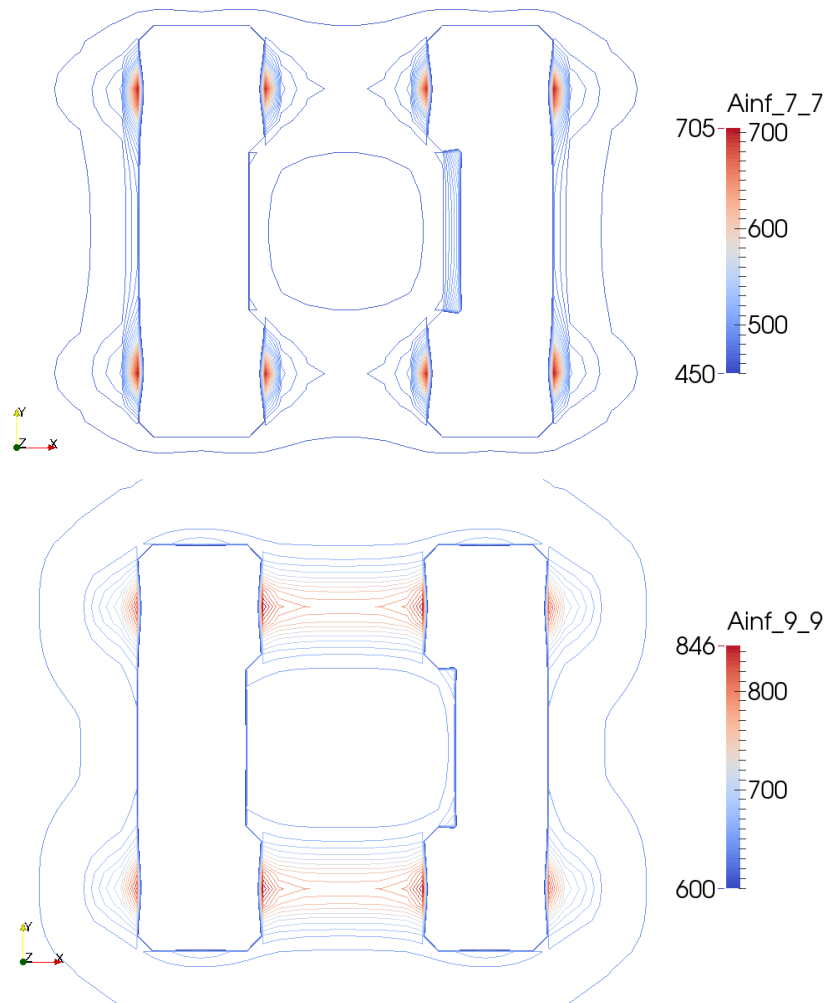


Figure 26: Infinite frequency added mass [tons] of ice cube at different location around the platform. $A_{inf_7_7}$: ice added mass in surge, $A_{inf_9_9}$: ice added mass in heave. Platform pontoons are along x-axis. Ice cube length is along x-axis

The variation of added mass as the ice gets closer to the platform is considered for translational modes of ice, i.e. surge, sway and heave. The ice model presented in Section 6.1 is modified by removing the convolution integrals in surge, sway and heave, and replacing it with the zero-frequency added mass in respective modes, hence neglecting the memory effects in these modes of motions. During the time domain simulations, the zero-frequency added mass values of ice in surge, sway and heave, are extracted from the pre-calculated values shown in Figure 25, considering ice and semi locations, as well as ice orientation. Figure 27 shows how the surge and heave added mass of ice is changing in time for a scenario where the ice is drifting in the negative x-axis towards the column of the semi. In addition to changing the added mass value of ice, the forces due to variation of added mass in time, i.e. $-\dot{A}\dot{\eta}$, is calculated and included as excitation force in the dynamic equation of ice.

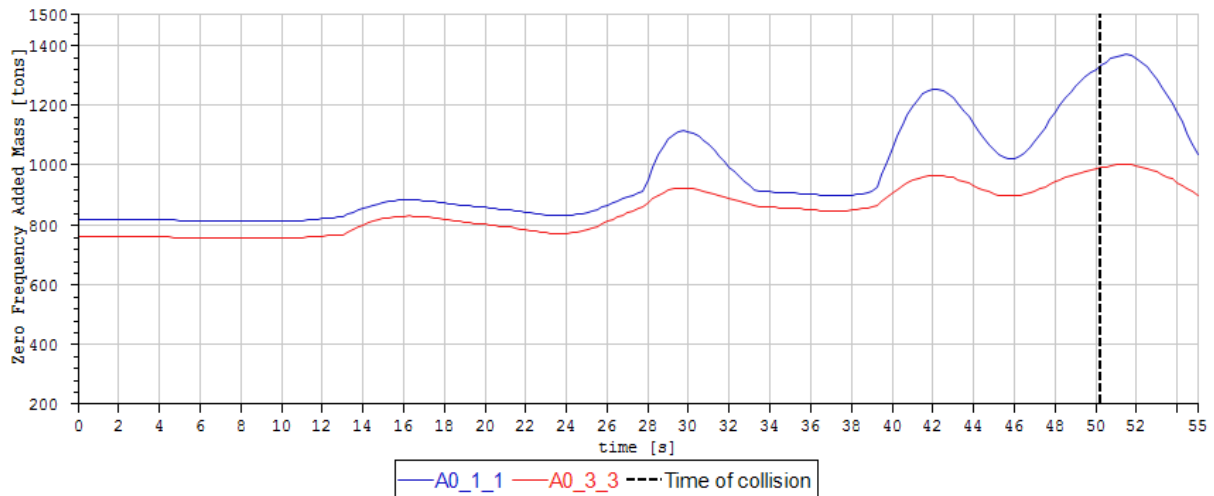


Figure 27: Variation of ice added mass with time, A0_1_1: zero frequency ice added mass in surge, A0_3_3: zero frequency ice added mass in heave. The time of collision is shown with dashed line. Wave condition: $H_s=9.8$ [m], $T_p=14.8$ [s], wave direction = 180 [deg]. Initial location of ice, $X=70$ [m], $Y=34$ [m]. Location of impact is column.

Figure 28 shows a comparison between the obtained motions of ice in surge and heave, when the ice starts 30 meters away from the platform column in X direction, and travel towards negative X-axis until collision. The wave's significant height, peak period, and direction are 9.8 [m], 14.8 [s], and 180 [deg], respectively. The results from the original linear model, with convolution integrals, i.e. memory effects, a liner model with a fixed zero frequency added mass, i.e. no memory effects, and the model where added mass is changing based on ice location are included. Comparing the responses for the models with and without convolution integrals, i.e. *Convolution* and *A0(constant)* in the figure, shows that the memory effects are almost negligible for the studied wave condition. This is expected, since the selected peak period corresponds to a linear wave length much longer than ice dimensions. Including the variation of added mass in time, slightly changes the responses in this case.

Figure 29 shows the obtained additional force due to variation of added mass in time until collision, and the comparison with the total excitation force in surge. It is clear that, in this case, the obtained repellent force at the time of impact is small comparing to the total excitation force on the ice, mainly due to small surge velocity. However, as will be discussed further in the following sections, the ice velocity at the time of impact is very sensitive to the initial conditions and selected seed for realizing irregular waves. Figure 30 shows the variation of added mass with time, and the comparison of obtained forces for the same case, but a different seed number. Here the repellent force at the time of impact is approximately one third of the total of the other excitation forces, which is considerably larger. A selection of cases is studied including this effect and presented in the following chapters.

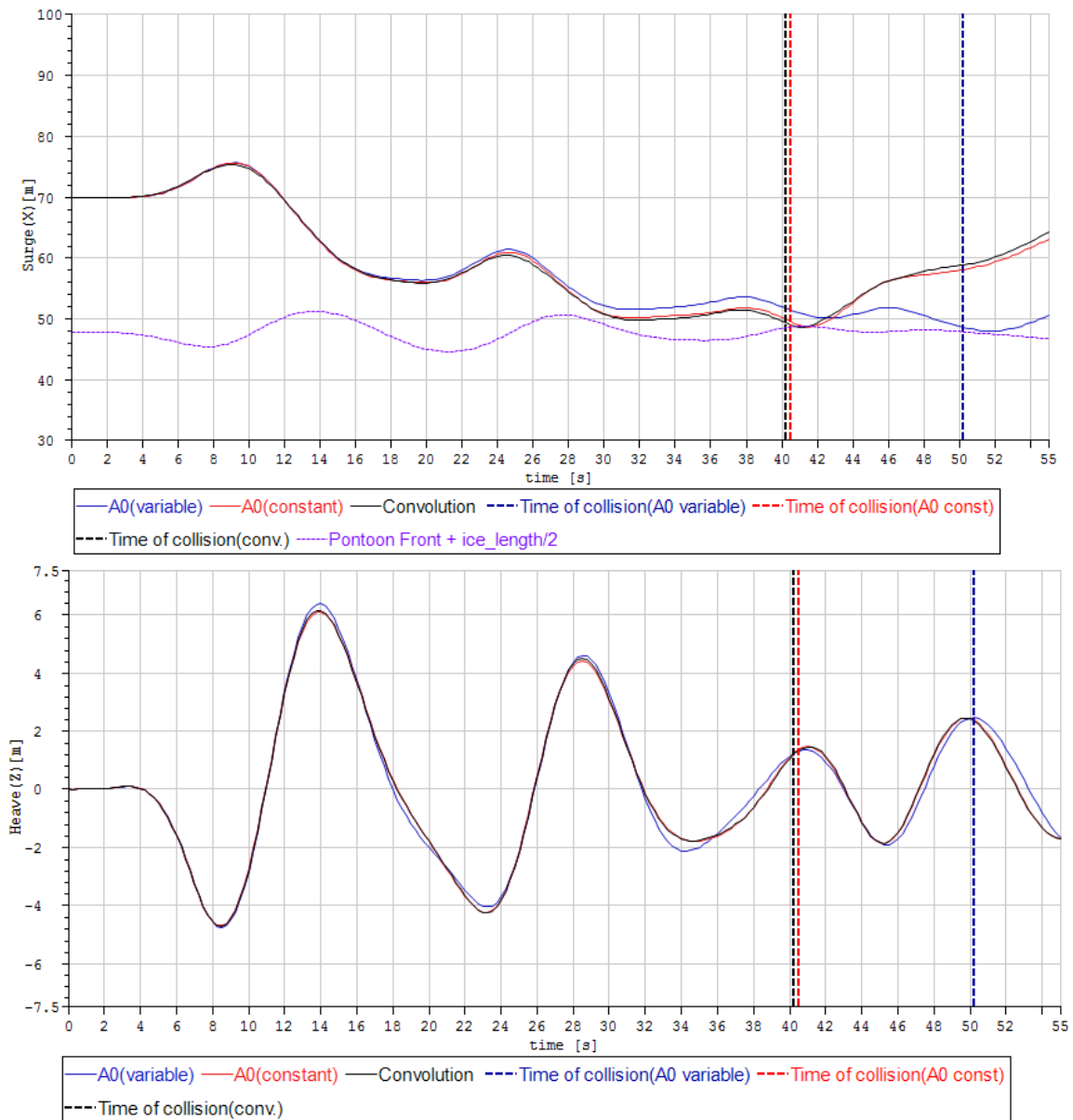


Figure 28: Comparison between ice surge and heave motion from linear models, A0(variable): consider variation of added mass as the ice gets closer to platform without memory effects, A0(constant): fixed value of zero frequency added mass, Convolution: memory effects by convolution integrals and fixed infinite frequency added mass. The time of collision in each case is shown with dashed line. Wave condition: $H_s=9.8$ [m], $T_p=14.8$ [s], wave direction = 180[deg]. Initial location of ice, $X=70$ [m], $Y=34$ [m]. Location of impact is column.

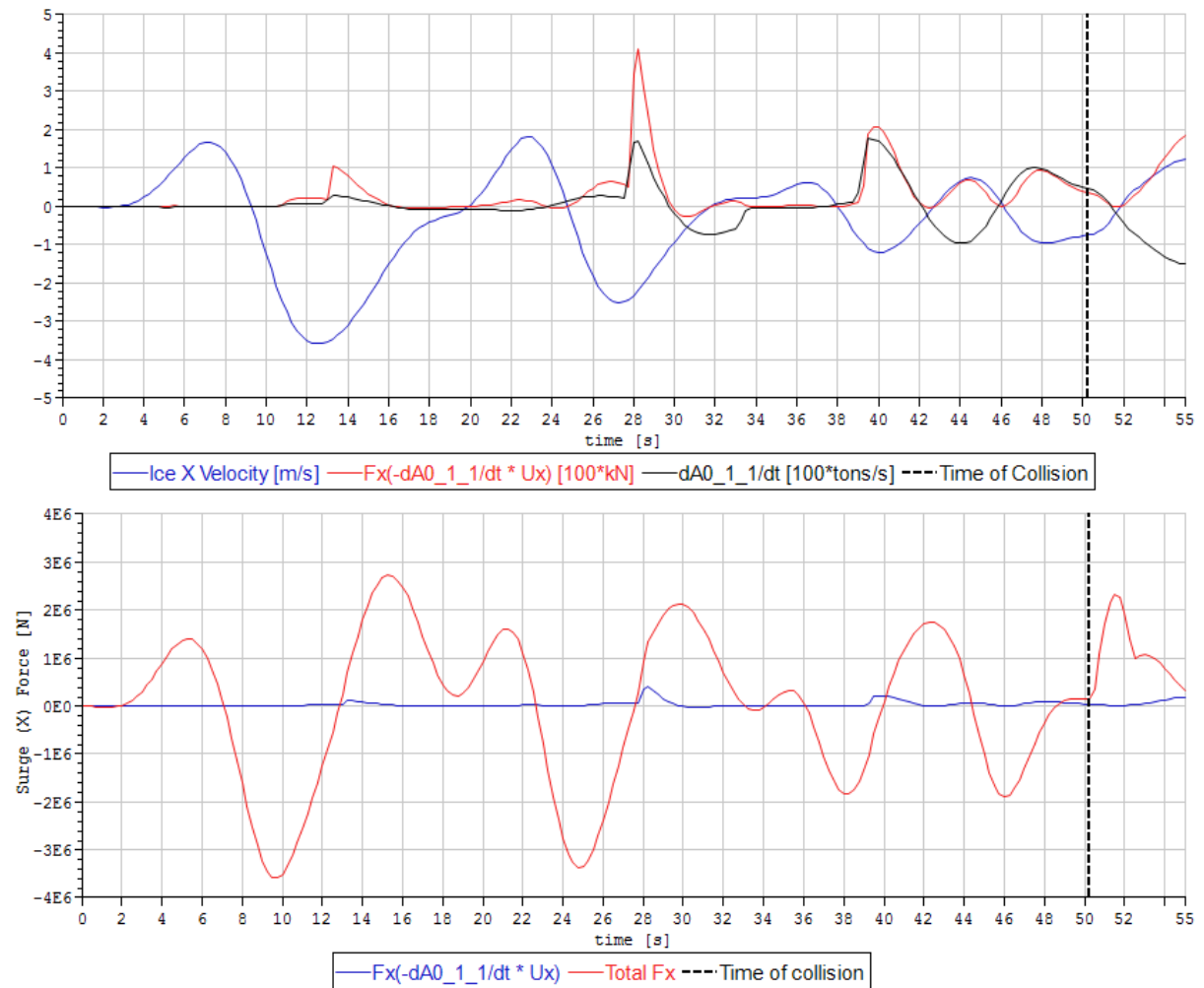


Figure 29: Comparison between forces on ice due to added mass variation and the total excitation force. The time of collision is shown with dashed line. Wave condition: $H_s=9.8$ [m], $T_p=14.8$ [s], wave direction = 180[deg]. Initial location of ice, $X=70$ [m], $Y=34$ [m], wave seed = 1. Location of impact is column.

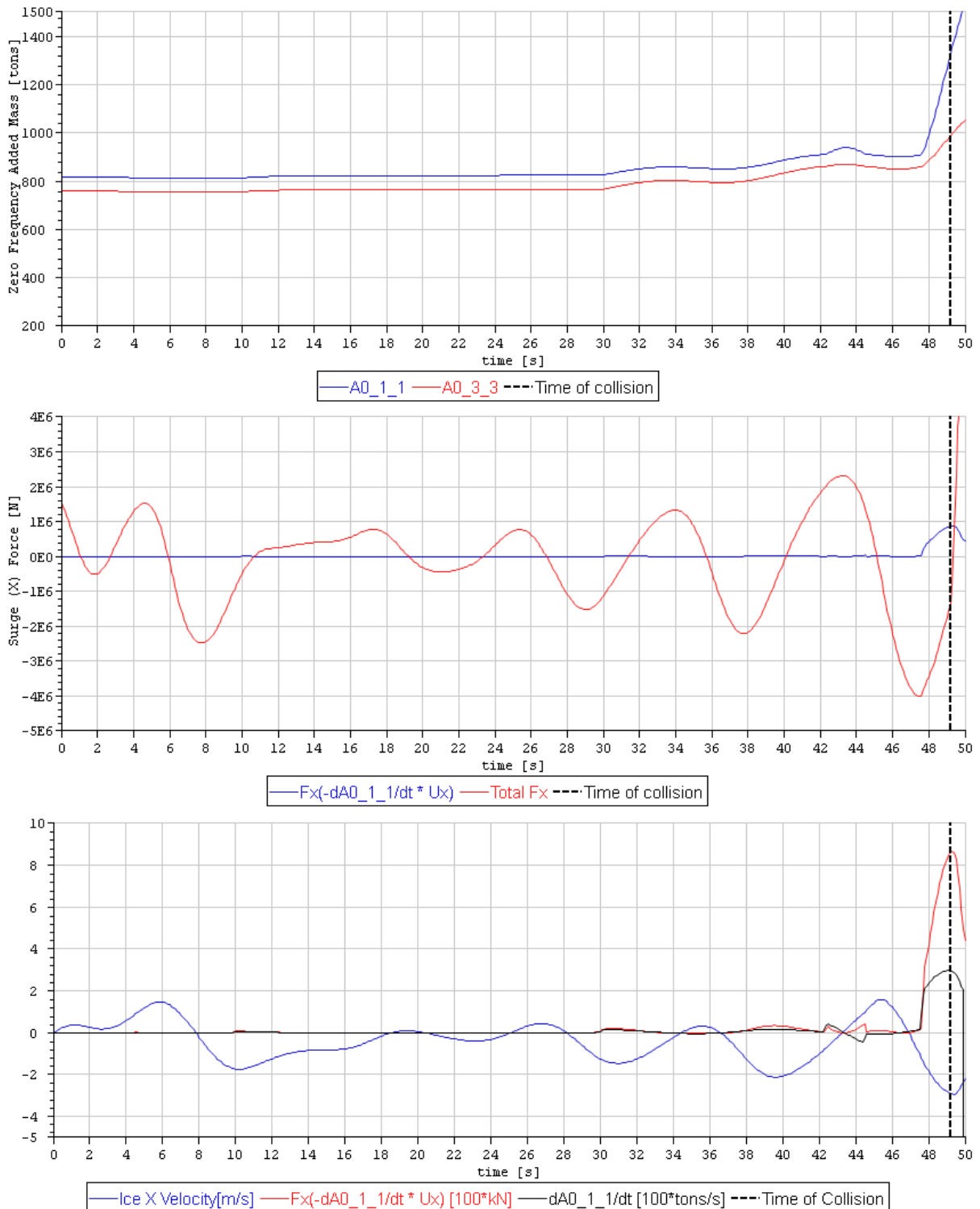


Figure 30: Variation of added mass in time (top), plus comparison between forces on ice due to added mass variation and the total excitation force. The time of collision is shown with dashed line. Wave condition: $H_s=9.8[m]$, $T_p=14.8[s]$, wave direction = $180[deg]$. Initial location of ice, $X=70[m]$, $Y=34[m]$, wave seed = 5. Location of impact is column.

The importance of including off-diagonal hydrodynamic coupling terms, which represent the interaction between the radiated wave from the platform and ice, must be investigated. These effects are not included in the present study. However, neglecting the effect of the ice on the platform, the nonlinear Froude-Krylov model described here could be generalized to use the total pressure field introduced by the platform to calculate forces, instead of the incident waves. In this way, the large part of the hydrodynamic interactions will be included consistently.

7.2 Improvements comparing to previous study

The present study is setup to provide a step further to better understand the complicated problem of ice, platform, dynamics and impact. In this regard following improvements have been done to the original study presented in [1].

The simulations are done in time domain. The impact scenario is highly dependent on the relative phase and location of ice and platform, which strongly varies with the selected wave realization. Adopting time domain simulations provide the possibility to study these dependencies directly. A probabilistic view of ice impact conditions could be established for each case using this simulation approach.

Selecting time-domain simulation gives way to introduce nonlinear effects into the simulation directly. In the present study, nonlinear viscous forces are introduced using Morison-type elements. Moreover, nonlinear Froude-Krylov forces are modelled in order to address the nonlinearities in buoyancy and wave excitation forces due to large variation in the ice's waterplane area as it moves vertically, and the fact that it can get completely submerged as it moves in waves. As shown in Sections 6.1.16.2.2.2 linear treatment of these nonlinearities can cause large over estimation of buoyancy and wave excitation forces, which intern reduces the accuracy of simulated ice motions.

A model for considering the variation of ice added mass, as it gets closer to platform, and the resulted repellent/attraction force is adopted here, while its importance is investigated for a selection of cases.

As it will be discussed, besides the ice shape, the initial location of the ice plays an important role in defining the impact location and velocities. This is investigated to large extend in the present study by considering different initial locations and collision paths.

7.3 Selected Cases

The selected environmental conditions for the present study are listed in Table 3, which consist of irregular waves only, i.e. current and wind are neglected. The stochastic waves are modelled using 3-parameter Jonswap spectrum. The wave realization is obtained through Fourier analysis by selecting a seed number to present a random selection of phases for wave components, similar to studies of ice in absence of platform presented in 6. Only the one-year return period waves are selected from [1] and included in the present study.

Table 3: Selected wave conditions.

Enviroment ID (EID)	Tp [s]	Hs[m]	Gamma
1	14.8	9.8	1.4
2	12	8.6	2.9
3	6.5	4.9	5

The two ice geometries presented in Section 4.2 are studied here, although the main focus is on the ice cube, where the geometry has been the centre of validation and CFD studies. Figure 31 shows a schematic view of the initial locations and orientations of ice relative to platform, and the selected wave

propagation directions. For the ice initial location to the right of the platform, positive x-axis, only the wave propagation along the x-axis is considered. The other wave propagation direction along y-axis is used with the initial location above platform, i.e. positive y-axis. The coordinates of the initial locations are listed in Table 4, while the platform's centre is placed at the origin.

Each combination of location and environment is simulated for 20 different seeds. The number of seeds is increased to 40 in a three cases and to 120 in a single case. Table 5 shows the specification of the selected cases studied.

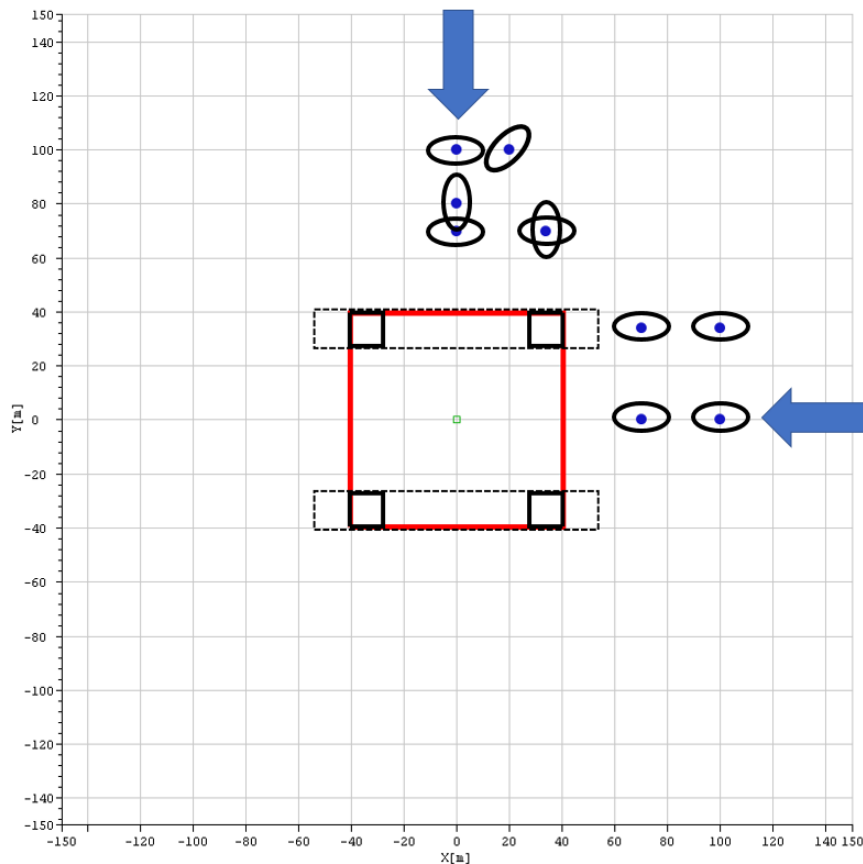


Figure 31: Schematic view of the platform and selected initial locations/orientations of ice. Blue dots show the centre of ice, while the ellipse demonstrates the orientation. Blue arrows show the selected propagation directions for waves.

Table 4: Initial location and orientations of ice used in the present study

Location ID (LID)	X[m]	Y[m]	Rz[deg]
1	70	0	0
2	100	0	0
3	70	34	0
4	100	34	0
5	0	70	0
6	0	100	0
7	34	70	0
8	0	80	90
9	34	70	90
10	20	100	45

Table 5: List of studies cases. Env. ID: Environmental condition ID, see Error! Reference source not found. for details. Loc. ID : ice initial location ID, see Table 4 and Figure 31 for details. Linear: linear model, NLFK: nonlinear Froude-Krylov model, NLFK_A0: nonlinear Froude-Krylov model plus the variation of zero-frequency added mass in time.

Case ID	Env. ID	Loc. ID	X [m]	Y [m]	Rz [deg]	Wave Direction [deg]	Num. Seeds	Geometry	Method	Collision Location
1	1	7	34	70	0	270	20	Spheroid	NLFK	Column
2	2	7	34	70	0	270	20	Spheroid	NLFK	Column
3	1	3	70	34	0	180	20	Cube	NLFK	Column
4	2	3	70	34	0	180	20	Cube	NLFK	Column
5	3	3	70	34	0	180	20	Cube	NLFK	Column
6	1	7	34	70	0	270	20	Cube	NLFK	Column
7	2	7	34	70	0	270	20	Cube	NLFK	Column
8	3	7	34	70	0	270	20	Cube	NLFK	Column
9	1	9	34	70	90	270	20	Cube	NLFK	Column
10	2	9	34	70	90	270	20	Cube	NLFK	Column
11	3	9	34	70	90	270	20	Cube	NLFK	Column
12	1	1	70	0	0	180	20	Cube	NLFK	Brace
13	1	2	100	0	0	180	20	Cube	NLFK	Brace
14	1	4	100	34	0	180	20	Cube	NLFK	Column
15	1	5	0	70	0	270	20	Cube	NLFK	Pontoon, Riser
16	1	8	0	80	90	270	40	Cube	NLFK	Pontoon, Riser
17	1	10	20	100	45	270	20	Cube	NLFK	Pontoon, Riser
18	1	7	34	70	0	270	40	Cube	Linear	Column
19	2	7	34	70	0	270	20	Cube	Linear	Column
20	3	7	34	70	0	270	20	Cube	Linear	Column
21	1	3	70	34	0	180	20	Cube	NLFK_A0	Column
22	1	8	0	80	90	270	120	Cube	NLFK_A0	Pontoon, Riser
23	1	8	0	80	90	270	40	Cube	NLFK_A0	Pontoon, Riser

7.4 Results and conclusions

The simulation results are presented here in terms of location and height of impact on the platform, and the magnitude of relative collision velocity. The estimated impact energy of ice is also calculated and presented.

7.4.1 Height and location of impact

The results for impact location from the cases presented in Table 5 which are calculated with NLFK method are superimposed and presented in Figure 32. The main focus of impact points is on the column, mainly because in most of the simulations the ice is positioned on the path of collision to column (location 3,4,7, and 9). When the ice is positioned on the centre line to the right of the platform, i.e. locations 1 and 2, it mainly hits the horizontal brace under the water which prevents it from coming in between the columns. When the ice is positioned above the platform on the centre line, i.e. locations 5,6, and 8, the ice either hits the top surface of the pontoon or find its way in between the columns and hit the inner cylinders which represent the risers here.

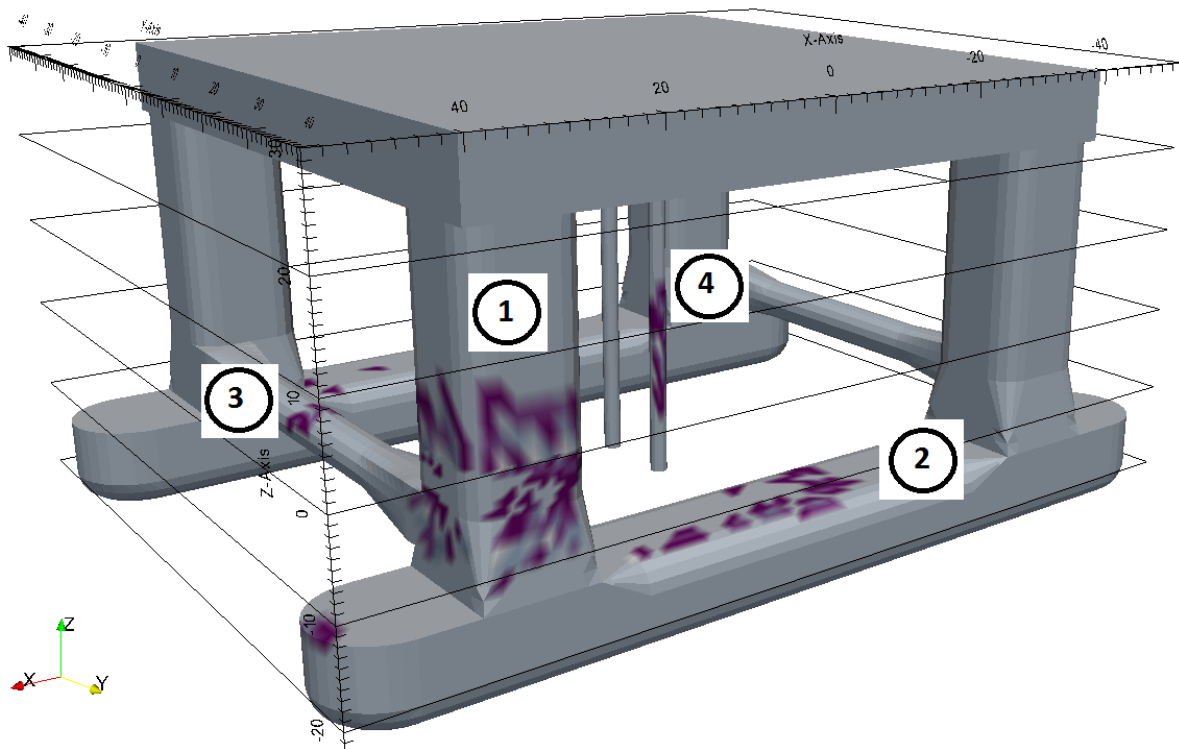


Figure 32: Super imposition of all collision points from the NLFK cases presented in Table 5. The dark areas show the approximate collision location. The four collision locations selected for processing are marked with numbers, 1: Column, 2:Pontoon, 3:Brace, 4:Riser.

The statistics for vertical location of impact on column and riser are presented all the relevant cases in Table 6 and Table 8, respectively. The values are for all the considered wave realizations seeds in each case. The vertical location of impact on pontoon and brace have much smaller variation and therefore not presented here. More details for these cases are included in Appendix A. Table 7 and Table 9 show the results of a Gumbel fit to the obtained values from different cases. However, based on the distribution of impact height presented in Figure 33, it is clear that the application of the Gumbel distribution is questionable at best, and the model, even at 56 seeds, is not fully converged. Distributions for the other studied scenarios are included in appendix A. Due to the complexity of the problem and dependency of

the results to the details of the ice and semi motion, it is not possible to identify any clear trend in dependency of the height of impact to the studied wave conditions, or methods.

Table 6: Statistical values for vertical location of collision [m] at column for different scenarios (Table 5). The location is measured from the mean water level, i.e. $Z=0$.

Case ID	Hs[m], Tp[s], WD[deg]	Max	Min	Mean	St. Dev.
1	9.8, 14.8, 270	3.67	-5.47	-1.5	2.31
2	8.6, 12.0, 270	0.73	-4.58	-2.03	1.44
3	9.8, 14.8, 180	1.47	-10.19	-3.61	4.58
4	8.6, 12.0, 180	2.93	-9.72	-1.85	4.44
5	4.9, 6.5, 180	1.47	-8.31	-2.92	3.89
6	9.8, 14.8, 270	5.13	-8.78	-1.22	4.06
7	8.6, 12.0, 270	5.13	-5.94	0.89	2.12
8	4.9, 6.5, 270	0.73	-8.78	-2.03	2.42
9	9.8, 14.8, 270	2.93	-8.78	-2.72	4.4
10	8.6, 12.0, 270	2.93	-9.72	-2.59	4.55
11	4.9, 6.5, 270	1.47	-8.78	-4.03	4.51
14	9.8, 14.8, 180	5.13	-10.19	-2.59	4.82
18	9.8, 14.8, 270	3.67	-8.31	-1.02	4.36
19	8.6, 12.0, 270	3.67	-8.31	0.72	2.93
20	4.9, 6.5, 270	1.47	-8.78	-0.83	3.27
21	9.8, 14.8, 180	3.67	-10.19	-5.4	3.82

Table 7: Statistical values based on Gumbel fit for the vertical location of collision [m] on column for different scenarios (Table 5). The location is measured from the mean water level, i.e. $Z=0$. MP: Most probable, Exp: expected, P90: 90 percent fractal.

Case ID	Hs[m], Tp[s], WD[deg]	MP	Exp	P90
1	9.8, 14.8, 270	-2.56	-1.89	1.61
2	8.6, 12.0, 270	-2.69	-2.27	-0.09
3	9.8, 14.8, 180	-5.71	-4.39	2.54
4	8.6, 12.0, 180	-3.88	-2.6	4.11
5	4.9, 6.5, 180	-4.7	-3.58	2.29
6	9.8, 14.8, 270	-3.08	-1.9	4.23
7	8.6, 12.0, 270	-0.08	0.53	3.72
8	4.9, 6.5, 270	-3.14	-2.44	1.21
9	9.8, 14.8, 270	-4.73	-3.46	3.16
10	8.6, 12.0, 270	-4.67	-3.36	3.5
11	4.9, 6.5, 270	-6.09	-4.79	2
14	9.8, 14.8, 180	-4.8	-3.4	3.88
18	9.8, 14.8, 270	-2.99	-1.75	4.75
19	8.6, 12.0, 270	-0.6	0.23	4.59
20	4.9, 6.5, 270	-2.3	-1.37	3.49
21	9.8, 14.8, 180	-7.17	-6.05	-0.22

Table 8: Statistical values for vertical location of collision [m] at risers for different scenarios (Table 5). The location is measured from the mean water level, i.e. Z=0.

Case ID	Hs[m], Tp[s], WD[deg]	Max	Min	Mean	St. Dev.
16	9.8, 14.8, 270	3.33	-8.67	-1.79	3.09
22	9.8, 14.8, 270	2.67	-6.67	-1.89	2.47
23	9.8, 14.8, 270	2.67	-5.33	-2.55	1.98

Table 9: Statistical values based on Gumbel fit for the vertical location of collision [m] on riser for different scenarios (Table 5). The location is measured from the mean water level, i.e. Z=0. MP: Most probable, Exp: expected, P90: 90 percent fractal.

Case ID	Hs[m], Tp[s], WD[deg]	MP	Exp	P90
16	9.8, 14.8, 270	-3.19	-2.3	2.32
22	9.8, 14.8, 270	-3.01	-2.3	1.36
23	9.8, 14.8, 270	-3.45	-2.88	0.09

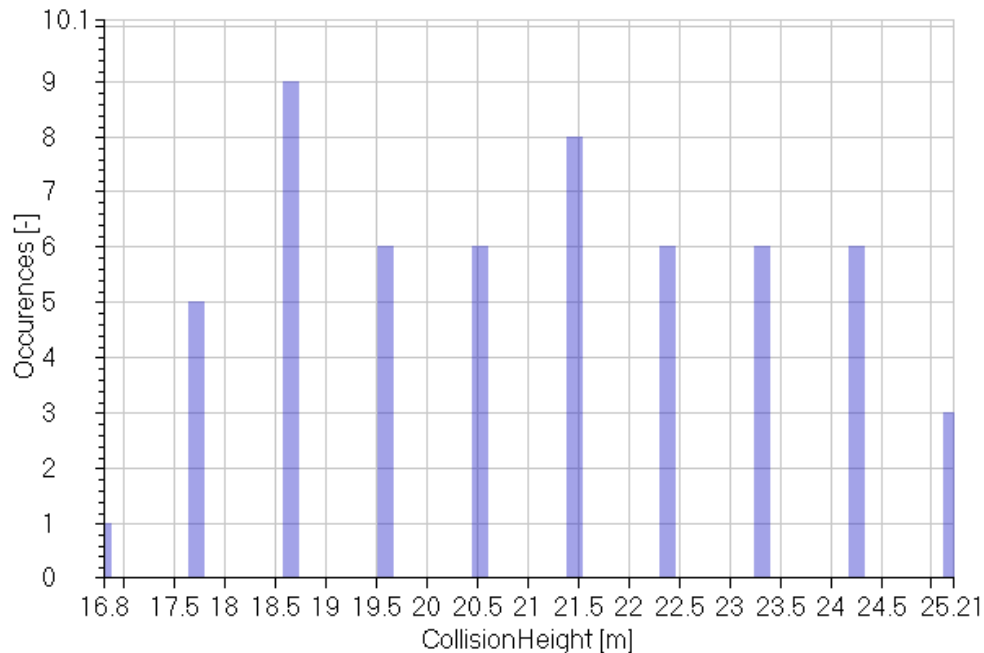


Figure 33: Distribution of collision height on risers for case 22, 56 different seeds. The collision height is measured from the bottom of semi, which is 23[m] below mean water line.

7.4.2 Velocity at the time of impact

Table 10 to Table 13 show the statistical values obtained for the relative collision velocity on the column, pontoon, brace, and riser, for the relevant cases listed in Table 5, respectively. As mentioned in Section 7.1.1, the relative collision velocity is obtained by

- finding the location of the impact point on the ice and platform surface,
- assuming the normal vector to platform's surface at the contact location to be the normal vector of the contact plain, i.e. collision vector.
- calculating the platform and ice velocity in the direction of the obtained collision vector.
- subtracting the obtained projected platform velocity from the projected ice velocity.

This velocity represents the relative velocity felt by the ice or platform at the time of impact. Table 14 to Table 17 present the outcome of fitting a Gumbel distribution to the simulations of each scenario. Figure 34 shows the distribution of the relative collision velocity on the column for case 3 with 20 seeds

(see Table 5 for case details). Similar to the results of impact height, the Gumbel model is not converged here for 20 seeds due to large scattering of the occurrences, and its applicability is questionable. Moreover, it is not possible to identify any clear trend in the magnitude of the velocity at the time of impact. A set of simulations with many more seeds is desirable to address the statistical variability of the problem.

Table 10: Statistical values for relative collision velocity [m/s] on the column for different scenarios (Table 5).

Case ID	Hs[m], Tp[s], WD[deg]	Max	Min	Mean	St. Dev.
1	9.8, 14.8, 270	2.38	0.09	0.78	0.64
2	8.6, 12.0, 270	2.16	0.04	0.66	0.69
3	9.8, 14.8, 180	3.9	0.38	1.66	1.1
4	8.6, 12.0, 180	5.28	0.44	2.25	1.31
5	4.9, 6.5, 180	4.5	0.24	2	1.16
6	9.8, 14.8, 270	3.46	0.15	1.59	1.04
7	8.6, 12.0, 270	4.23	0.24	2.12	1.13
8	4.9, 6.5, 270	2.77	0.42	1.44	0.61
9	9.8, 14.8, 270	3.9	0.27	2.06	1.11
10	8.6, 12.0, 270	5.16	0.67	2.24	1.22
11	4.9, 6.5, 270	4.52	0.37	1.91	1.2
14	9.8, 14.8, 180	4.73	0.47	1.87	1.17
18	9.8, 14.8, 270	2.89	0.03	1.05	0.65
19	8.6, 12.0, 270	3.54	0.31	1.59	0.79
20	4.9, 6.5, 270	3.03	0.03	1.21	0.7
21	9.8, 14.8, 180	2.64	0.14	1.07	0.65

Table 11: Statistical values for relative collision velocity [m/s] on the pontoon for different scenarios (Table 5).

Case ID	Hs[m], Tp[s], WD[deg]	Max	Min	Mean	St. Dev.
15	9.8, 14.8, 270	2.16	0.16	1.19	0.62
16	9.8, 14.8, 270	1.82	0.08	0.92	0.53
17	9.8, 14.8, 270	1.87	0.03	0.9	0.62
22	9.8, 14.8, 270	3.42	0.03	1.01	0.68
23	9.8, 14.8, 270	2.01	0.07	1	0.6

Table 12: Statistical values for relative collision velocity [m/s] on the brace for different scenarios (Table 5).

Case ID	Hs[m], Tp[s], WD[deg]	Max	Min	Mean	St. Dev.
12	9.8, 14.8, 180	2.49	0.18	1.23	0.64
13	9.8, 14.8, 180	3.13	0.18	1.51	0.8

Table 13: Statistical values for relative collision velocity [m/s] on the riser for different scenarios (Table 5).

Case ID	Hs[m], Tp[s], WD[deg]	Max	Min	Mean	St. Dev.
16	9.8, 14.8, 270	2.46	0.21	1.27	0.49
22	9.8, 14.8, 270	3.54	0.24	1.53	0.71
23	9.8, 14.8, 270	2.57	0.4	1.4	0.61

Table 14: Statistical values from a Gumbel fit to the results for relative collision velocity [m/s] on the column for different scenarios (Table 5). MP: Most probable, Exp: expected, P90: 90 percent fractal.

Case ID	Hs[m], Tp[s], WD[deg]	MP	Exp	P90
1	9.8, 14.8, 270	0.49	0.67	1.64
2	8.6, 12.0, 270	0.35	0.55	1.59
3	9.8, 14.8, 180	1.15	1.47	3.13
4	8.6, 12.0, 180	1.65	2.03	4.01
5	4.9, 6.5, 180	1.47	1.8	3.55
6	9.8, 14.8, 270	1.11	1.41	2.98
7	8.6, 12.0, 270	1.61	1.93	3.64
8	4.9, 6.5, 270	1.15	1.33	2.26
9	9.8, 14.8, 270	1.55	1.87	3.55
10	8.6, 12.0, 270	1.69	2.04	3.87
11	4.9, 6.5, 270	1.36	1.7	3.52
14	9.8, 14.8, 180	1.33	1.67	3.44
18	9.8, 14.8, 270	0.76	0.95	1.91
19	8.6, 12.0, 270	1.23	1.45	2.63
20	4.9, 6.5, 270	0.9	1.1	2.14
21	9.8, 14.8, 180	0.77	0.96	1.95

Table 15: Statistical values from a Gumbel fit to the results for relative collision velocity [m/s] on the pontoon for different scenarios (Table 5). MP: Most probable, Exp: expected, P90: 90 percent fractal.

Case ID	Hs[m], Tp[s], WD[deg]	MP	Exp	P90
15	9.8, 14.8, 270	0.9	1.08	2.04
16	9.8, 14.8, 270	0.68	0.83	1.65
17	9.8, 14.8, 270	0.61	0.8	1.76
22	9.8, 14.8, 270	0.7	0.9	1.91
23	9.8, 14.8, 270	0.72	0.89	1.8

Table 16: Statistical values from a Gumbel fit to the results for relative collision velocity [m/s] on the brace for different scenarios (Table 5). MP: Most probable, Exp: expected, P90: 90 percent fractal.

Case ID	Hs[m], Tp[s], WD[deg]	MP	Exp	P90
12	9.8, 14.8, 180	0.94	1.12	2.08
13	9.8, 14.8, 180	1.14	1.38	2.59

Table 17: Statistical values from a Gumbel fit to the results for relative collision velocity [m/s] on the riser for different scenarios (Table 5). MP: Most probable, Exp: expected, P90: 90 percent fractal.

Case ID	Hs[m], Tp[s], WD[deg]	MP	Exp	P90
16	9.8, 14.8, 270	1.04	1.18	1.92
22	9.8, 14.8, 270	1.21	1.41	2.46
23	9.8, 14.8, 270	1.13	1.3	2.21

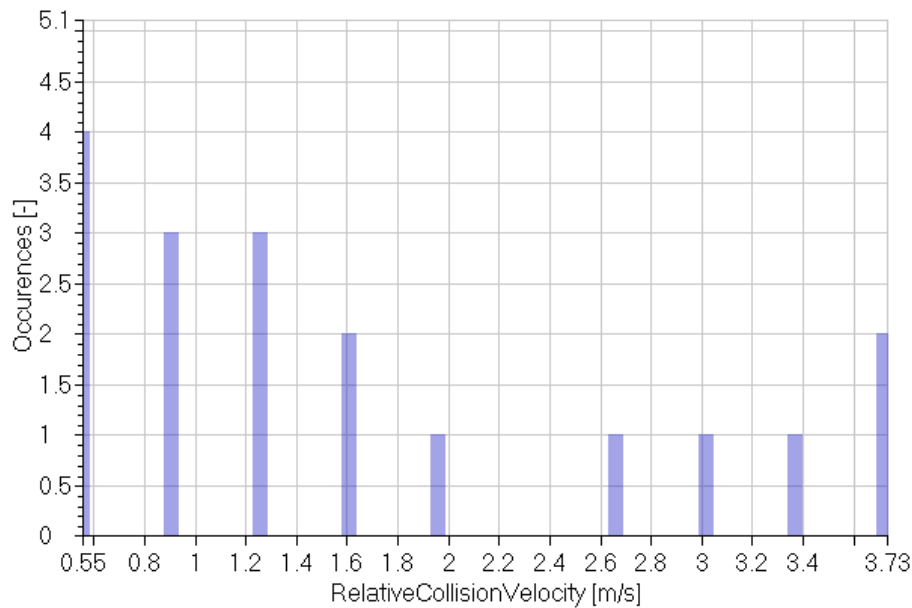


Figure 34: Distribution of relative collision velocity of the column for case 3. Hs=9.8[m], Tp=14.8[s], Wave direction=180[deg]. See Table 5 for more details.

7.4.2.1 The influence of NLFK_A0 model on relative collision velocity on column

The results from the nonlinear Froude-Krylov and nonlinear Froude-Krylov model with variation of added mass for relative collision velocity are compared in Table 18 and Table 19. A direct comparison of the two case suggest that implementation of repellent force due to variation of added mass decreases the expected collision velocity. However, it is important to note the strong variability of the results to the studies samples and the need for studying a larger number of seeds, as will be future shown in the next section.

Table 18: Statistical values for relative collision velocity [m/s] on the column for cases 3 and 21 (Table 5).

Case ID	Hs[m], Tp[s], WD[deg]	Max	Min	Mean	St. Dev.	Seeds	Method
3	9.8, 14.8, 180	3.9	0.38	1.66	1.1	20	NLFK
21	9.8, 14.8, 180	2.64	0.14	1.07	0.65	20	NLFK_A0

Table 19: Statistical values from a Gumbel fit to the results for relative collision velocity [m/s] on the column for cases 3 and 21 (Table 5). MP: Most probable, Exp: expected, P90: 90 percent fractal.

Case ID	Hs[m], Tp[s], WD[deg]	MP	Exp	P90	Seeds	Method
3	9.8, 14.8, 180	1.15	1.47	3.13	20	NLFK
21	9.8, 14.8, 180	0.77	0.96	1.95	20	NLFK_A0

7.4.2.2 Relative collision velocity at the pontoon

A closer look into the results obtained for collision on the pontoon is presented here. Figure 35 shows the obtained velocities at the time of collision for 64 seeds out of 120 from case 22, where ice collides with the pontoon. Figure 36 shows the collision vector components for the same cases. The vertical components of collision vector (Z-component) is almost one in all the cases, suggesting that the ice hits the pontoon from the top in a vertical motion. Therefore, the relative collision velocity in Figure 35 is mainly the relative vertical velocity of the ice and platform. As expected the magnitude of relative collision velocity is smaller than the magnitude of ice total translational velocity, suggesting that a portion of the total ice kinetic energy will contribute in impact. However, in some cases, the two can be quite close.

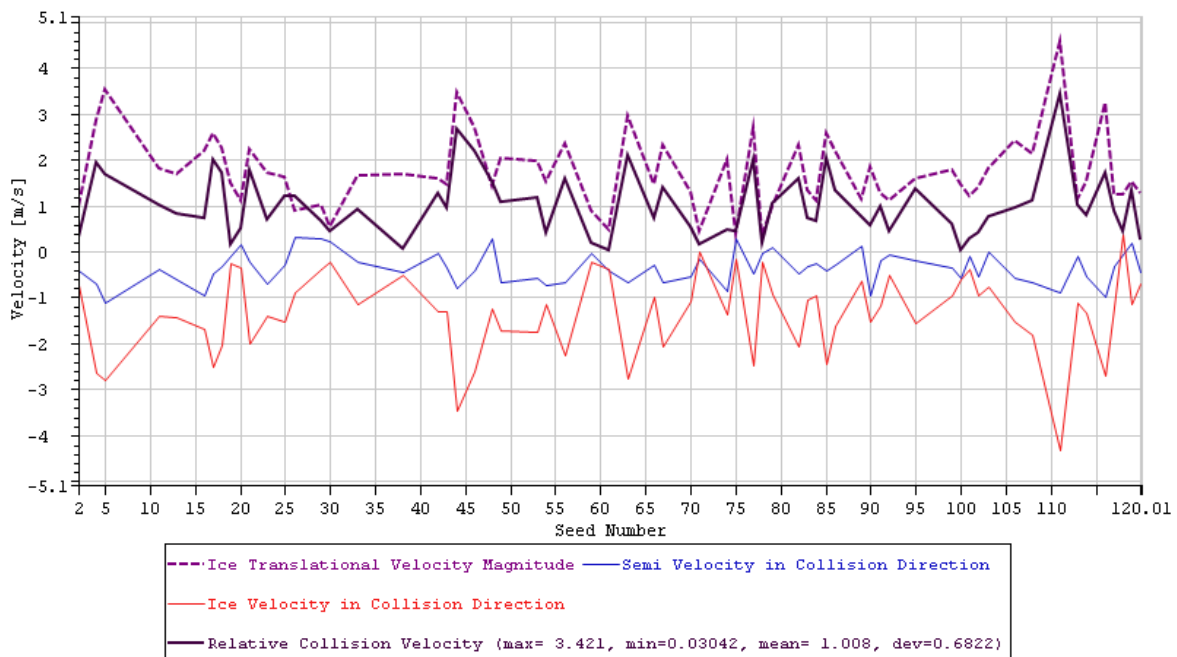


Figure 35: Velocities at the time of collision to the pontoon for different seeds in case 22, i.e. $H_s=9.8$ [m], $T_p=14.8$ [s], wave direction = 270[deg]. Ice initial location, $X=0$ [m], $Y=80$ [m], $R_z=90$ [deg].

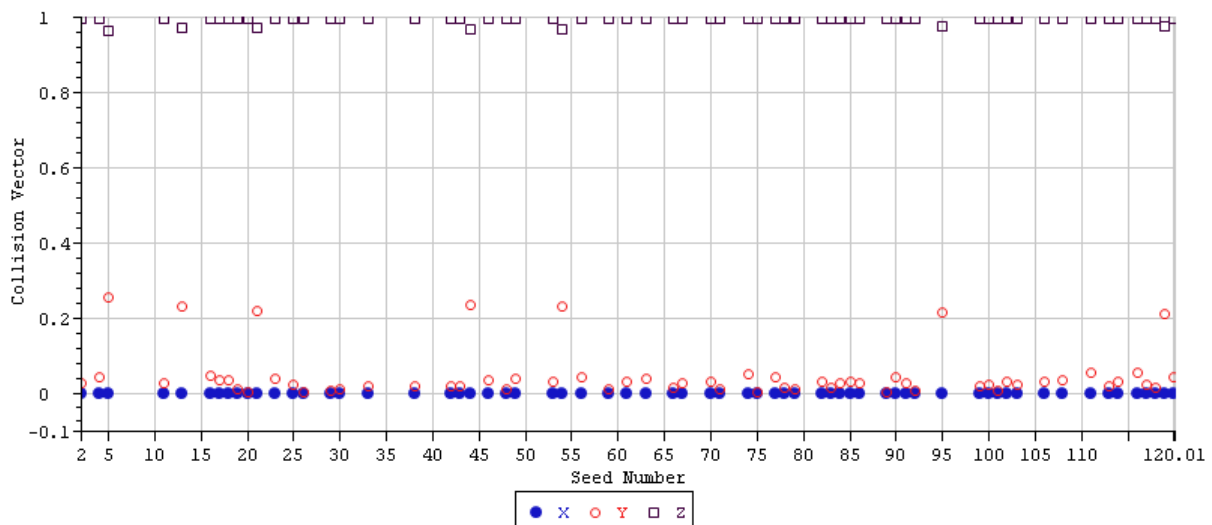


Figure 36: Components of collision vector on the pontoon for different seeds in case 22, i.e. $H_s=9.8$ [m], $T_p=14.8$ [s], wave direction = 270[deg]. Ice initial location, $X=0$ [m], $Y=80$ [m], $R_z=90$ [deg].

Table 20 and Table 21 shows the results for relative collision velocity from three cases with the same environmental condition, but different number of seeds and calculation method. Comparing the results for case 16 and 23, which uses the same setup but different calculation method, suggests consideration of variation of added mass as the ice gets closer to the platform increases the relative collision velocity. This is opposite of what has been observed for collision on the column. However, the collision vector, and hence the ice's mode of motion which contributes to collision, is different in the two cases, i.e. one is surge, the other is heave. The fact that only variation of heave added mass due to horizontal location of ice is included may be a factor as well.

Table 20: Statistical values for relative collision velocity on the pontoon for cases 16, 22 and 23 (Table 5).

Case ID	Hs[m], Tp[s], WD[deg]	Max	Min	Mean	St. Dev.	Seeds	Method
16	9.8, 14.8, 270	1.82	0.08	0.92	0.53	20	NLFK
22	9.8, 14.8, 270	3.42	0.03	1.01	0.68	120	NLFK_A0
23	9.8, 14.8, 270	2.01	0.07	1	0.6	40	NLFK_A0

Table 21: Statistical values from a Gumbel fit to the results for relative collision velocity on the pontoon for cases 16, 22 and 23 (Table 5). MP: Most probable, Exp: expected, P90: 90 percent fractal.

Case ID	Hs[m], Tp[s], WD[deg]	MP	Exp	P90	Seeds	Method
16	9.8, 14.8, 270	0.68	0.83	1.65	20	NLFK
22	9.8, 14.8, 270	0.7	0.9	1.91	120	NLFK_A0
23	9.8, 14.8, 270	0.72	0.89	1.8	40	NLFK_A0

Figure 37 shows a comparison of relative collision velocity distribution for cases 22 and 23. The two cases have the same condition, except for the number of seeds which are, 120 and 40 respectively. In case 23, 64 out of 120 seeds result in pontoon collision and hence reported here. The number for case 22 is 18 out of 40. The comparison of the two distributions clearly show how increasing the number of seeds, considering the same collision scenario, could lead to a better statistical representation of the values.

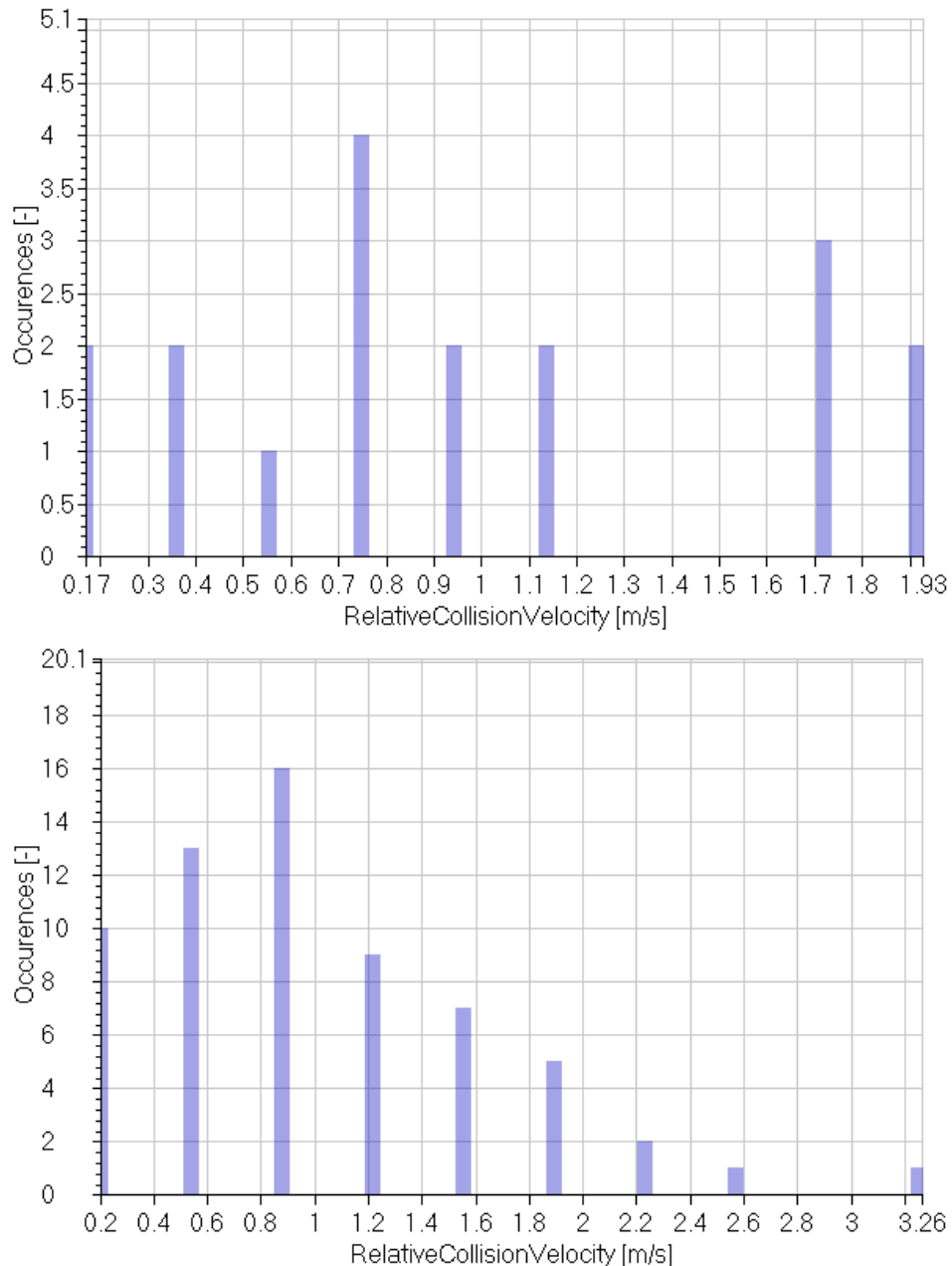


Figure 37: Distribution of relative collision velocity on the pontoon from case 23 with 40 seeds (top), and case 22 with 120 seeds (bottom). $H_s=9.8[m]$, $T_p=14.8[s]$, wave direction = $270[deg]$. Ice initial location, $X=0[m]$, $Y=80[m]$, $R_z=90[deg]$.

7.4.3 Kinetic energy at the time of impact

An estimation of the impact energy of the ice cube, with the mass of 1432 tons, is presented in Table 22 to Table 25, for collision on the column, pontoon, brace, and riser, respectively. The statistical values, i.e. samples max and mean, as well as Gumbel estimations, for relative collision velocity are used in the calculations. As mentioned before, added mass values are affected by the presence of the platform. Moreover, the applicability of zero or infinite frequency added mass in this case depends on the speed of collision and solidity of ice. Here, the relevant zero-frequency added mass, considering the proximity effect, and the collision direction, is adopted in the calculations, which is a conservative approach to selecting the infinite frequency added mass.

Table 22: Estimated impact energy [MJ] for the ice cube on the column. The ice's zero-frequency added mass in surge close to the platform column, i.e. A0_1_1 = 1350[tons], is used in the calculations. MP: Most probable, Exp: expected, P90: 90 percent fractal, based on Gumbel fit to relative collision velocities.

Case ID	Hs[m], Tp[s], WD[deg]	Sample Mean	Sample Max	MP	Exp	P90
3	9.8, 14.8, 180	3.8	21.2	1.8	3.0	13.6
4	8.6, 12.0, 180	7.0	38.8	3.8	5.7	22.4
5	4.9, 6.5, 180	5.6	28.2	3.0	4.5	17.5
6	9.8, 14.8, 270	3.5	16.7	1.7	2.8	12.4
7	8.6, 12.0, 270	6.3	24.9	3.6	5.2	18.4
8	4.9, 6.5, 270	2.9	10.7	1.8	2.5	7.1
9	9.8, 14.8, 270	5.9	21.2	3.3	4.9	17.5
10	8.6, 12.0, 270	7.0	37.0	4.0	5.8	20.8
11	4.9, 6.5, 270	5.1	28.4	2.6	4.0	17.2
14	9.8, 14.8, 180	4.9	31.1	2.5	3.9	16.5
18	9.8, 14.8, 270	1.5	11.6	0.8	1.3	5.1
19	8.6, 12.0, 270	3.5	17.4	2.1	2.9	9.6
20	4.9, 6.5, 270	2.0	12.8	1.1	1.7	6.4
21	9.8, 14.8, 180	1.6	9.7	0.8	1.3	5.3

Table 23: Estimated impact energy [MJ] for the ice cube on the pontoon. The ice's zero-frequency added mass in heave when the ice is on the pontoon, i.e. A0_3_3 = 900[tons], is used in the calculations. MP: Most probable, Exp: expected, P90: 90 percent fractal, based on Gumbel fit to relative collision velocities.

Case ID	Hs[m], Tp[s], WD[deg]	Sample Mean	Sample Max	MP	Exp	P90
15	9.8, 14.8, 270	1.7	5.4	0.9	1.4	4.9
16	9.8, 14.8, 270	1.0	3.9	0.5	0.8	3.2
17	9.8, 14.8, 270	0.9	4.1	0.4	0.7	3.6
22	9.8, 14.8, 270	1.2	13.6	0.6	0.9	4.3
23	9.8, 14.8, 270	1.2	4.7	0.6	0.9	3.8

Table 24: Estimated impact energy [MJ] for the ice cube on the brace. The ice's zero-frequency added mass in surge when the ice is far away, i.e. $A0_1_1 = 810$ [tons], is used in the calculations. MP: Most probable, Exp: expected, P90: 90 percent fractal, based on Gumbel fit to relative collision velocities.

Case ID	Hs[m], Tp[s], WD[deg]	Sample Mean	Sample Max	MP	Exp	P90
12	9.8, 14.8, 180	1.7	7.0	1.0	1.4	4.8
13	9.8, 14.8, 180	2.6	11.0	1.5	2.1	7.5

Table 25: Estimated impact energy [MJ] for the ice cube on the riser. The ice's zero-frequency added mass in surge when the ice is far away, i.e. $A0_1_1 = 810$ [tons], is used in the calculations. MP: Most probable, Exp: expected, P90: 90 percent fractal, based on Gumbel fit to relative collision velocities.

Case ID	Hs[m], Tp[s], WD[deg]	Sample Mean	Sample Max	MP	Exp	P90
16	9.8, 14.8, 270	1.8	6.8	1.2	1.6	4.1
22	9.8, 14.8, 270	2.6	14.0	1.6	2.2	6.8
23	9.8, 14.8, 270	2.2	7.4	1.4	1.9	5.5

In all the cases considered here, the ice, when placed transverse to the waves, rotate and align itself with the waves before collision. Therefore, it is assumed that the collision is always happening in the longitudinal direction of ice, and hence the surge added mass is used in all horizontal collisions. When the collision vector is vertical, e.g. on the pontoon, then the heave zero-frequency added mass is adopted.

As expected, the obtained impact energies, similar to collision velocities, are highly dependent on the selected wave realization and initial conditions. Moreover, the assumptions made for the impact process (Section 7.1.1), mainly neglecting the crushing of ice during impact, will introduce inaccuracies in the present estimations of impact energy. A more complete impact solver, including models for ice crushing and hydrodynamic interaction during impact, is desirable. Then it would be possible to simulate the impact, starting from the ice and platform's velocities and positions at the time of impact, as identified here, and estimate the actual energy transfer between the two.

8 Proposal of simplified model test for verification and illustration of the numerical results

In the numerical simulations one has identified that the hydrodynamic motion of glacial ice masses and its interaction with semisubmersible drilling units are quite complex and challenging. We will therefore suggest investigating the behaviour of the motions and interaction by a simplified model test in an ocean basin. Three phenomena could be studied further in a model test programme:

- How does the glassier ice mass move in waves when there is no hydrodynamic interaction with the semi-submersible?
- How does the glassier ice mass move when it is close to the semi-submersible?
- What is the glassier ice mass behaviour when is about to collide with the platform?

The first question could be investigated by doing a model test with an "artificial" glacial ice model in an ocean basin. The ice model is kept in stationary positions and exposed to waves. This can be regarded as a stationary approach where one can obtain high confidence statistics of the motions of glacial ice mass in waves.

The second question could be investigated by looking into a similar test, but where both the ice mass and the platform are kept in stationary positions and exposed to waves in the basin. This can also be regarded as a stationary approach where one can obtain high confidence statistics of the motions of the two bodies.

The third question could be investigated by letting the "artificial" ice mass be freely floating in waves and let it collide with the semi-submersible. This can be regarded as a transient approach where one will need several realizations to obtain enough statistics of the behaviour of the two bodies. One must expect that there will be somewhat less confidence in these data but still is expected to give valuable input to the complex behaviour of the simulated situation.

The "artificial" glacial ice should be modelled with a correct scaled density, probably made by a solid plastic material or foam material (Divinicell). In order to keep the ice mass model in a stationary position (no drifting) it is suggested using an artificial, soft mooring system which will give similar wave frequency motion as it will have when it is free floating. Similar results could also be obtained using numerical simulation of the same system including the soft mooring. Hence one could achieve high quality data for verification of ice mass motions in the numerical simulation.

The same semi-submersible model in the model test as used in the present numerical study should be used as that will allow for reusing an exciting a scale model and a numerical model of the platform, confer Table 1 and Figure 1.

Figure 38 shows a simple sketch of the proposed model test set-up. The platform will be moored using a linear spring system which is fixed to gondola/transverse system. This gondola/transverse system is running in rail above the basin and can therefore be used to locate the platform in various position in the ocean basin with a minimum of rigging time. The motion of the platform will be measured by use of optical tracking system.

The ice mass model may be full submerged due to wave motions. Accordingly, one must be able to measure the motions even in this situation. We suggest using an accelerometer/gyro system and/or an optical tracking system. The latter may either be an above-water or an under-water tracking system. For

using the above-water tracking system, one will use a slender tube with three optical markers that always will be above the water.

In the sketch below, it is indicated that the artificial mooring system consist of nearly vertical mooring lines with linear springs. This is suggested because it will give flexibility in location of the platform close to the ice mass. The drawback is that it will affect the hydrostatic stiffness of the ice mass and to some extent include viscous damping. The vertical stiffness of the mooring system is planned to be soft, in order to reduce the effect on the wave frequency motions and to minimize the effect of the hydrostatic stiffness. In the numerical validations one should consider to also include the artificial mooring system in the model. This way, it will be possible to make a direct comparison. It is also possible to replace the vertical mooring system in the numerical model with an equivalent horizontal system in order to study the effect of the hydrostatic stiffness. An alternative to the vertical mooring system is a horizontal mooring system. The main drawback with this system is less flexibility when positioning the platform near the ice model. The selection of artificial mooring system should be further examined during detailed design of a model test program.

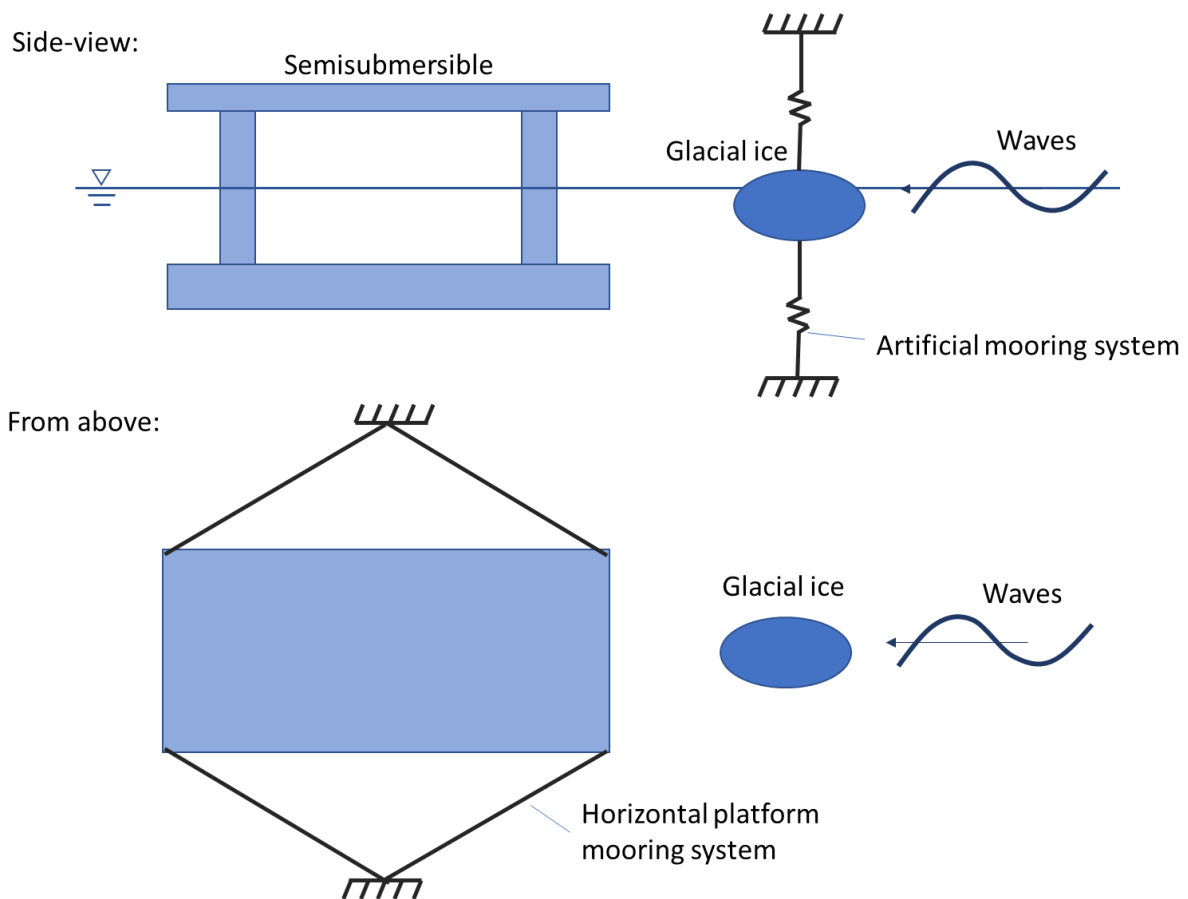


Figure 38 Sketch of proposed model test setup

9 References

- [1] DNVGL, «Ptil - Konstruksjonssikkerhet i arktiske områder (ST5) - Glacial ice impact,» Report No. 2017-0425, Rev. 2., March, 2018.
- [2] T. Sayeed, B. Colbourne, B. Quinton, D. Molyneux, H. Peng og D. Spencer, «A review of icebergs and bergy bit hydrodynamic interaction with offshore structures,» *Cold Regions Science and Technology*, vol. 135, pp. 34-50, 2017.
- [3] A. Tsarau, R. Lubbad og S. Løset, «Recent advances in modelling the hydrodynamic effects on ice motion and ice-structure interactions offshore,» i *Proceedings of the 23rd International Conference on Port and Ocean Engineering under Arctic Conditions, (POAC15)*, Trondheim, Norway, 2015.
- [4] V. M. Arunachalam, J. J. Murray og D. B. Muggeridge, «Short term motion analysis of icebergs in linear waves,» *Cold Regions Science and Technology*, vol. 13, nr. 3, pp. 247-258, 1987.
- [5] J. H. Lever og D. Sen, «A method to upgrade ice berg velocity statistics to include wave induced motion,» *Journal of Offshore Mech. Arct. Eng.*, vol. 109, nr. 2, pp. 278-286, 1987.
- [6] J. H. Lever, B. Colbourne og L. Mak, «A model study of the wave-induced motion of small icebergs and bergy bits,» *Journal of Offshore Mech. Arct. Eng.*, vol. 110, nr. 1, pp. 101-107, 1988.
- [7] J. H. Lever, D. Sen og D. Attwood, «The influence of shape on iceberg wave-induced velocity statistics,» *Journal of Offshore Mech. Arct. Eng.*, vol. 112, nr. 3, pp. 263-269, 1990.
- [8] J. H. Lever, D. Attwood og D. Sen, «Factors affecting the prediction of wave-induced iceberg motion,» *Cold Regions Science and Technology*, vol. 15, pp. 177-190, 1988.
- [9] D. Attwood, «Wave induced motions of small ice masses (Master thesis),» Memorial University of Newfoundland, 1986.
- [10] Hay and Company Consultants Inc, «Motion and impact of icebergs, Environmental studies revolving Funds report 004,» Ottawa, 1986.
- [11] M. Isaacson og F. J. D. Stritto, «Motion of an ice mass near a large offshore structure,» i *Offshore Technology Conference*, Houston, Texas, 1986.
- [12] K. F. Cheung, «Hydrodynamic interactions between ice masses and large offshore structures (Master thesis),» University of British Columbia, 1987.
- [13] M. Isaacson og K. F. Cheung, «Influence of added mass on ice impacts,» *Can. J. Civ. Eng.*, vol. 15, nr. 4, pp. 698-708, 1988.
- [14] M. Isaacson og K. McTaggart, «Influence of hydrodynamic effects on iceberg collisions,» *Can. J. Civ. Eng.*, vol. 17, nr. 3, pp. 329-337, 1990.
- [15] V. A. Chernetsov, A. A. Malyutin og S. L. Karlinsky, «Floating production platform for polar seas designed to resist iceberg impact,» i *Proceedings of Eighteenth International Offshore and Polar Eng. Conf.*, 2008.
- [16] S. L. Karlinsky og V. A. Chernetsov, «Floating production unit resistance to iceberg impact,» i *Proceedings of the Twentieth International Offshore and Polar Engineering Conference*, 2010.
- [17] S. G. Lee, I. H. Lee, Y. H. Baek, N. Couty, S. G. Geoff og J. M. Quenez, «Membrane-type LNG carrier side collision with iceberg - effect of impact conditions on structural response through a sensitivity analysis,» i *Presentated at 6th Ann Arctic Shipping Summit*, Helsinki, Finland, 2010.
- [18] M. A. Salvaggio og M. Rojansky, «The importance of wave-driven icebergs impacting an offshore structure,» i *Offshore Technology Conference*, Houston, Texas, 1986.

- [19] L. M. Mak, J. H. Lever, M. J. Hinchey og D. Duthinh, «Wave-induced bergy bit motion near a floating oil production platform,» i *Proceedings of the 9th International Conference on Offshore Mechanics and Arctic Engineering*, Houston, Texas, 1990.
- [20] D. J. McGovern og W. Bai, «Experimental study on kinematics of sea ice floes in regular waves,» *Cold Regions Science and Technology*, vol. 103, pp. 15-30, 2014.
- [21] M. Isaacson og K. McTaggart, «Iceberg drift motions near a large structure,» i *Proceedings of the First Pacific/Asia Offshore Mechanics Symposium*, Seoul, Korea, 1990.
- [22] A. B. Cammaert og G. P. Tsinker, «Impact of large ice floes and icebergs on marine structures,» i *Proceedings of the Sixth International Conference on Port and Ocean Engineering under Arctic Conditions*, Quebec, Canada, 1981.
- [23] A. S. Swamidas, H. El-Tahan og M. Arockiasamy, «Structural integrity of semisubmersibles and gravity platforms to bergy-bit/iceberg impact,» i *Offshore Technology Conference*, Houston, Texas, 1986.
- [24] K. Holthe, «A numerical model for predicting the response of concrete gravity platforms to iceberg impact,» i *Proceedings of the International Conference on Port and Ocean Engineering under Arctic Conditions*, Luleå, Sweden, 1989.
- [25] Z. Liu og J. Amdahl, «A new formulation of the impact mechanics of ship collisions and its application to a ship-iceberg collision,» *Marine Structures*, vol. 23, pp. 360-384, 2010.
- [26] D. Bass, H. Gaskill og N. Riggs, «Analysis of iceberg impact with gravity base structures,» i *Proceedings of the 4th International Conference on Offshore Mechanics and Arctic Engineering*, Dallas, Texas, 1985.
- [27] N. Fonseca og C. Stansberg, «Wave drift forces and low frequency damping on the exwave semisubmersible,» i *Proceedings of OMAE2017*, Trondheim, Norway, 2017.
- [28] O. Faltinsen, *Sea loads on ships and offshore structures*, Cambridge University Press, 1990.
- [29] M. Greenshow og L. Yanbao, «Added mass for circular cyliners near to or penetrating fluid boundaries - review, extension and application to water-entry, -exit and slamming,» *Ocean Engng*, vol. 14, nr. 4, pp. 325-348, 1987.
- [30] X. Xiang og O. M. Faltinsen, «Maneuvering of Two Interacting Ships in Calm Water,» i *11th International Symposium on Practical Design of Ships and Other Floating Structures*, Rio de Janeiro, RJ, Brazil, 2010.
- [31] R. D. Blevins, *Applied Fluid Dynamics Handbook*, Krieger Pub Co, 2003.
- [32] Statoil, «Barents East blocks metocean design basis,» Document no. ME2015-005, November, 2015.
- [33] BaSEC - Barents Sea Exploration Collaboration, «Fysisk miljø i Barentshavet sørøst,» <https://www.norskoljeoggass.no/globalassets/dokumenter/miljo/barents-sea-exploration-collaboration/basec-rapport-1---fysisk-miljo-i-barentshavet-sorost.pdf>, 2016.
- [34] R. O. Foschi og M. Isaacson, «A study of wave-iceberg load combination factors,» i *Proceedings of the Sixth International Offshore and Polar Conference*, Los Angeles, California, 1996.
- [35] R. O. Foschi, M. Isaacson, N. Allyn og S. Yee, «Assessment of the wave-iceberg load combination factor,» *Int. J. Offshore Polar Eng.*, vol. 8, nr. 1, pp. 1-8, 1998.
- [36] R. O. Foschi, M. Isaacson, N. Allyn og S. Yee, «Combined wave-iceberg loading on offshore structures,» *Can. J. Civ. Eng.*, vol. 23, nr. 5, pp. 1099-1110, 1996.
- [37] R. O. Foschi, M. Isaacson, S. Allyn og S. Yee, «Assessment of the wave-iceberg load combination factor,» i *Proceedings of the Seventh International Offshore and Polar Engineering Conference*, 1997.

- [38] R. O. Foschi, M. Isaacson og M. Allyn, «Reliability calibration of a wave-iceberg interaction load combination factor,» i *Proceedings of the 23rd International Conference on Offshore Mechanics and Arctic Engineering*, Vancouver, British Columbia, 2004.

Appendix A

Collision on the Column

1 Collision Scenario Number 1

	1	2	3	4	5
Signals		Max	Min	Mean	St. Dev.
RelativeCollisionVelocity	[m/s]	2.38	0.09	0.78	0.64
IceVelocity	[m/s]	3.96	0.84	2.28	0.92
CollisionHeight	[m]	26.67	17.53	21.5	2.31

Table 26: Statistical values calculated for collision scenario number 1.

	1	2	3	4
Signals		MP	Exp	P90
RelativeCollisionVelocity	[m/s]	0.49	0.67	1.64
IceVelocity	[m/s]	1.86	2.13	3.52
CollisionHeight	[m]	20.44	21.11	24.61

Table 27: Statistical values calculated for collision scenario number 1.

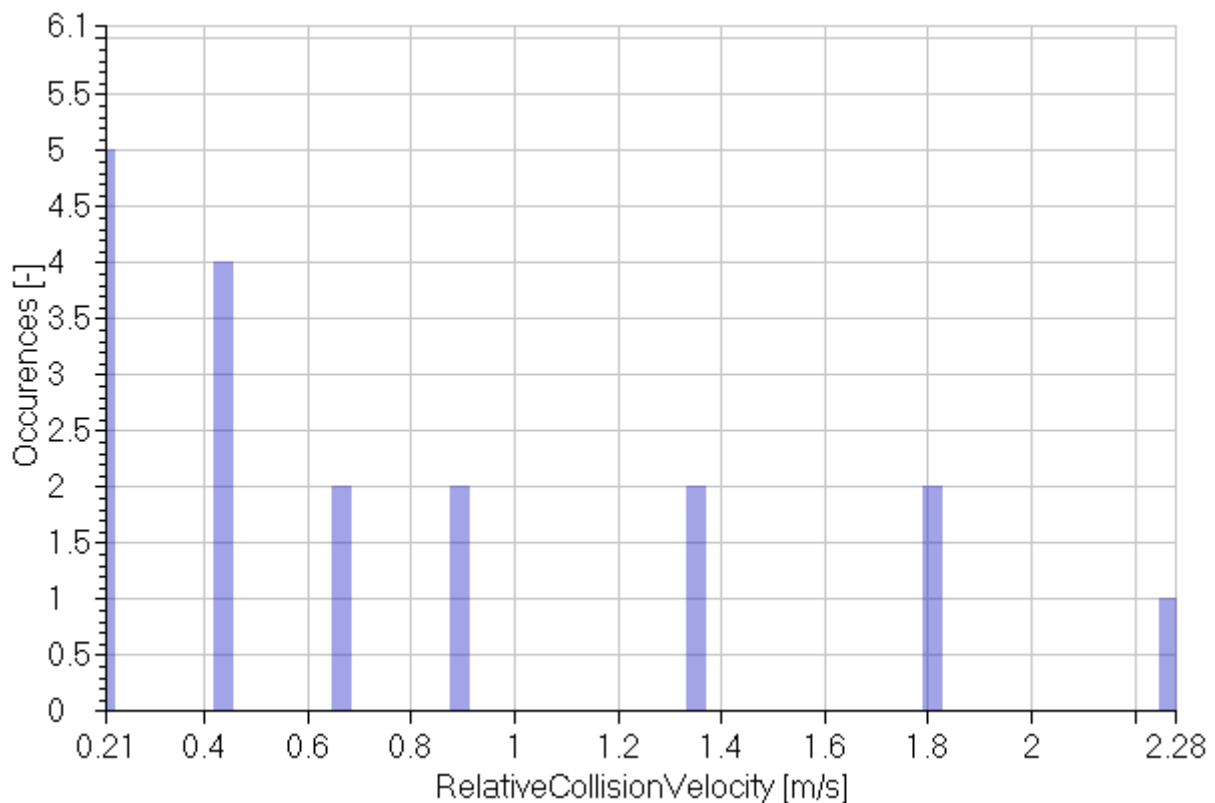


Figure 39: collision scenario number 1

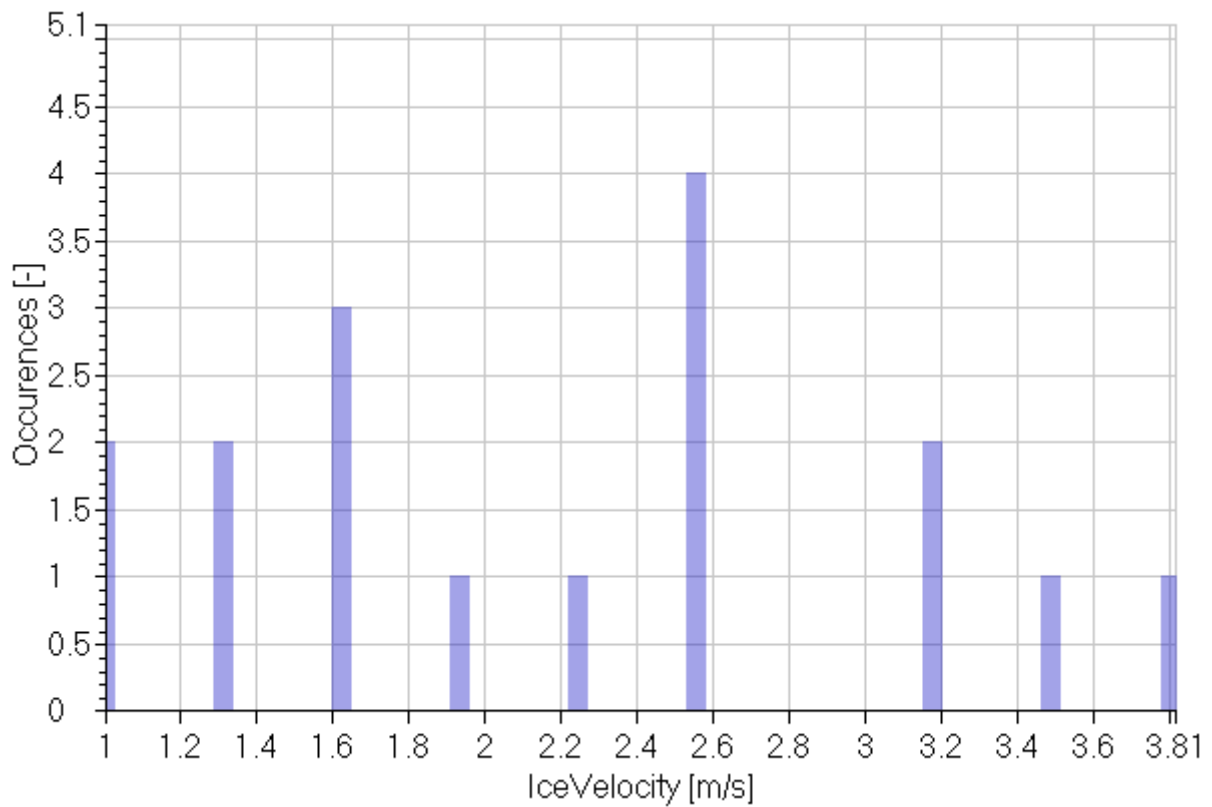


Figure 40: collision scenario number 1

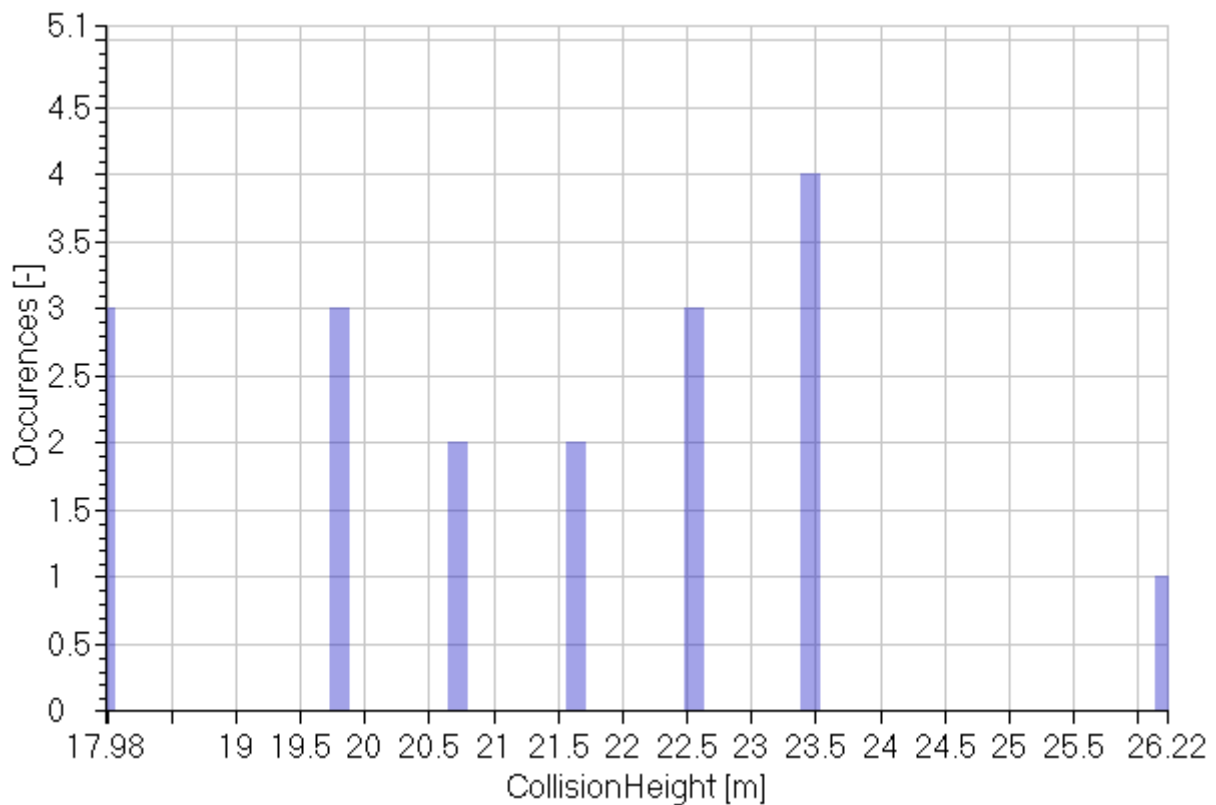


Figure 41: collision scenario number 1

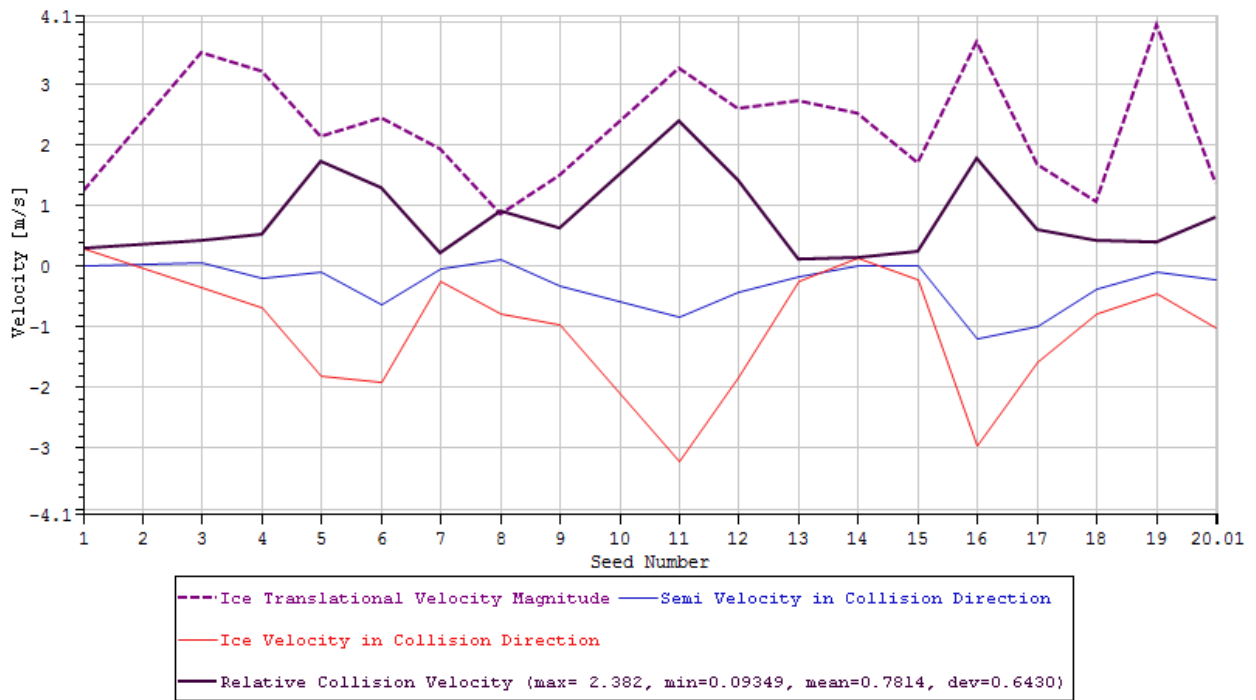


Figure 42: Total and relative collision velocities of ice and platform for different seeds, for case number 1.

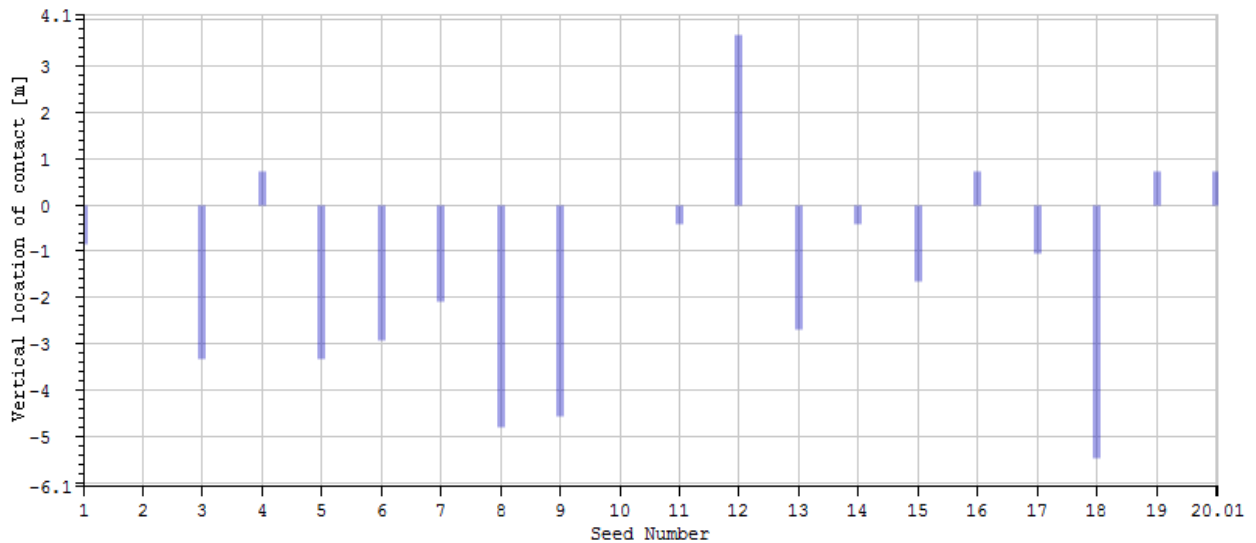


Figure 43: Vertical location of impact on the platform for different seeds, for case number 1.

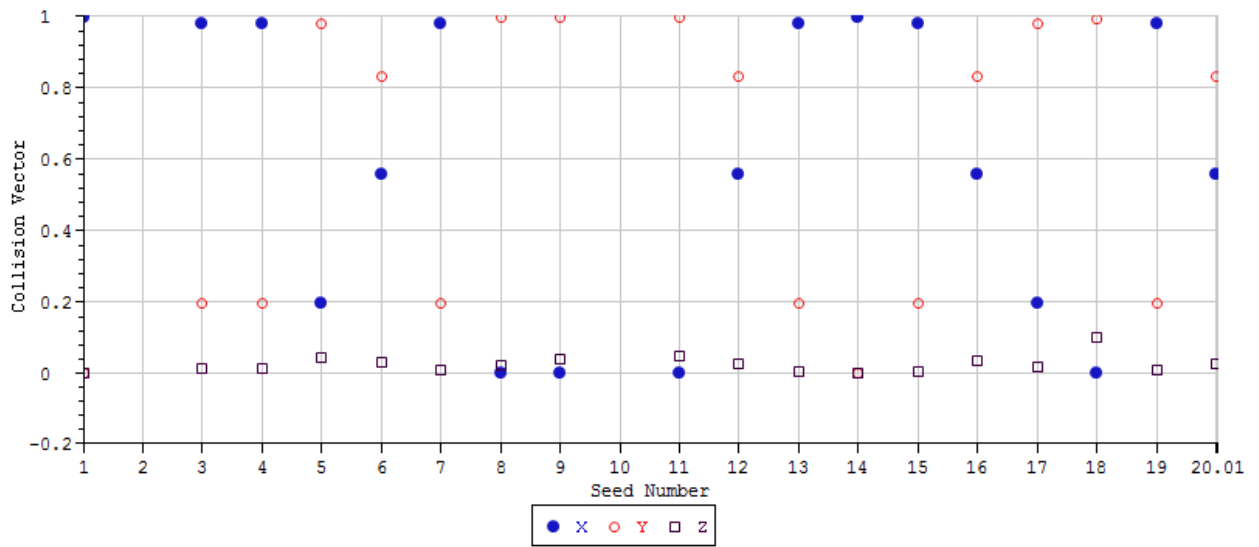


Figure 44: Collision vector components for different seeds, for case number 1.

2 Collision Scenario Number 2

	1	2	3	4	5
Signals		Max	Min	Mean	St. Dev.
RelativeCollisionVelocity	[m/s]	2.16	0.04	0.66	0.69
IceVelocity	[m/s]	3.13	0.74	2.11	0.65
CollisionHeight	[m]	23.73	18.42	20.97	1.44

Table 28: Statistical values calculated for collision scenario number 2.

	1	2	3	4
Signals		MP	Exp	P90
RelativeCollisionVelocity	[m/s]	0.35	0.55	1.59
IceVelocity	[m/s]	1.82	2	2.98
CollisionHeight	[m]	20.31	20.73	22.91

Table 29: Statistical values calculated for collision scenario number 2.

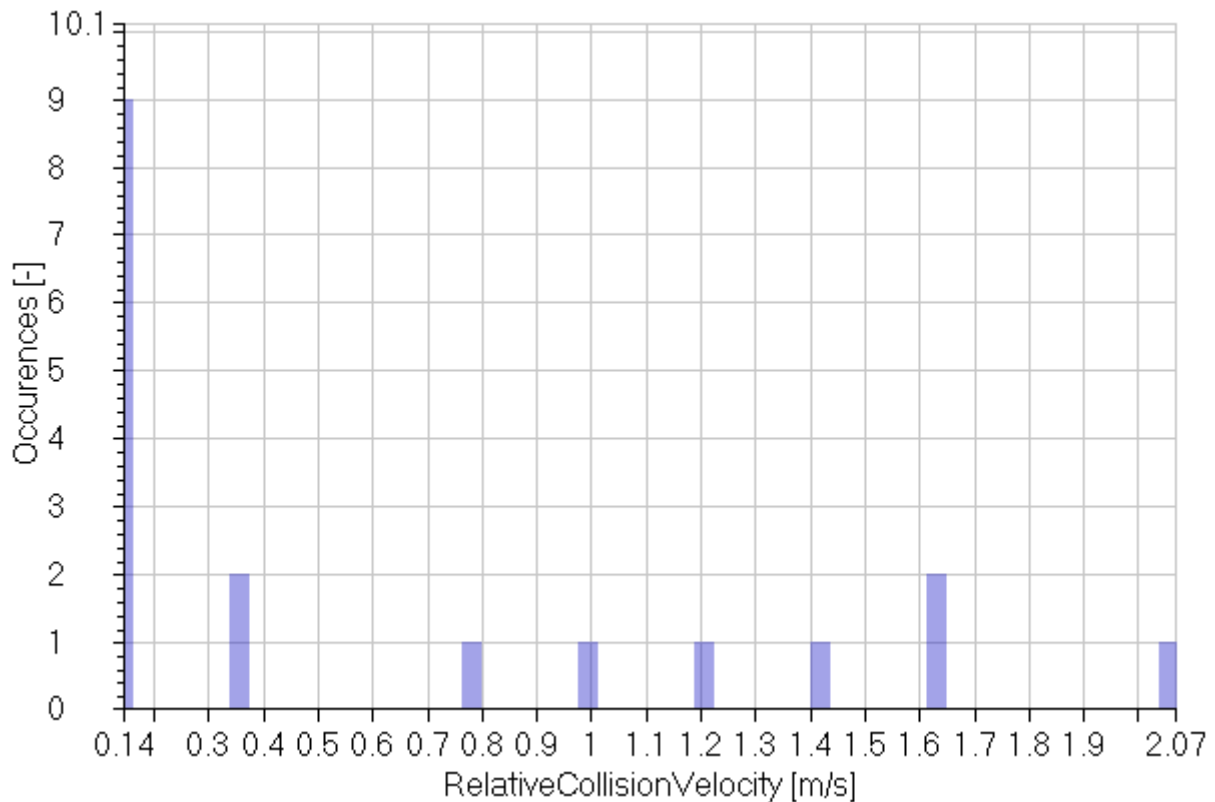


Figure 45: collision scenario number 2

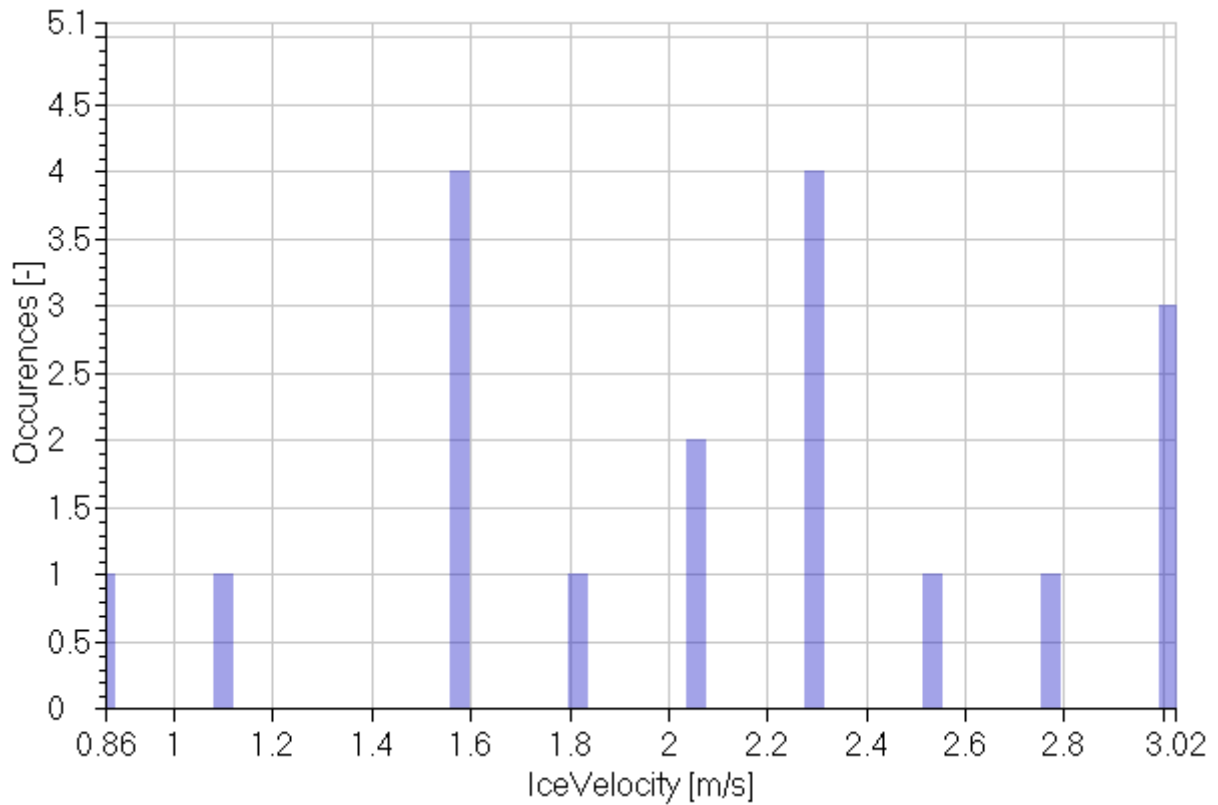


Figure 46: collision scenario number 2

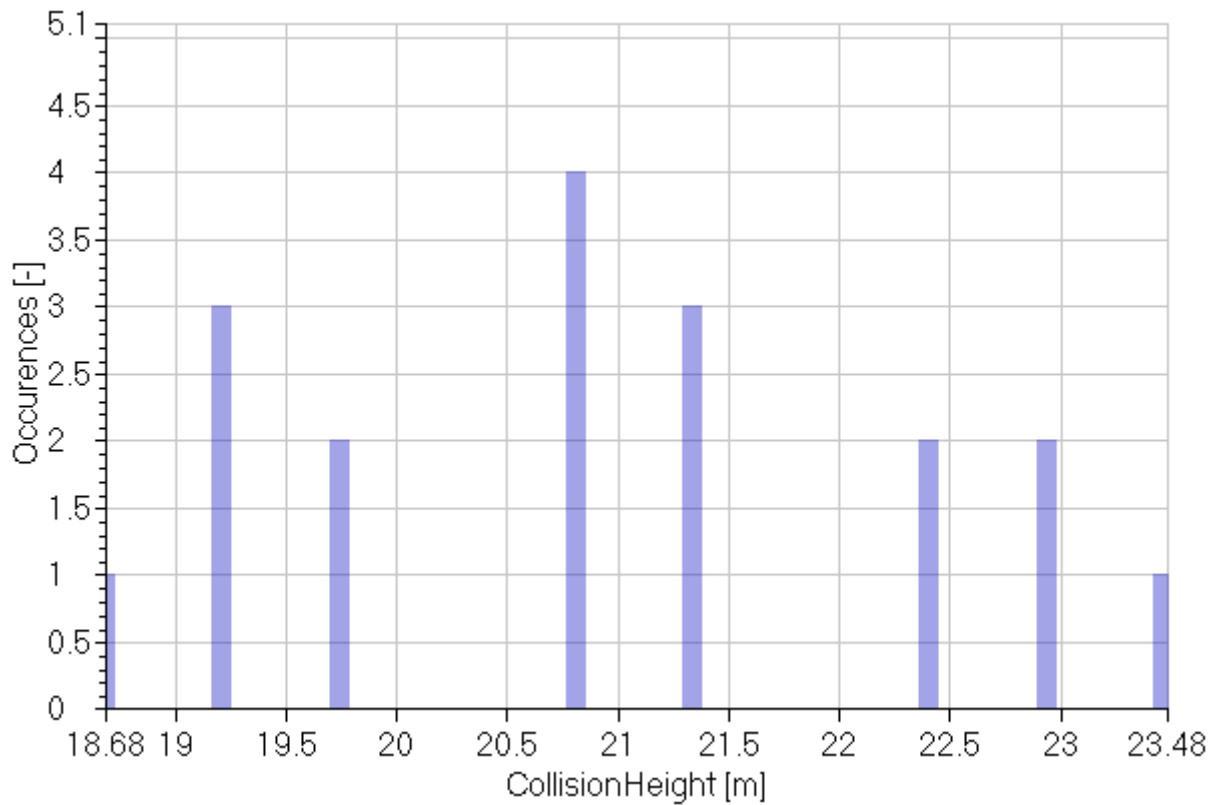


Figure 47: collision scenario number 2

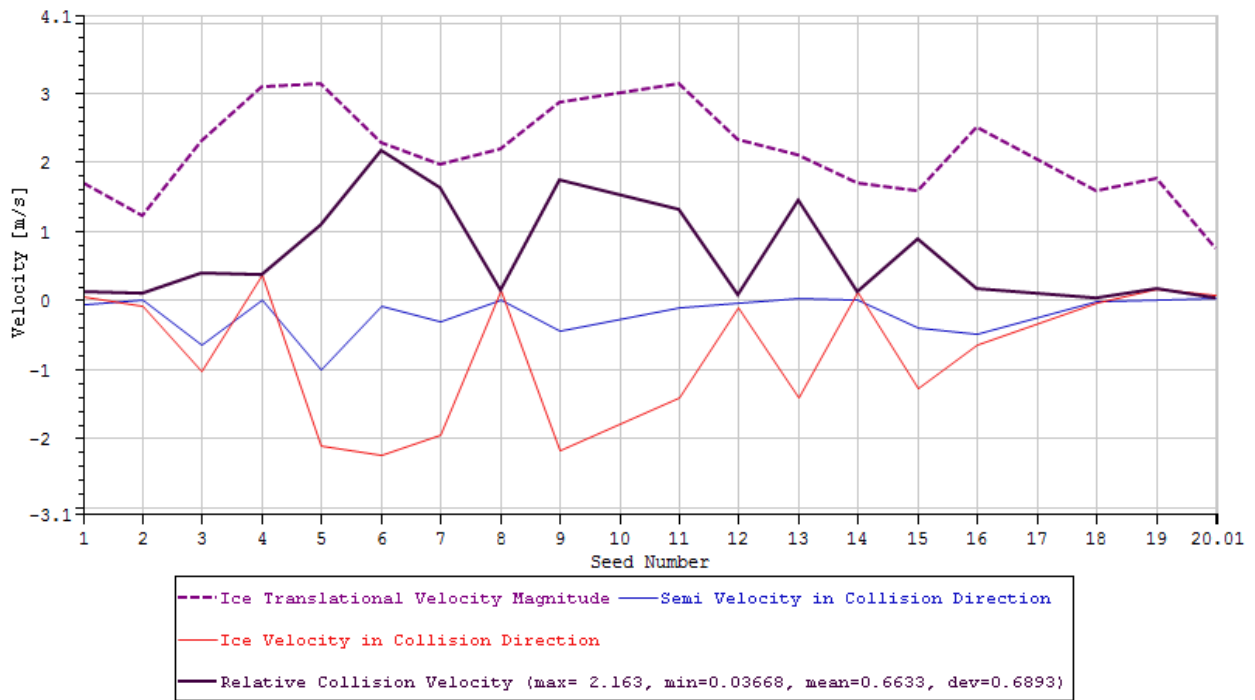


Figure 48: Total and relative collision velocities of ice and platform for different seeds, for case number 2.

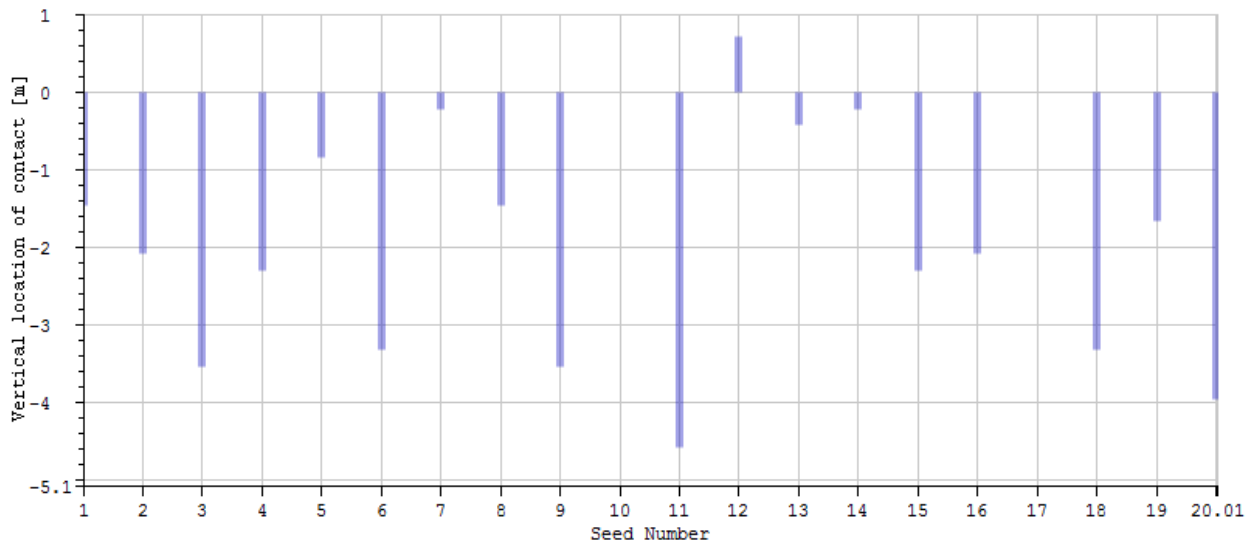


Figure 49: Vertical location of impact on the platform for different seeds, for case number 2.

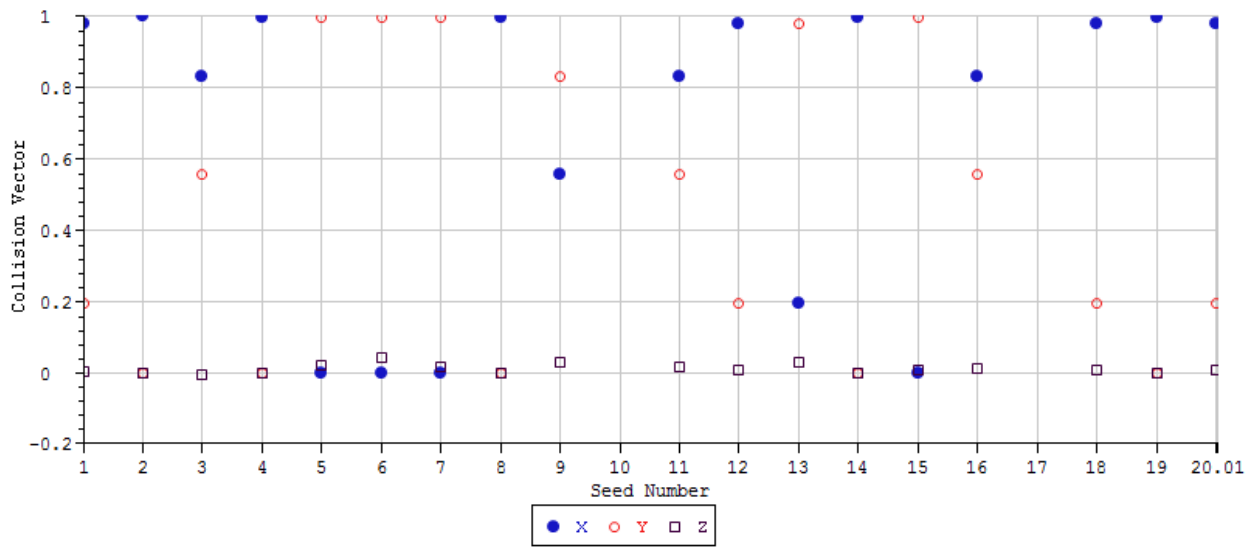


Figure 50: Collision vector components for different seeds, for case number 2.

3 Collision Scenario Number 3

	1	2	3	4	5
Signals		Max	Min	Mean	St. Dev.
RelativeCollisionVelocity	[m/s]	3.9	0.38	1.66	1.1
IceVelocity	[m/s]	4.83	0.6	2.21	1.17
CollisionHeight	[m]	24.47	12.81	19.39	4.58

Table 30: Statistical values calculated for collision scenario number 3.

	1	2	3	4
Signals		MP	Exp	P90
RelativeCollisionVelocity	[m/s]	1.15	1.47	3.13
IceVelocity	[m/s]	1.67	2.01	3.78
CollisionHeight	[m]	17.29	18.61	25.54

Table 31: Statistical values calculated for collision scenario number 3.

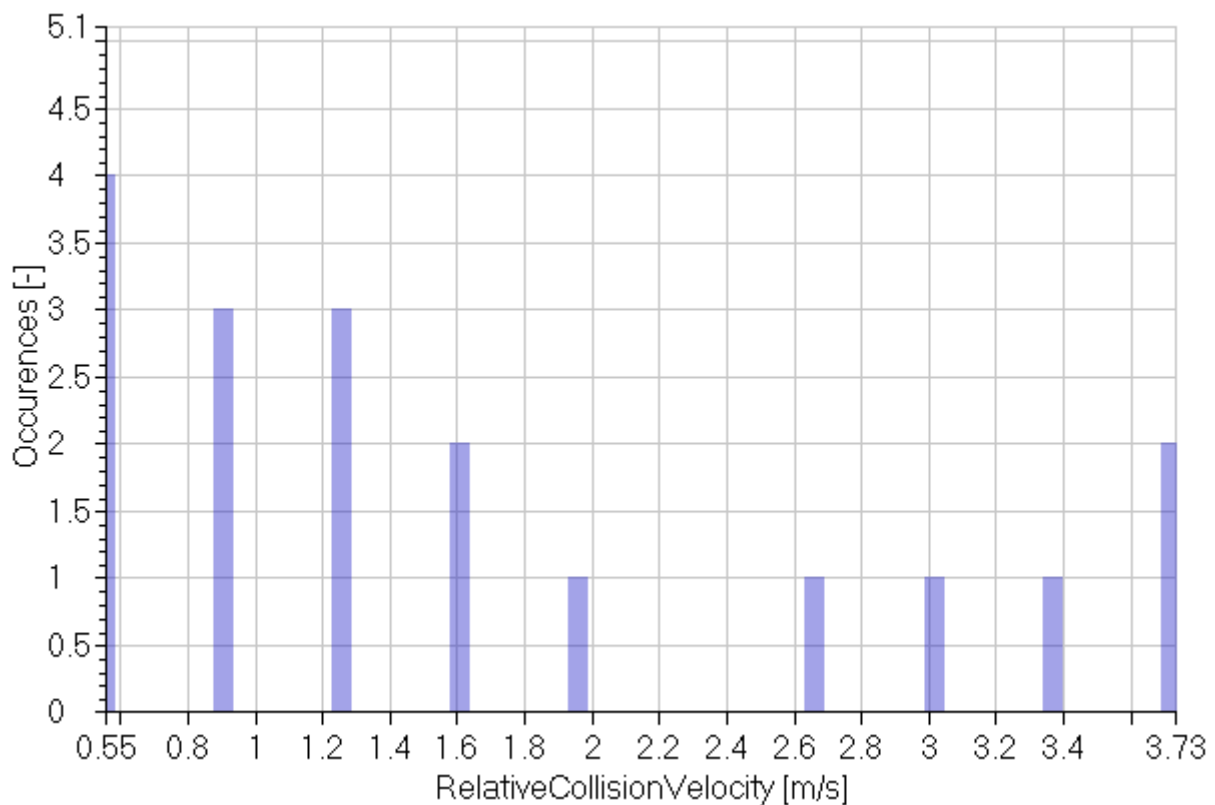


Figure 51: collision scenario number 3

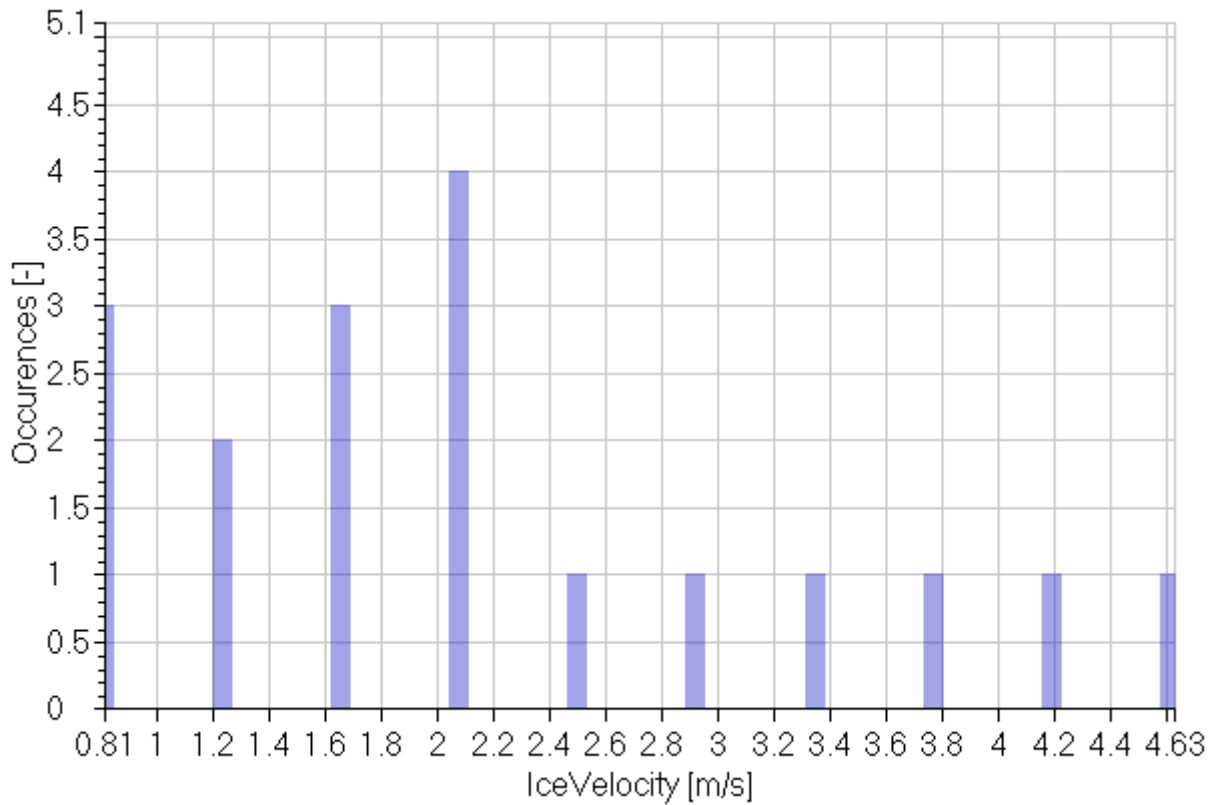


Figure 52: collision scenario number 3

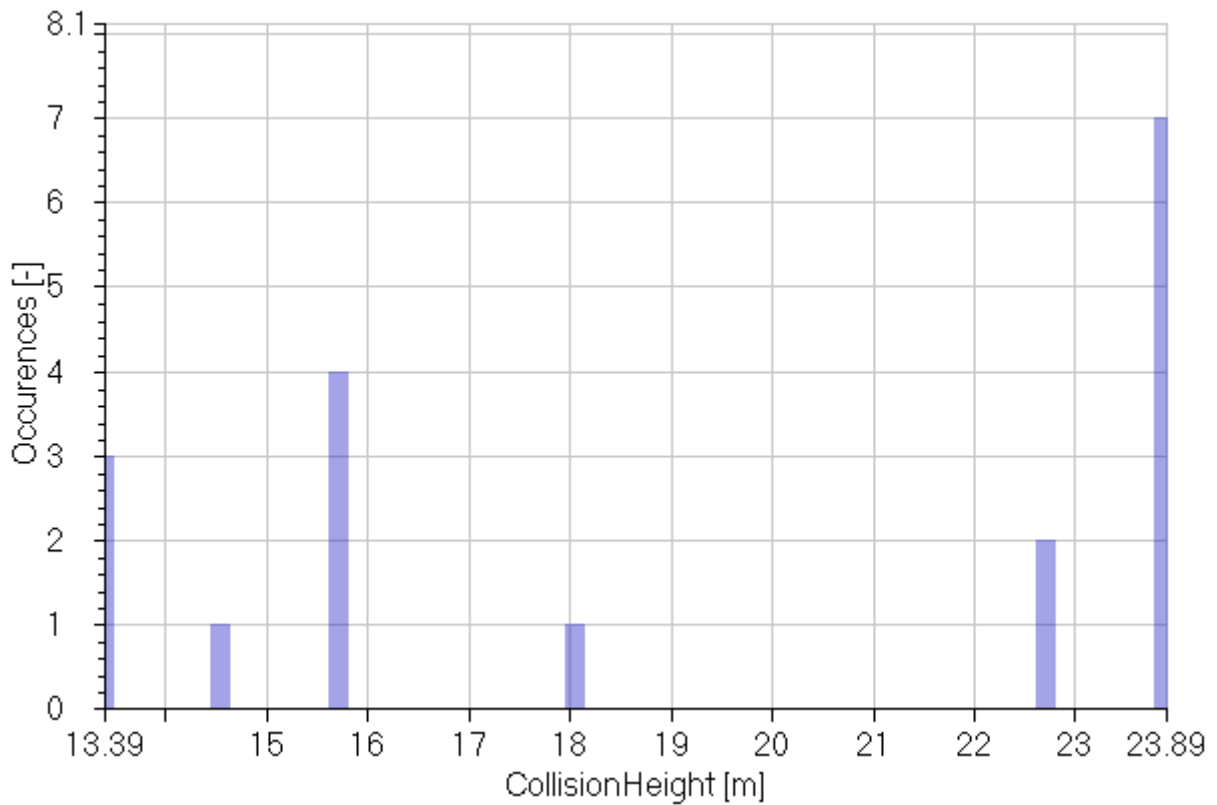


Figure 53: collision scenario number 3

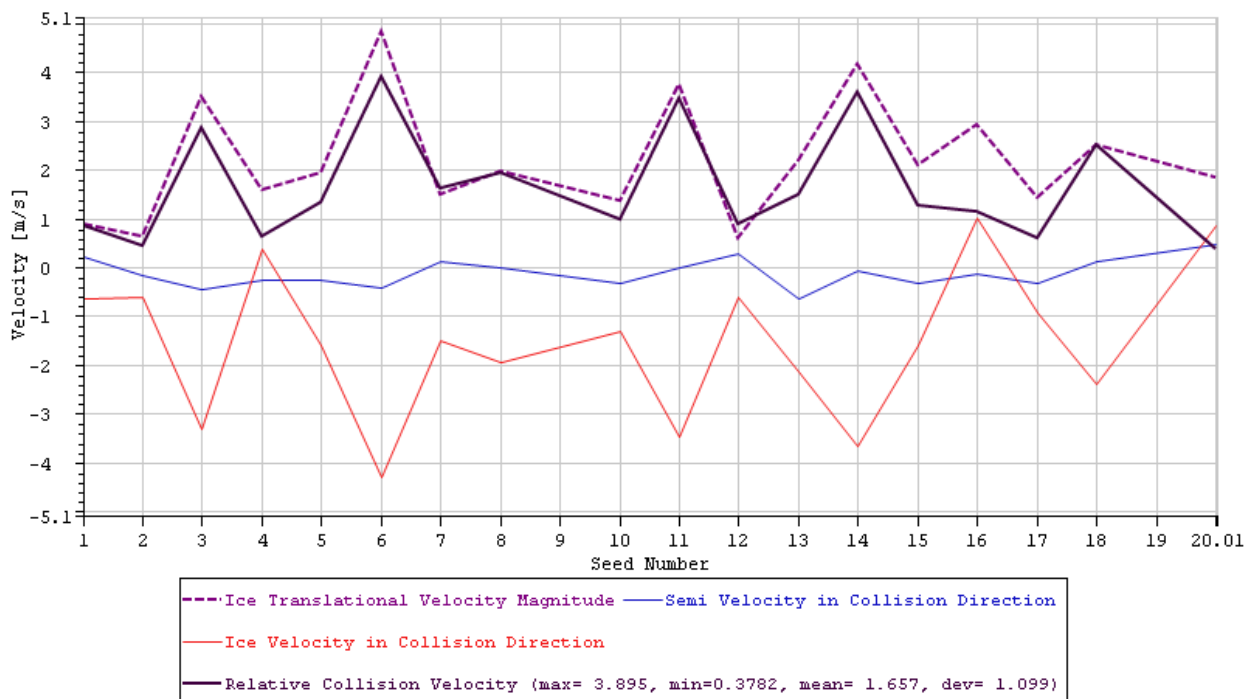


Figure 54: Total and relative collision velocities of ice and platform for different seeds, for case number 3.

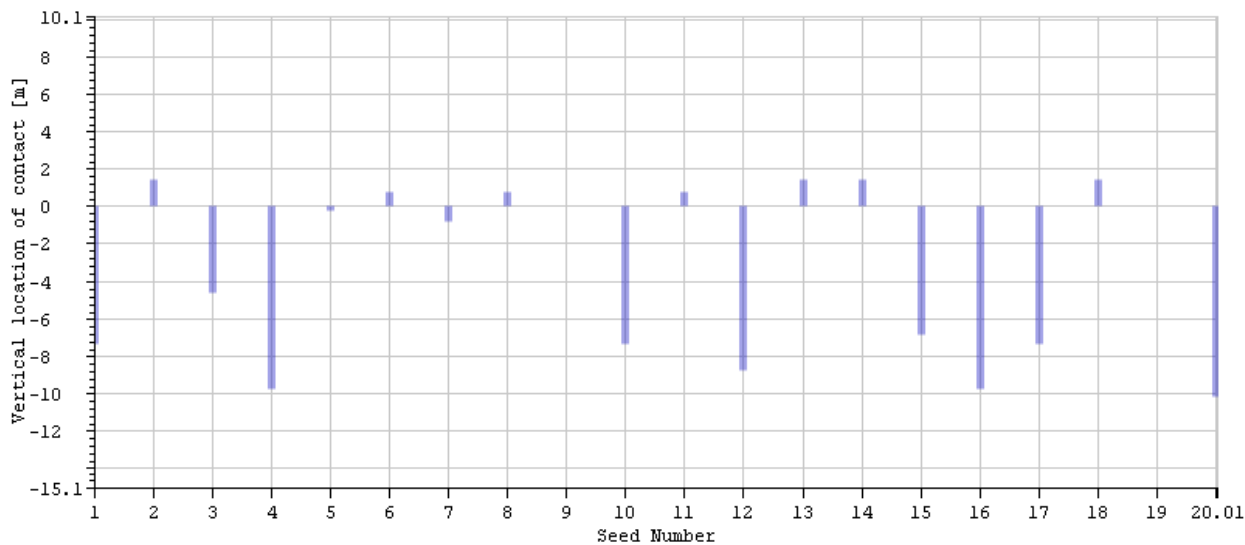


Figure 55: Vertical location of impact on the platform for different seeds, for case number 3.

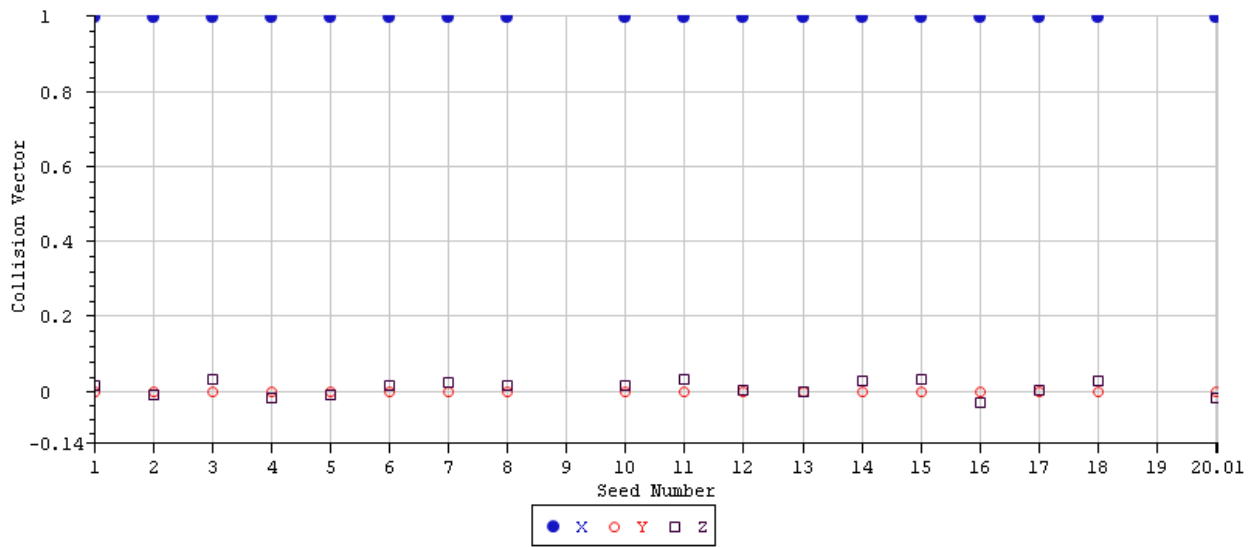


Figure 56: Collision vector components for different seeds, for case number 3.

4 Collision Scenario Number 4

	1	2	3	4	5
Signals		Max	Min	Mean	St. Dev.
RelativeCollisionVelocity	[m/s]	5.28	0.44	2.25	1.31
IceVelocity	[m/s]	5.32	0.42	2.56	1.33
CollisionHeight	[m]	25.93	13.28	21.15	4.44

Table 32: Statistical values calculated for collision scenario number 4.

	1	2	3	4
Signals		MP	Exp	P90
RelativeCollisionVelocity	[m/s]	1.65	2.03	4.01
IceVelocity	[m/s]	1.96	2.34	4.34
CollisionHeight	[m]	19.12	20.4	27.11

Table 33: Statistical values calculated for collision scenario number 4.

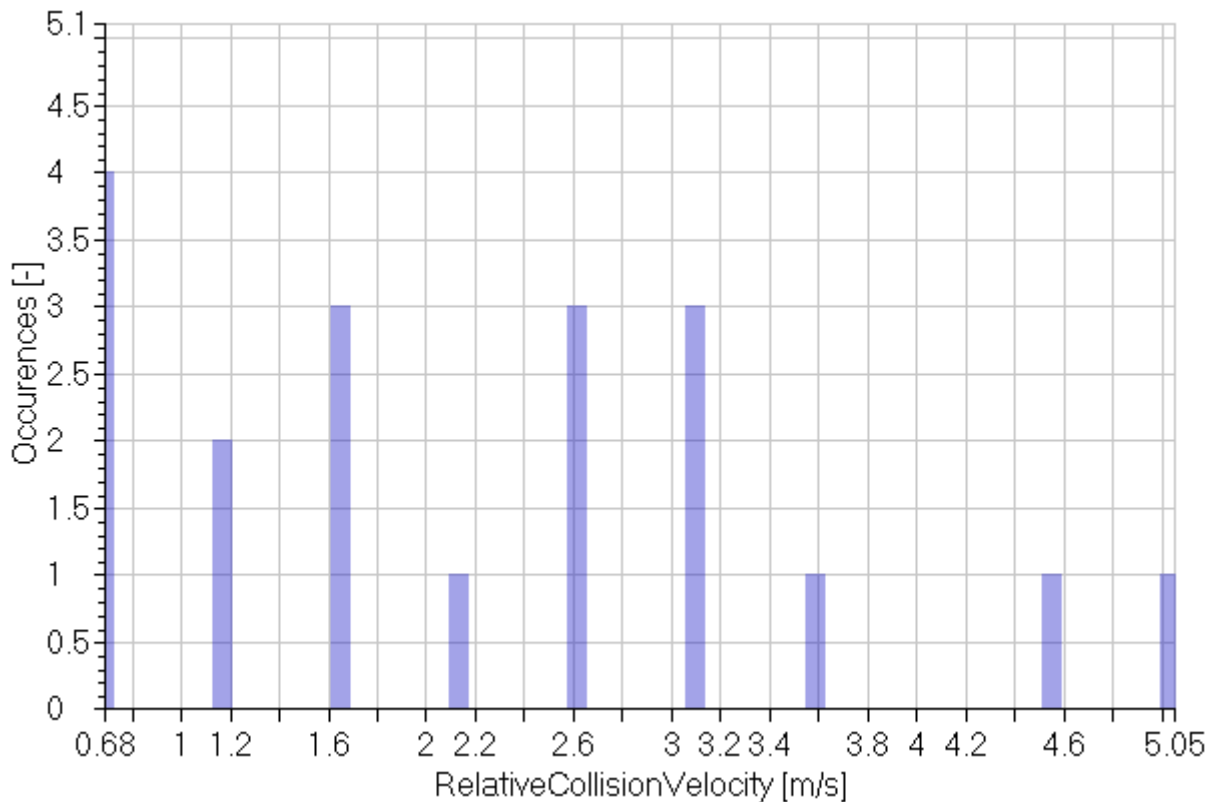


Figure 57: collision scenario number 4

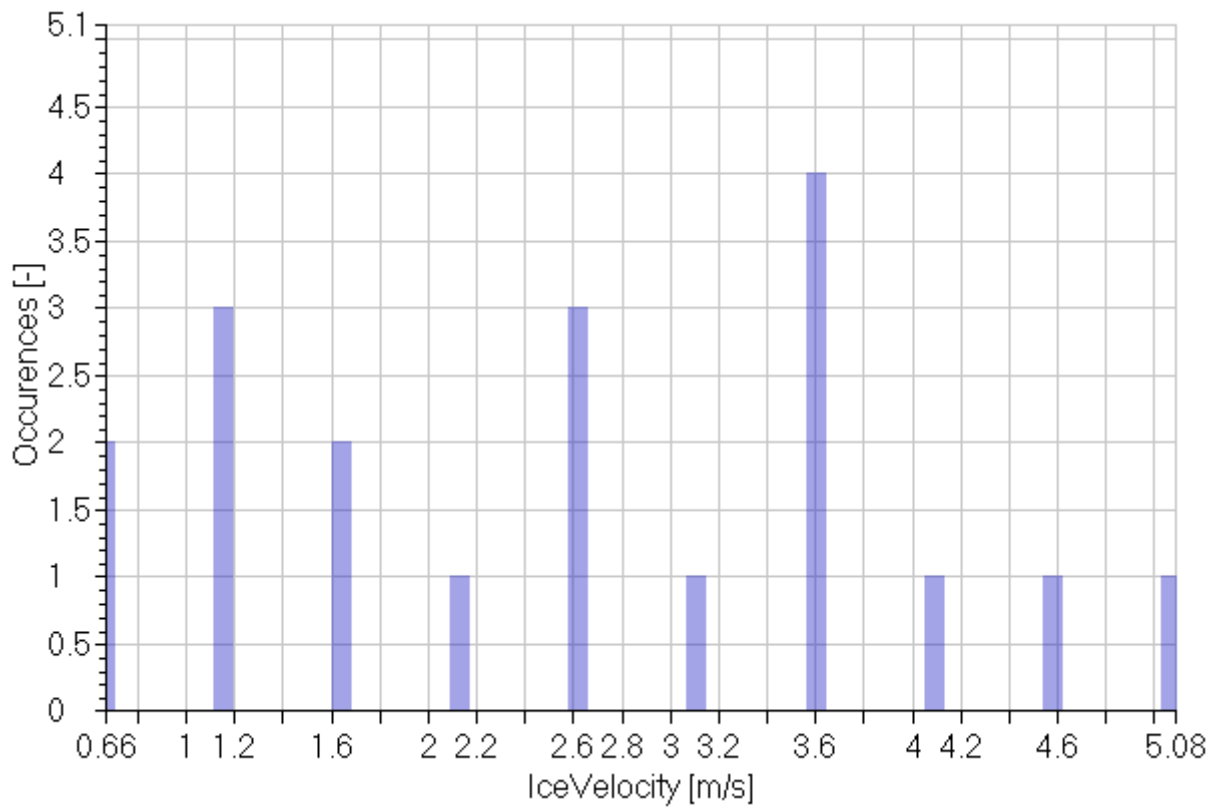


Figure 58: collision scenario number 4

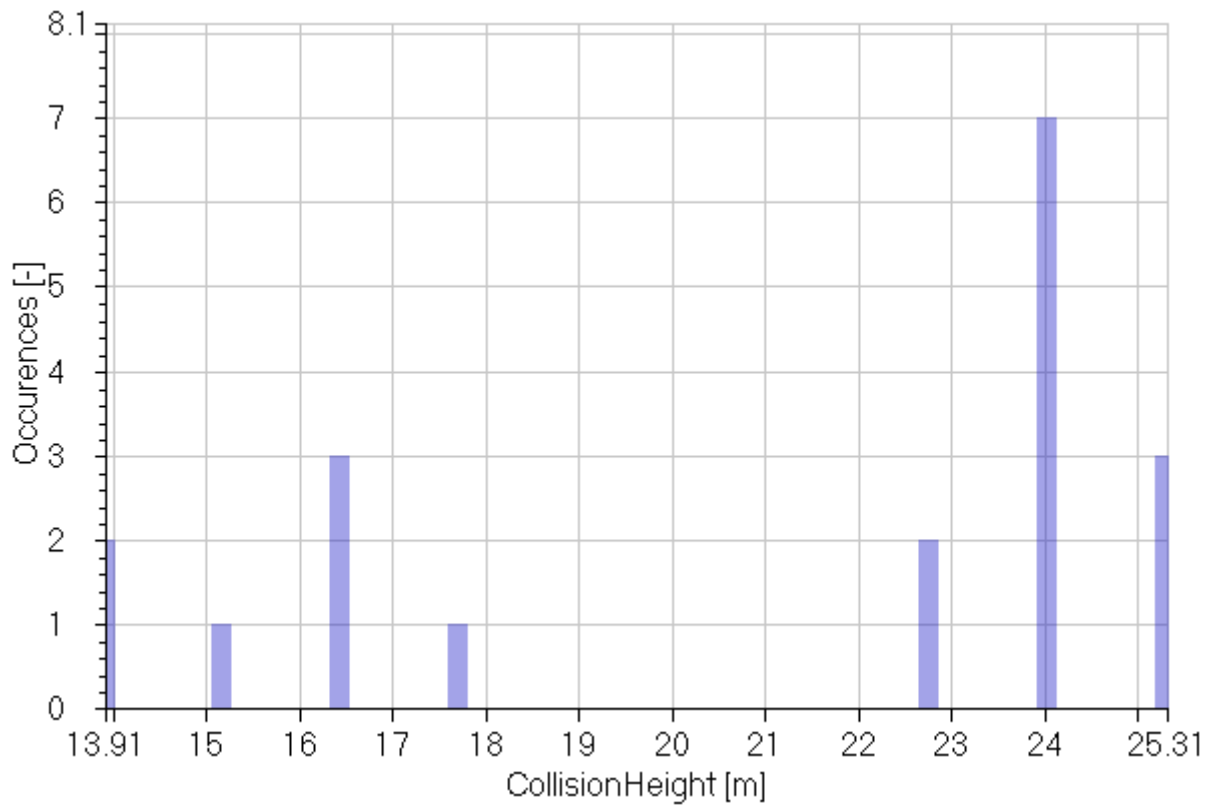


Figure 59: collision scenario number 4

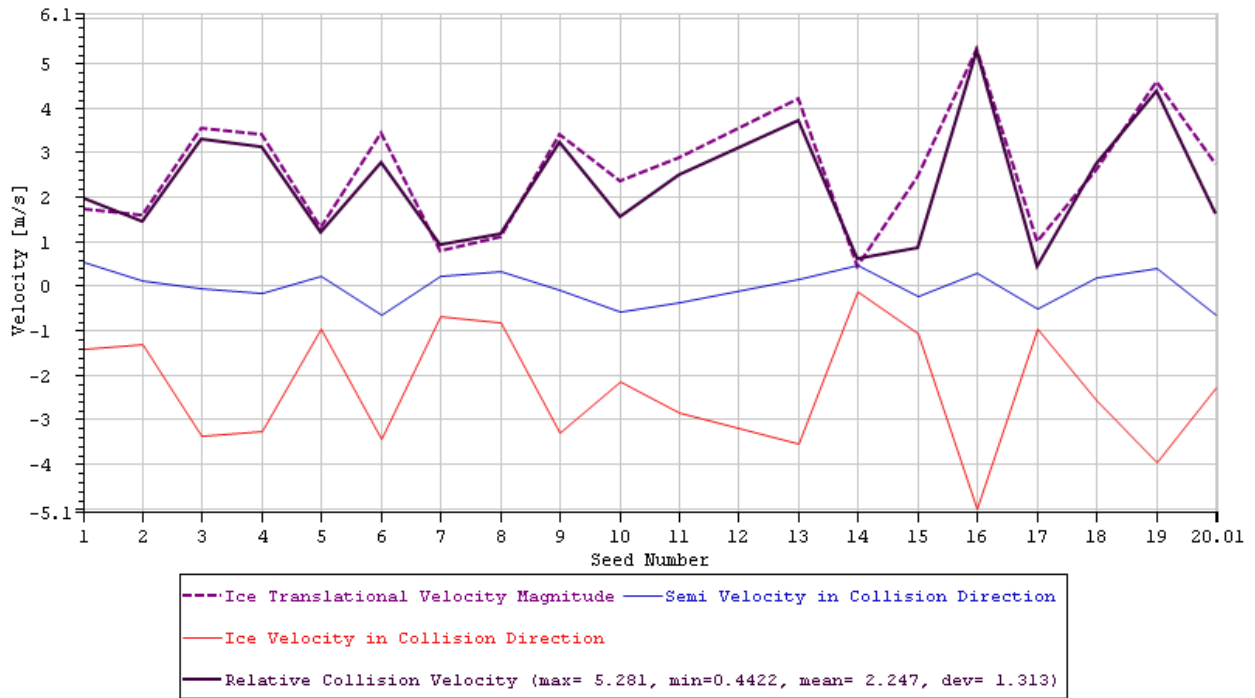


Figure 60: Total and relative collision velocities of ice and platform for different seeds, for case number 4.

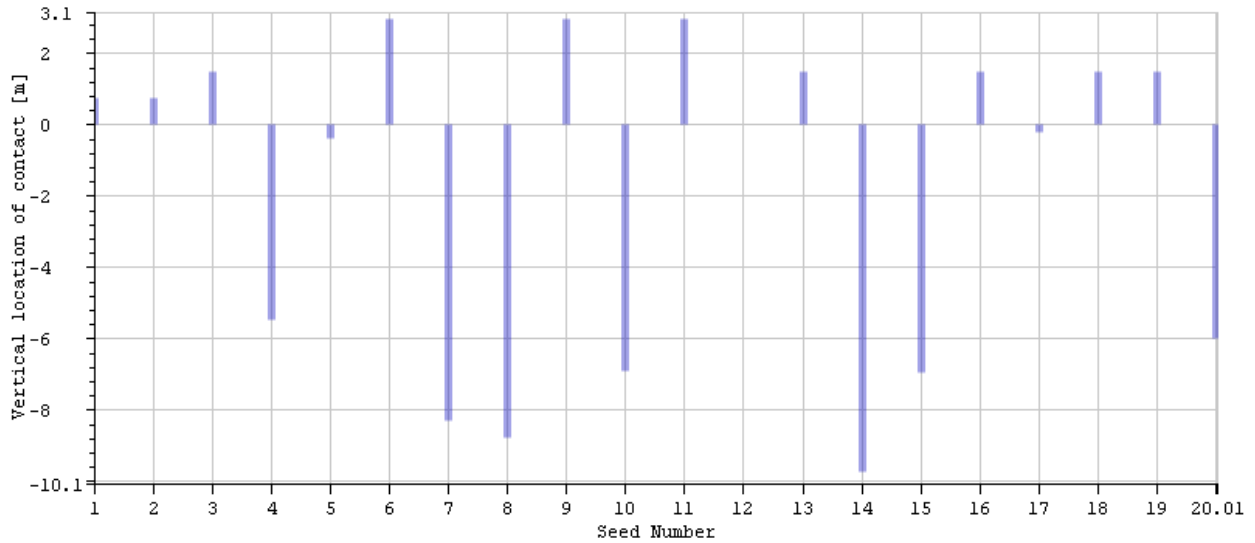


Figure 61: Vertical location of impact on the platform for different seeds, for case number 4.

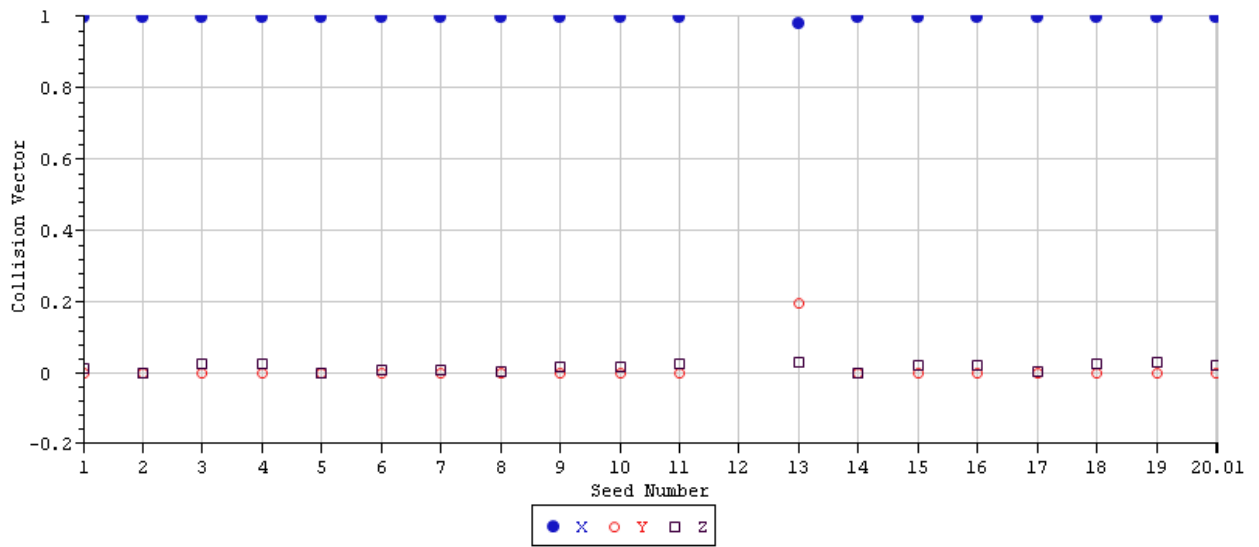


Figure 62: Collision vector components for different seeds, for case number 4.

5 Collision Scenario Number 5

	1	2	3	4	5
Signals		Max	Min	Mean	St. Dev.
RelativeCollisionVelocity	[m/s]	4.5	0.24	2	1.16
IceVelocity	[m/s]	4.27	0.65	2.11	1.02
CollisionHeight	[m]	24.47	14.69	20.08	3.89

Table 34: Statistical values calculated for collision scenario number 5.

	1	2	3	4
Signals		MP	Exp	P90
RelativeCollisionVelocity	[m/s]	1.47	1.8	3.55
IceVelocity	[m/s]	1.65	1.94	3.48
CollisionHeight	[m]	18.3	19.42	25.29

Table 35: Statistical values calculated for collision scenario number 5.

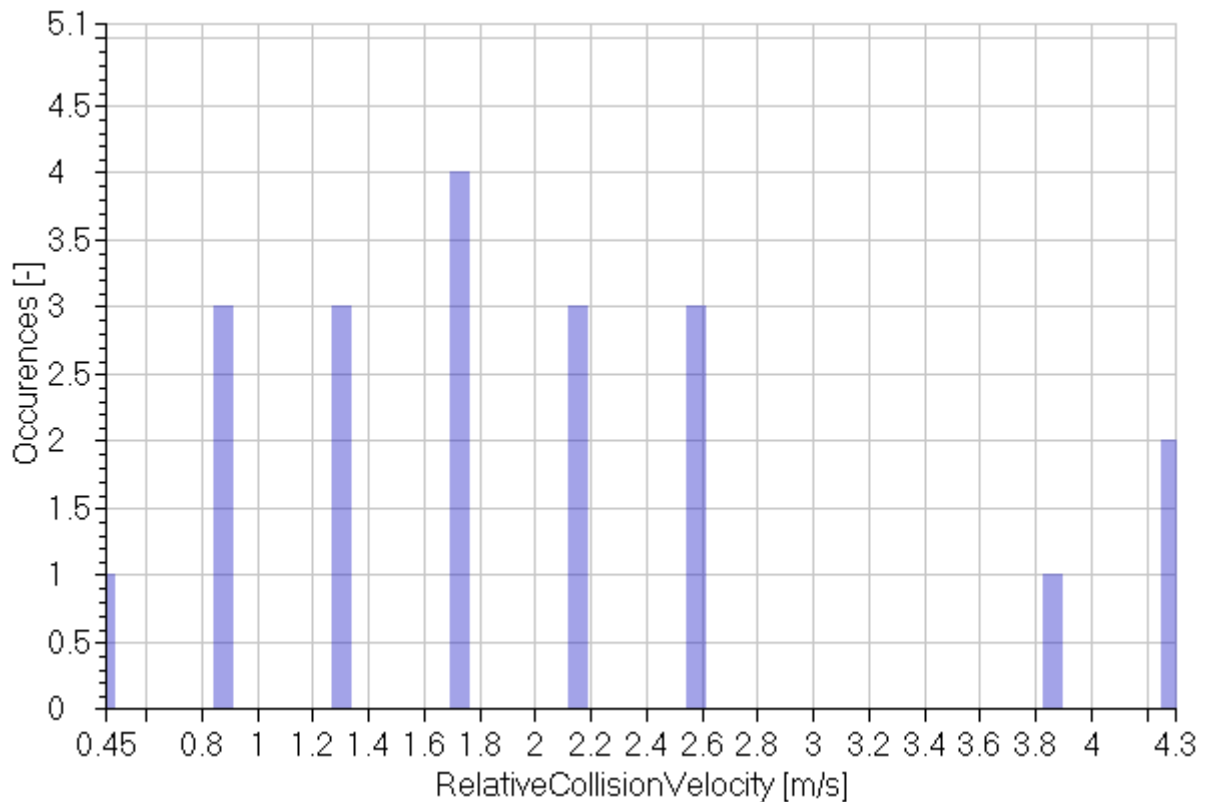


Figure 63: collision scenario number 5

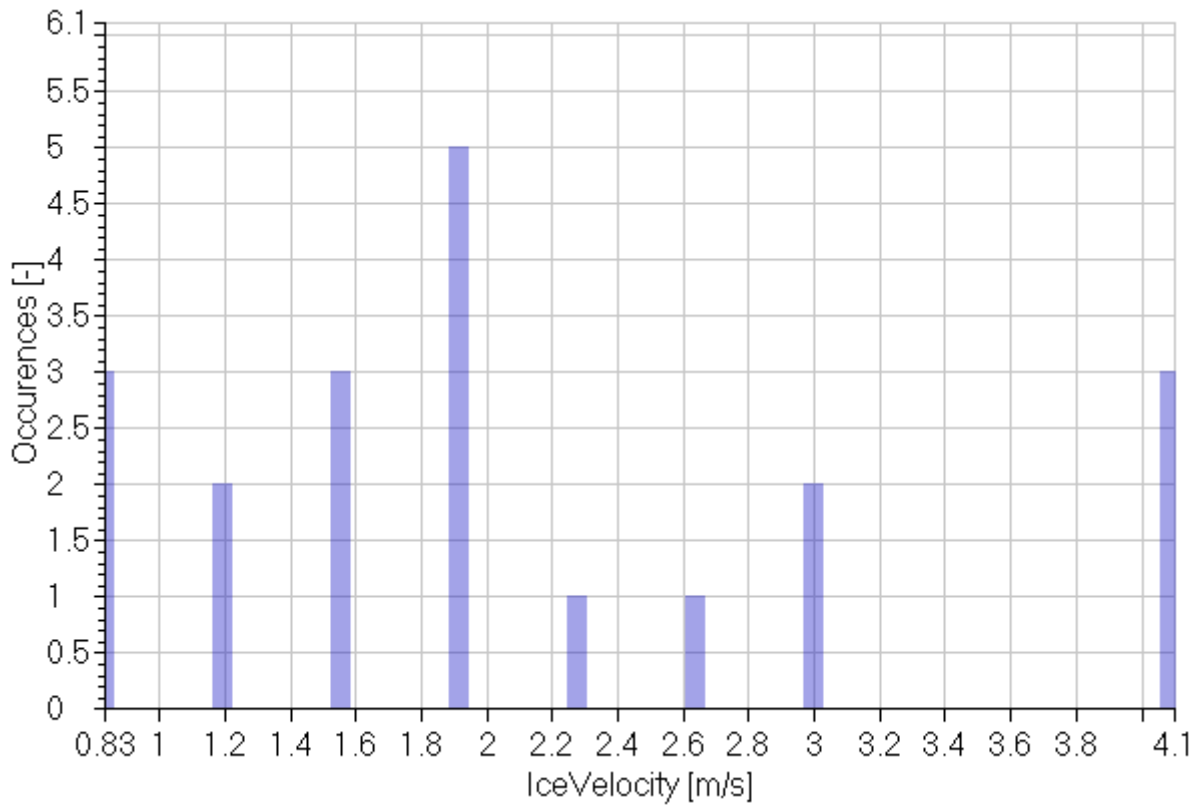


Figure 64: collision scenario number 5

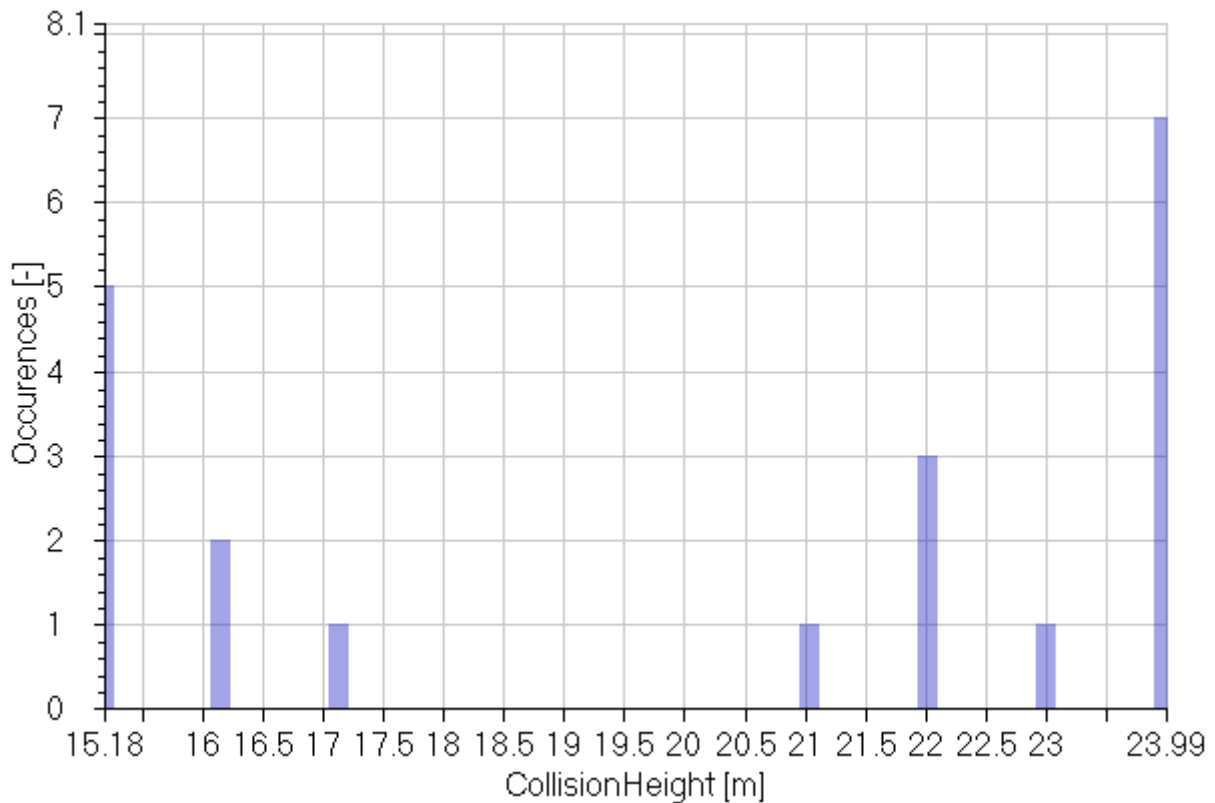


Figure 65: collision scenario number 5

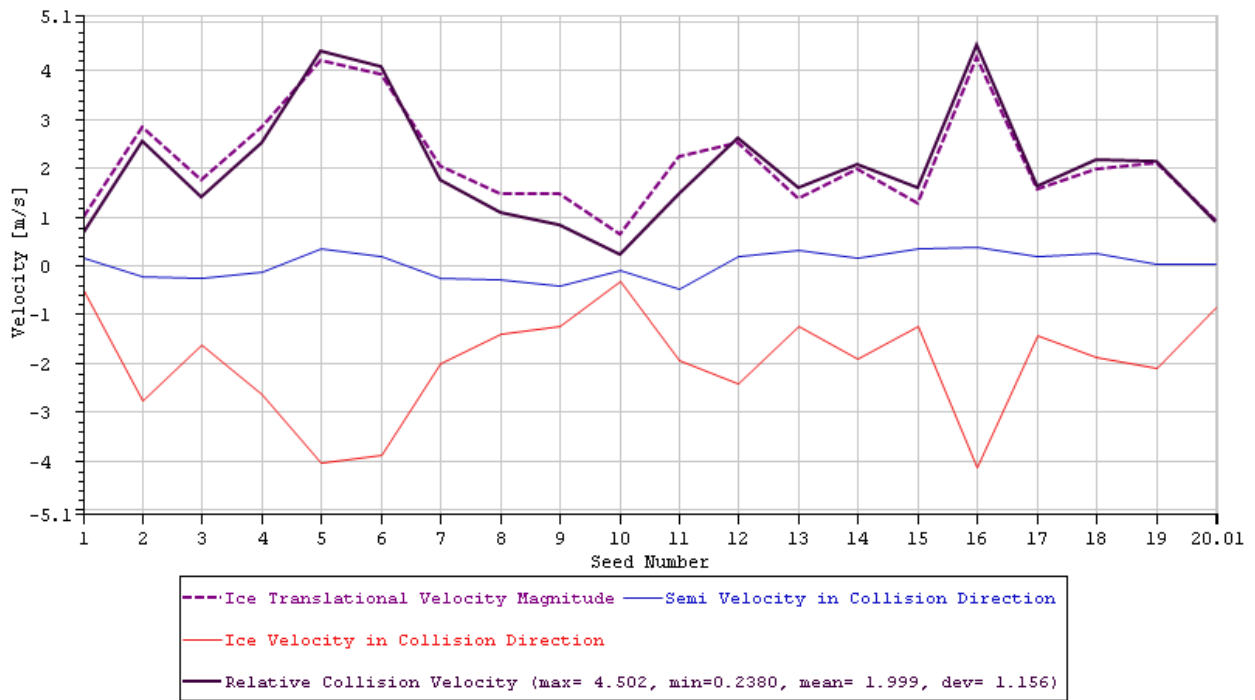


Figure 66: Total and relative collision velocities of ice and platform for different seeds, for case number 5.

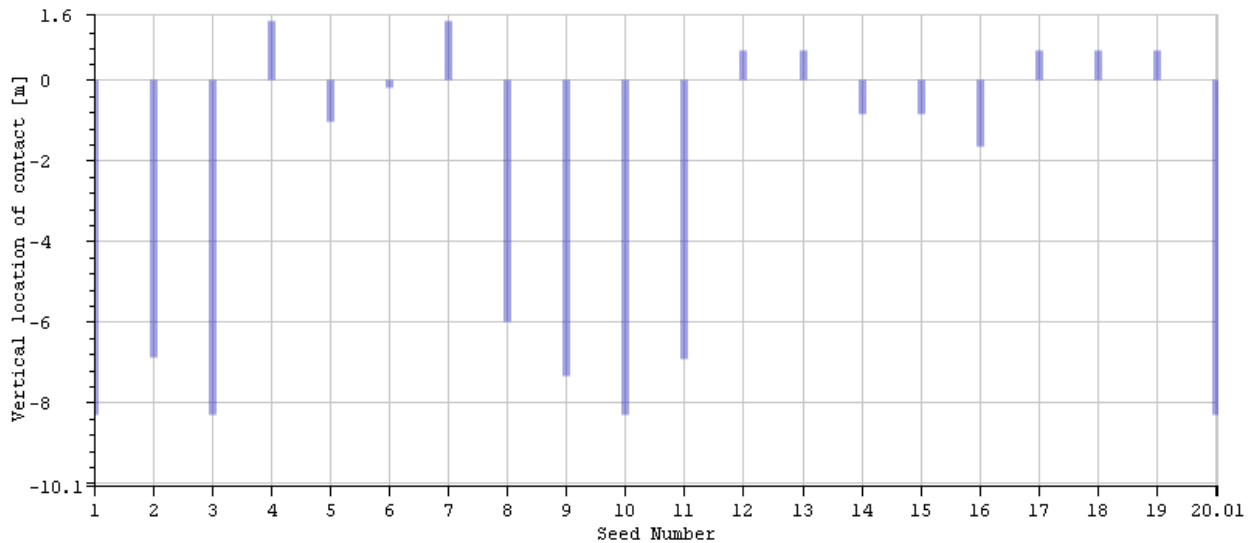


Figure 67: Vertical location of impact on the platform for different seeds, for case number 5.

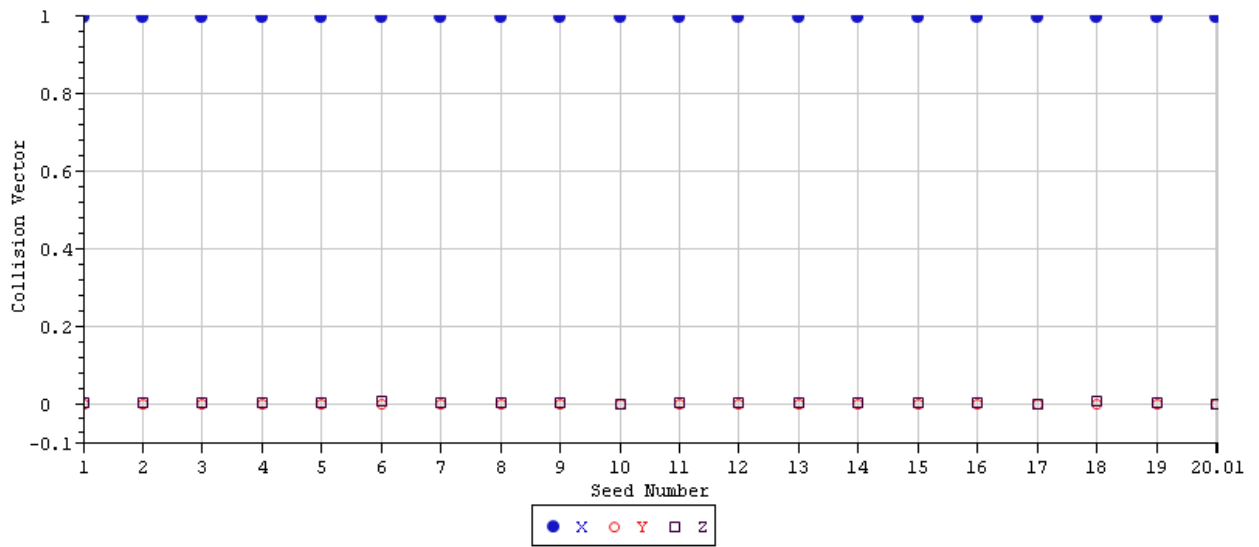


Figure 68: Collision vector components for different seeds, for case number 5.

6 Collision Scenario Number 6

	1	2	3	4	5
Signals		Max	Min	Mean	St. Dev.
RelativeCollisionVelocity	[m/s]	3.46	0.15	1.59	1.04
IceVelocity	[m/s]	5.02	0.93	2.41	1.13
CollisionHeight	[m]	28.13	14.22	21.78	4.06

Table 36: Statistical values calculated for collision scenario number 6.

	1	2	3	4
Signals		MP	Exp	P90
RelativeCollisionVelocity	[m/s]	1.11	1.41	2.98
IceVelocity	[m/s]	1.89	2.22	3.92
CollisionHeight	[m]	19.92	21.1	27.23

Table 37: Statistical values calculated for collision scenario number 6.

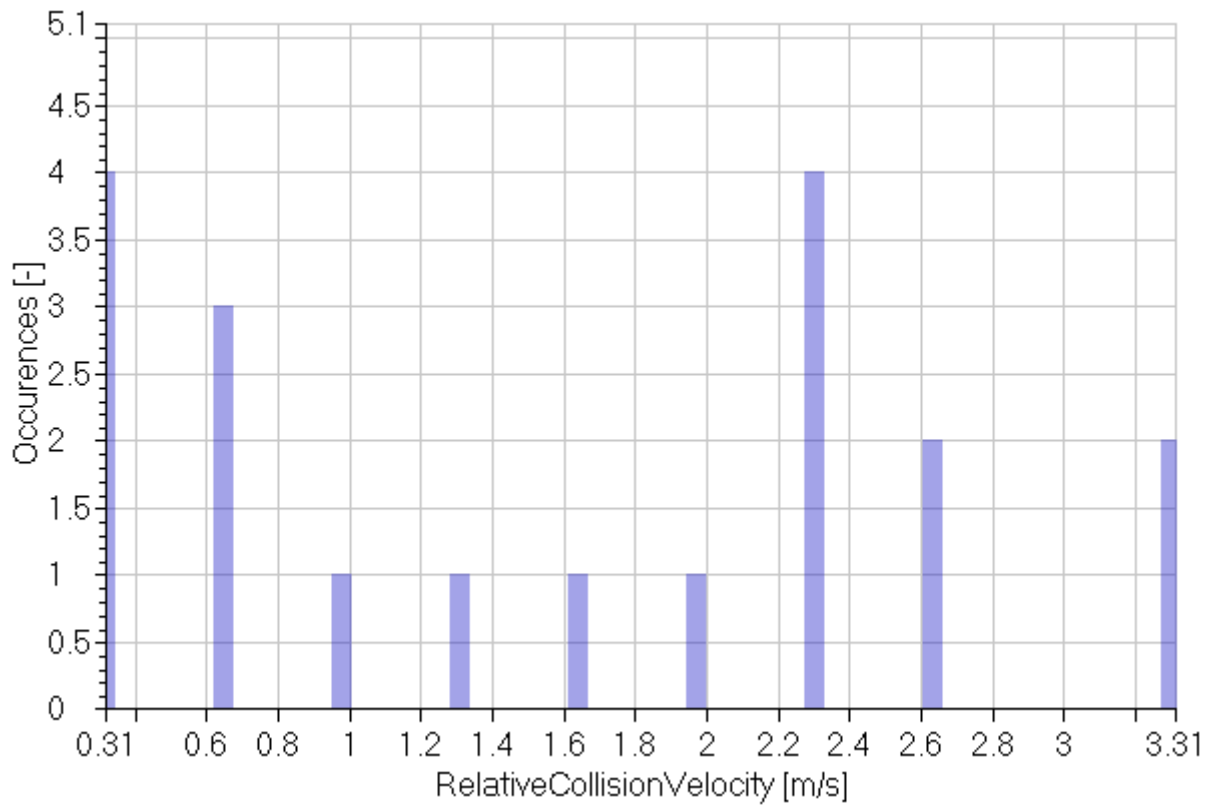


Figure 69: collision scenario number 6

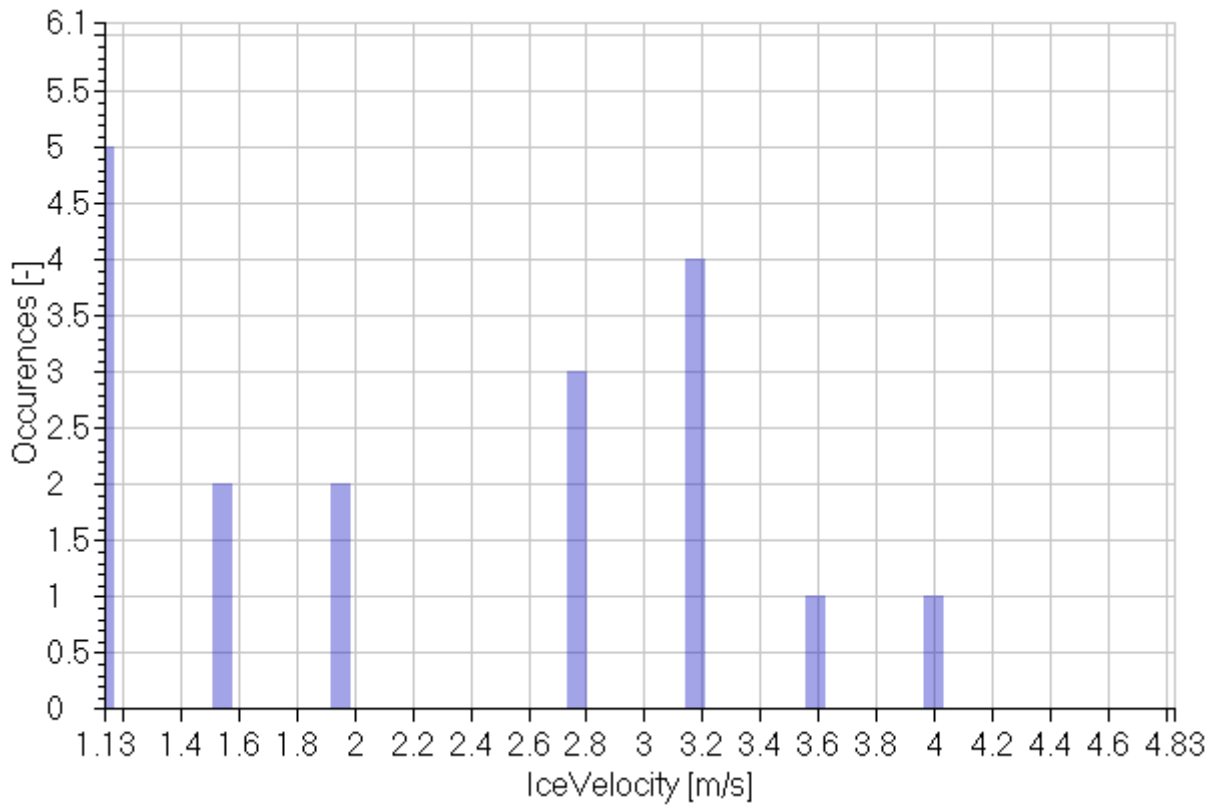


Figure 70: collision scenario number 6

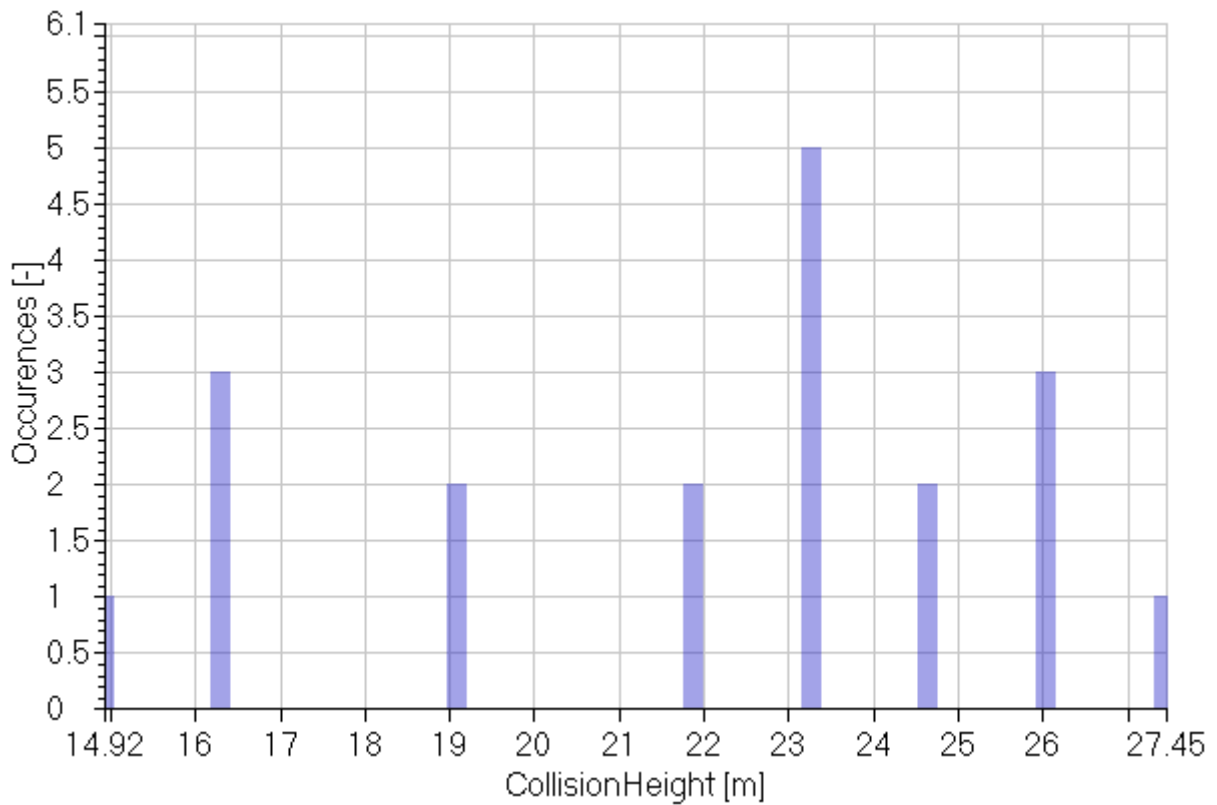


Figure 71: collision scenario number 6

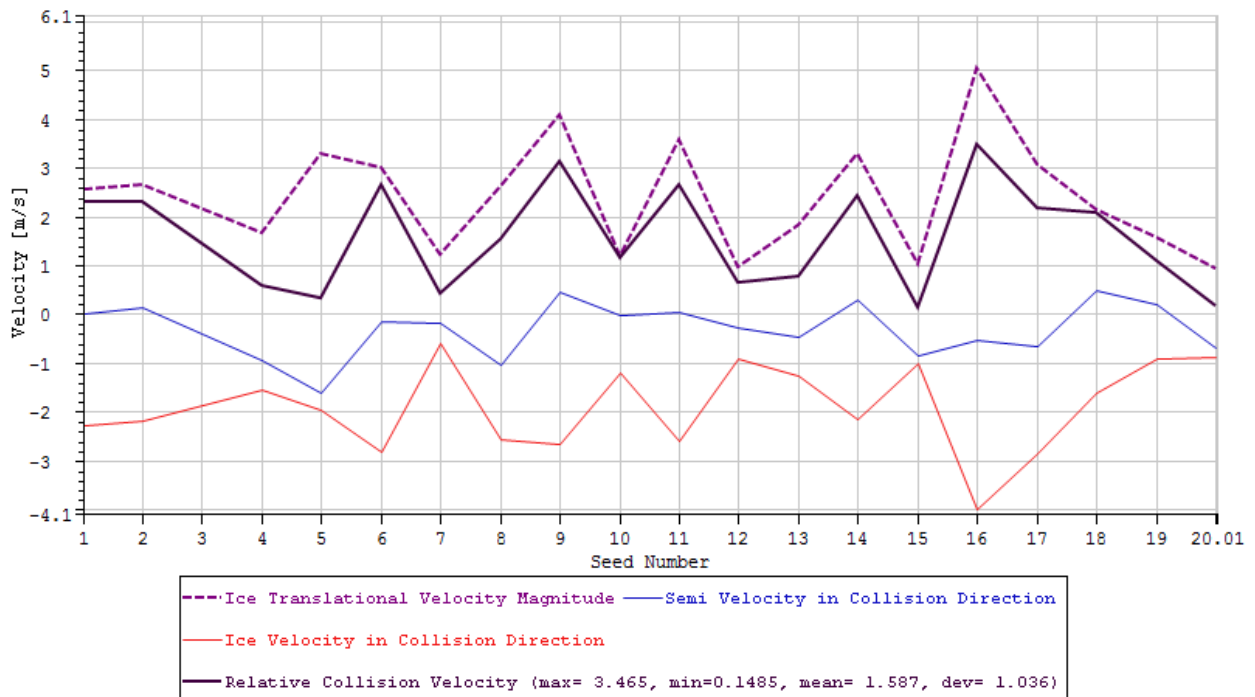


Figure 72: Total and relative collision velocities of ice and platform for different seeds, for case number 6.

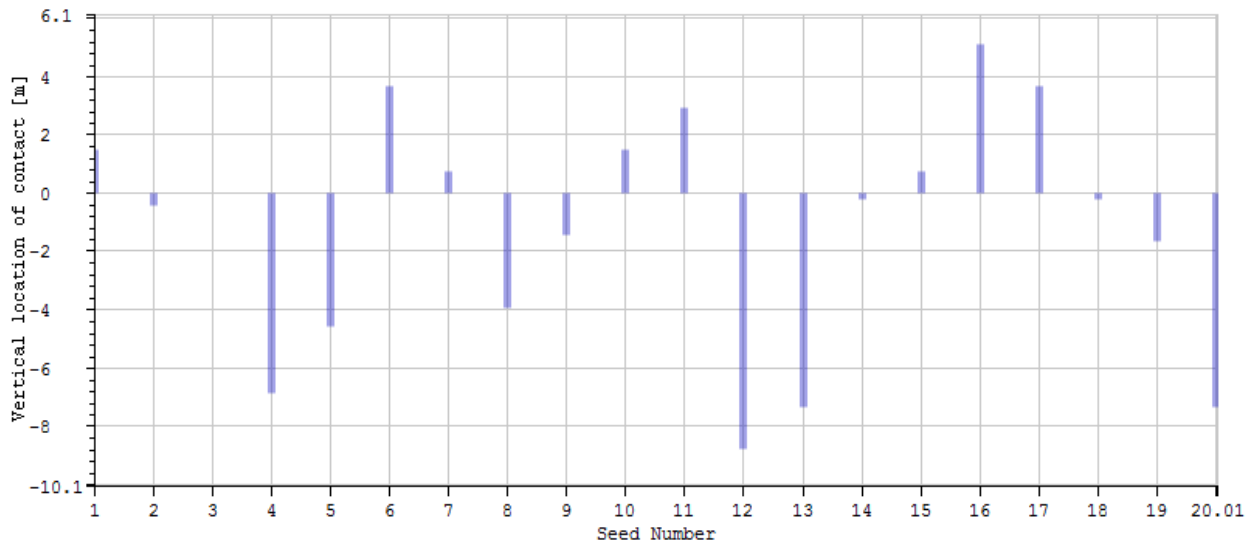


Figure 73: Vertical location of impact on the platform for different seeds, for case number 6.

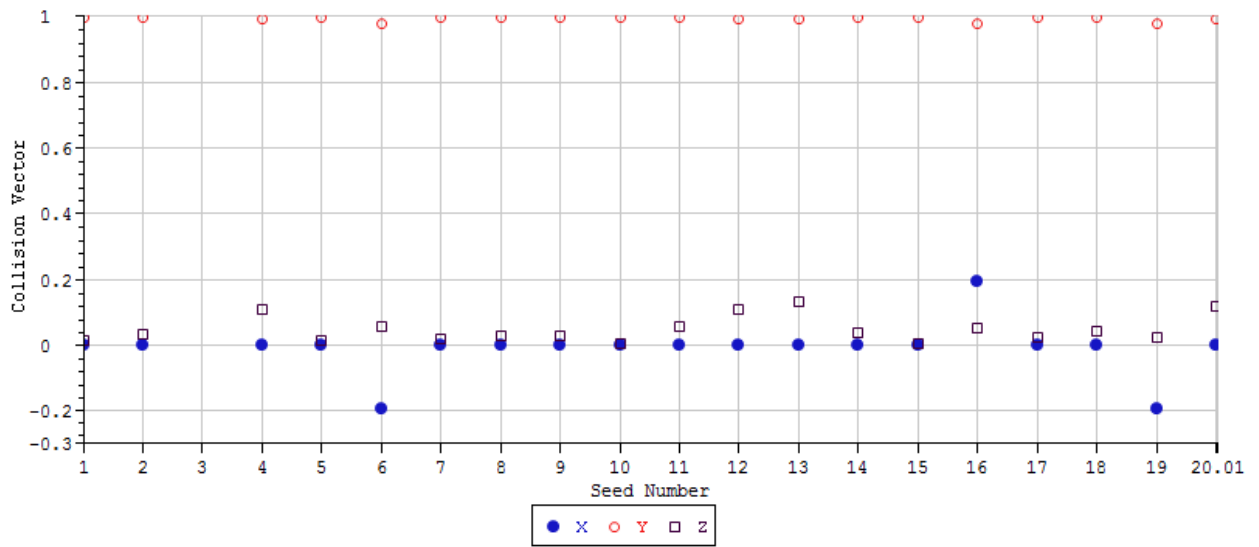


Figure 74: Collision vector components for different seeds, for case number 6.

7 Collision Scenario Number 7

	1	2	3	4	5
Signals		Max	Min	Mean	St. Dev.
RelativeCollisionVelocity	[m/s]	4.23	0.24	2.12	1.13
IceVelocity	[m/s]	5	0.75	2.52	1.05
CollisionHeight	[m]	28.13	17.06	23.89	2.12

Table 38: Statistical values calculated for collision scenario number 7.

	1	2	3	4
Signals		MP	Exp	P90
RelativeCollisionVelocity	[m/s]	1.61	1.93	3.64
IceVelocity	[m/s]	2.04	2.34	3.92
CollisionHeight	[m]	22.92	23.53	26.72

Table 39: Statistical values calculated for collision scenario number 7.

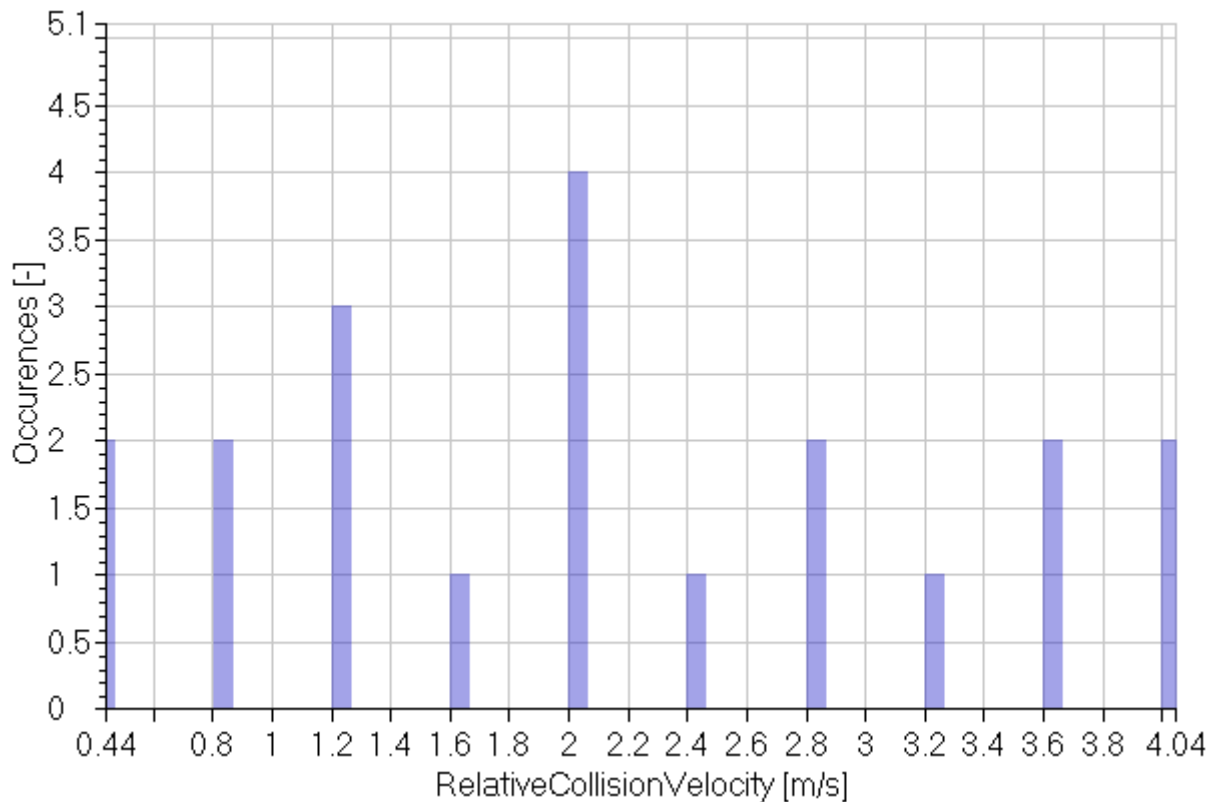


Figure 75: collision scenario number 7

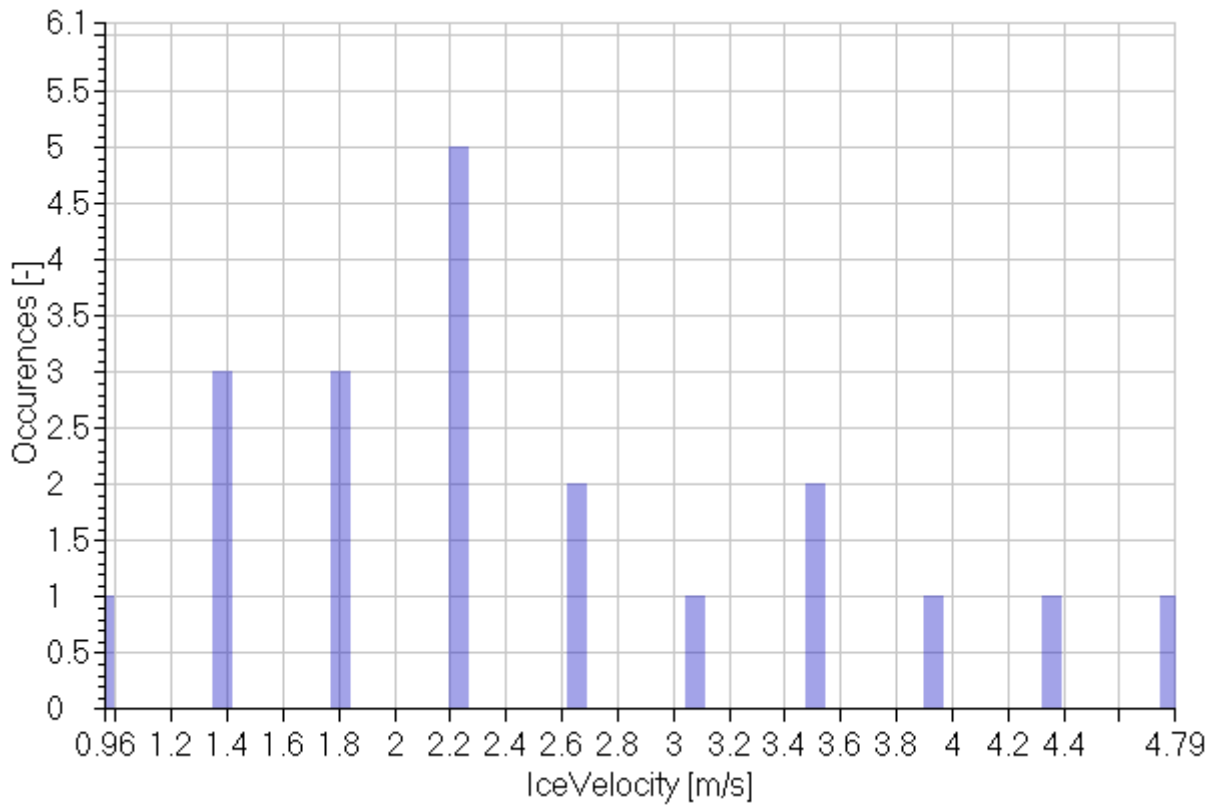


Figure 76: collision scenario number 7

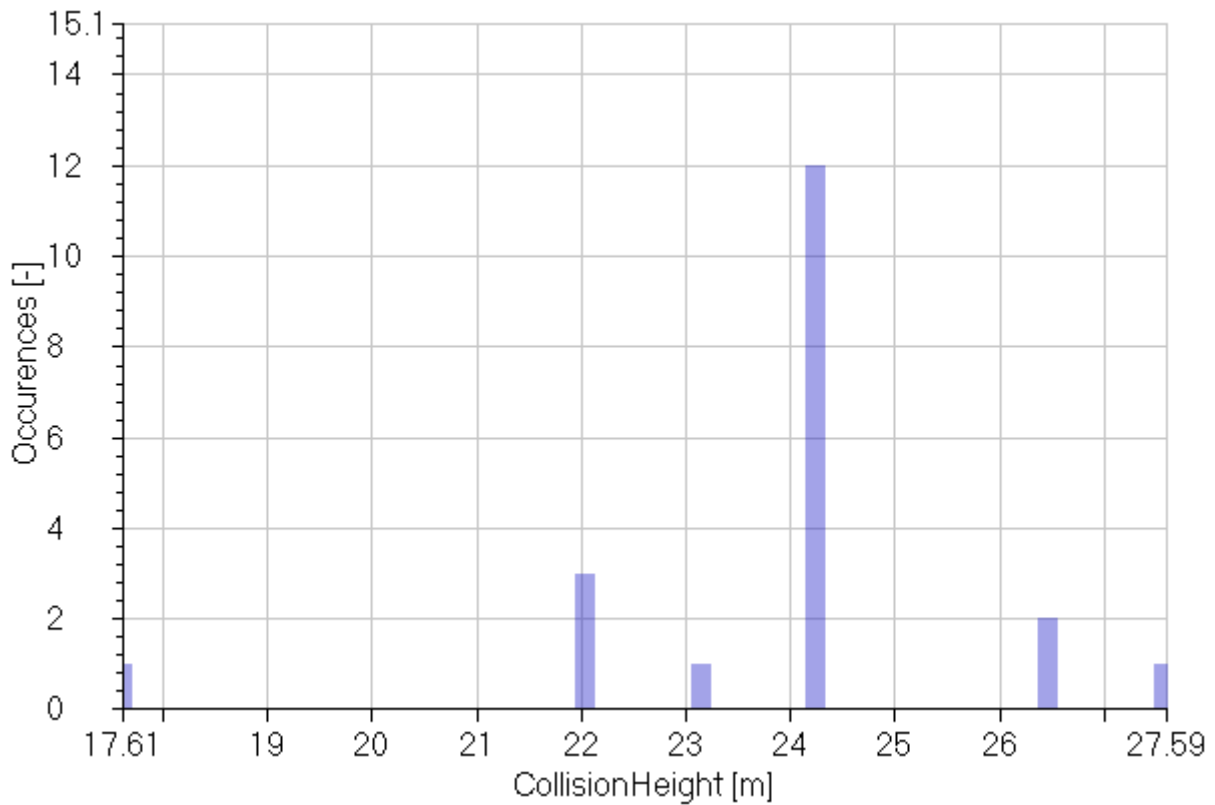


Figure 77: collision scenario number 7

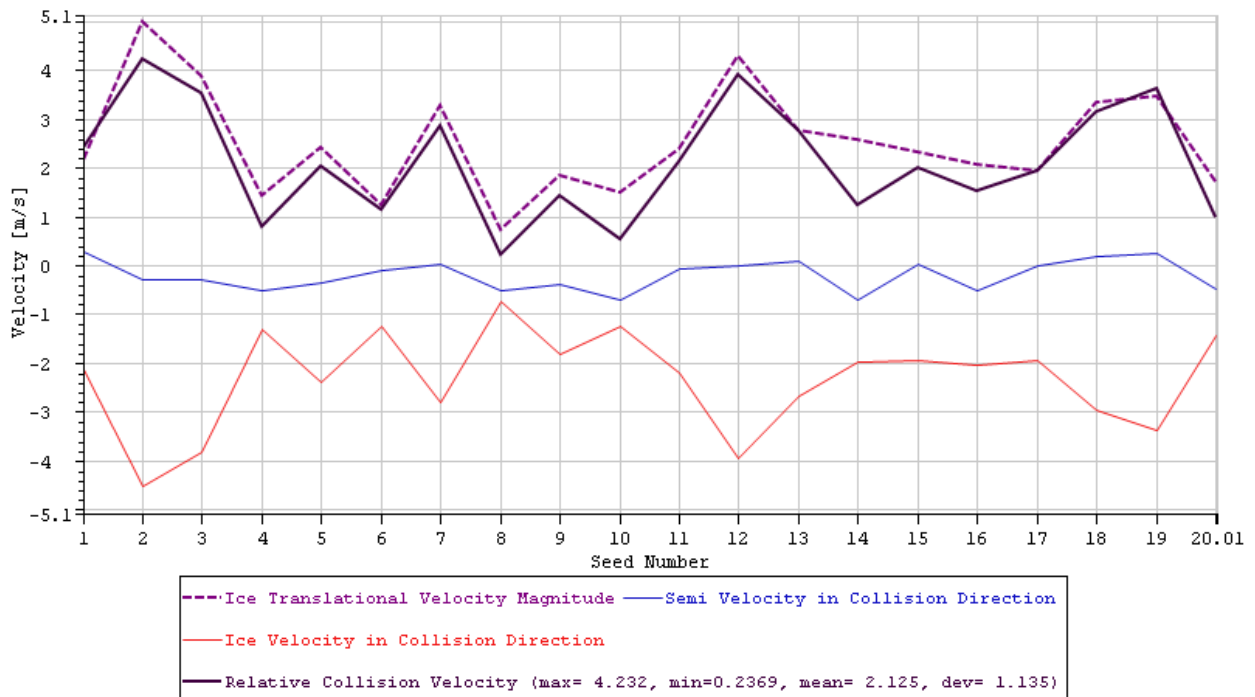


Figure 78: Total and relative collision velocities of ice and platform for different seeds, for case number 7.

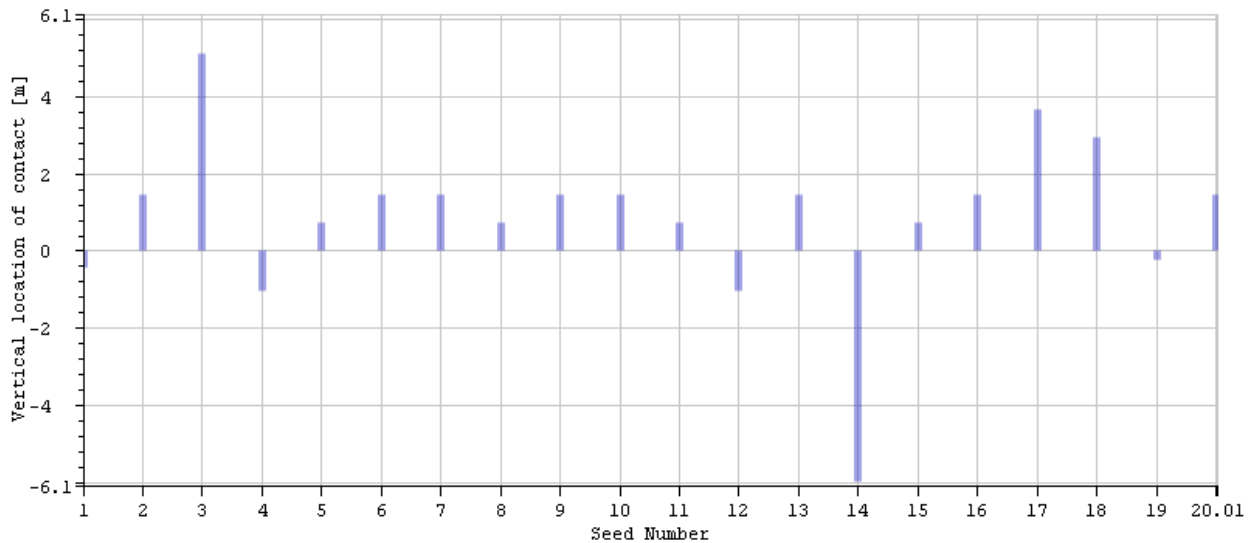


Figure 79: Vertical location of impact on the platform for different seeds, for case number 7.

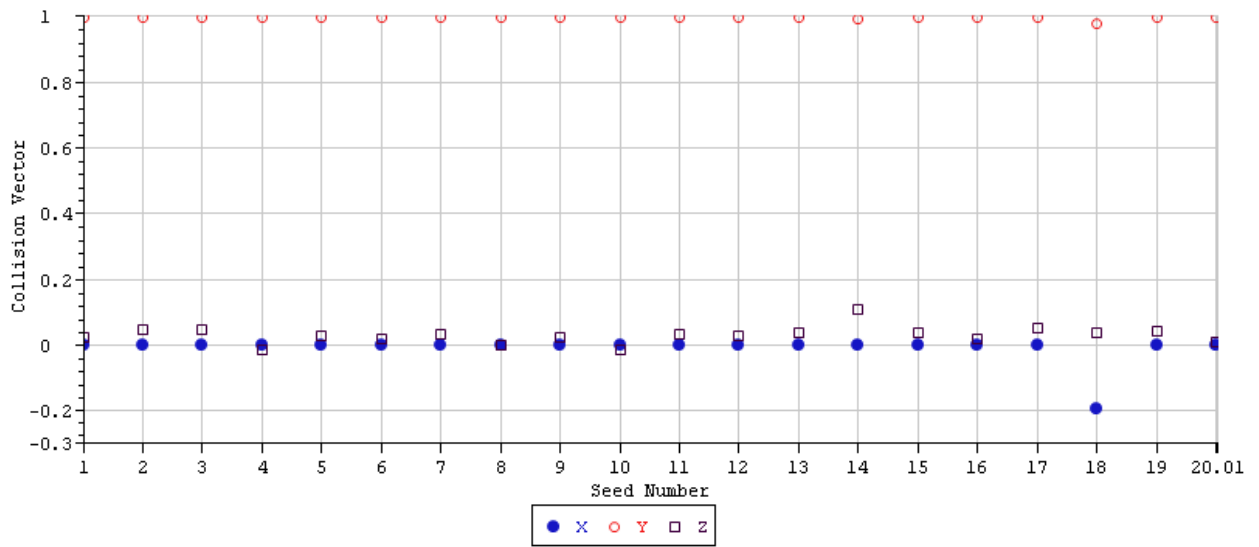


Figure 80: Collision vector components for different seeds, for case number 7.

8 Collision Scenario Number 8

	1	2	3	4	5
Signals		Max	Min	Mean	St. Dev.
RelativeCollisionVelocity	[m/s]	2.77	0.42	1.44	0.61
IceVelocity	[m/s]	2.77	0.65	1.63	0.57
CollisionHeight	[m]	23.73	14.22	20.97	2.42

Table 40: Statistical values calculated for collision scenario number 8.

	1	2	3	4
Signals		MP	Exp	P90
RelativeCollisionVelocity	[m/s]	1.15	1.33	2.26
IceVelocity	[m/s]	1.36	1.53	2.39
CollisionHeight	[m]	19.86	20.56	24.21

Table 41: Statistical values calculated for collision scenario number 8.

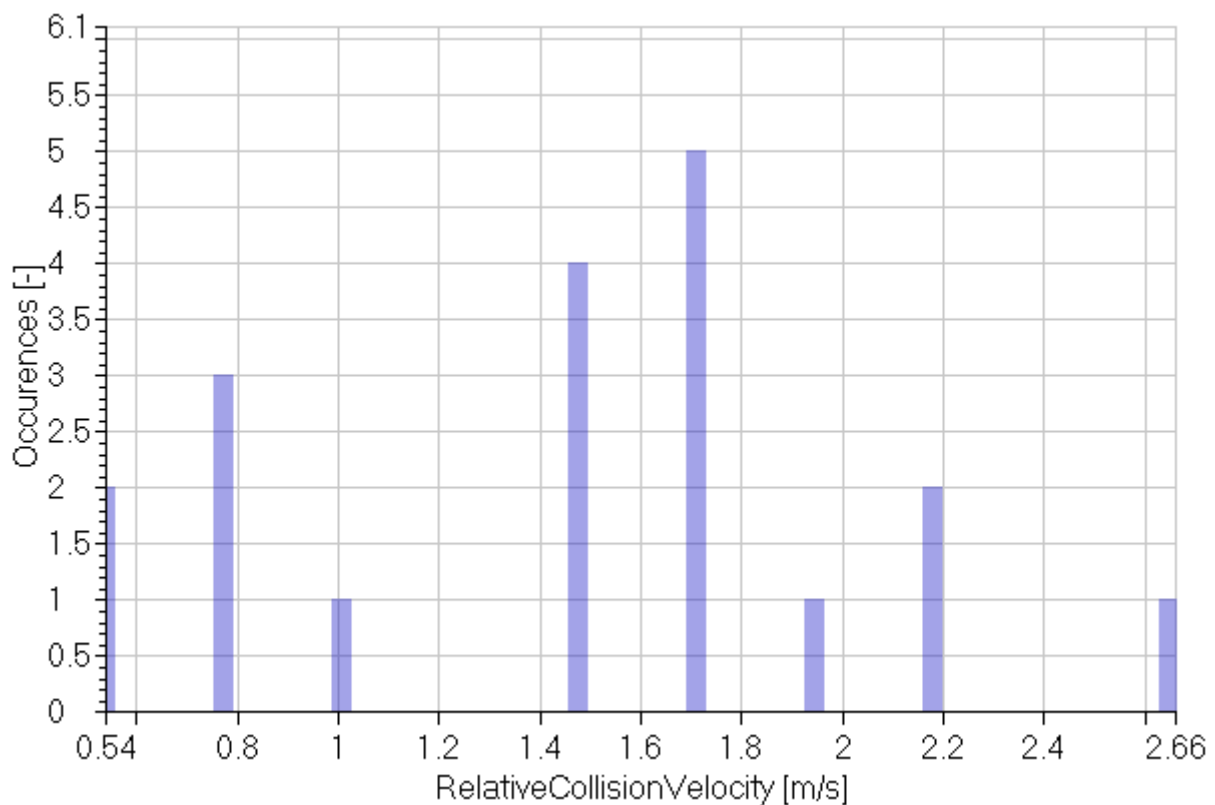


Figure 81: collision scenario number 8

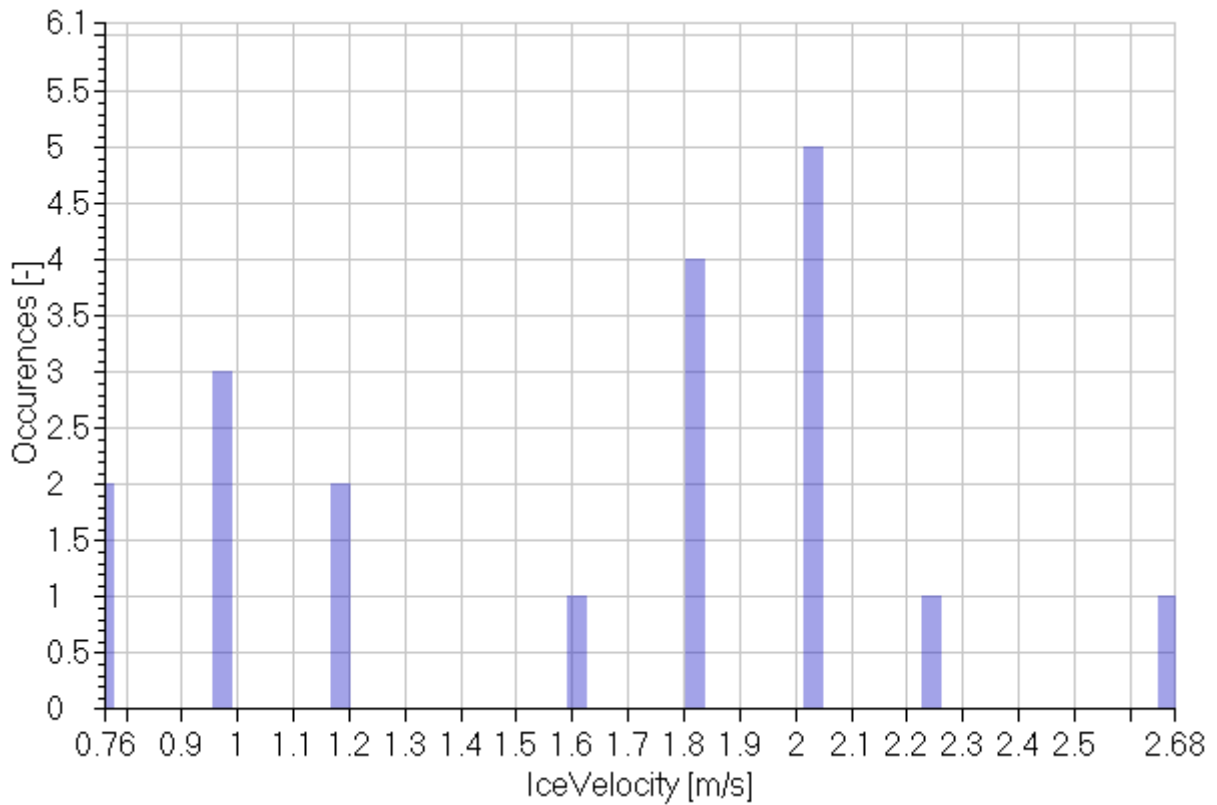


Figure 82: collision scenario number 8

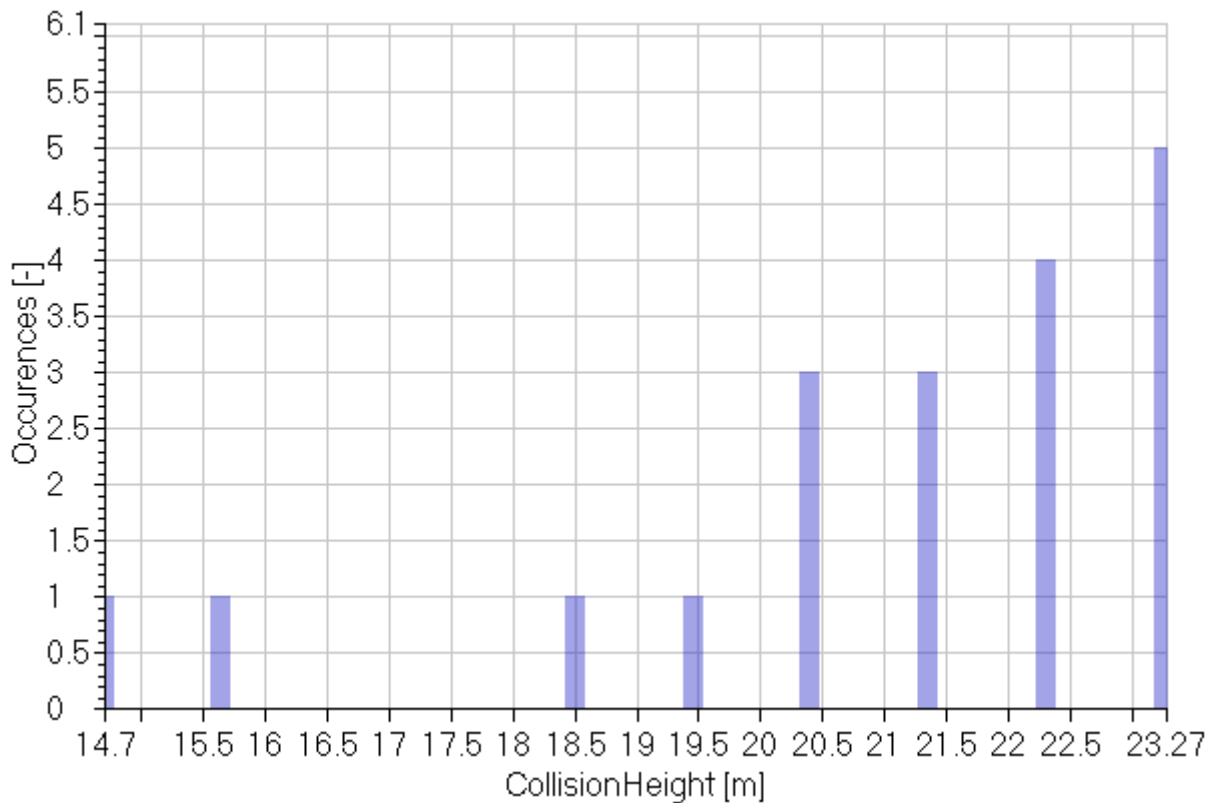


Figure 83: collision scenario number 8

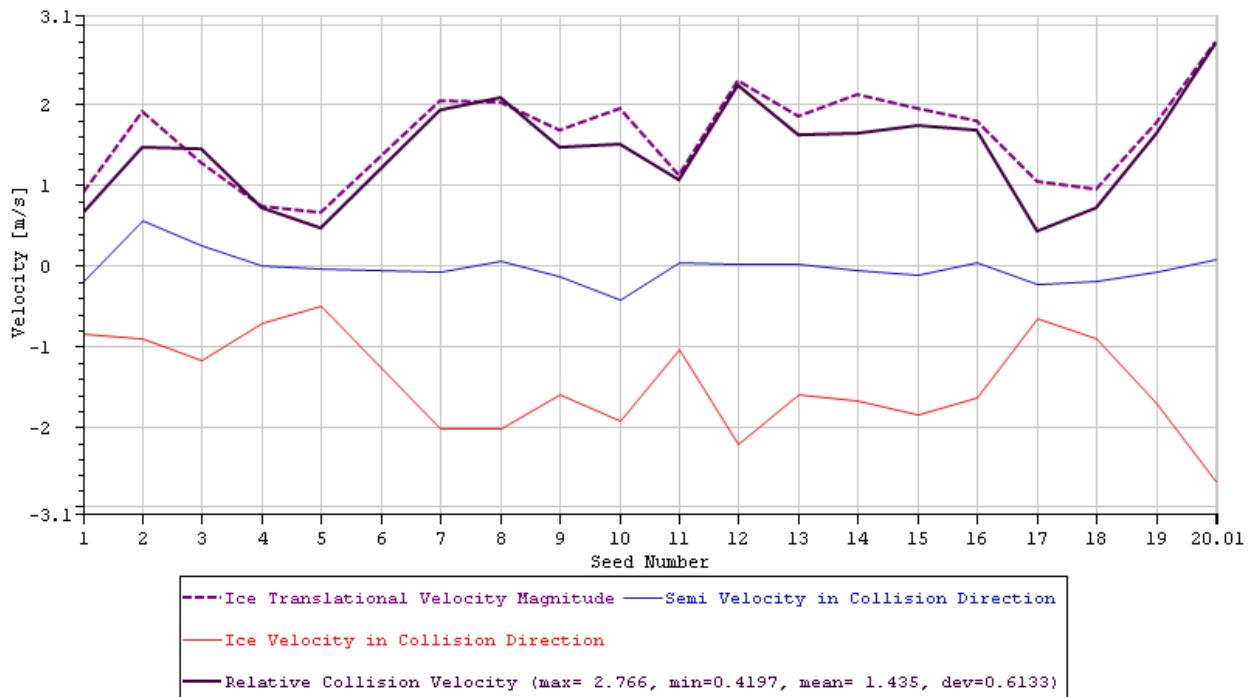


Figure 84: Total and relative collision velocities of ice and platform for different seeds, for case number 8.

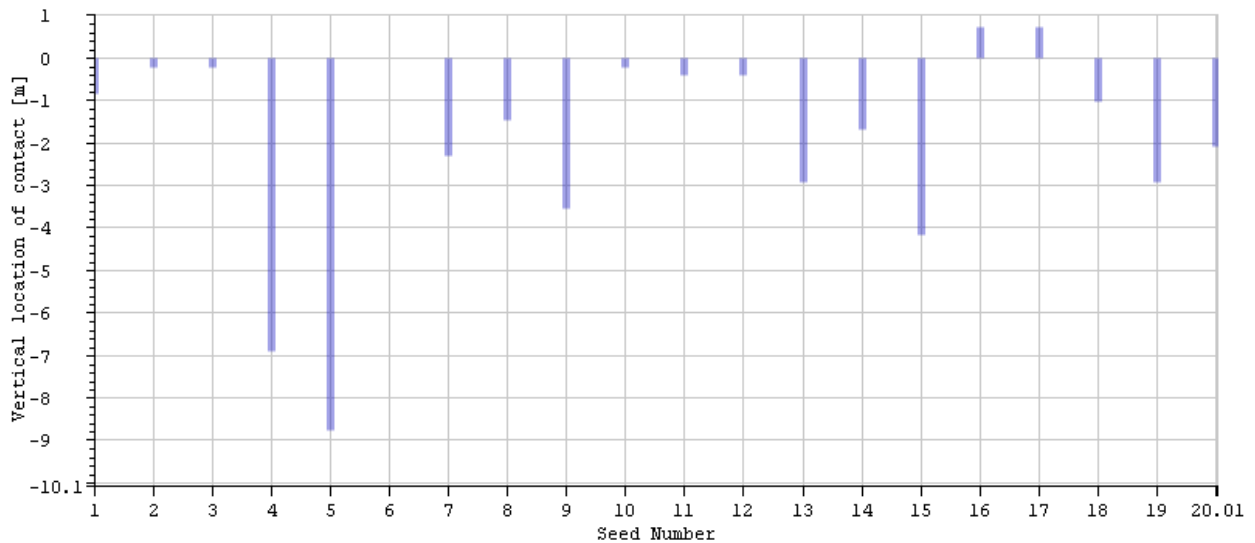


Figure 85: Vertical location of impact on the platform for different seeds, for case number 8.

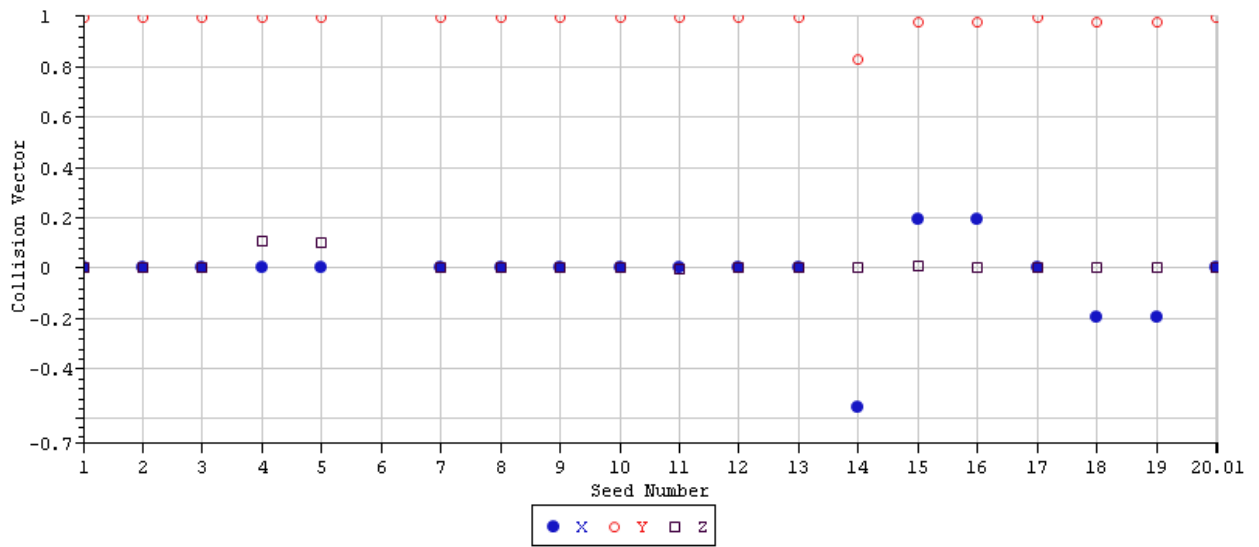


Figure 86: Collision vector components for different seeds, for case number 8.

9 Collision Scenario Number 9

	1	2	3	4	5
Signals		Max	Min	Mean	St. Dev.
RelativeCollisionVelocity	[m/s]	3.9	0.27	2.06	1.11
IceVelocity	[m/s]	4.87	0.73	2.48	1.2
CollisionHeight	[m]	25.93	14.22	20.28	4.4

Table 42: Statistical values calculated for collision scenario number 9.

	1	2	3	4
Signals		MP	Exp	P90
RelativeCollisionVelocity	[m/s]	1.55	1.87	3.55
IceVelocity	[m/s]	1.93	2.28	4.08
CollisionHeight	[m]	18.27	19.54	26.16

Table 43: Statistical values calculated for collision scenario number 9.

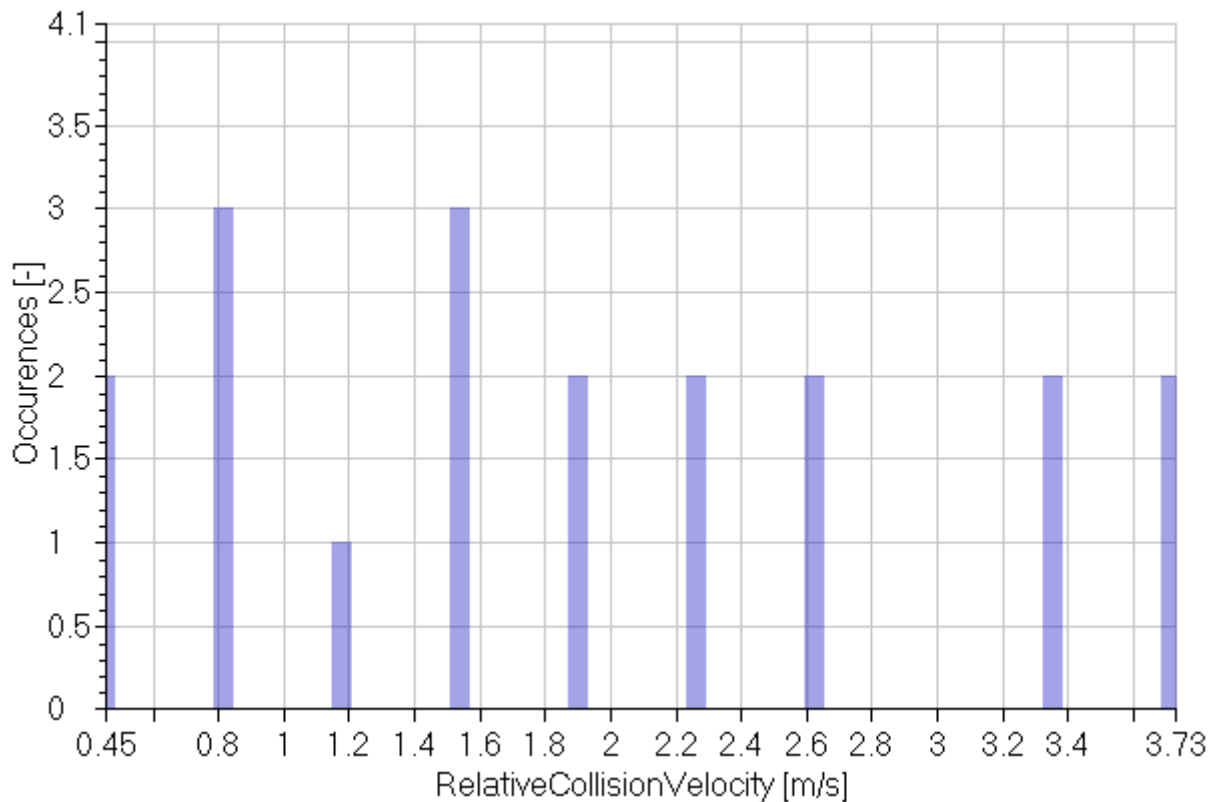


Figure 87: collision scenario number 9

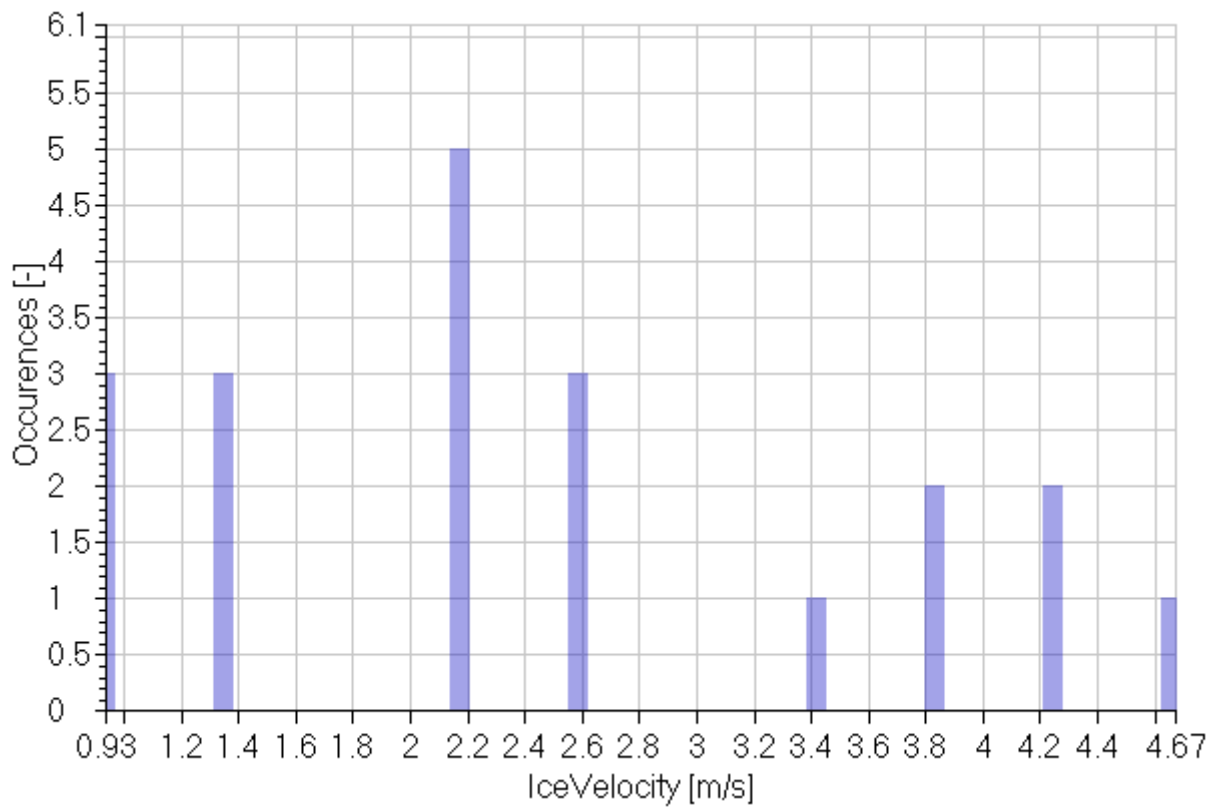


Figure 88: collision scenario number 9

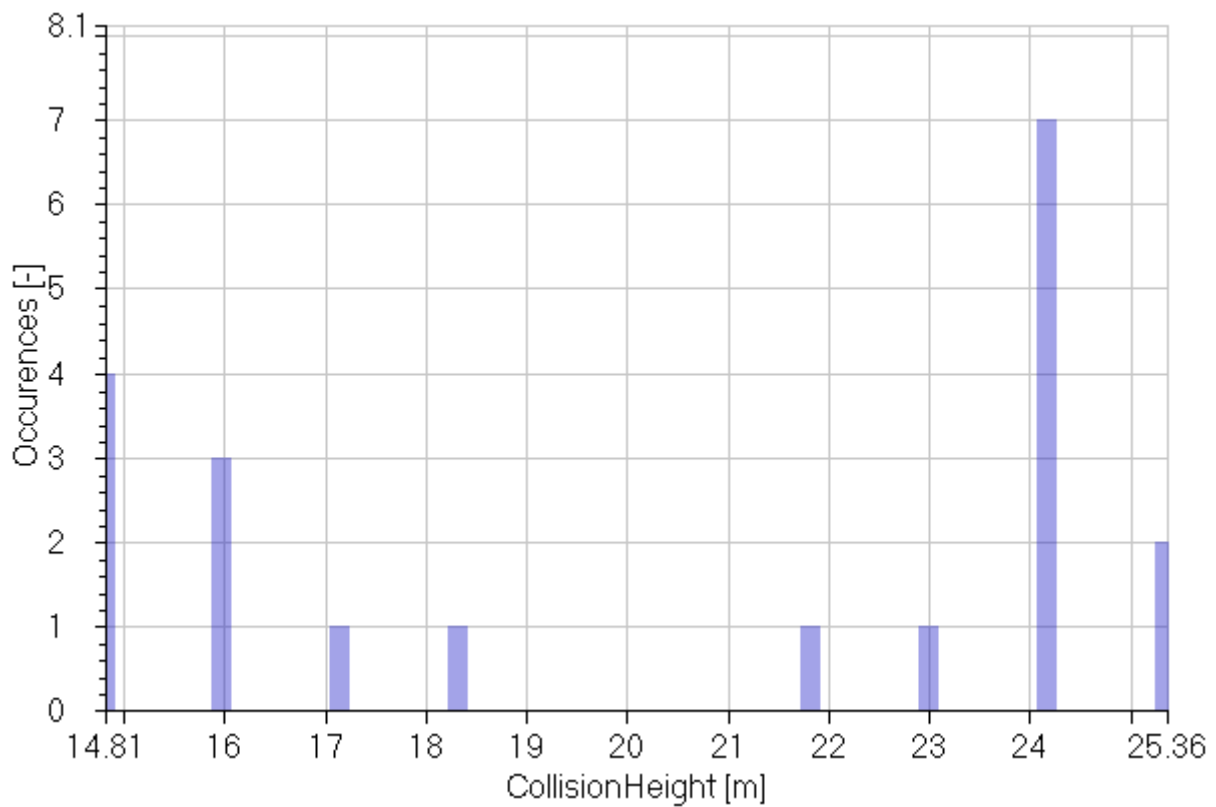


Figure 89: collision scenario number 9

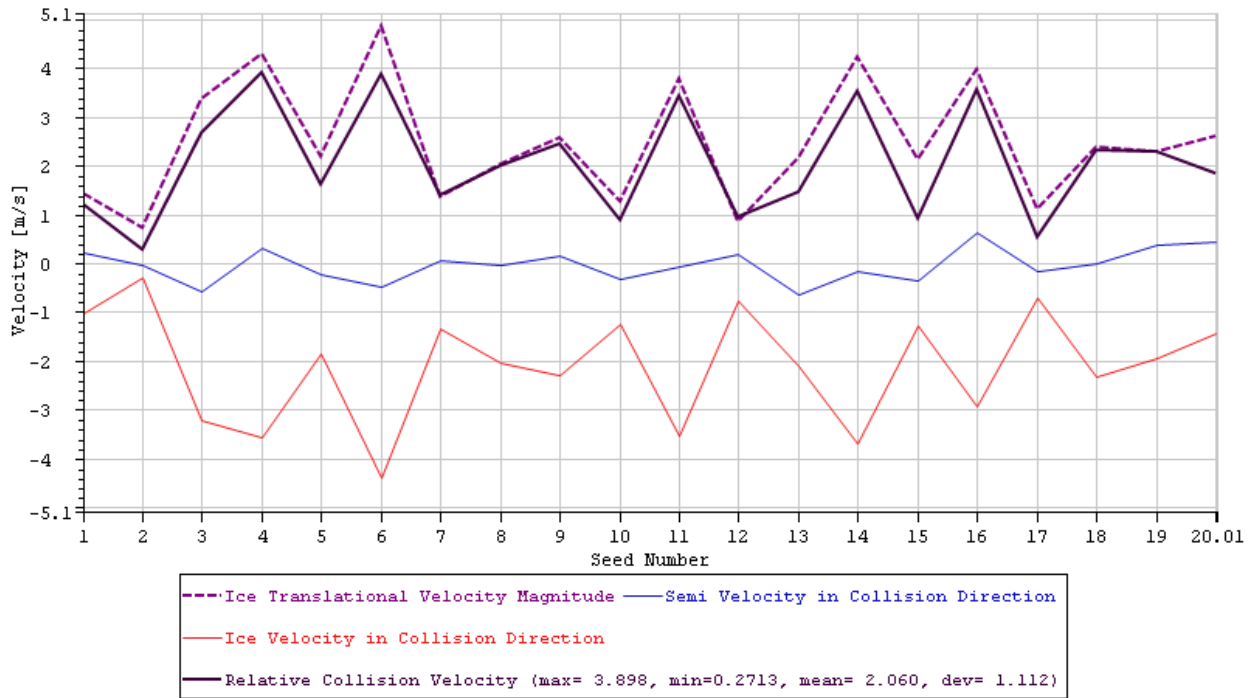


Figure 90: Total and relative collision velocities of ice and platform for different seeds, for case number 9.

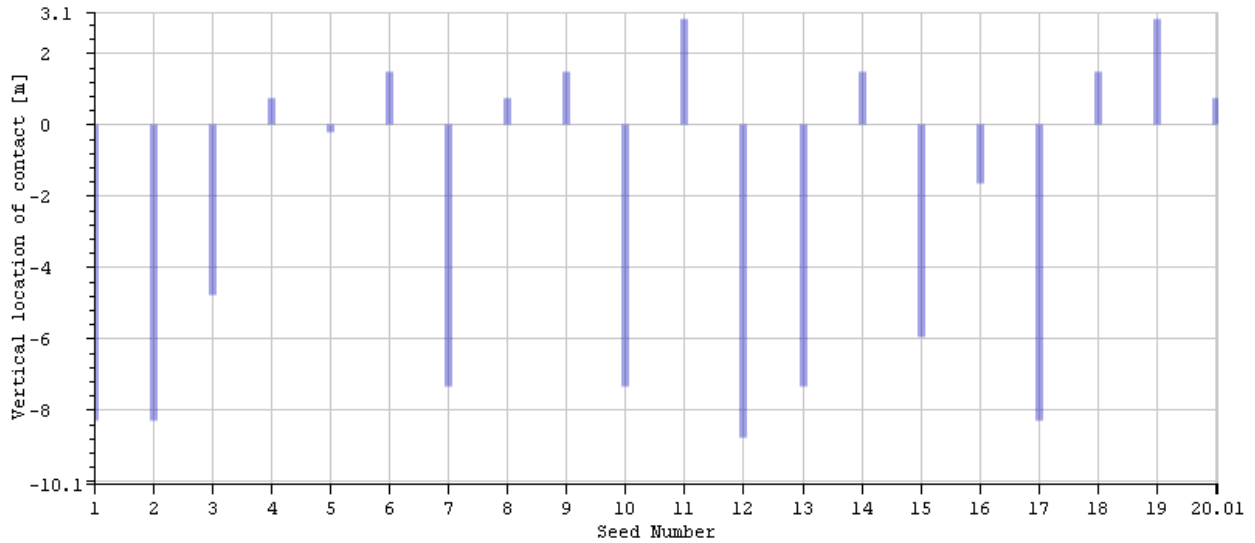


Figure 91: Vertical location of impact on the platform for different seeds, for case number 9.

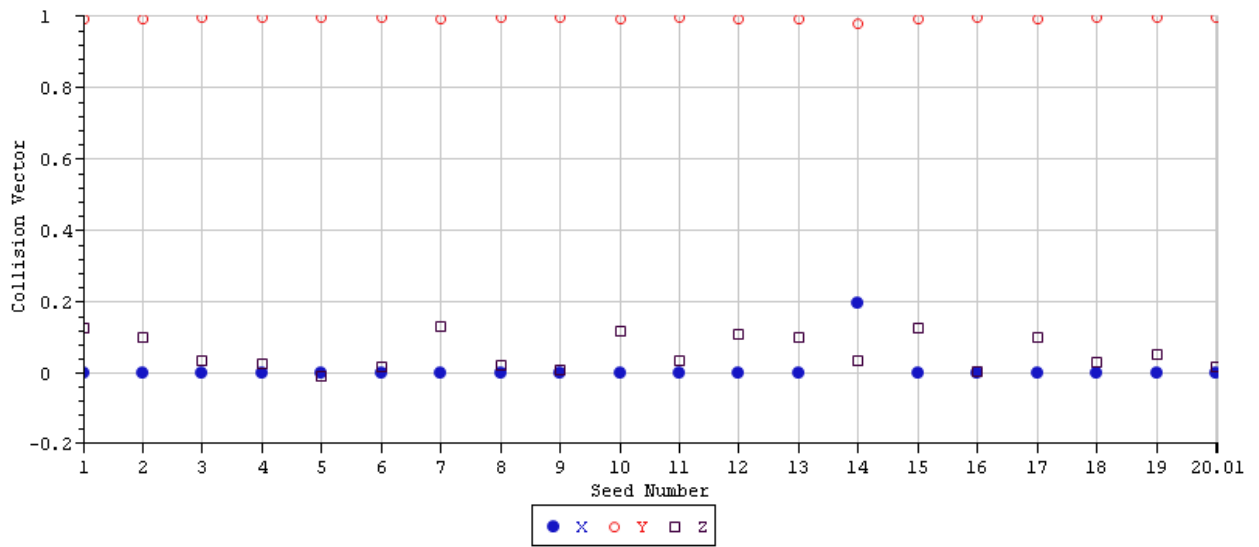


Figure 92: Collision vector components for different seeds, for case number 9.

10 Collision Scenario Number 10

	1	2	3	4	5
Signals		Max	Min	Mean	St. Dev.
RelativeCollisionVelocity	[m/s]	5.16	0.67	2.24	1.22
IceVelocity	[m/s]	5.34	0.63	2.5	1.28
CollisionHeight	[m]	25.93	13.28	20.41	4.55

Table 44: Statistical values calculated for collision scenario number 10.

	1	2	3	4
Signals		MP	Exp	P90
RelativeCollisionVelocity	[m/s]	1.69	2.04	3.87
IceVelocity	[m/s]	1.91	2.28	4.21
CollisionHeight	[m]	18.33	19.64	26.5

Table 45: Statistical values calculated for collision scenario number 10.

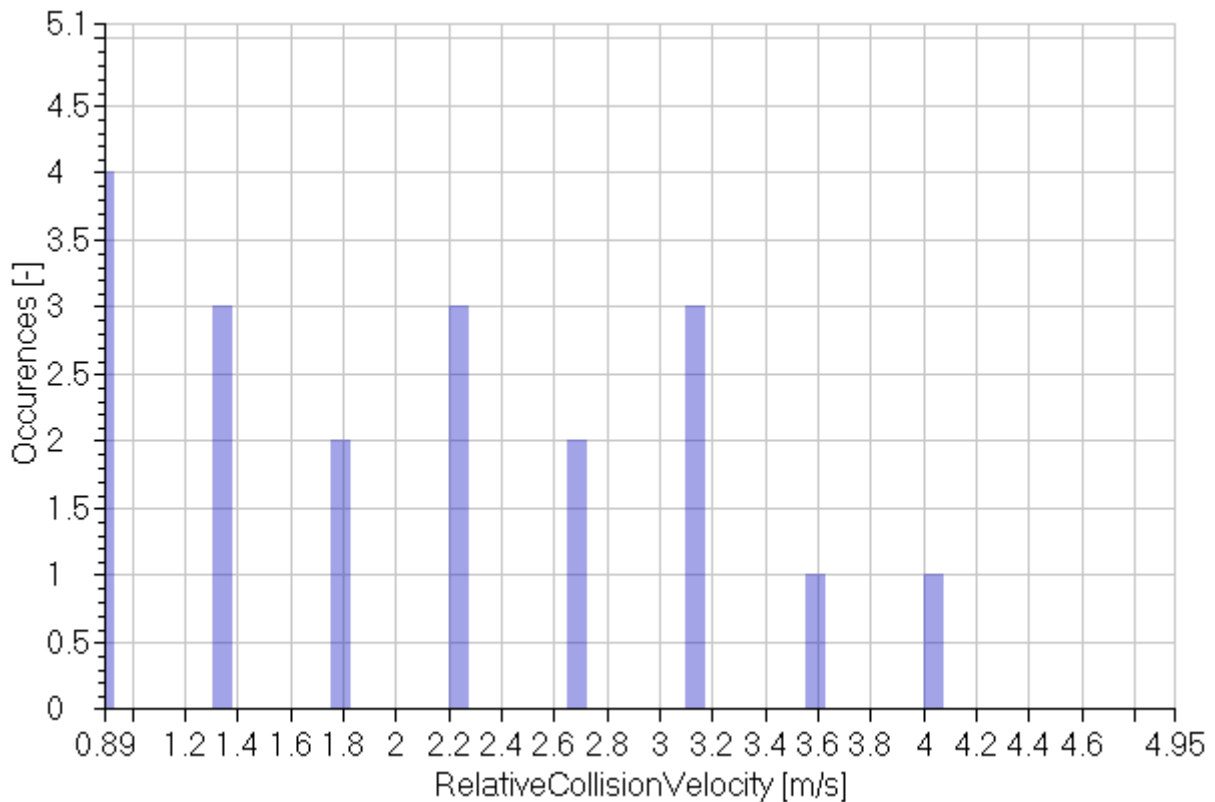


Figure 93: collision scenario number 10

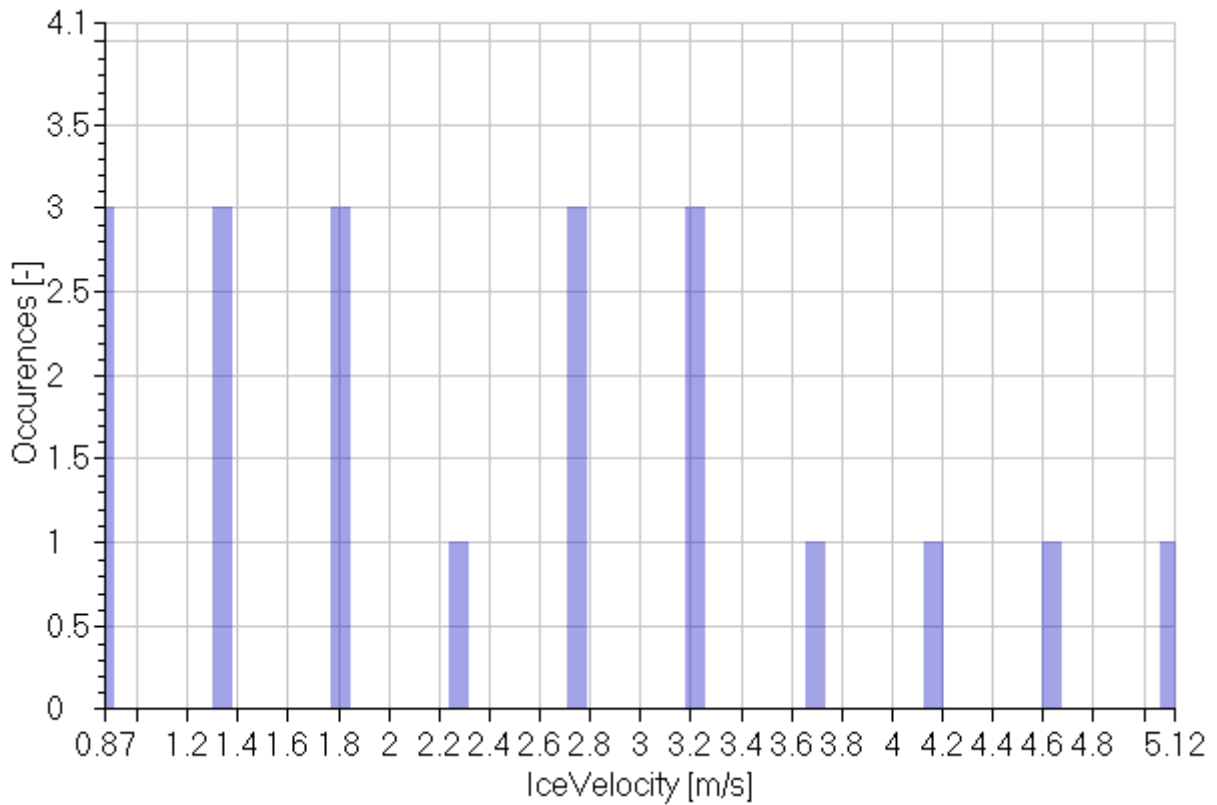


Figure 94: collision scenario number 10

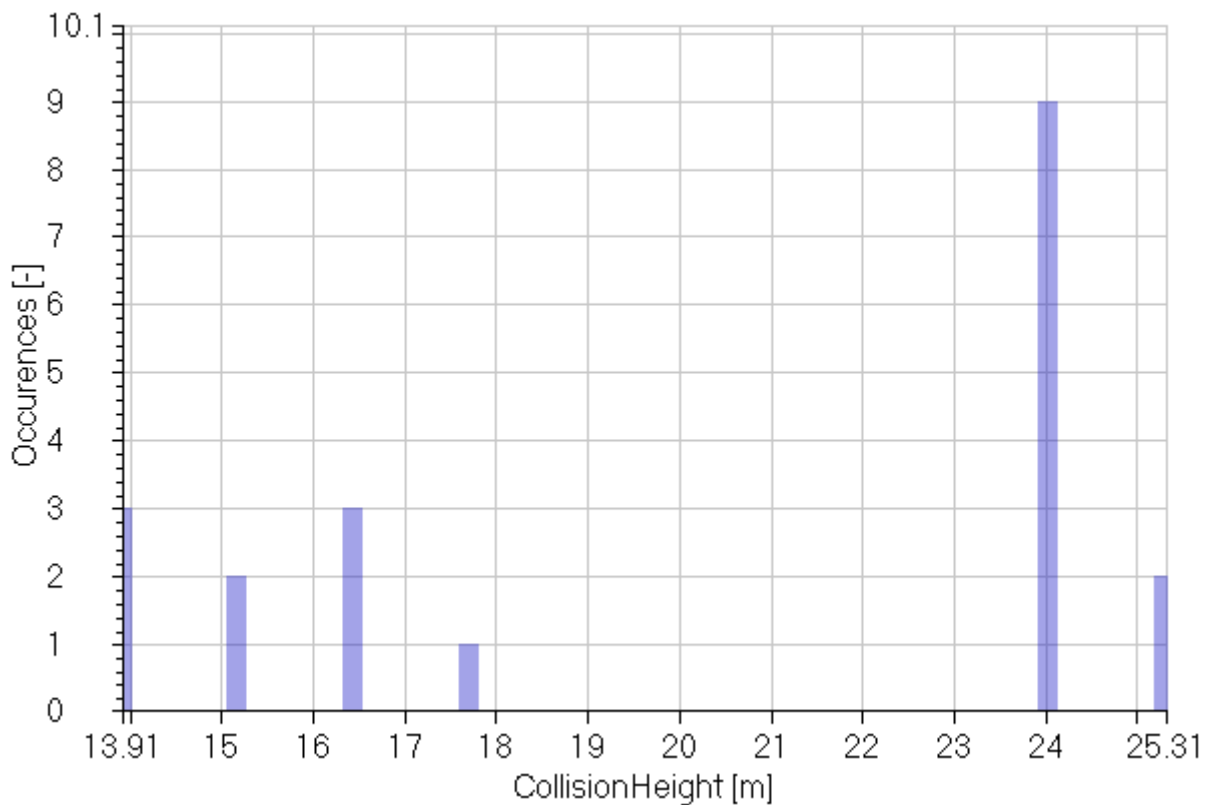


Figure 95: collision scenario number 10

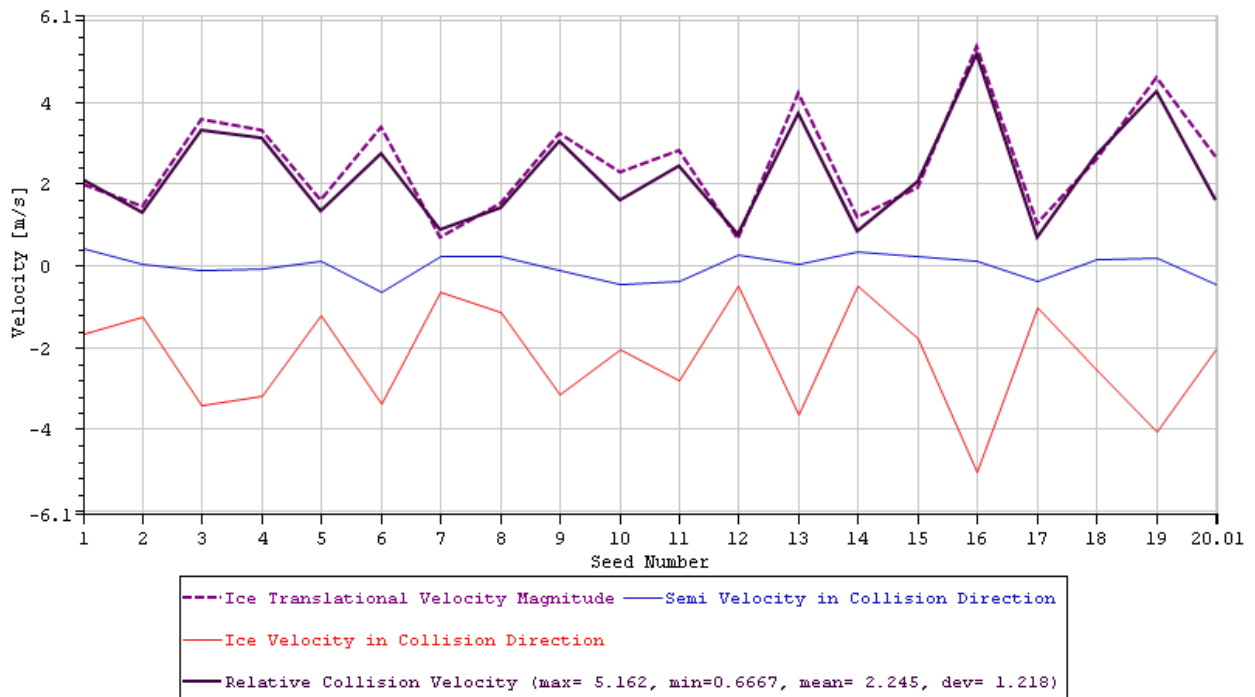


Figure 96: Total and relative collision velocities of ice and platform for different seeds, for case number 10.

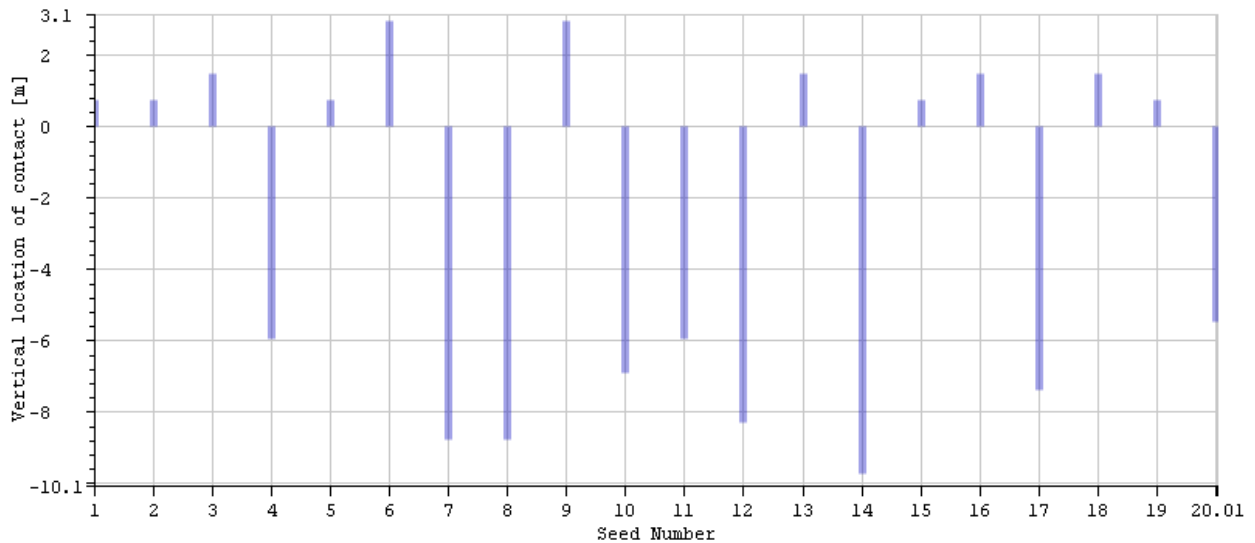


Figure 97: Vertical location of impact on the platform for different seeds, for case number 10.

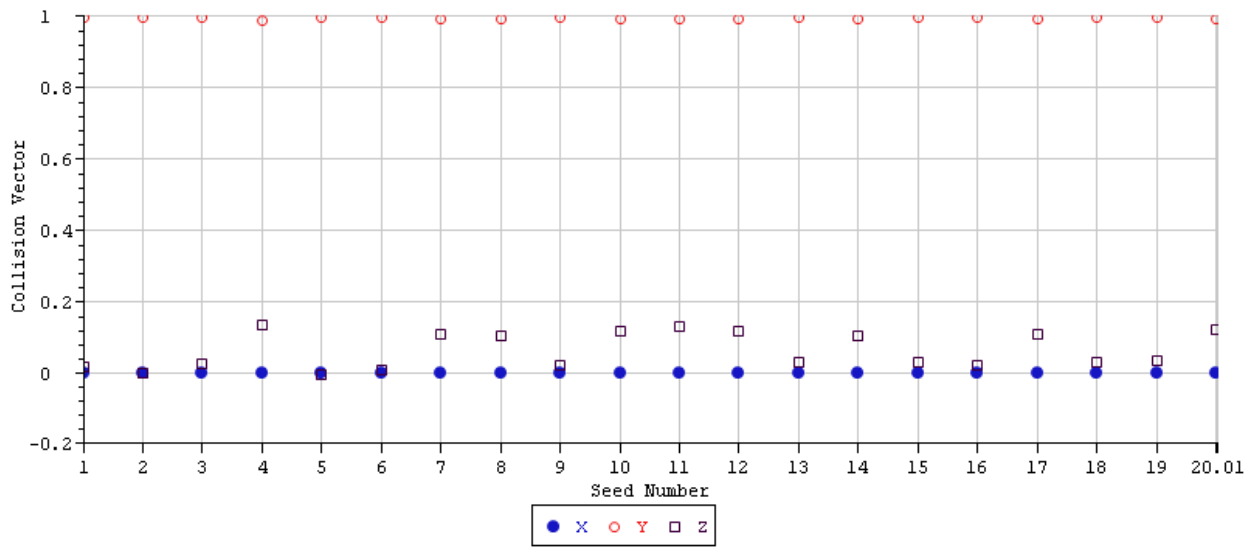


Figure 98: Collision vector components for different seeds, for case number 10.

11 Collision Scenario Number 11

	1	2	3	4	5
Signals		Max	Min	Mean	St. Dev.
RelativeCollisionVelocity	[m/s]	4.52	0.37	1.91	1.2
IceVelocity	[m/s]	4.32	0.37	2.05	1.07
CollisionHeight	[m]	24.47	14.22	18.97	4.51

Table 46: Statistical values calculated for collision scenario number 11.

	1	2	3	4
Signals		MP	Exp	P90
RelativeCollisionVelocity	[m/s]	1.36	1.7	3.52
IceVelocity	[m/s]	1.57	1.87	3.49
CollisionHeight	[m]	16.91	18.21	25

Table 47: Statistical values calculated for collision scenario number 11.

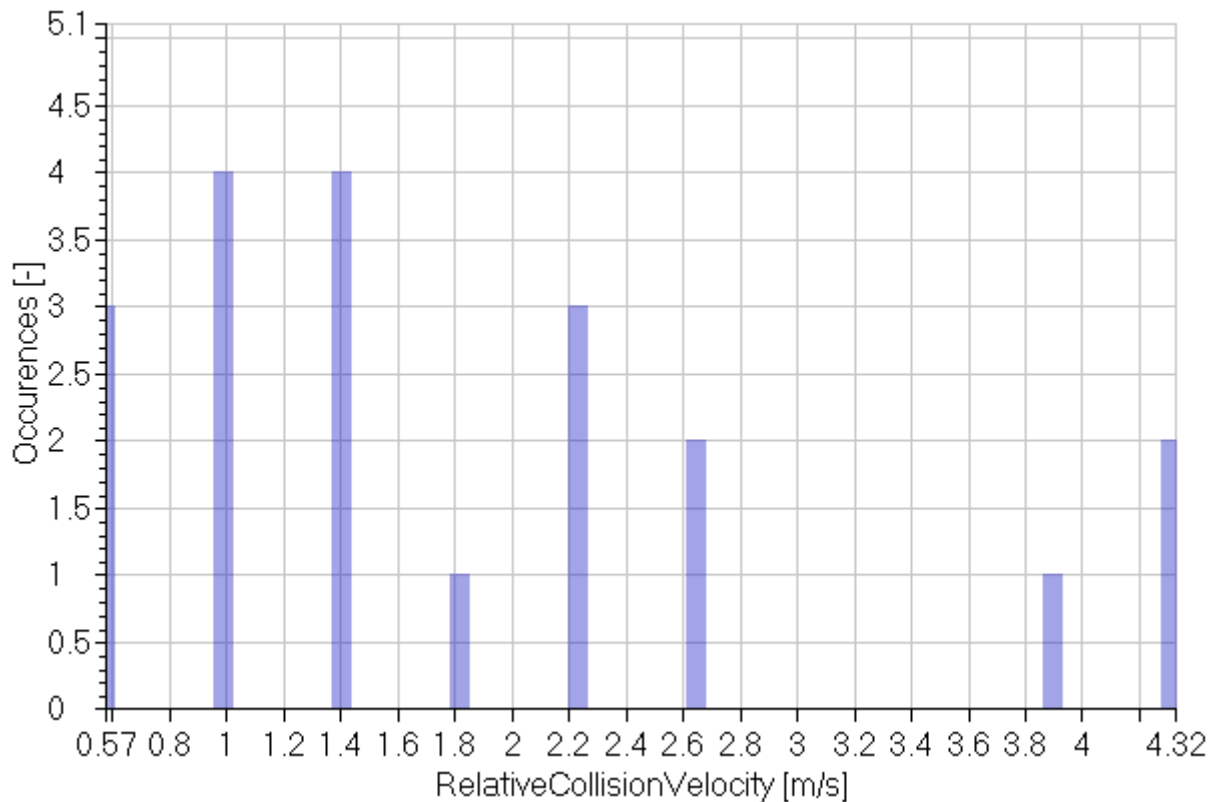


Figure 99: collision scenario number 11

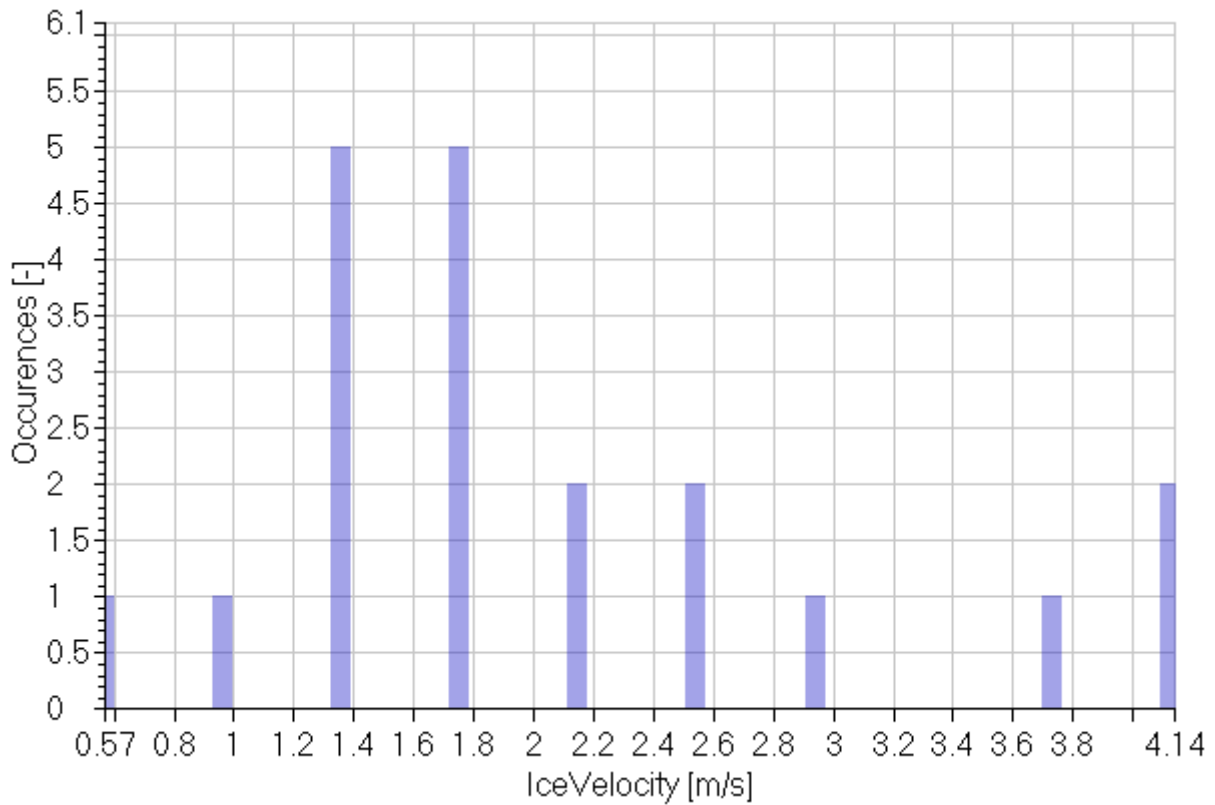


Figure 100: collision scenario number 11

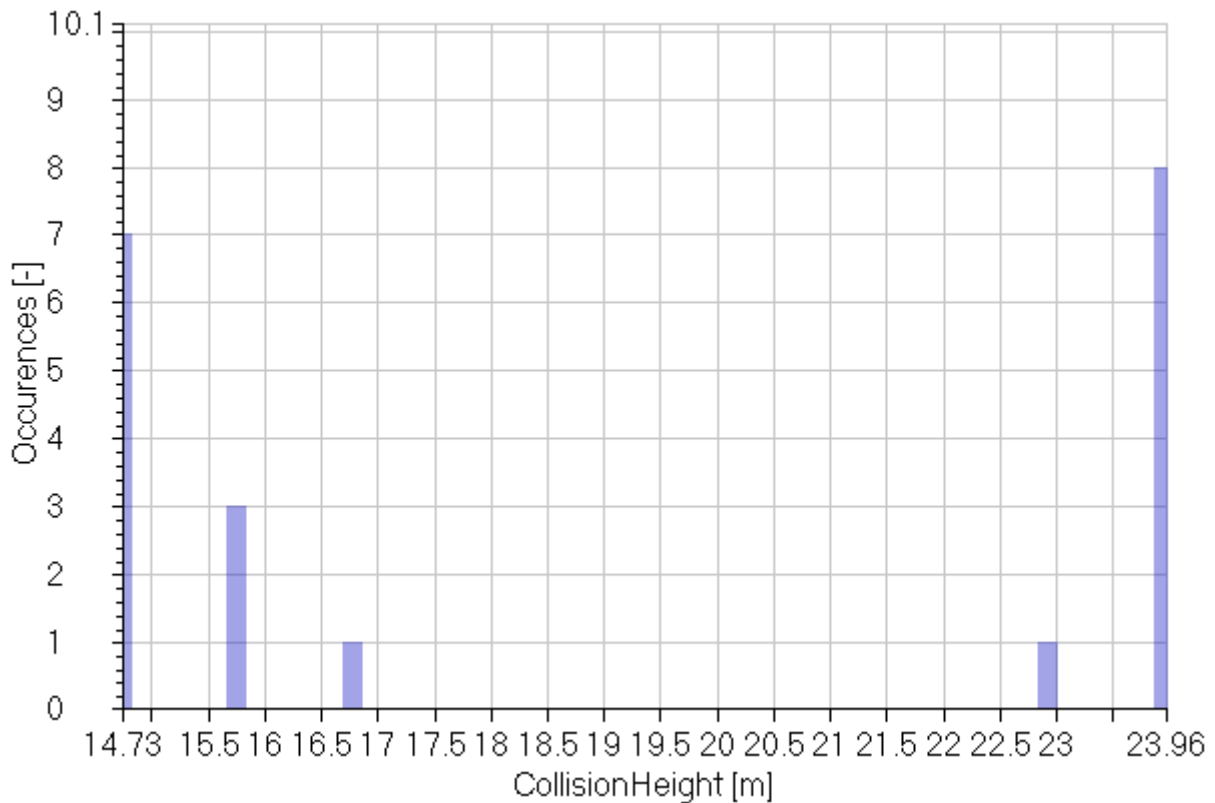


Figure 101: collision scenario number 11

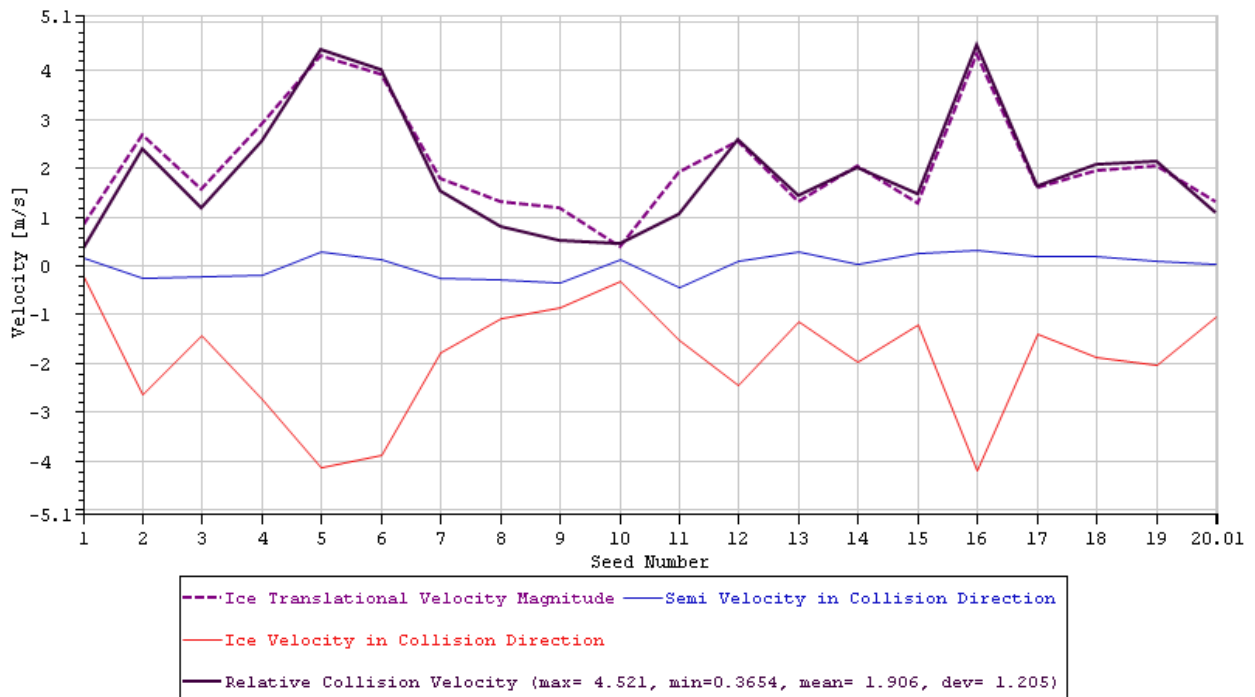


Figure 102: Total and relative collision velocities of ice and platform for different seeds, for case number 11.

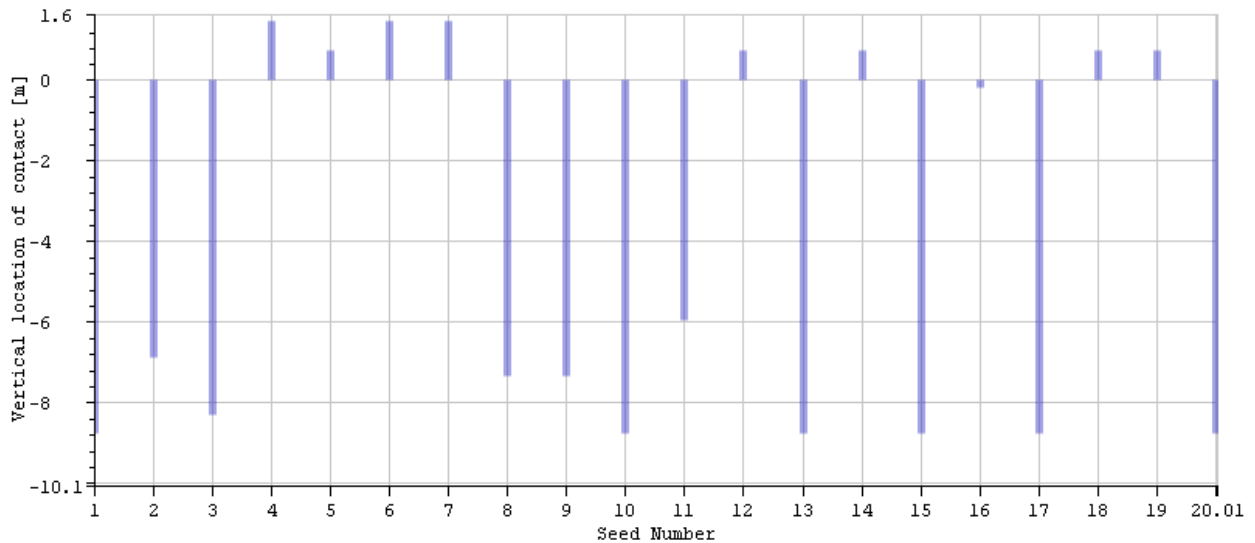


Figure 103: Vertical location of impact on the platform for different seeds, for case number 11.

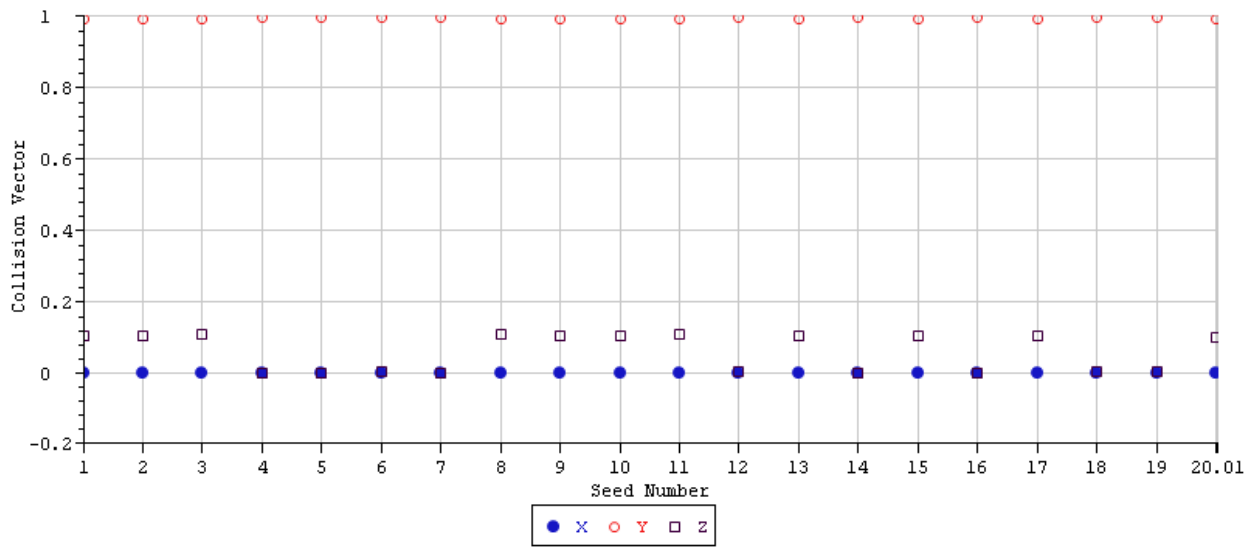


Figure 104: Collision vector components for different seeds, for case number 11.

12 Collision Scenario Number 14

	1	2	3	4	5
Signals		Max	Min	Mean	St. Dev.
RelativeCollisionVelocity	[m/s]	4.73	0.47	1.87	1.17
IceVelocity	[m/s]	5.75	0.73	2.52	1.25
CollisionHeight	[m]	28.13	12.81	20.41	4.82

Table 48: Statistical values calculated for collision scenario number 14.

	1	2	3	4
Signals		MP	Exp	P90
RelativeCollisionVelocity	[m/s]	1.33	1.67	3.44
IceVelocity	[m/s]	1.95	2.31	4.21
CollisionHeight	[m]	18.2	19.6	26.88

Table 49: Statistical values calculated for collision scenario number 14.

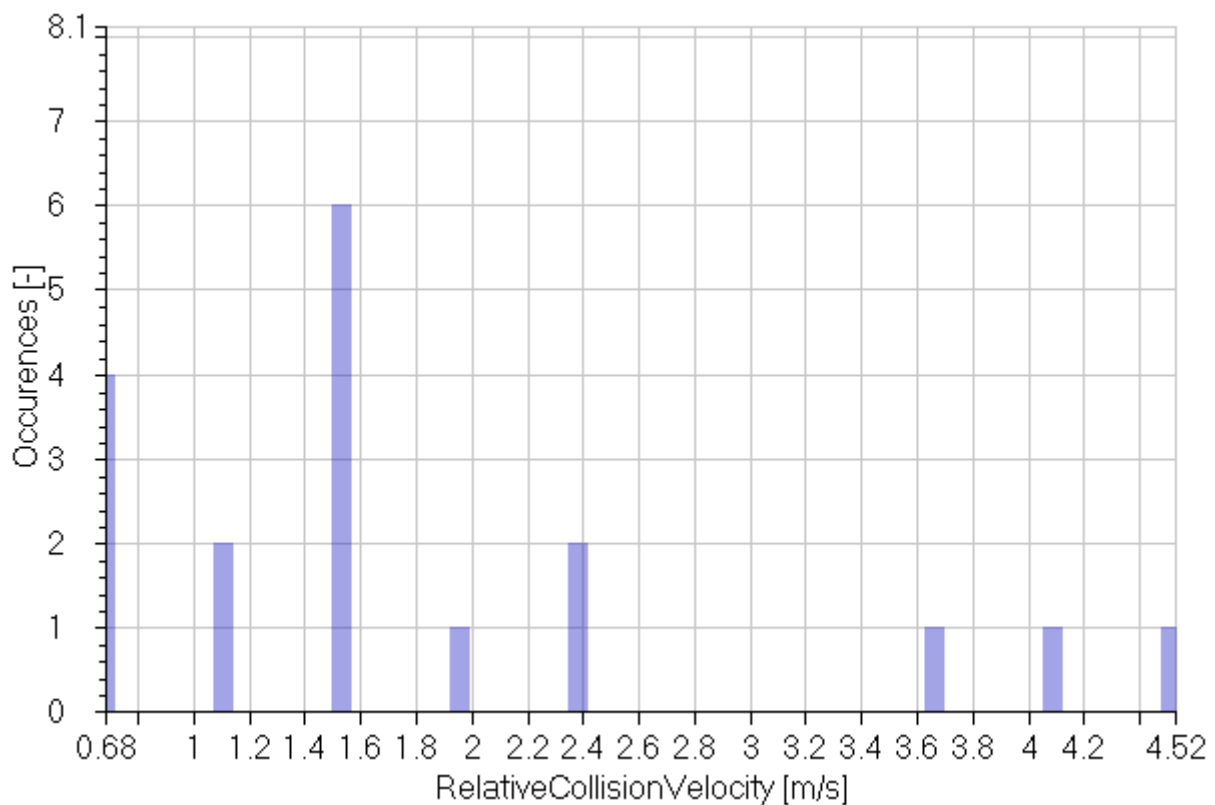


Figure 105: collision scenario number 14

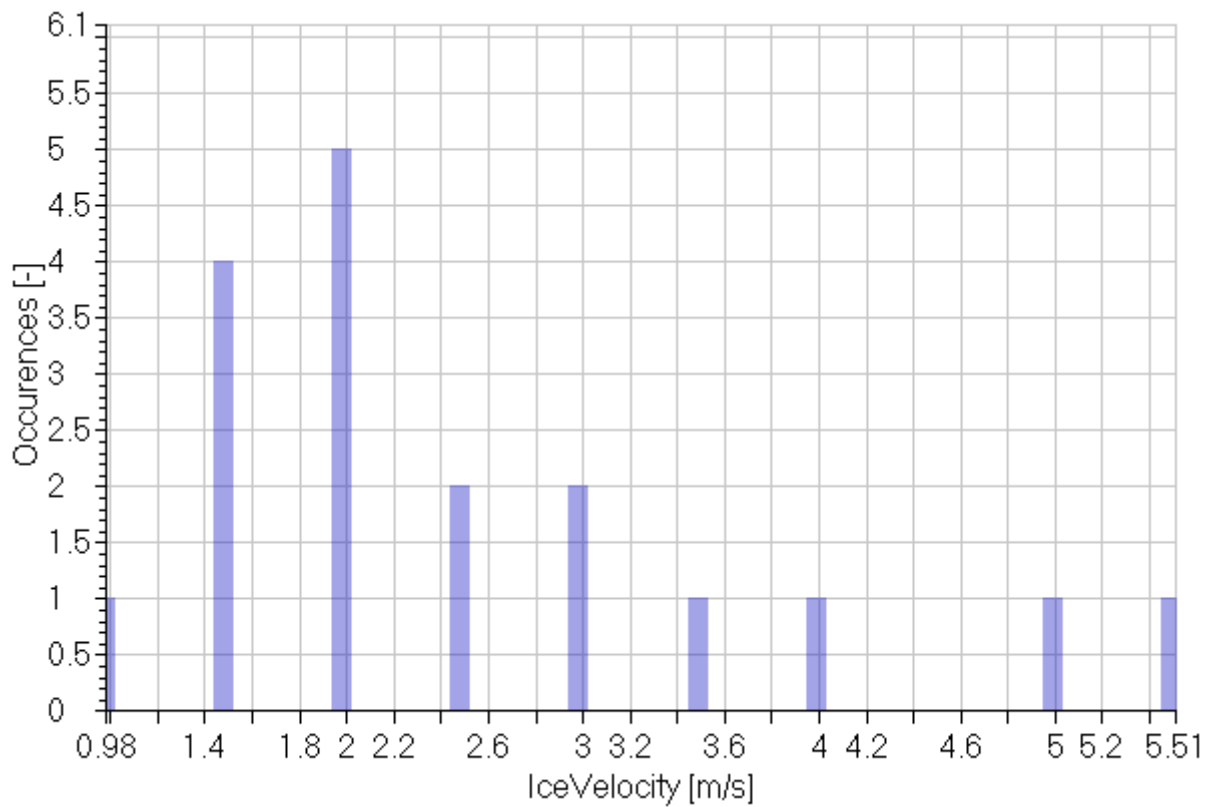


Figure 106: collision scenario number 14

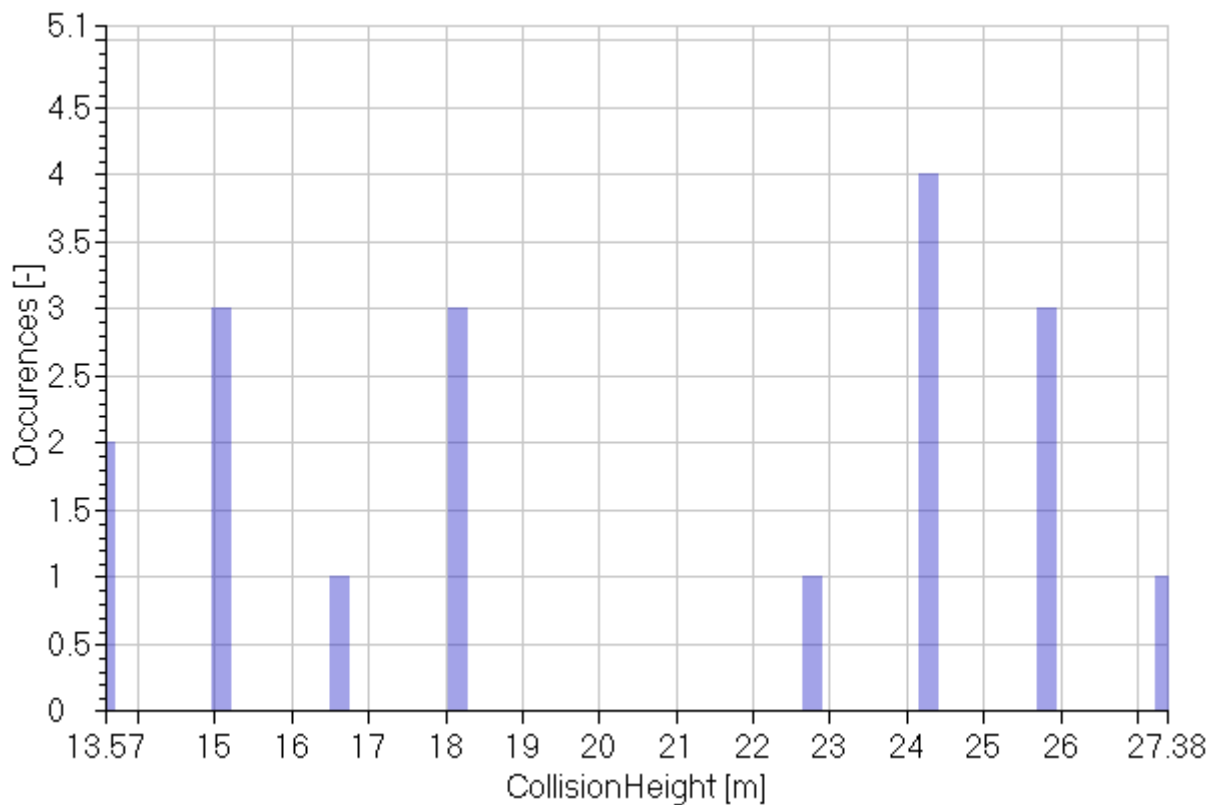


Figure 107: collision scenario number 14

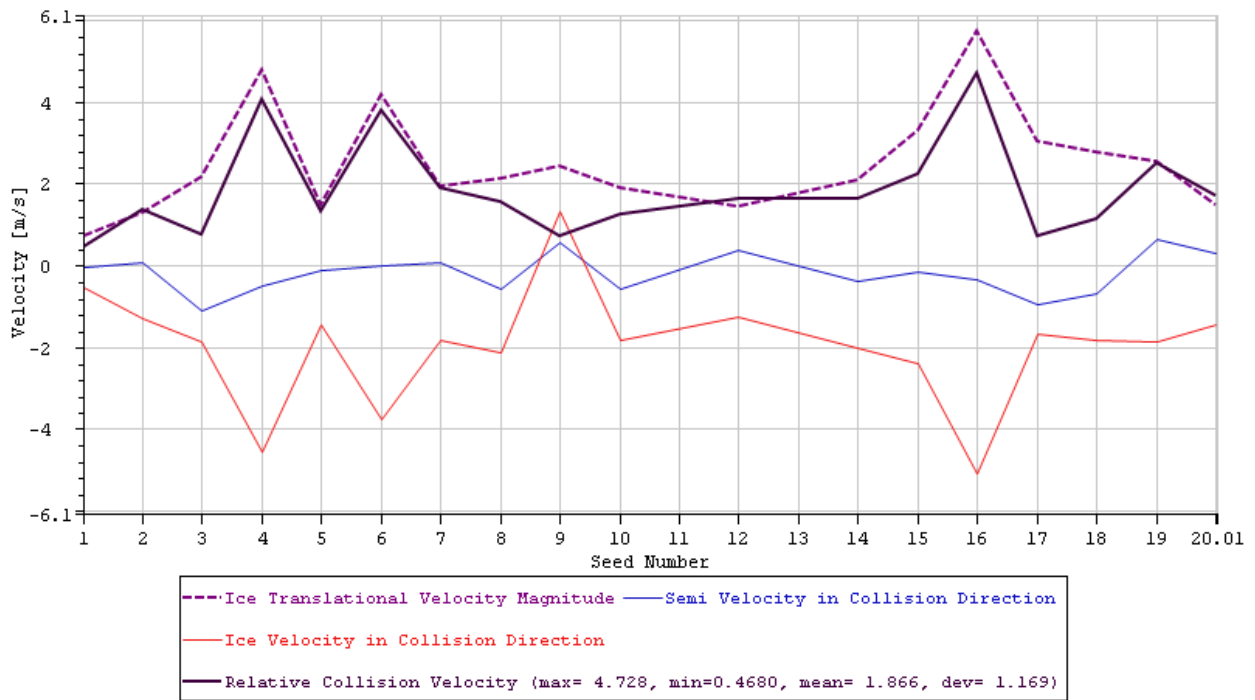


Figure 108: Total and relative collision velocities of ice and platform for different seeds, for case number 14.

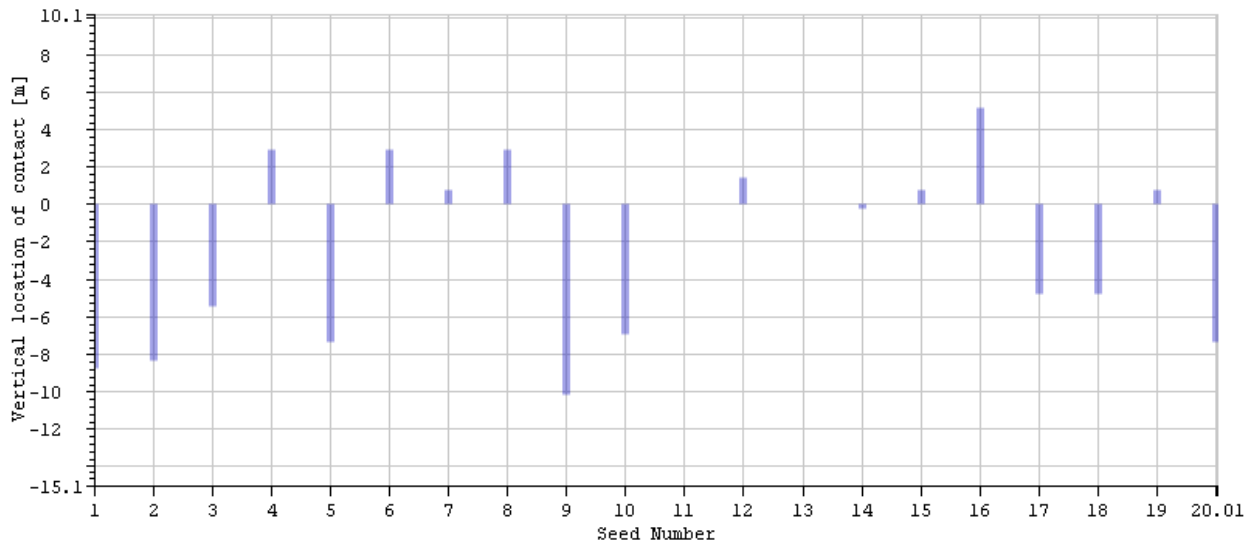


Figure 109: Vertical location of impact on the platform for different seeds, for case number 14.

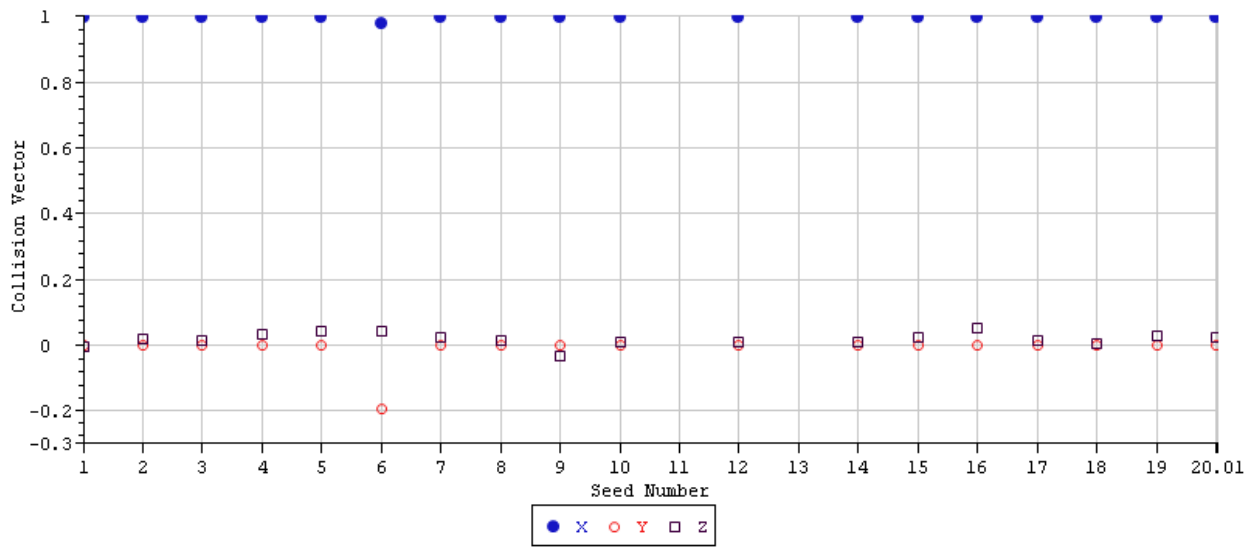


Figure 110: Collision vector components for different seeds, for case number 14.

13 Collision Scenario Number 18

	1	2	3	4	5
Signals		Max	Min	Mean	St. Dev.
RelativeCollisionVelocity	[m/s]	2.89	0.03	1.05	0.65
IceVelocity	[m/s]	3.23	0.45	1.8	0.63
CollisionHeight	[m]	26.67	14.69	21.98	4.36

Table 50: Statistical values calculated for collision scenario number 18.

	1	2	3	4
Signals		MP	Exp	P90
RelativeCollisionVelocity	[m/s]	0.76	0.95	1.91
IceVelocity	[m/s]	1.51	1.69	2.64
CollisionHeight	[m]	20.01	21.25	27.75

Table 51: Statistical values calculated for collision scenario number 18.

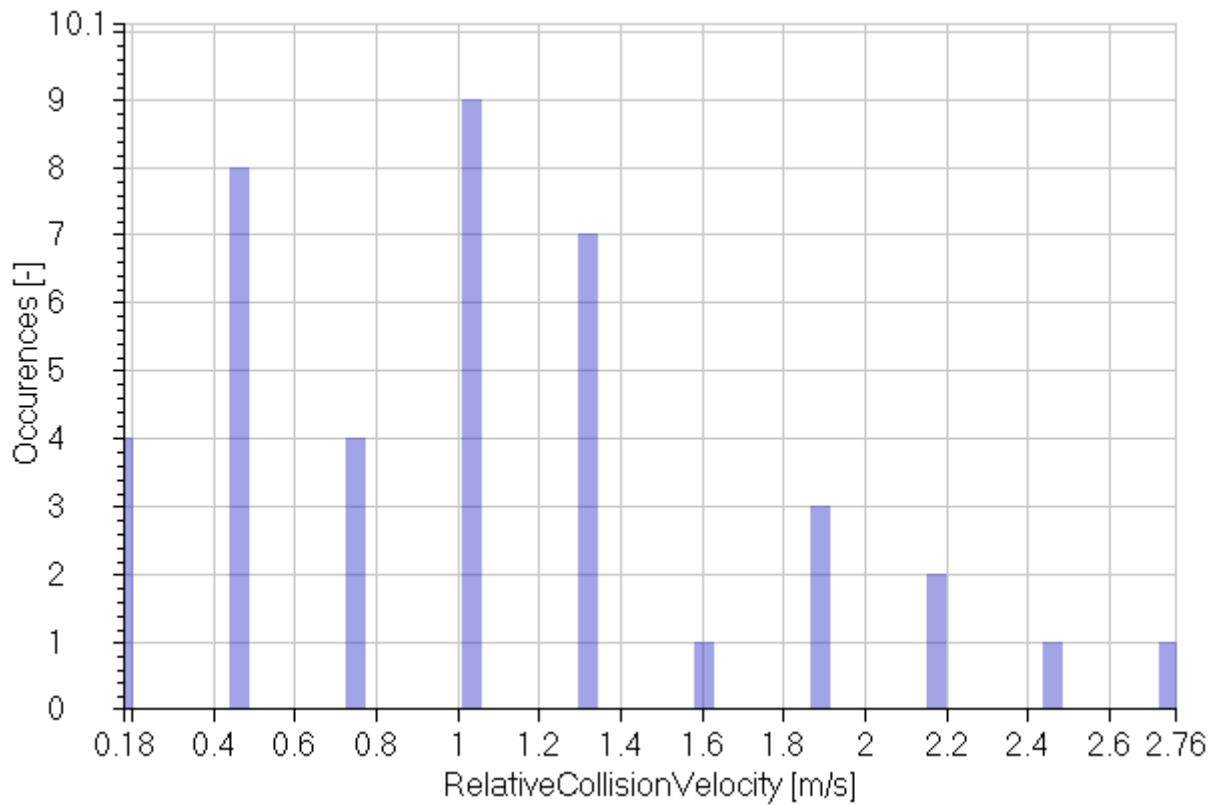


Figure 111: collision scenario number 18

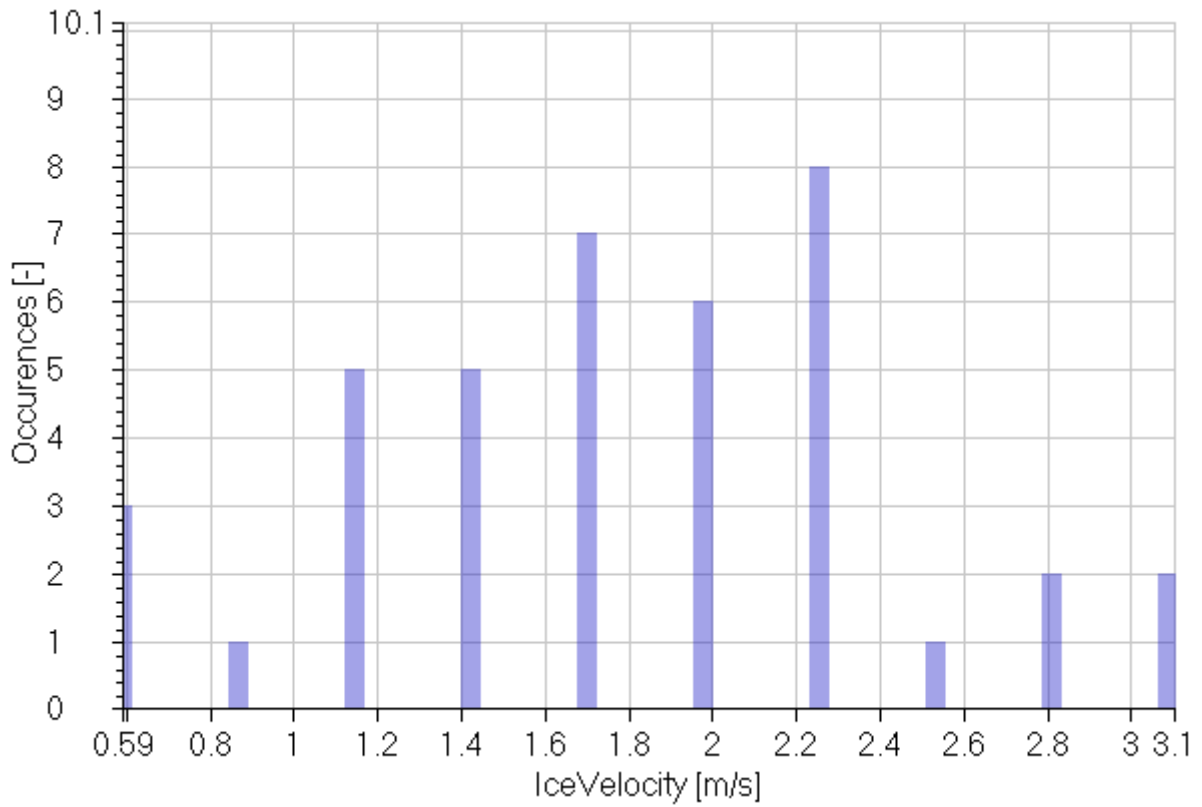


Figure 112: collision scenario number 18

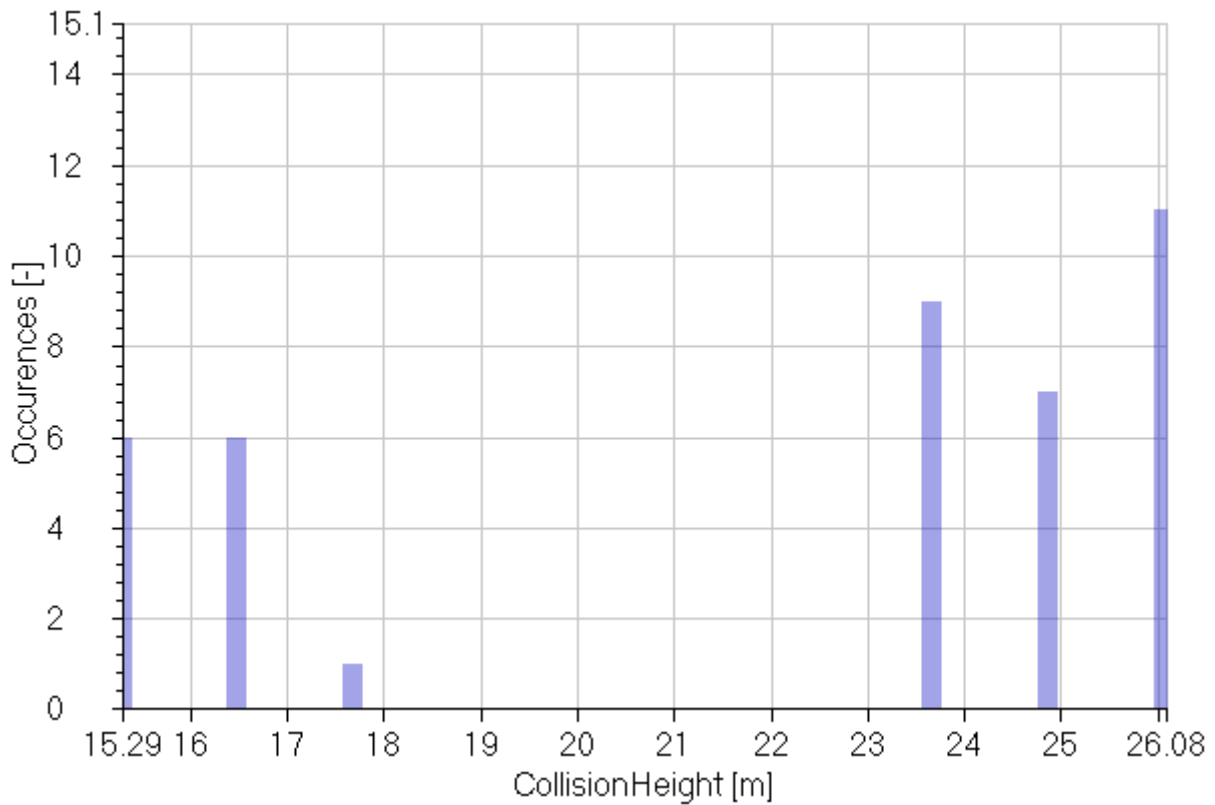


Figure 113: collision scenario number 18

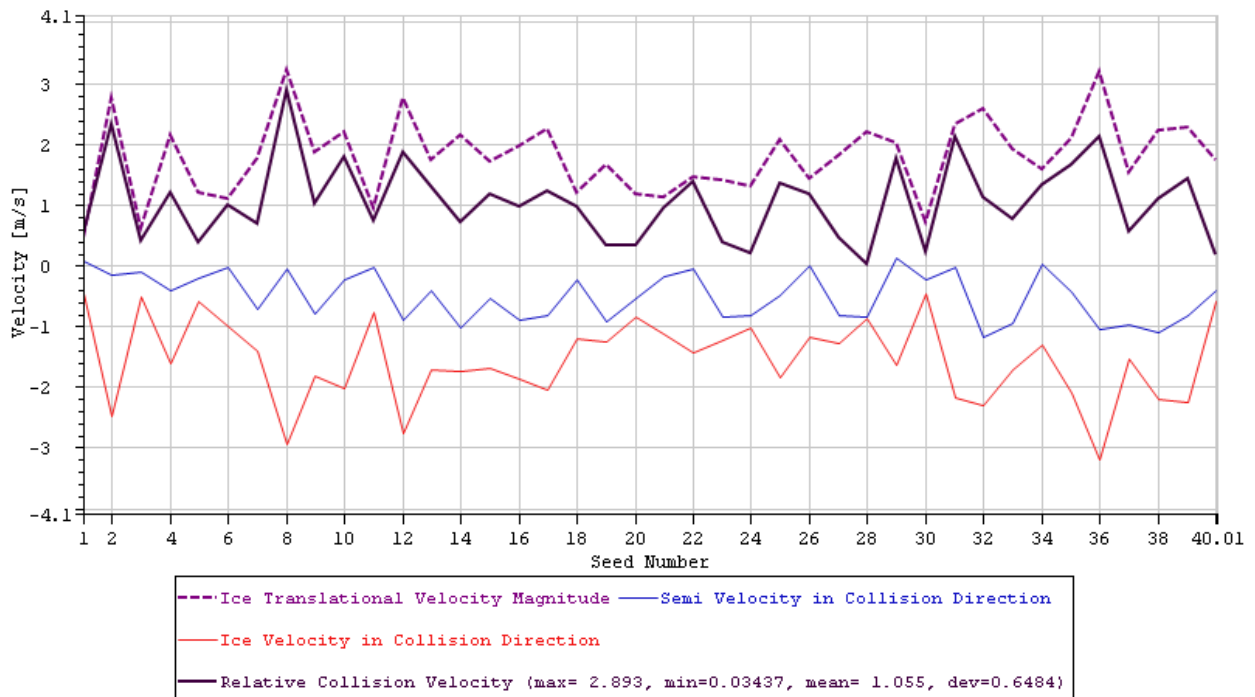


Figure 114: Total and relative collision velocities of ice and platform for different seeds, for case number 18.

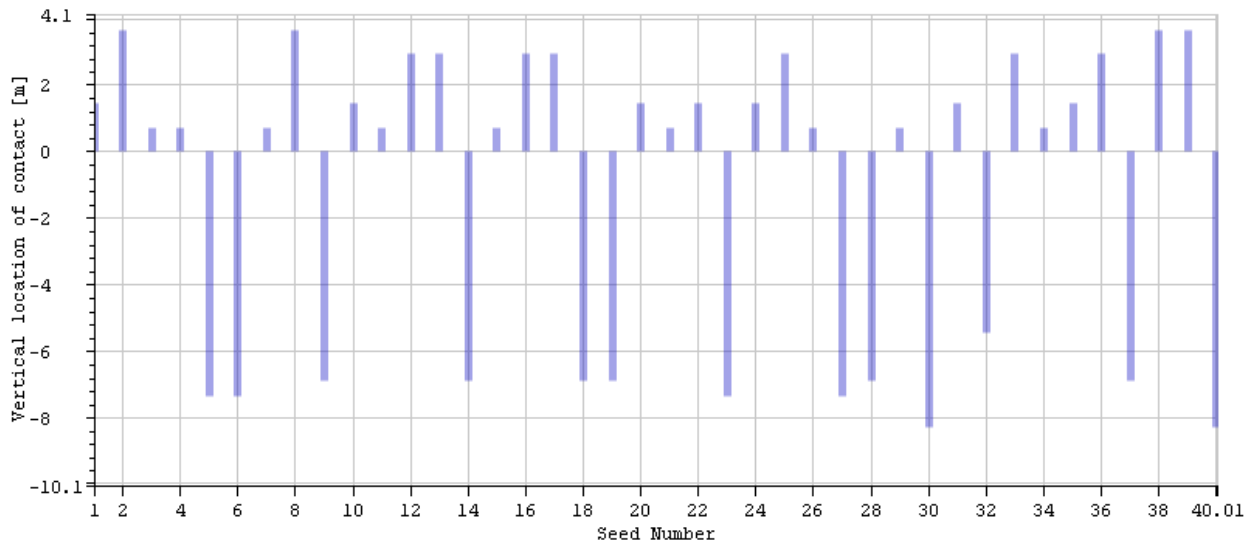


Figure 115: Vertical location of impact on the platform for different seeds, for case number 18.

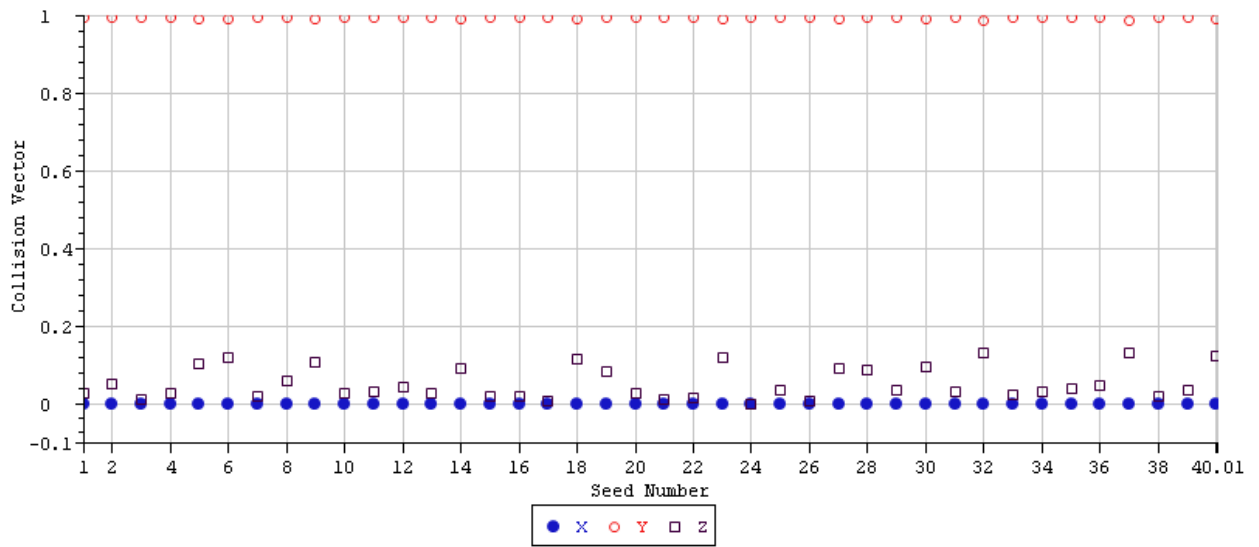


Figure 116: Collision vector components for different seeds, for case number 18.

14 Collision Scenario Number 19

	1	2	3	4	5
Signals		Max	Min	Mean	St. Dev.
RelativeCollisionVelocity	[m/s]	3.54	0.31	1.59	0.79
IceVelocity	[m/s]	3.96	0.42	1.99	0.76
CollisionHeight	[m]	26.67	14.69	23.72	2.93

Table 52: Statistical values calculated for collision scenario number 19.

	1	2	3	4
Signals		MP	Exp	P90
RelativeCollisionVelocity	[m/s]	1.23	1.45	2.63
IceVelocity	[m/s]	1.64	1.86	2.99
CollisionHeight	[m]	22.4	23.23	27.59

Table 53: Statistical values calculated for collision scenario number 19.

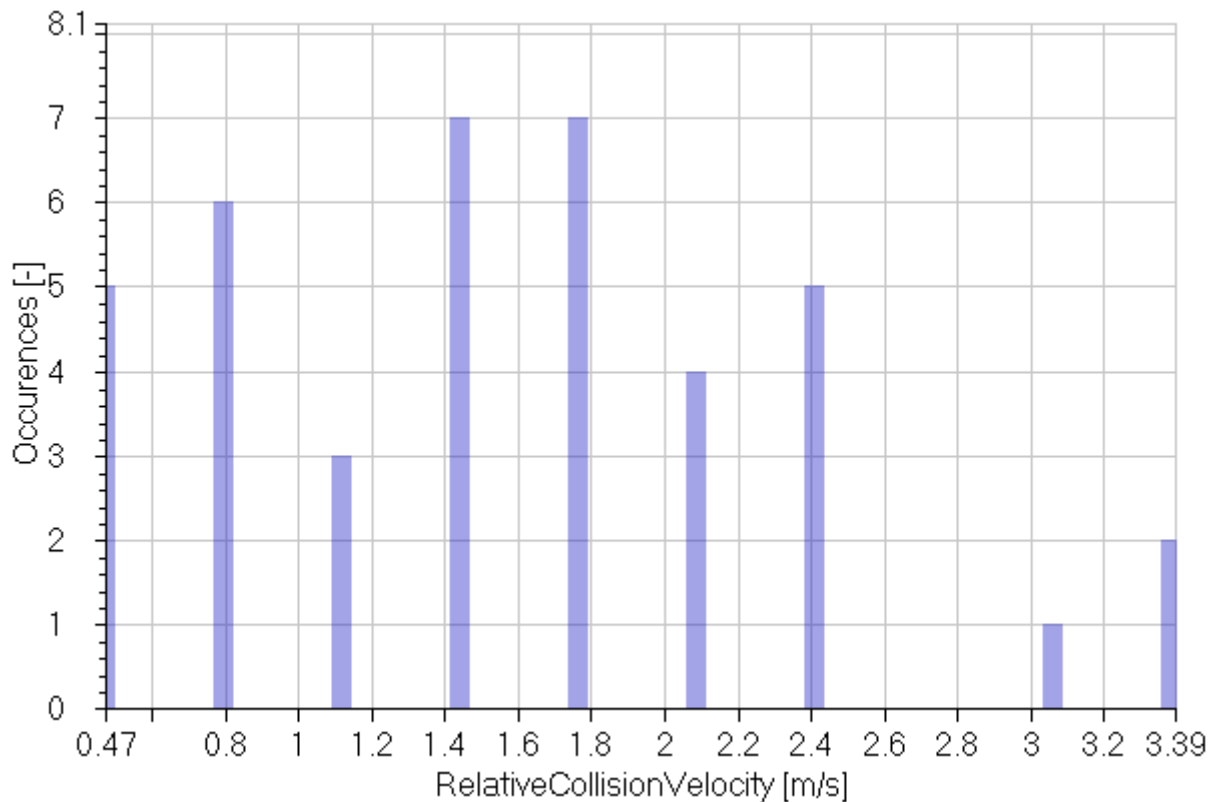


Figure 117: collision scenario number 19

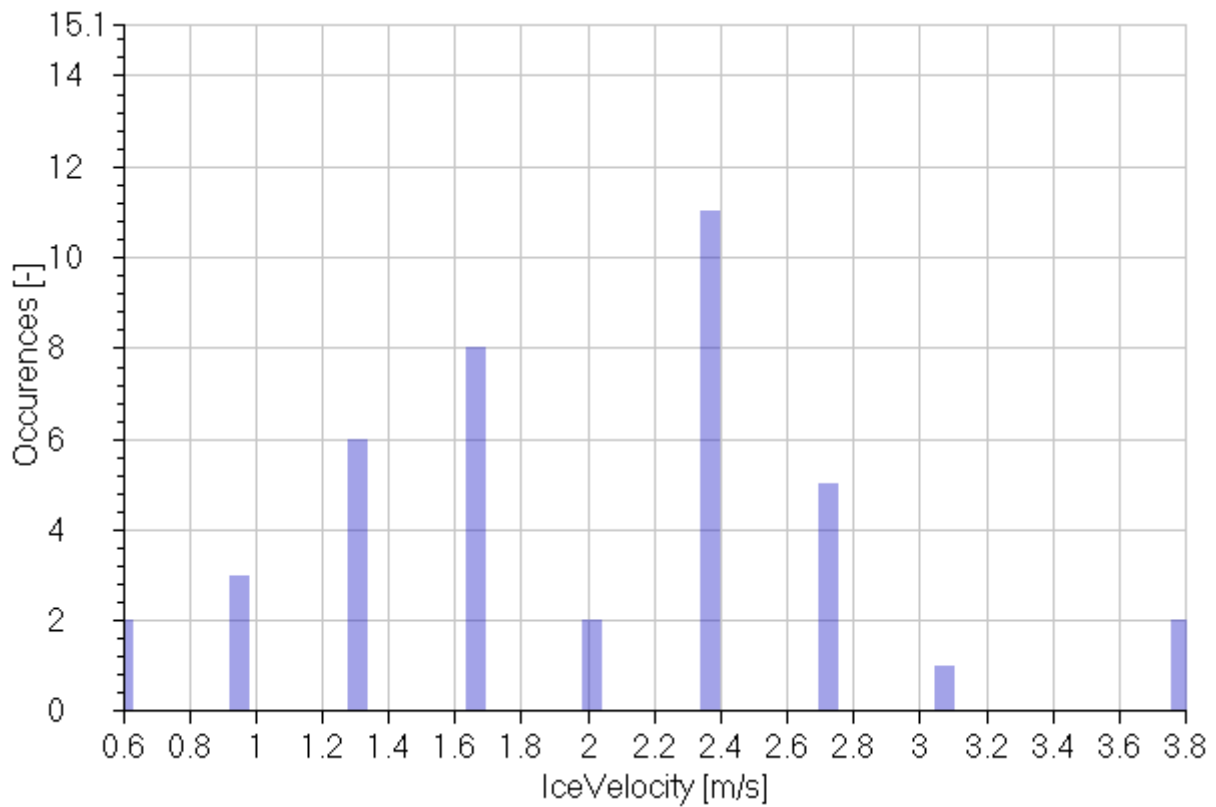


Figure 118: collision scenario number 19

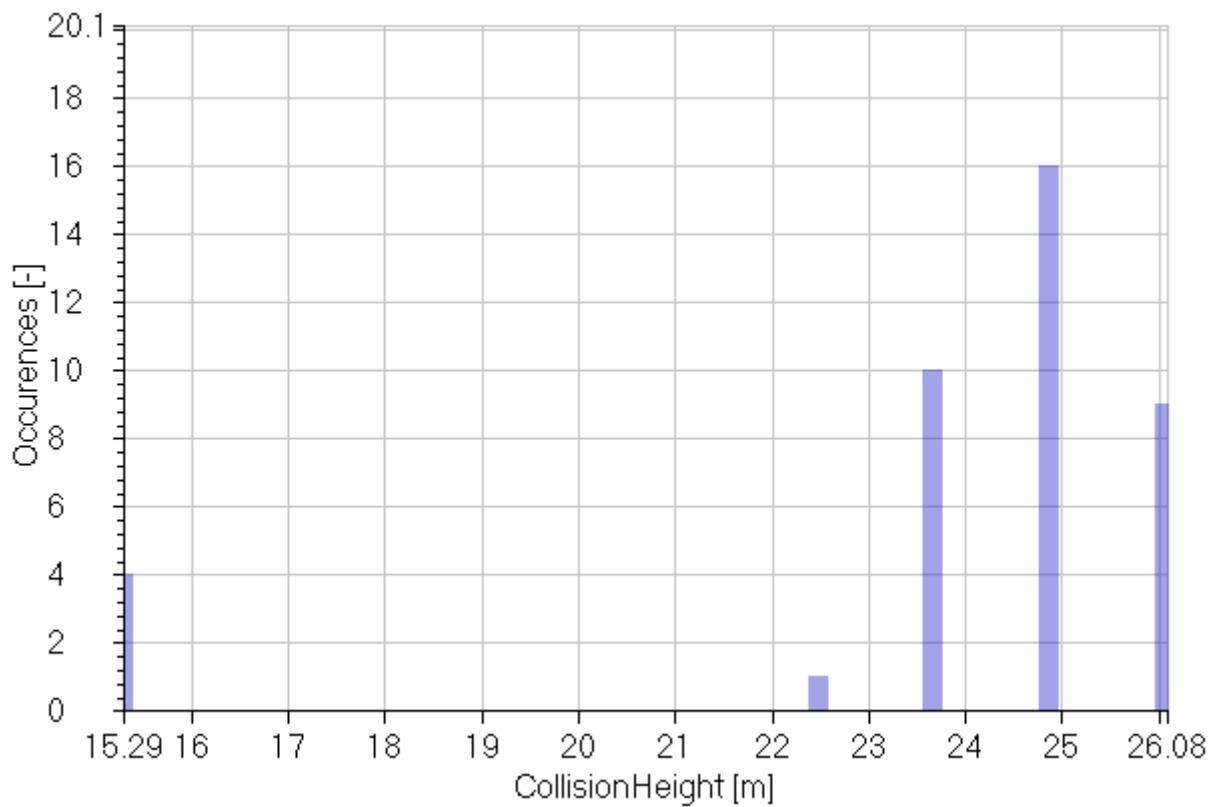


Figure 119: collision scenario number 19

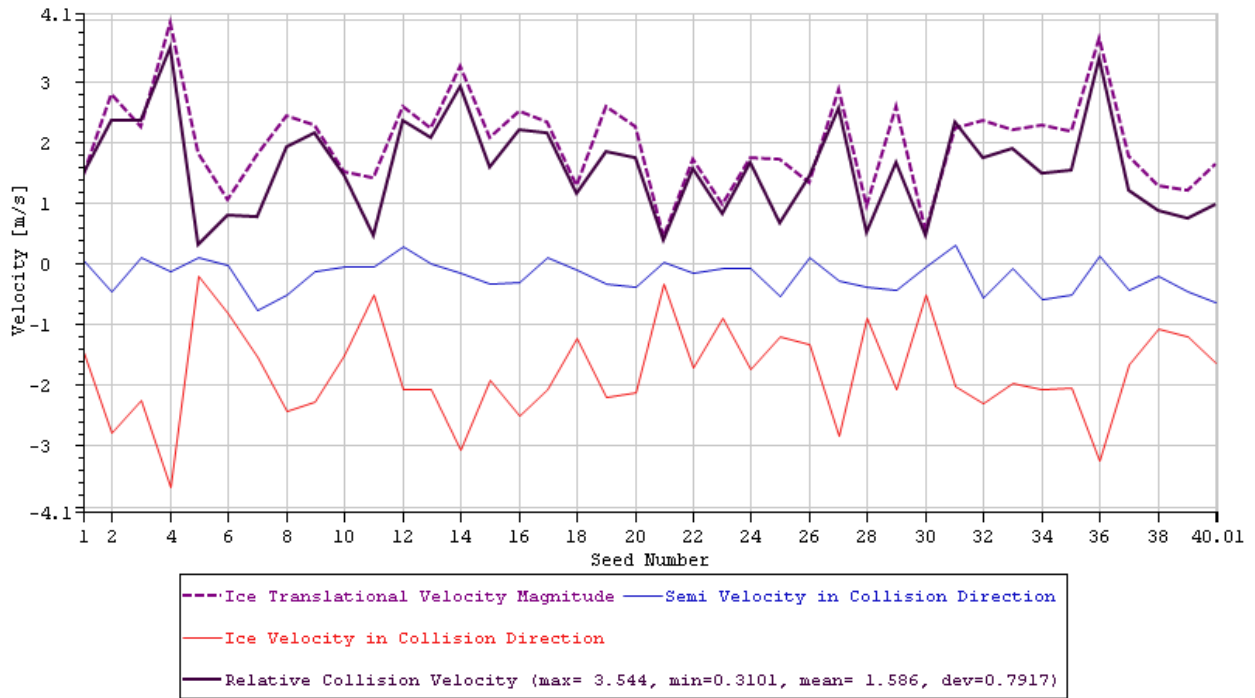


Figure 120: Total and relative collision velocities of ice and platform for different seeds, for case number 19.

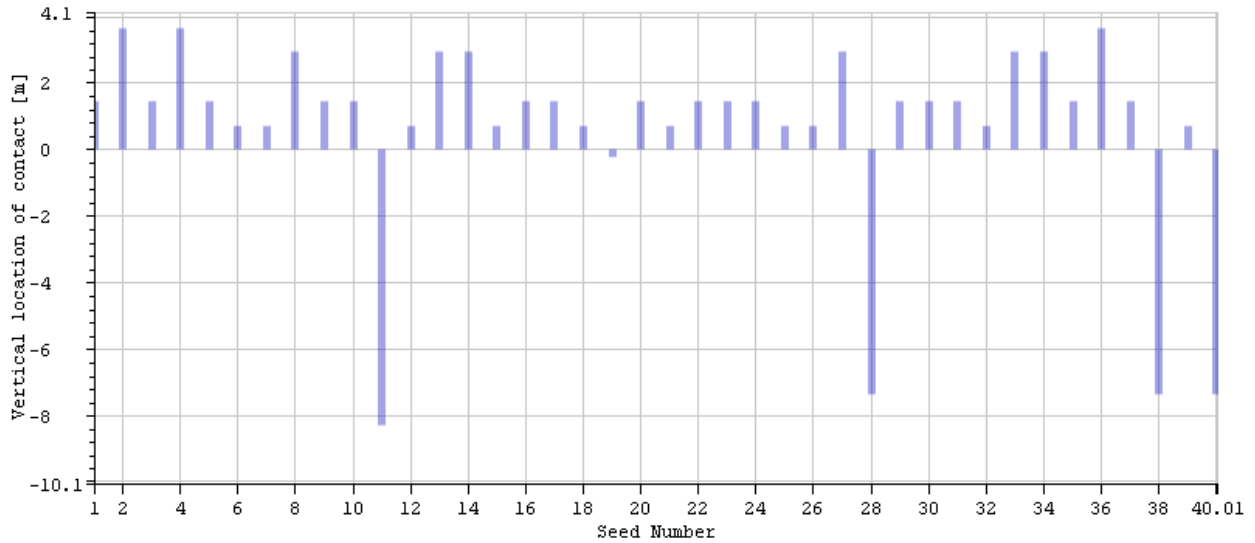


Figure 121: Vertical location of impact on the platform for different seeds, for case number 19.

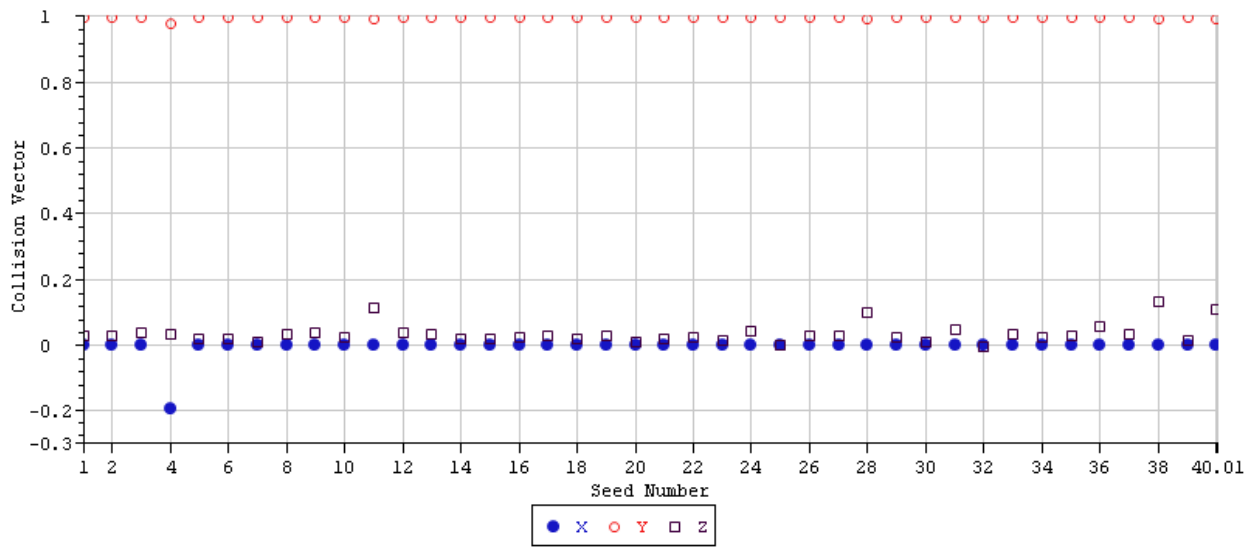


Figure 122: Collision vector components for different seeds, for case number 19.

15 Collision Scenario Number 20

	1	2	3	4	5
Signals		Max	Min	Mean	St. Dev.
RelativeCollisionVelocity	[m/s]	3.03	0.03	1.21	0.7
IceVelocity	[m/s]	3.14	0.21	1.49	0.74
CollisionHeight	[m]	24.47	14.22	22.17	3.27

Table 54: Statistical values calculated for collision scenario number 20.

	1	2	3	4
Signals		MP	Exp	P90
RelativeCollisionVelocity	[m/s]	0.9	1.1	2.14
IceVelocity	[m/s]	1.16	1.37	2.46
CollisionHeight	[m]	20.7	21.63	26.49

Table 55: Statistical values calculated for collision scenario number 20.

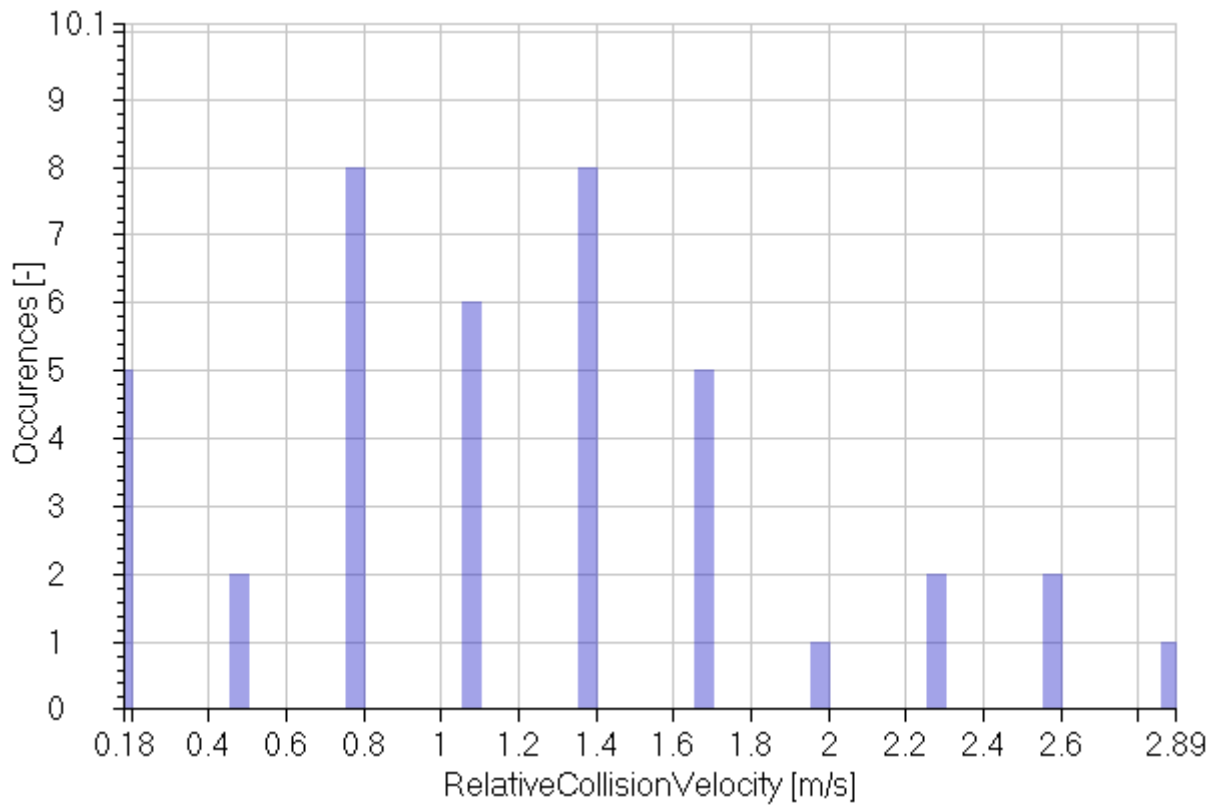


Figure 123: collision scenario number 20

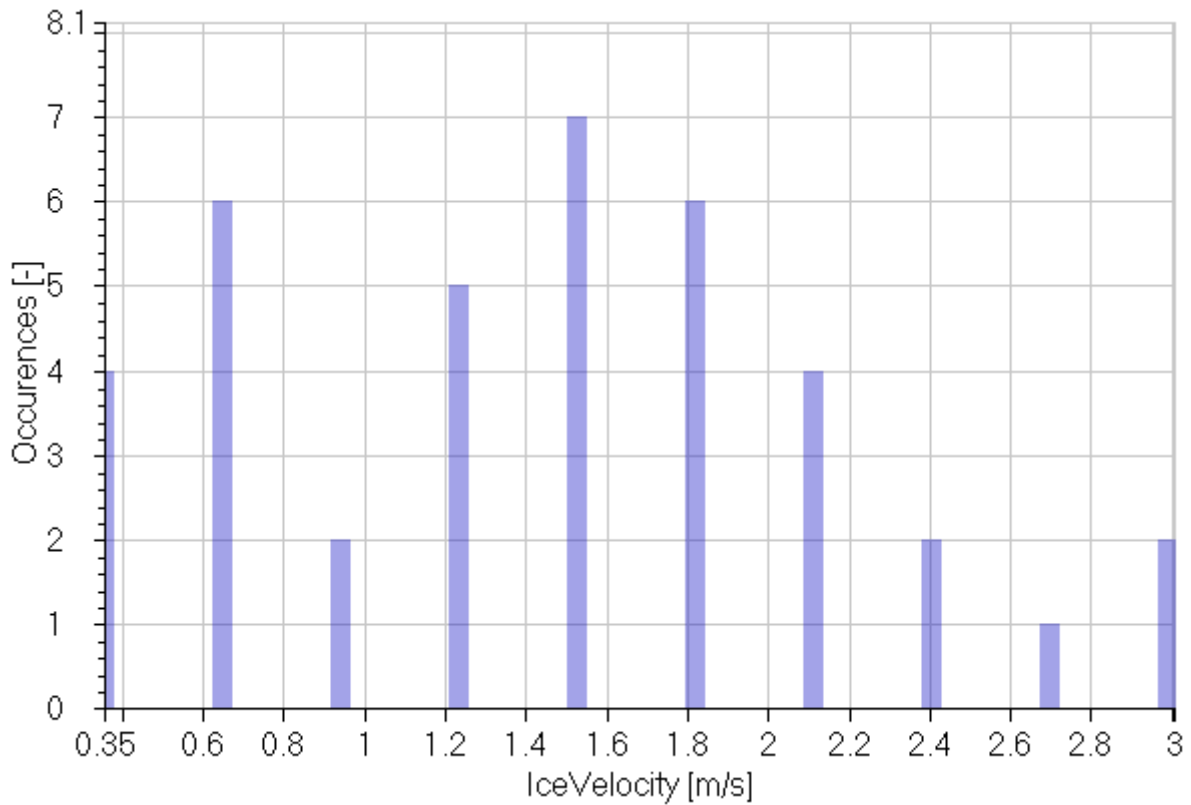


Figure 124: collision scenario number 20

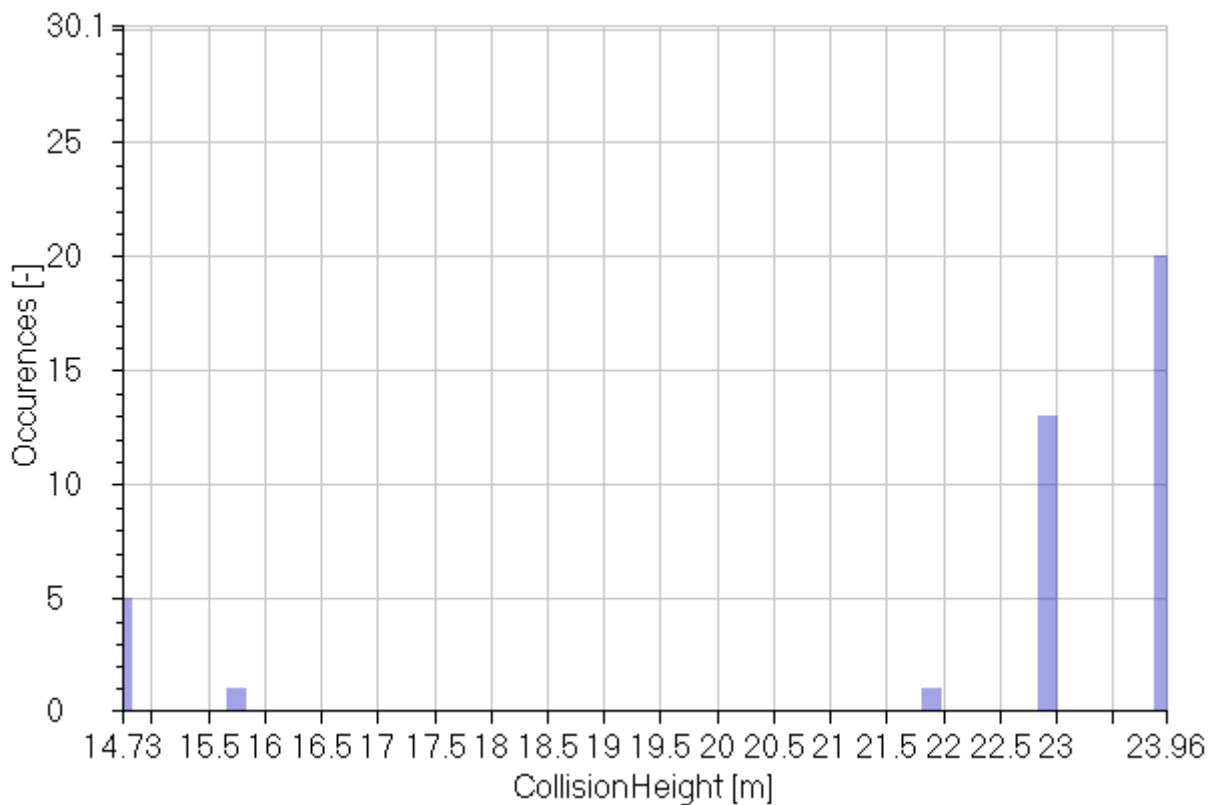


Figure 125: collision scenario number 20

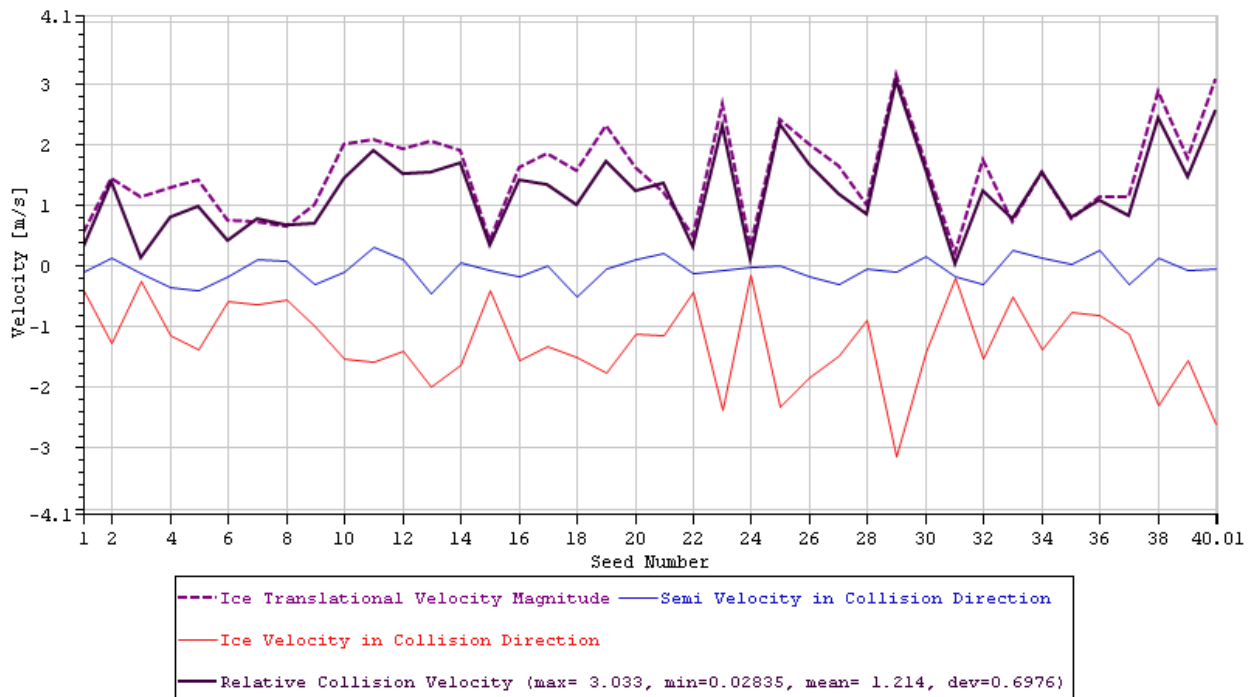


Figure 126: Total and relative collision velocities of ice and platform for different seeds, for case number 20.

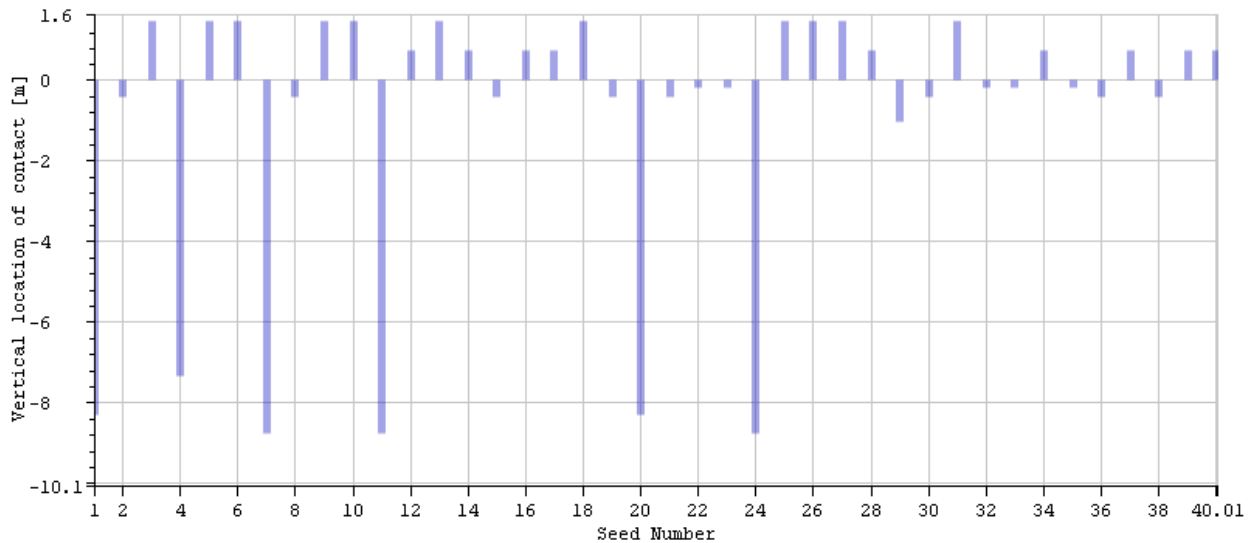


Figure 127: Vertical location of impact on the platform for different seeds, for case number 20.

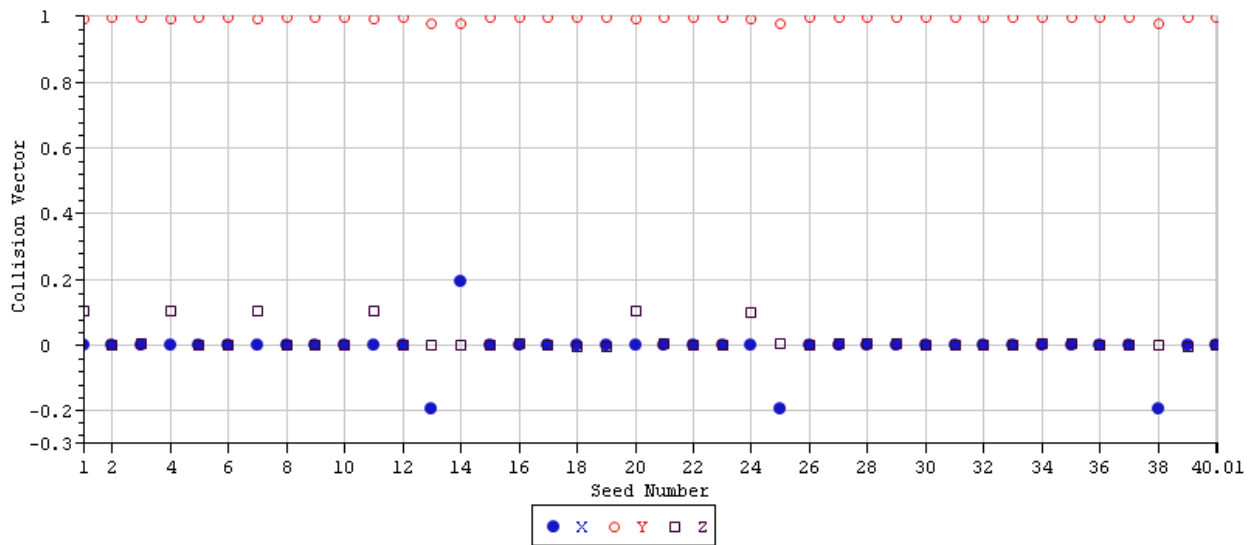


Figure 128: Collision vector components for different seeds, for case number 20.

16 Collision Scenario Number 21

	1	2	3	4	5
Signals		Max	Min	Mean	St. Dev.
RelativeCollisionVelocity	[m/s]	2.64	0.14	1.07	0.65
IceVelocity	[m/s]	3.73	0.7	2.06	0.84
CollisionHeight	[m]	26.67	12.81	17.6	3.82

Table 56: Statistical values calculated for collision scenario number 21.

	1	2	3	4
Signals		MP	Exp	P90
RelativeCollisionVelocity	[m/s]	0.77	0.96	1.95
IceVelocity	[m/s]	1.67	1.92	3.2
CollisionHeight	[m]	15.83	16.95	22.78

Table 57: Statistical values calculated for collision scenario number 21.

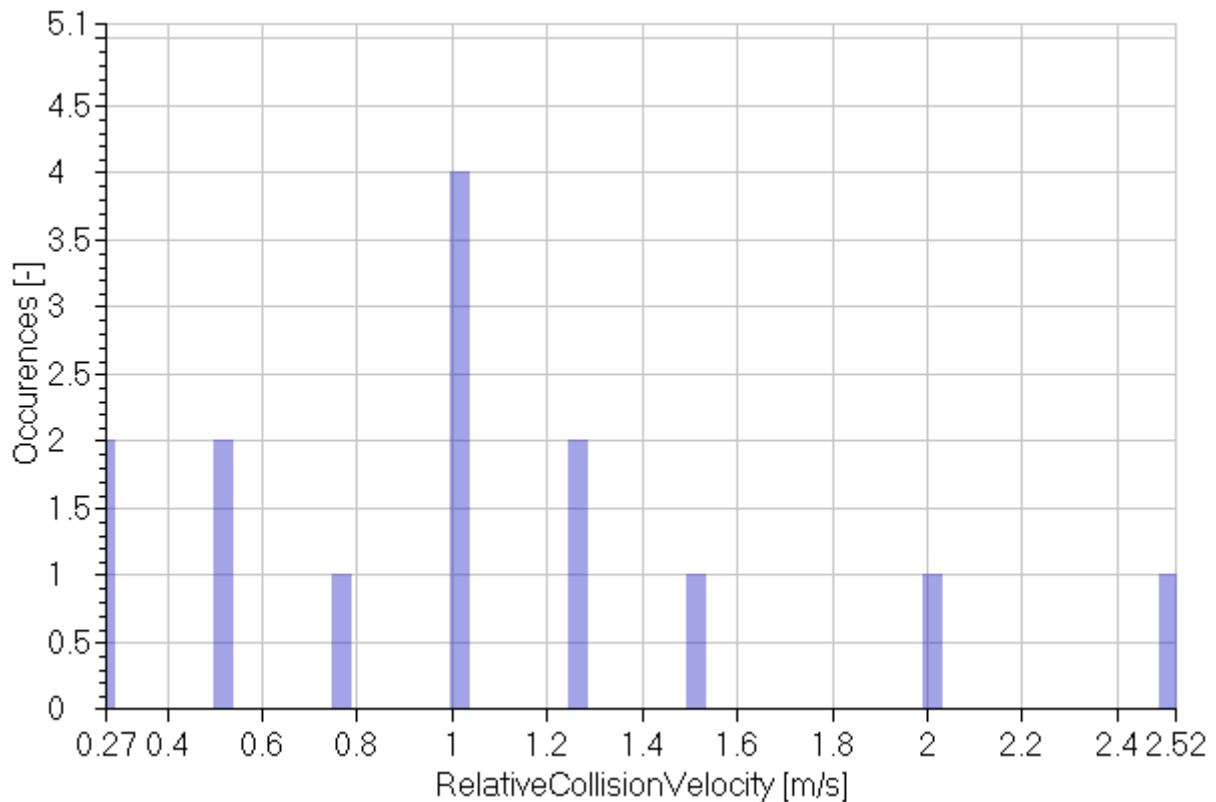


Figure 129: collision scenario number 21

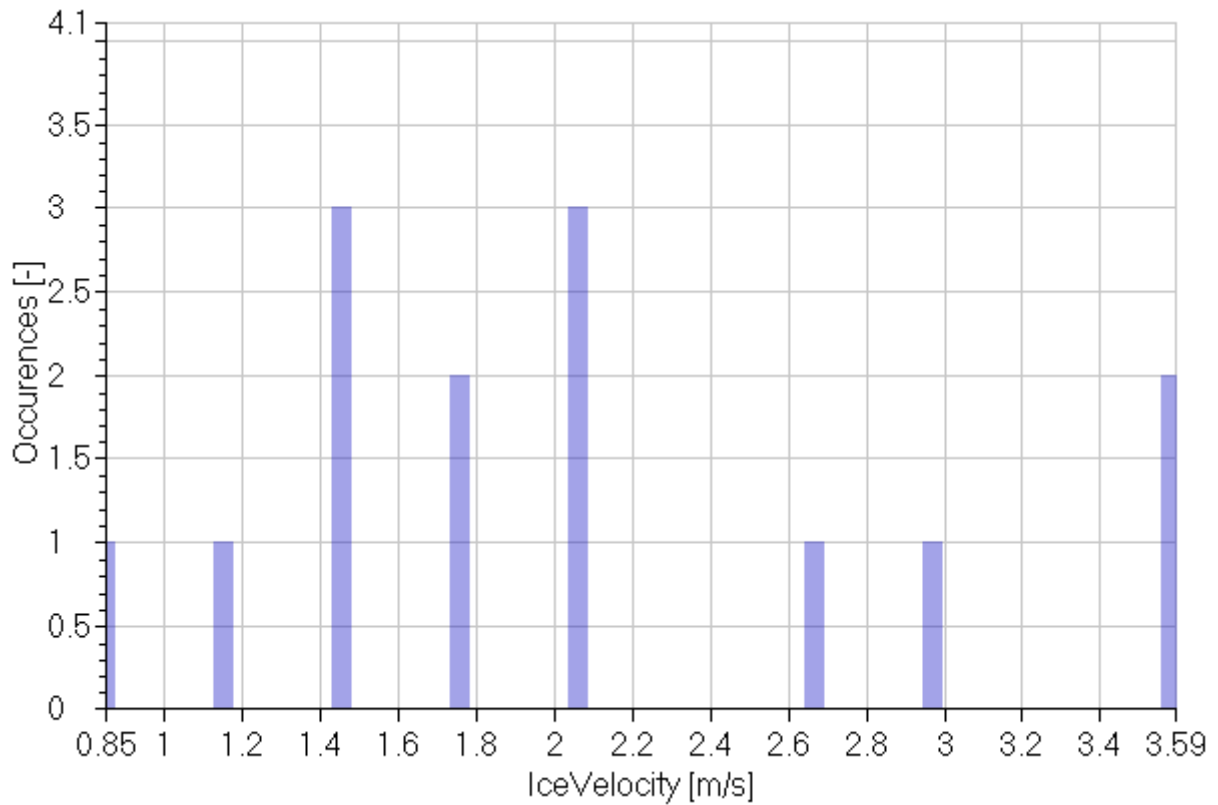


Figure 130: collision scenario number 21

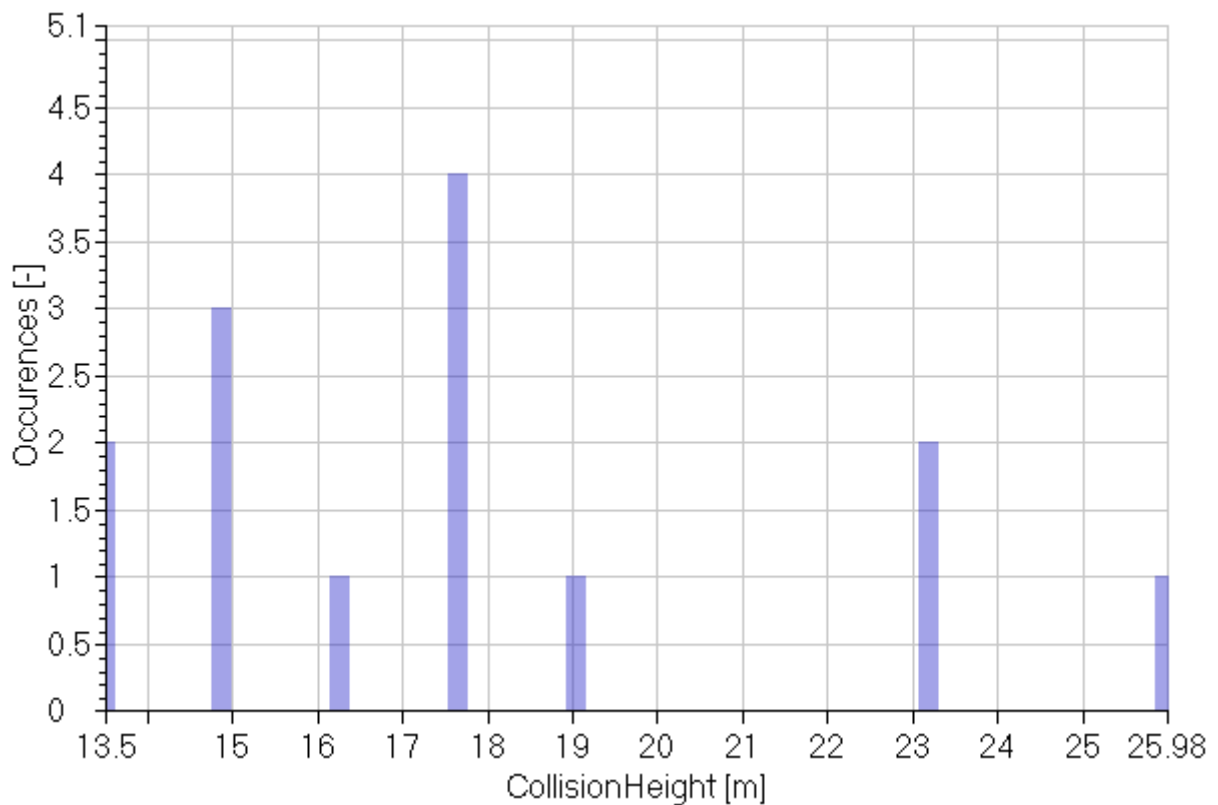


Figure 131: collision scenario number 21

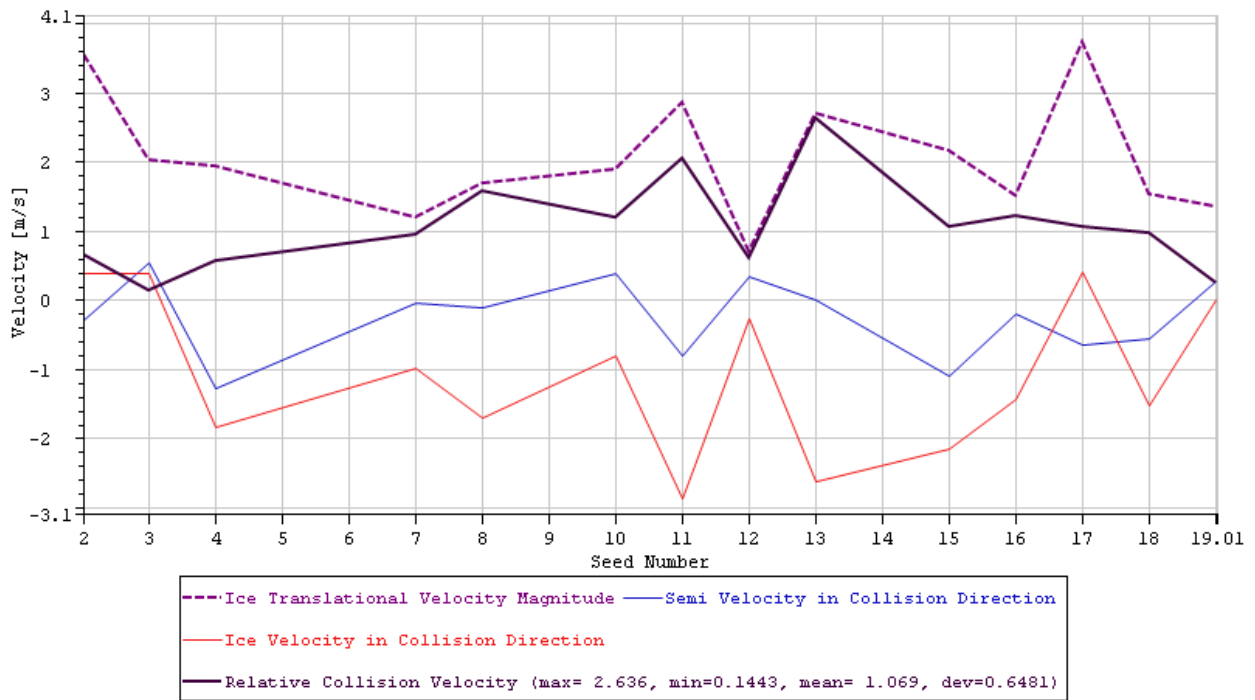


Figure 132: Total and relative collision velocities of ice and platform for different seeds, for case number 21.

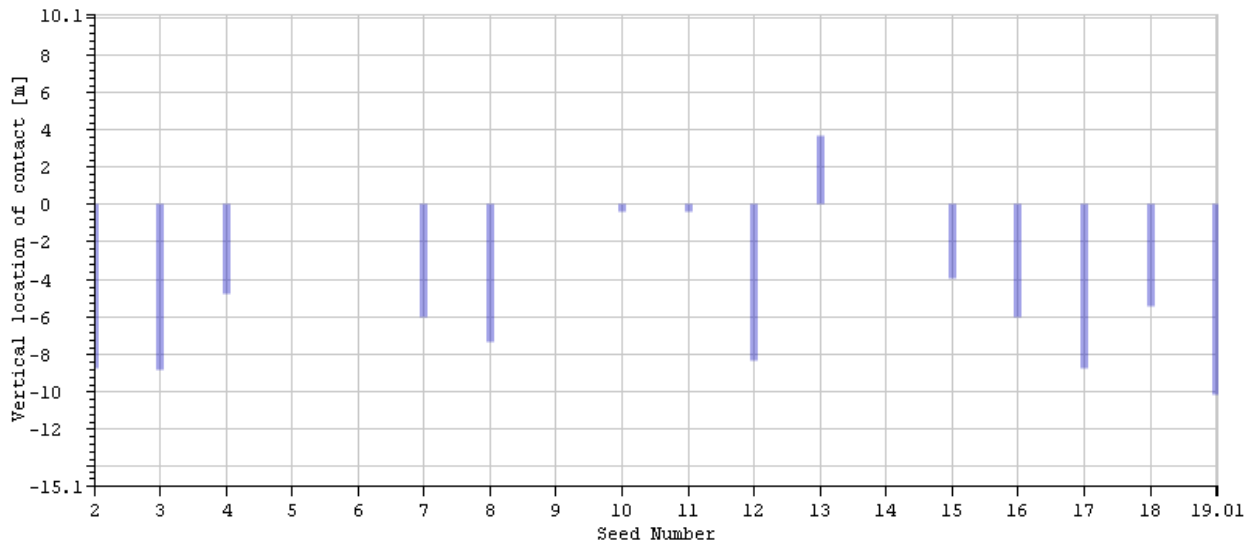


Figure 133: Vertical location of impact on the platform for different seeds, for case number 21.

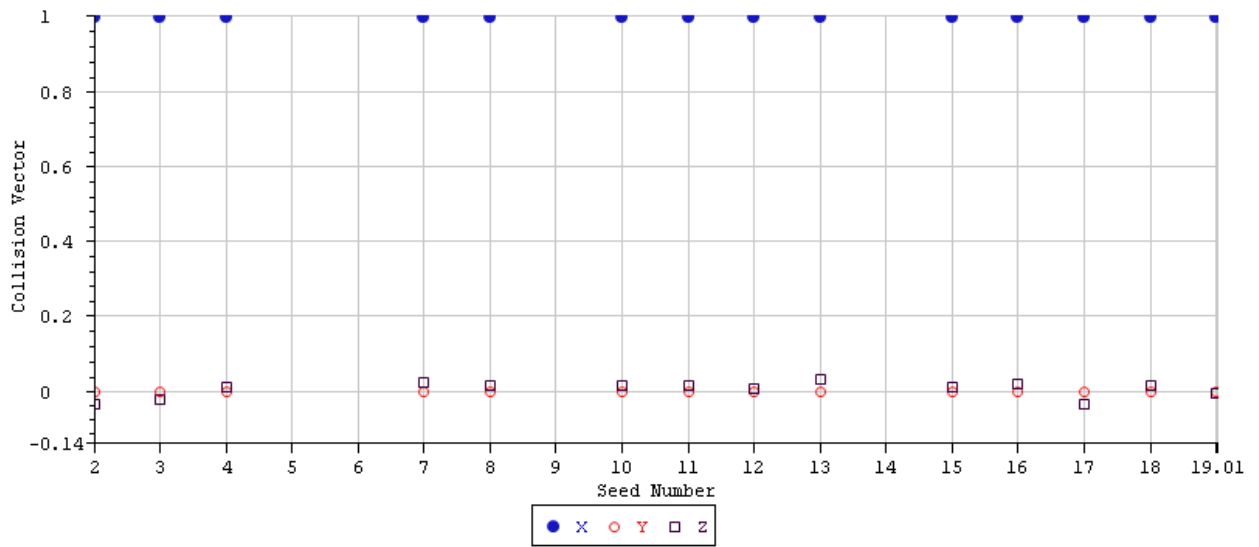


Figure 134: Collision vector components for different seeds, for case number 21.

Collision on the Pontoon

17 Collision Scenario Number 15

	1	2	3	4	5
Signals		Max	Min	Mean	St. Dev.
RelativeCollisionVelocity	[m/s]	2.16	0.16	1.19	0.62
IceVelocity	[m/s]	3.51	1.37	2.33	0.73
CollisionHeight	[m]	9.5	9.35	9.48	0.05

Table 58: Statistical values calculated for collision scenario number 15.

	1	2	3	4
Signals		MP	Exp	P90
RelativeCollisionVelocity	[m/s]	0.9	1.08	2.04
IceVelocity	[m/s]	1.99	2.2	3.32
CollisionHeight	[m]	9.46	9.47	9.54

Table 59: Statistical values calculated for collision scenario number 15.

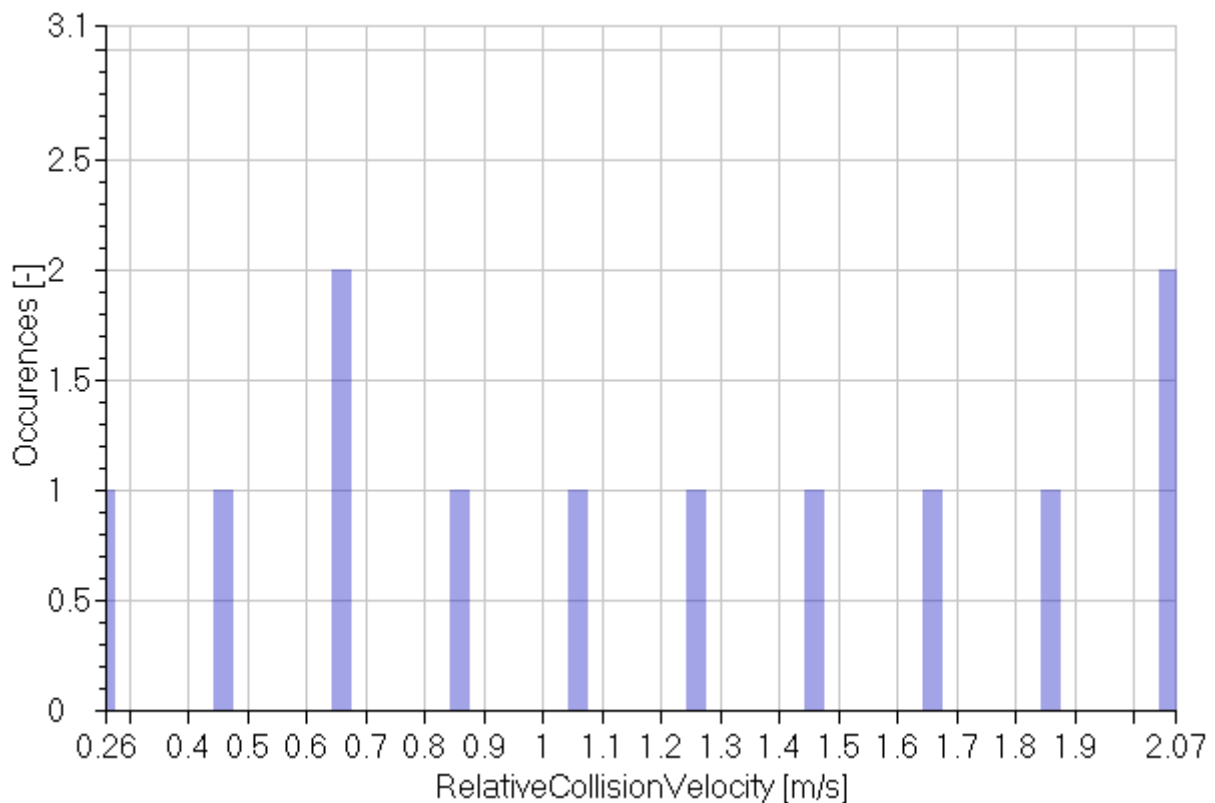


Figure 135: collision scenario number 15

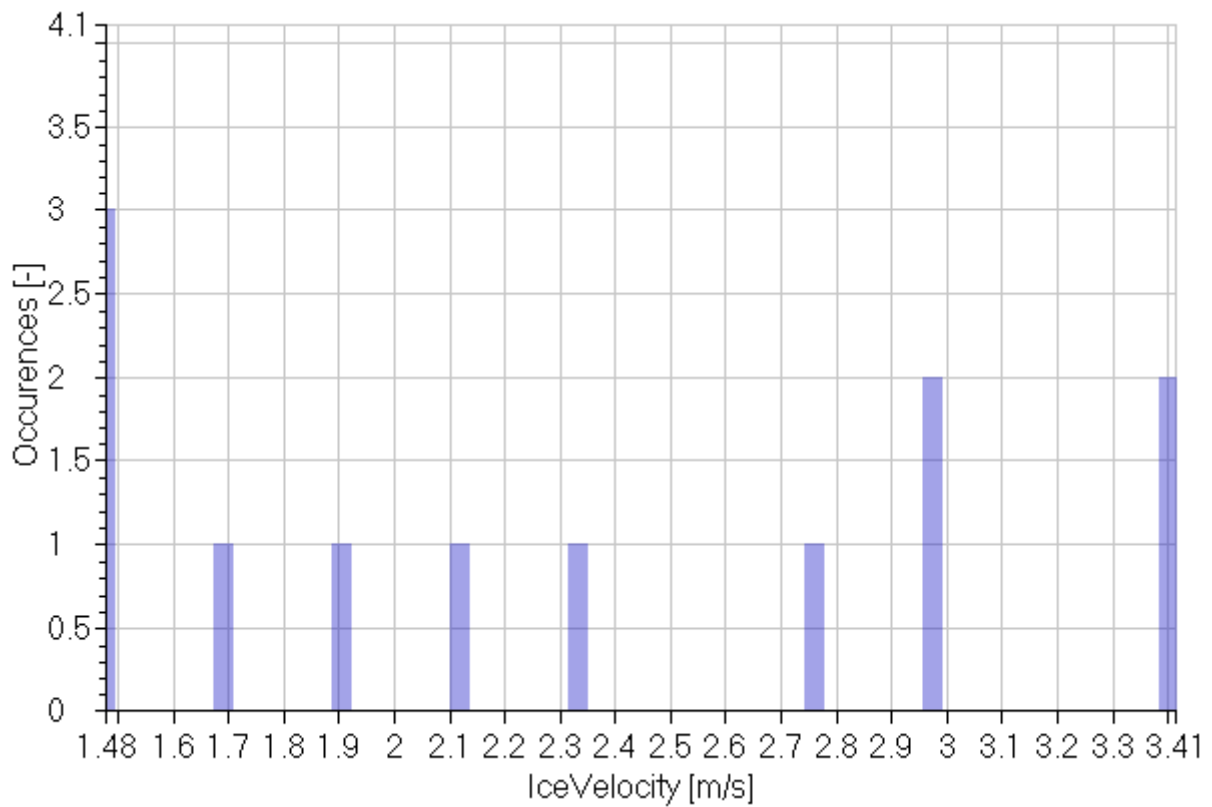


Figure 136: collision scenario number 15

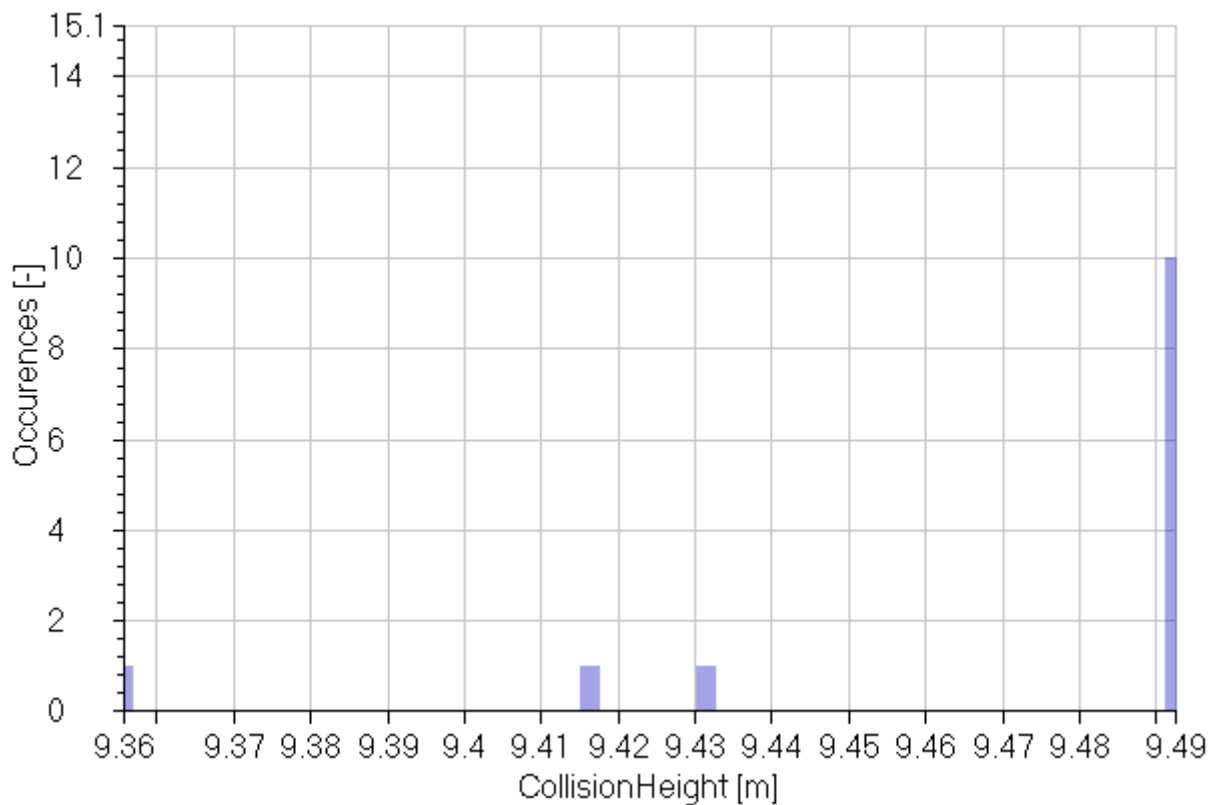


Figure 137: collision scenario number 15

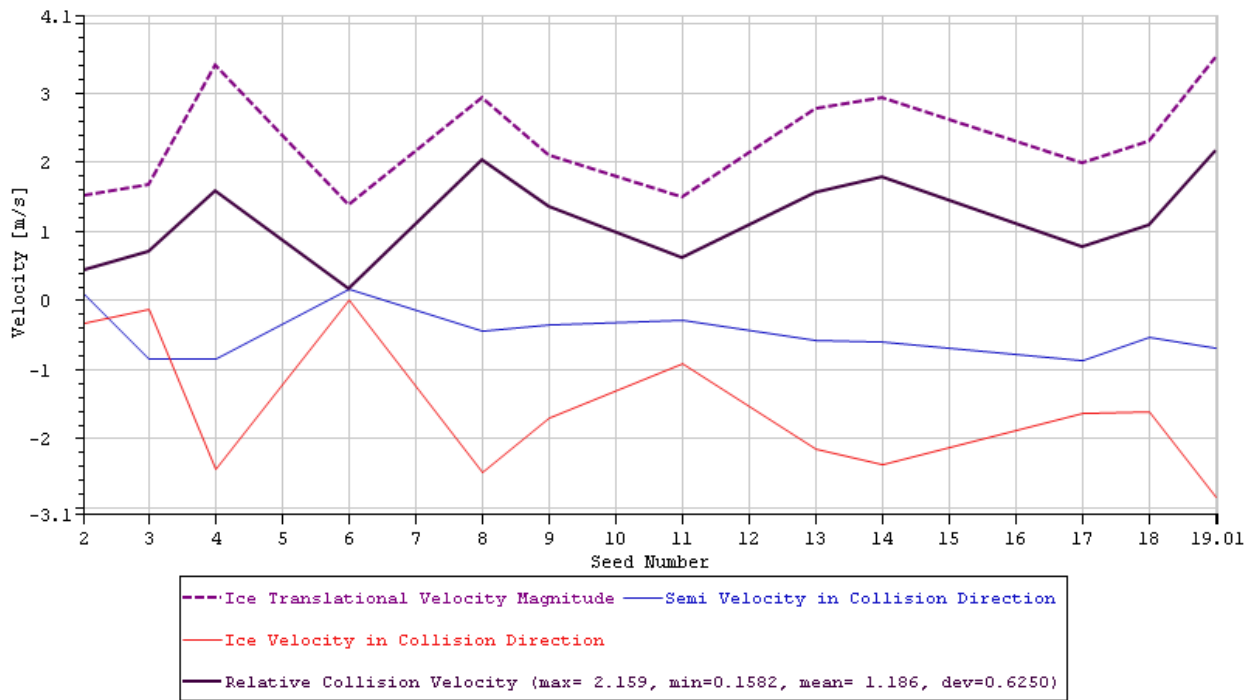


Figure 138: Total and relative collision velocities of ice and platform for different seeds, for case number 15.

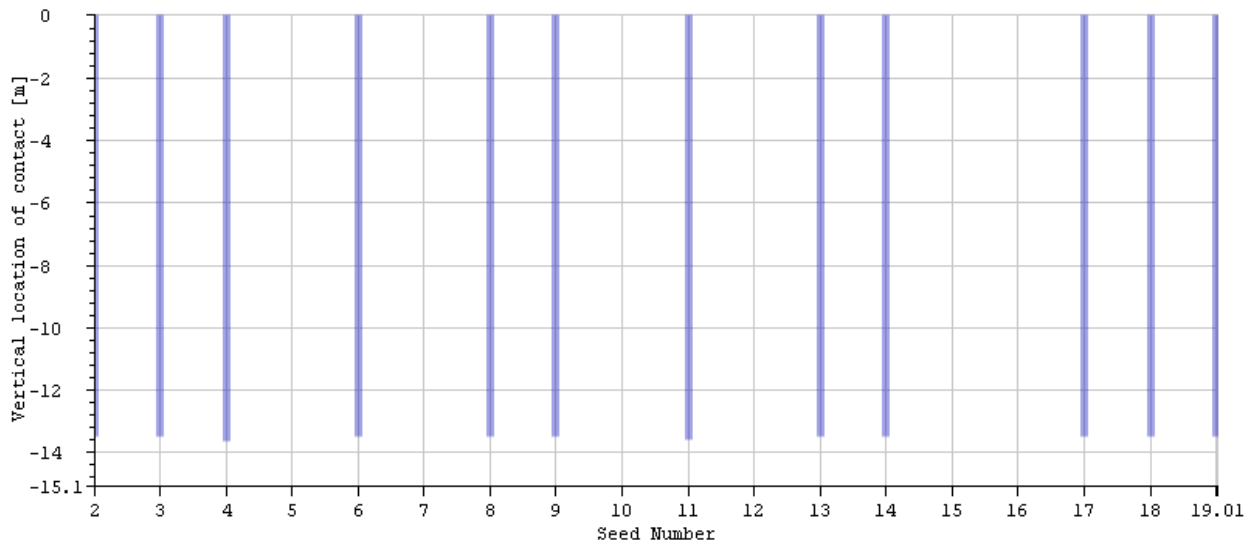


Figure 139: Vertical location of impact on the platform for different seeds, for case number 15.

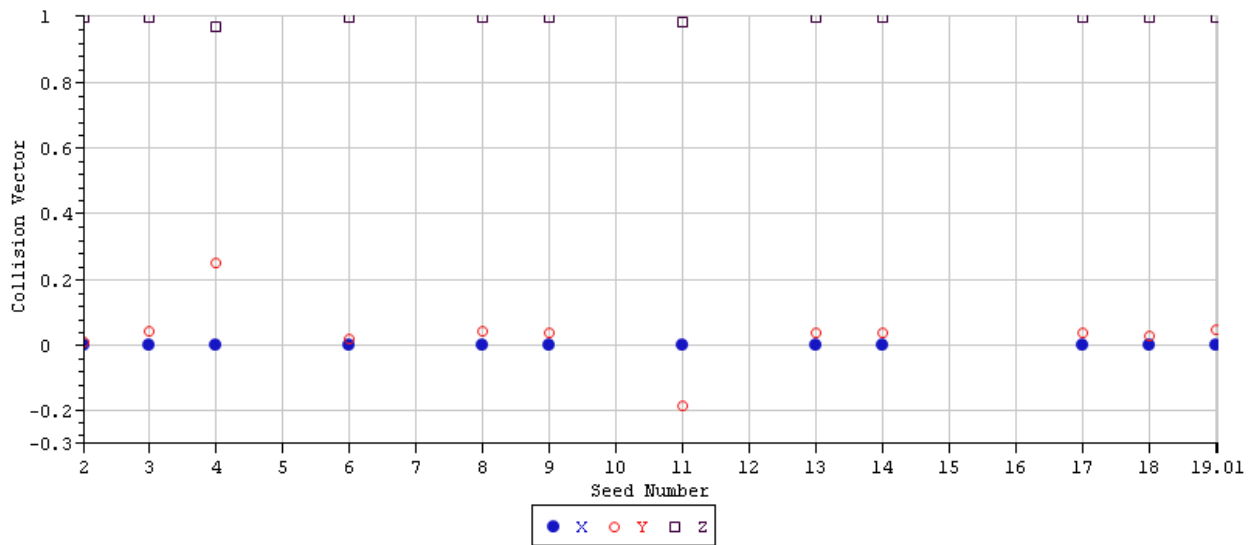


Figure 140: Collision vector components for different seeds, for case number 15.

18 Collision Scenario Number 16

	1	2	3	4	5
Signals		Max	Min	Mean	St. Dev.
RelativeCollisionVelocity	[m/s]	1.82	0.08	0.92	0.53
IceVelocity	[m/s]	3.24	0.37	1.57	0.76
CollisionHeight	[m]	9.5	9.35	9.47	0.05

Table 60: Statistical values calculated for collision scenario number 16.

	1	2	3	4
Signals		MP	Exp	P90
RelativeCollisionVelocity	[m/s]	0.68	0.83	1.65
IceVelocity	[m/s]	1.22	1.44	2.6
CollisionHeight	[m]	9.45	9.46	9.55

Table 61: Statistical values calculated for collision scenario number 16.

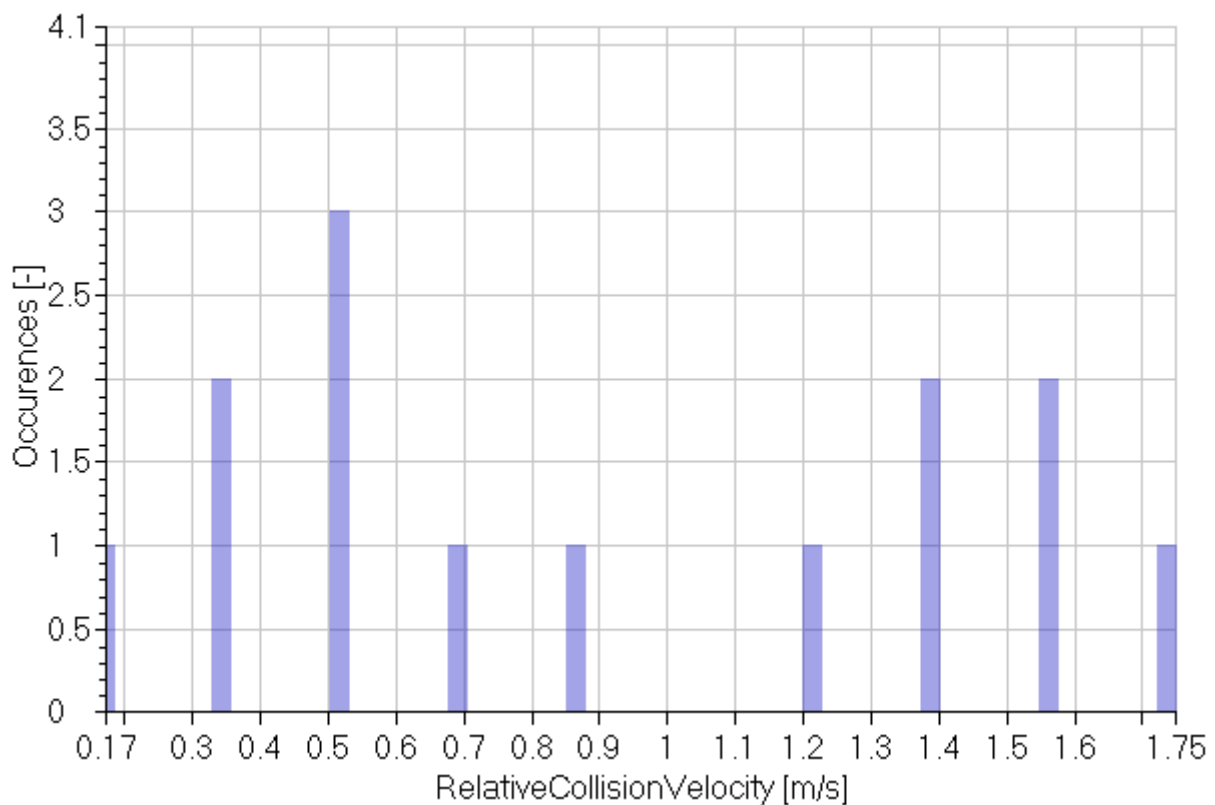


Figure 141: collision scenario number 16

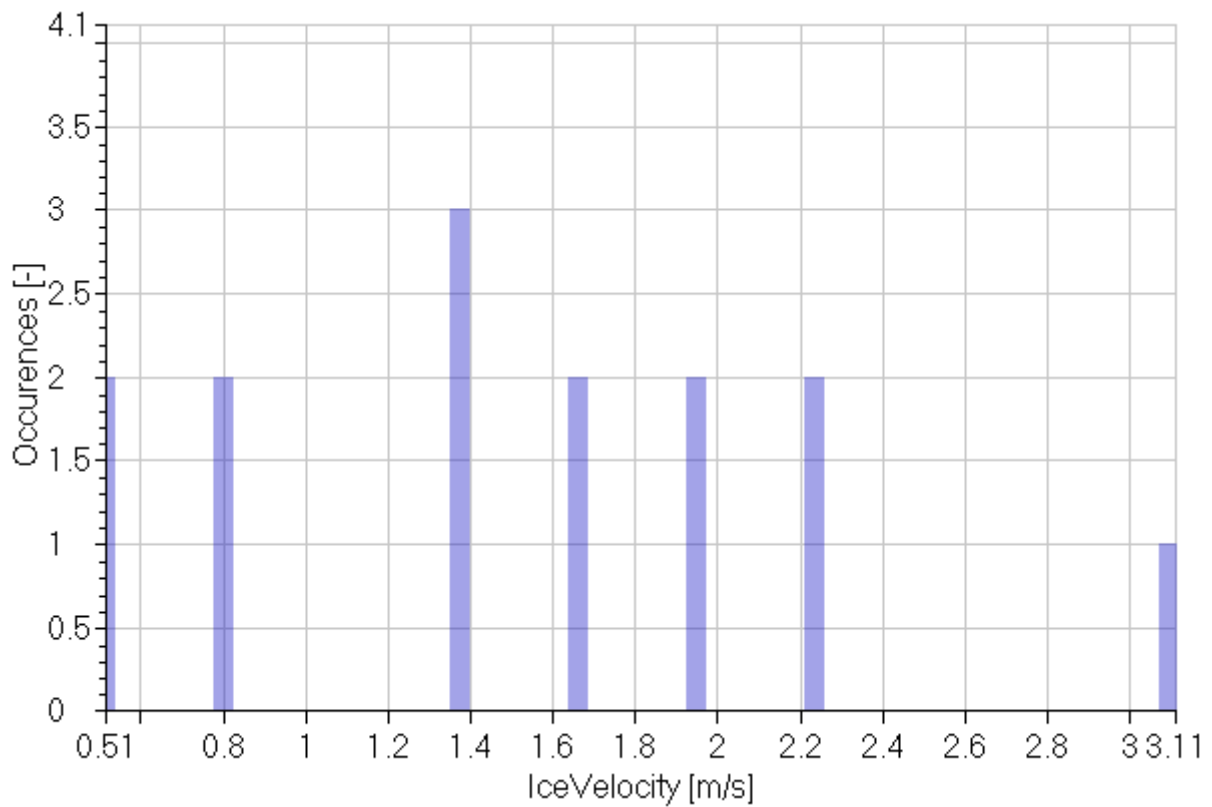


Figure 142: collision scenario number 16

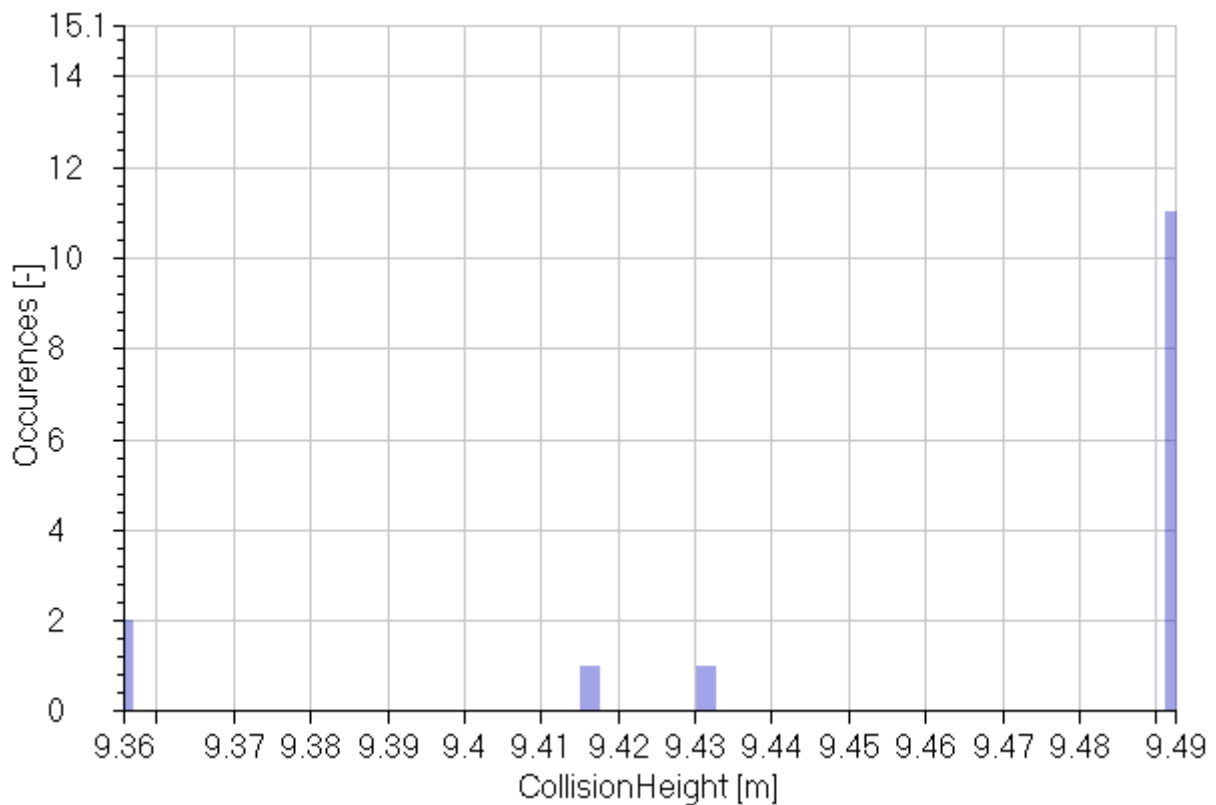


Figure 143: collision scenario number 16

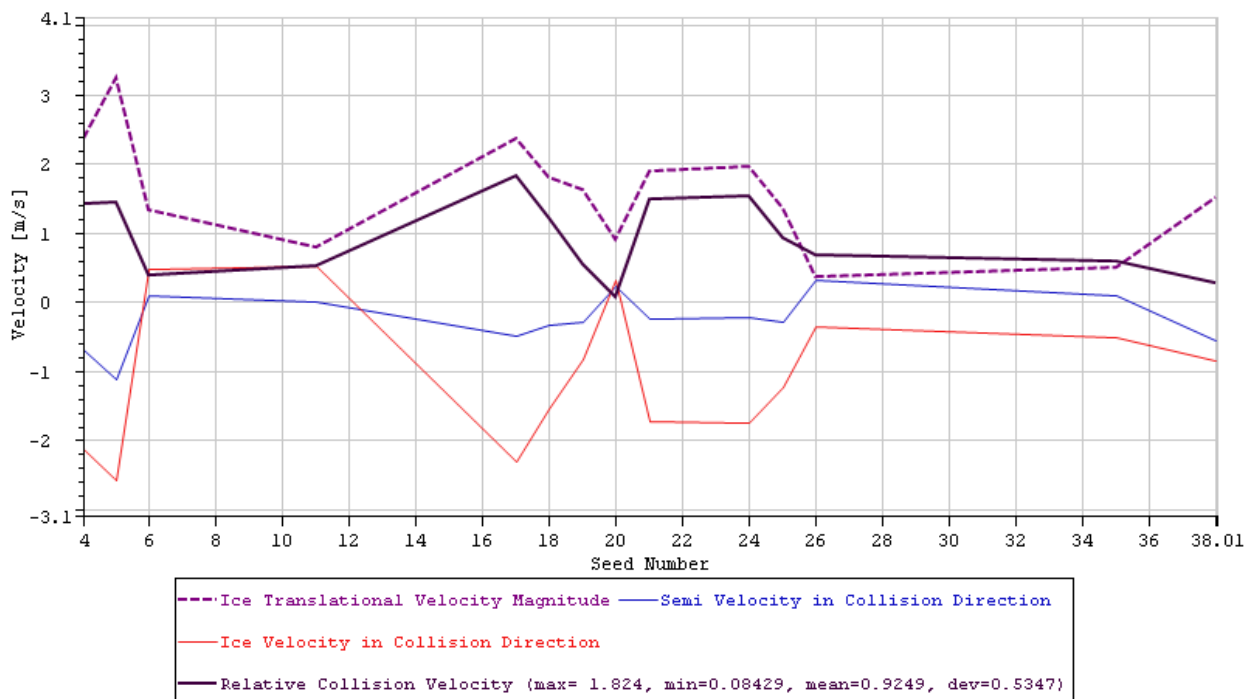


Figure 144: Total and relative collision velocities of ice and platform for different seeds, for case number 16.

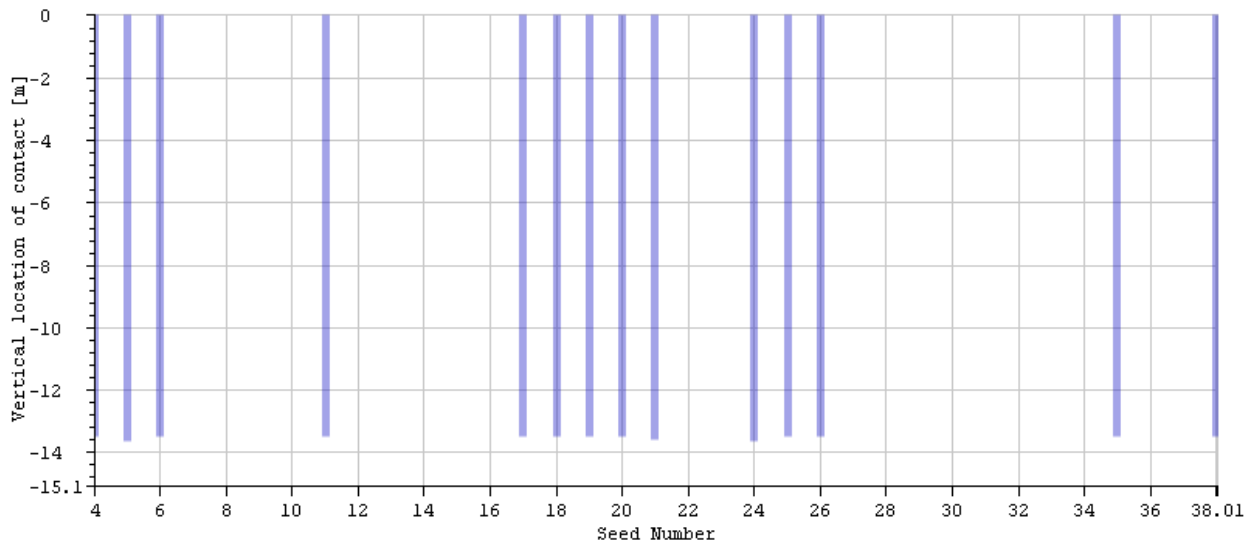


Figure 145: Vertical location of impact on the platform for different seeds, for case number 16.

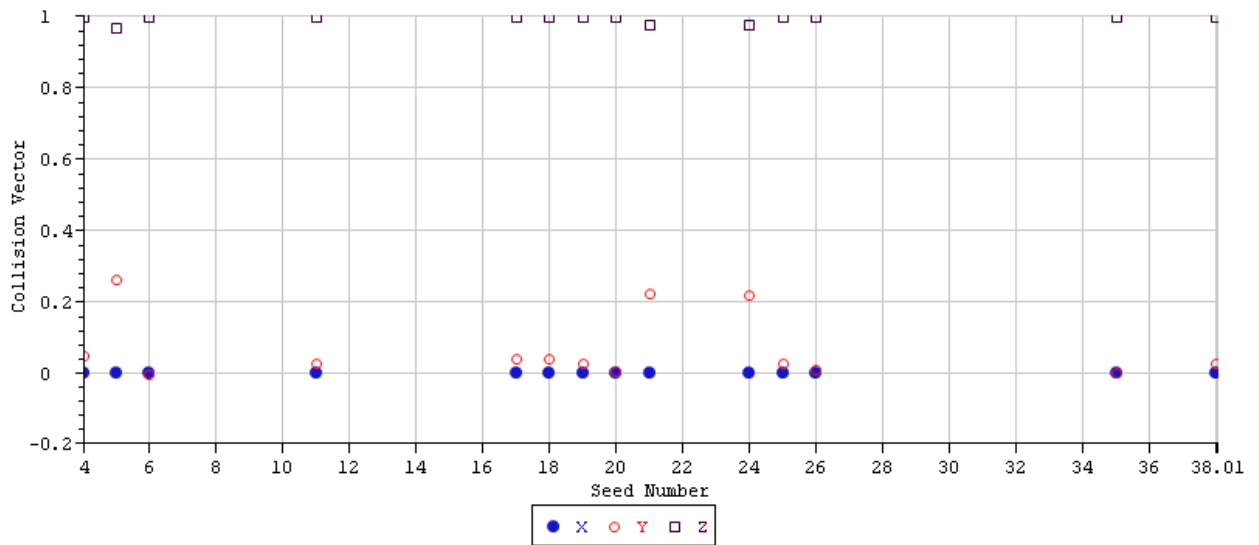


Figure 146: Collision vector components for different seeds, for case number 16.

19 Collision Scenario Number 17

	1	2	3	4	5
Signals		Max	Min	Mean	St. Dev.
RelativeCollisionVelocity	[m/s]	1.87	0.03	0.9	0.62
IceVelocity	[m/s]	3.41	0.28	1.51	0.88
CollisionHeight	[m]	9.5	9.44	9.5	0.02

Table 62: Statistical values calculated for collision scenario number 17.

	1	2	3	4
Signals		MP	Exp	P90
RelativeCollisionVelocity	[m/s]	0.61	0.8	1.76
IceVelocity	[m/s]	1.1	1.36	2.71
CollisionHeight	[m]	9.49	9.49	9.52

Table 63: Statistical values calculated for collision scenario number 17.

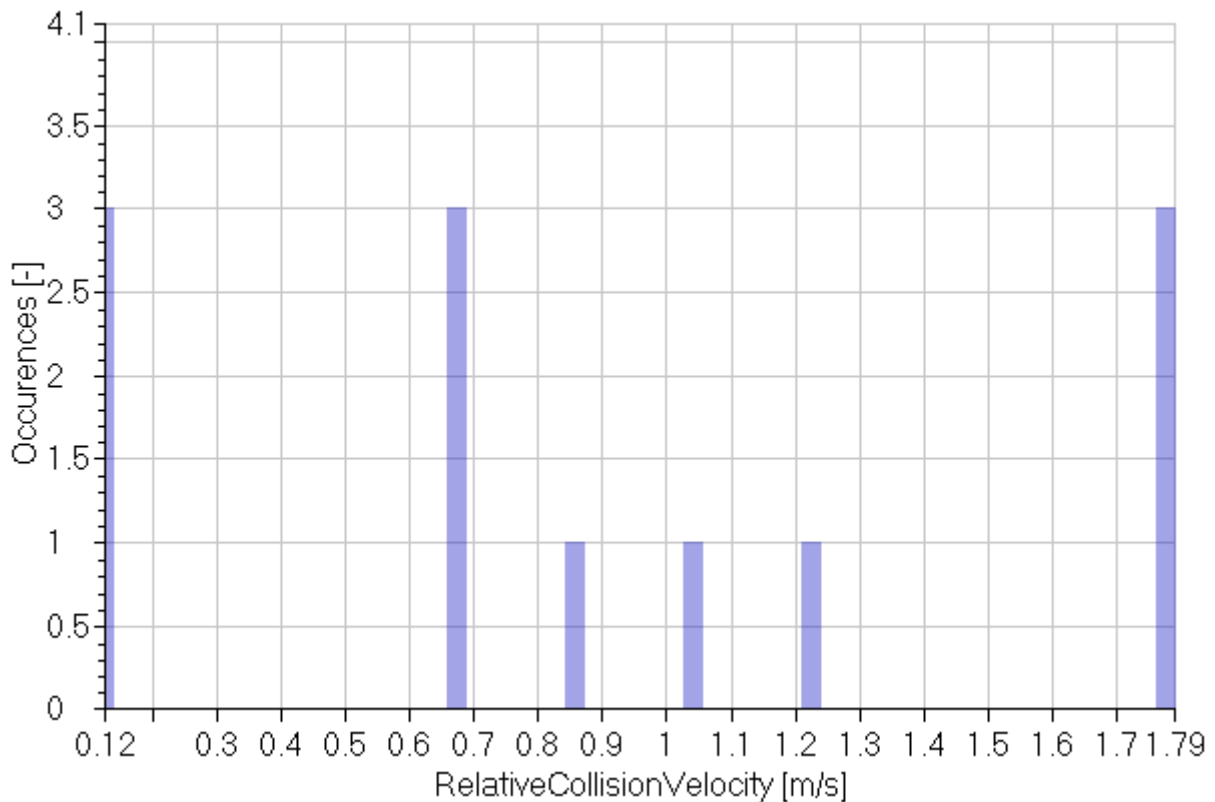


Figure 147: collision scenario number 17

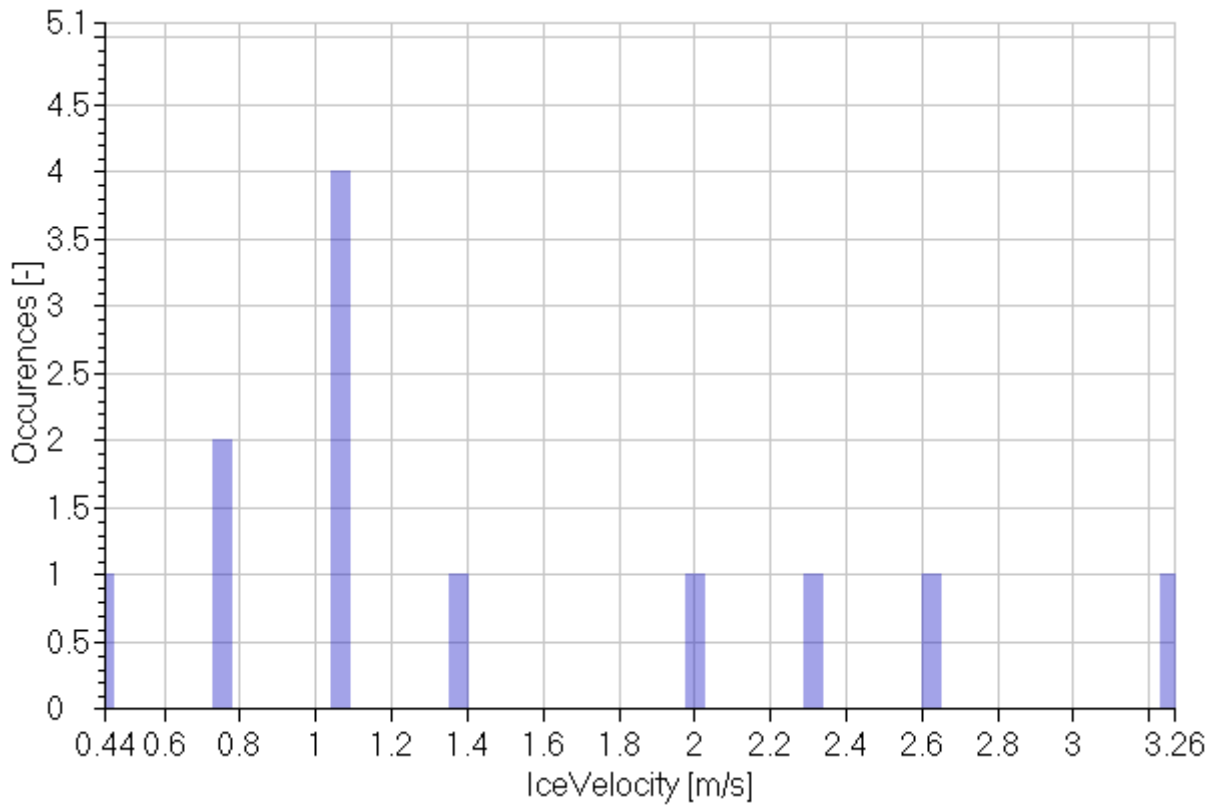


Figure 148: collision scenario number 17

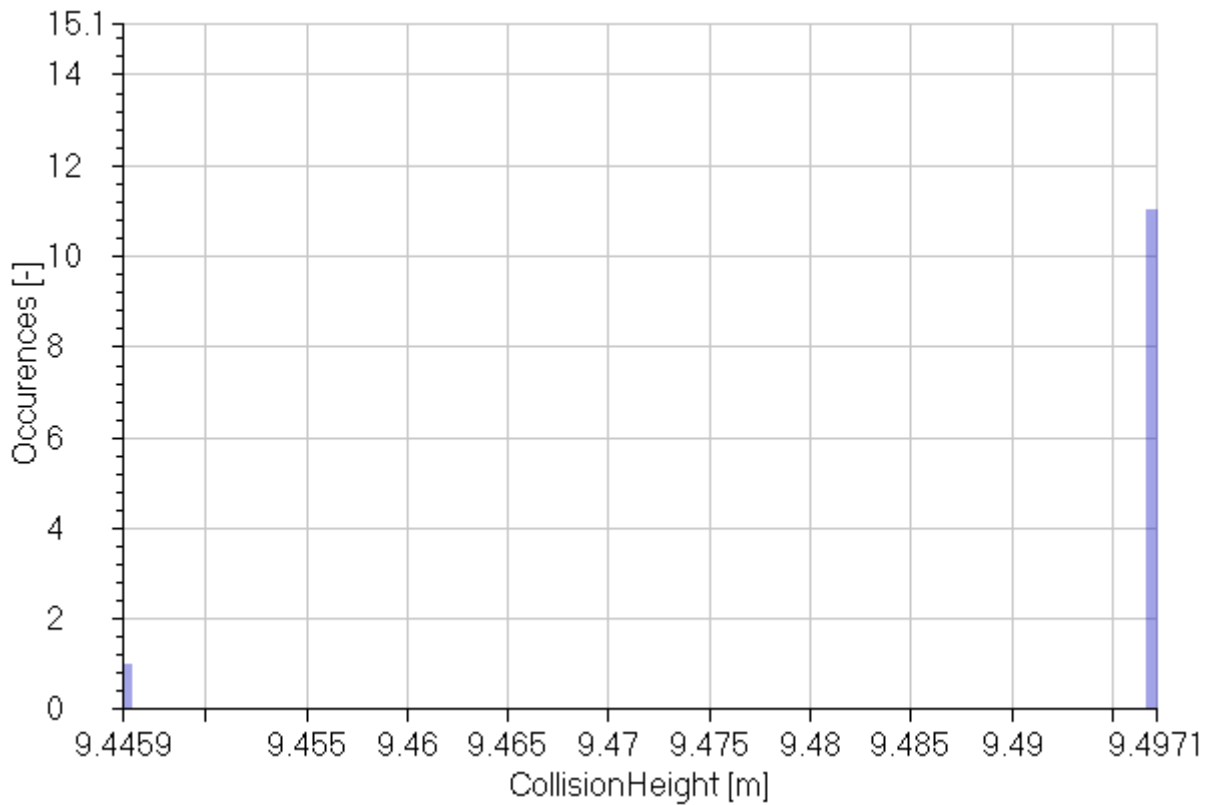


Figure 149: collision scenario number 17

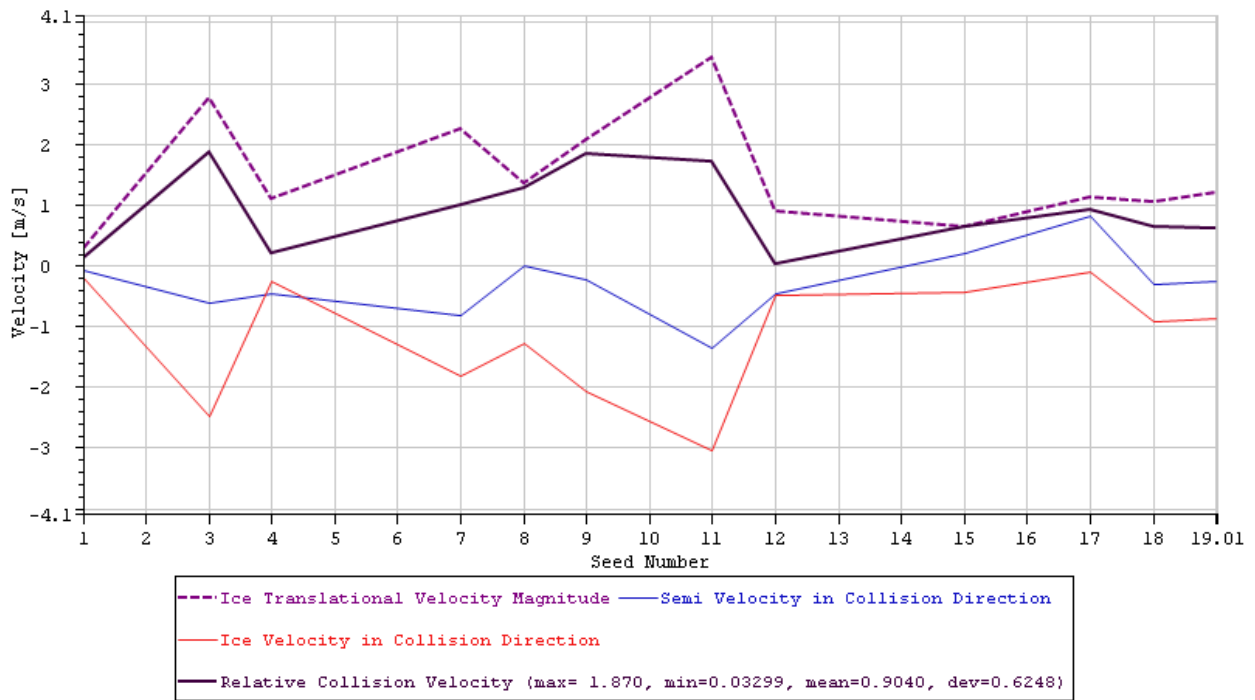


Figure 150: Total and relative collision velocities of ice and platform for different seeds, for case number 17.

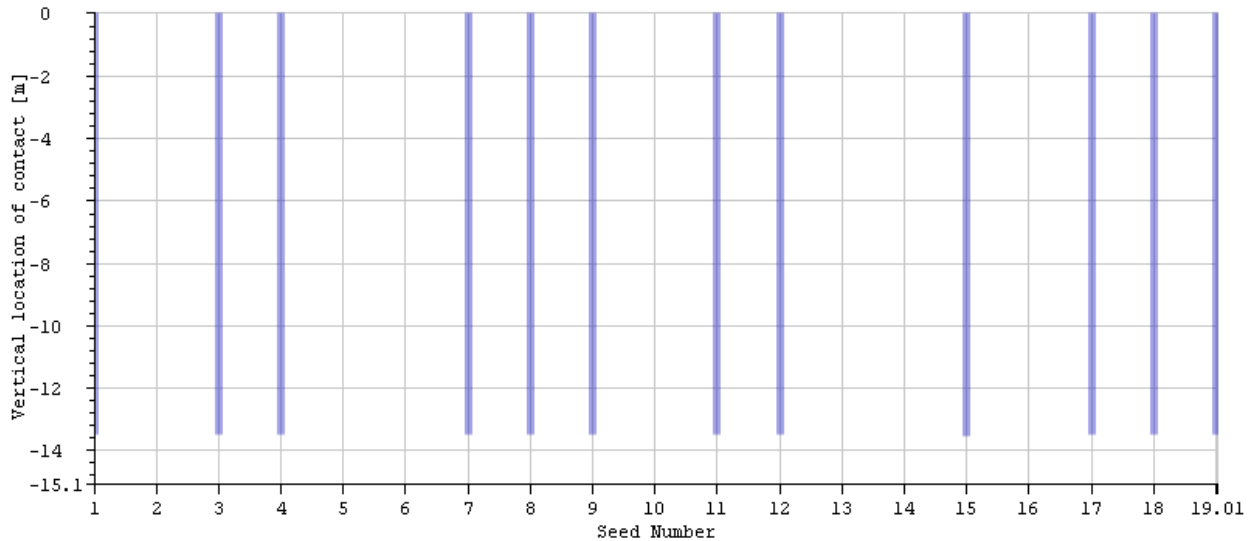


Figure 151: Vertical location of impact on the platform for different seeds, for case number 17.

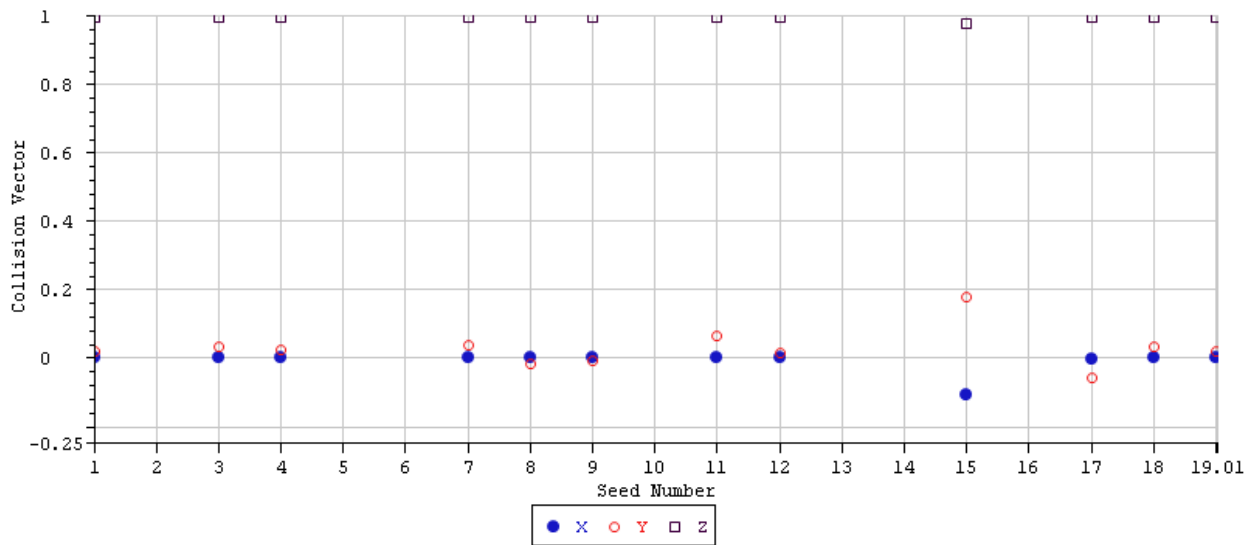


Figure 152: Collision vector components for different seeds, for case number 17.

20 Collision Scenario Number 22

	1	2	3	4	5
Signals		Max	Min	Mean	St. Dev.
RelativeCollisionVelocity	[m/s]	3.42	0.03	1.01	0.68
IceVelocity	[m/s]	4.57	0.36	1.74	0.8
CollisionHeight	[m]	9.5	9.35	9.49	0.04

Table 64: Statistical values calculated for collision scenario number 22.

	1	2	3	4
Signals		MP	Exp	P90
RelativeCollisionVelocity	[m/s]	0.7	0.9	1.91
IceVelocity	[m/s]	1.38	1.6	2.79
CollisionHeight	[m]	9.47	9.48	9.54

Table 65: Statistical values calculated for collision scenario number 22.

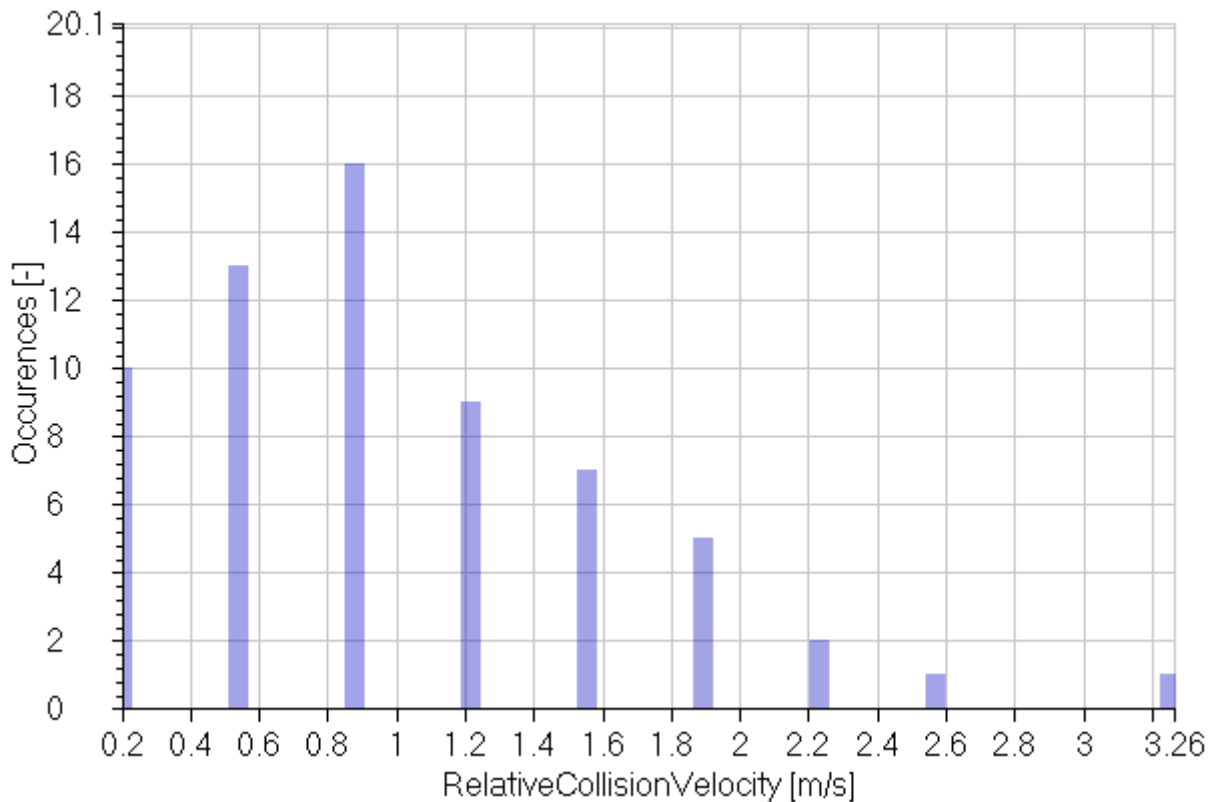


Figure 153: collision scenario number 22

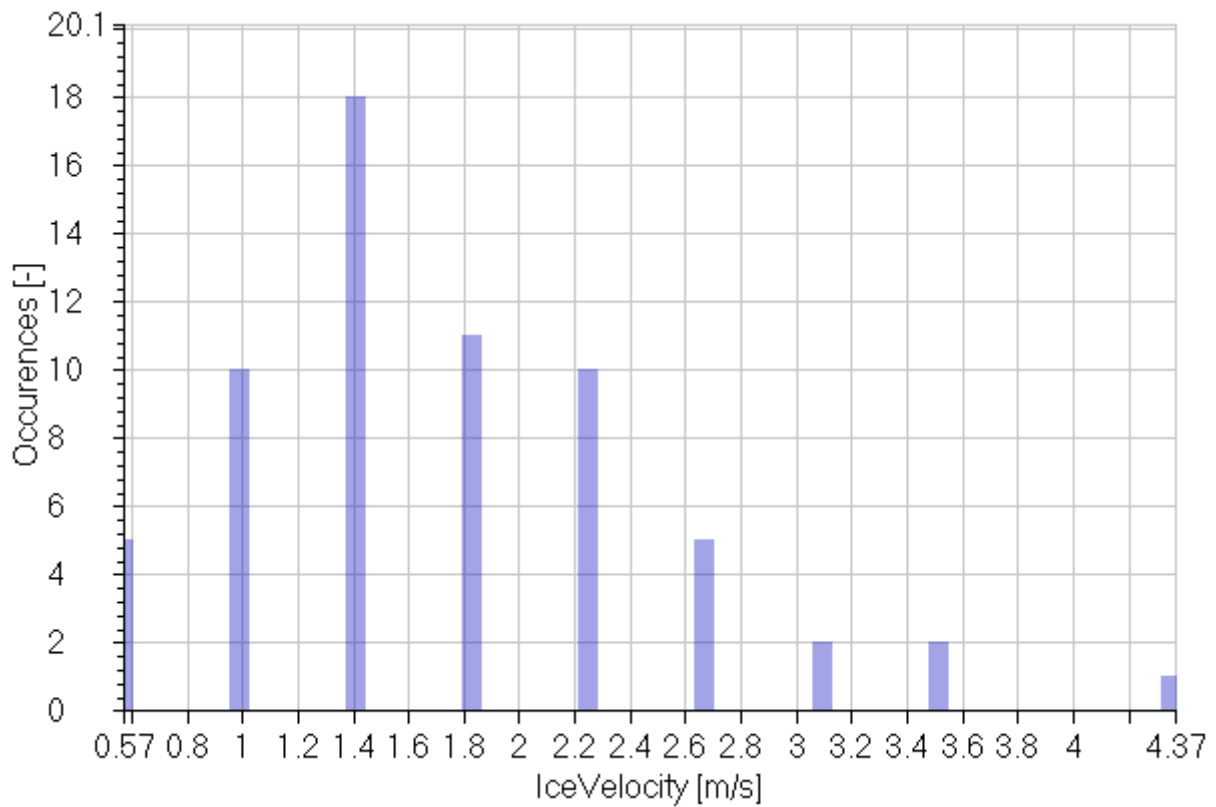


Figure 154: collision scenario number 22

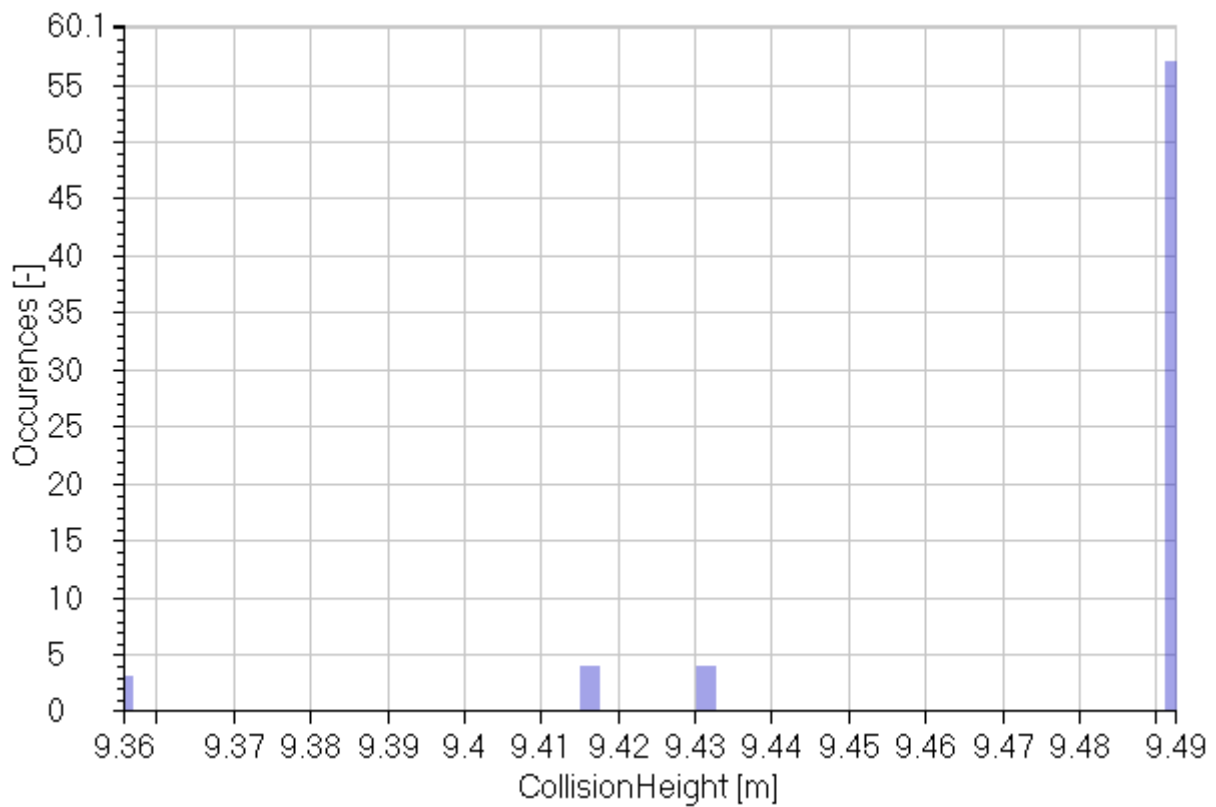


Figure 155: collision scenario number 22

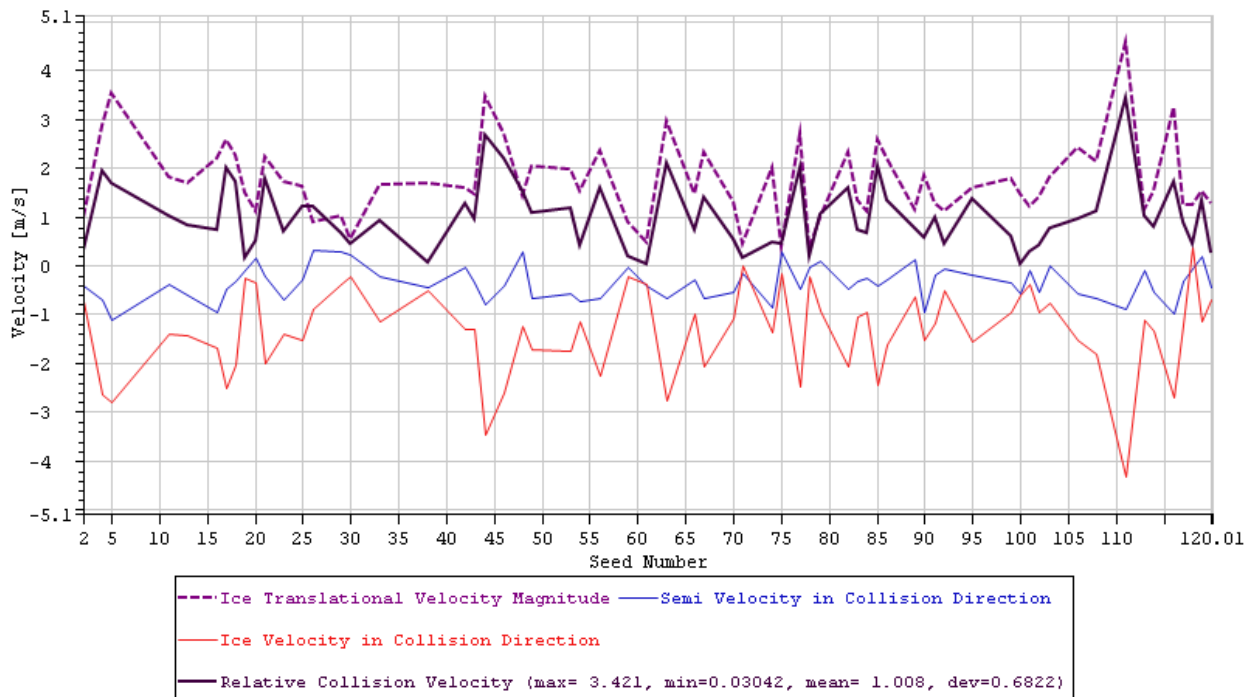


Figure 156: Total and relative collision velocities of ice and platform for different seeds, for case number 22.

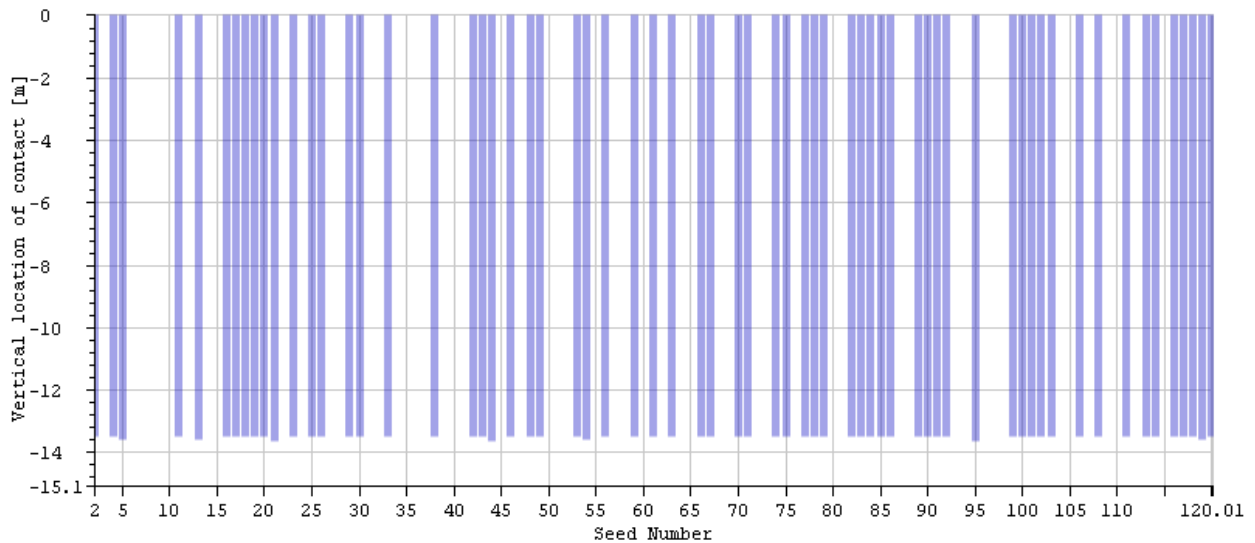


Figure 157: Vertical location of impact on the platform for different seeds, for case number 22.

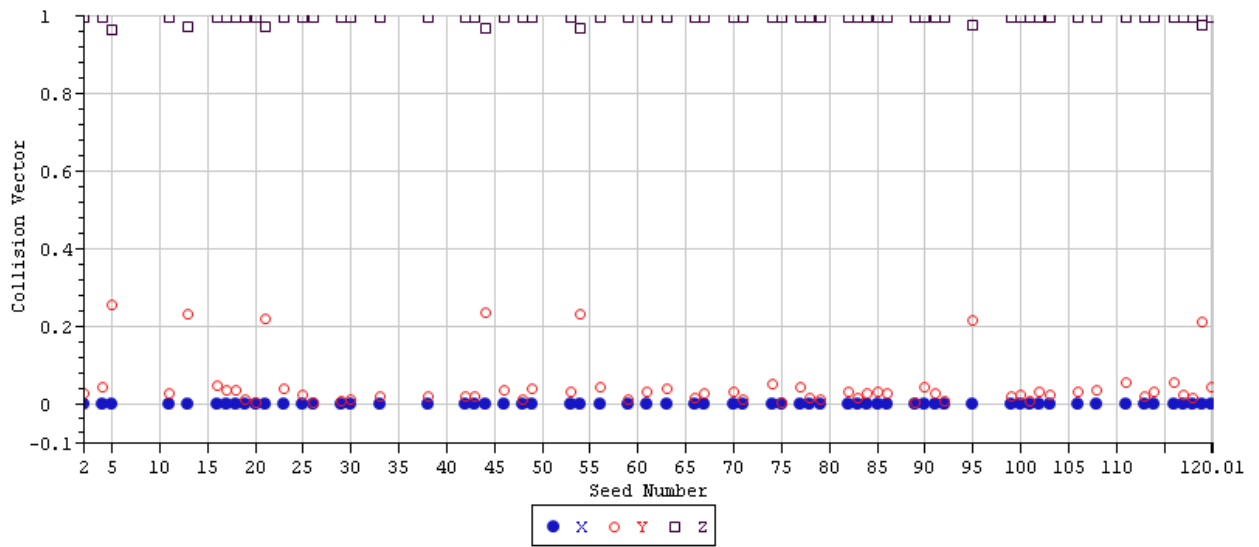


Figure 158: Collision vector components for different seeds, for case number 22.

21 Collision Scenario Number 23

	1	2	3	4	5
Signals		Max	Min	Mean	St. Dev.
RelativeCollisionVelocity	[m/s]	2.01	0.07	1	0.6
IceVelocity	[m/s]	3.54	0.53	1.77	0.73
CollisionHeight	[m]	9.5	9.35	9.48	0.04

Table 66: Statistical values calculated for collision scenario number 23.

	1	2	3	4
Signals		MP	Exp	P90
RelativeCollisionVelocity	[m/s]	0.72	0.89	1.8
IceVelocity	[m/s]	1.43	1.64	2.75
CollisionHeight	[m]	9.46	9.48	9.54

Table 67: Statistical values calculated for collision scenario number 23.

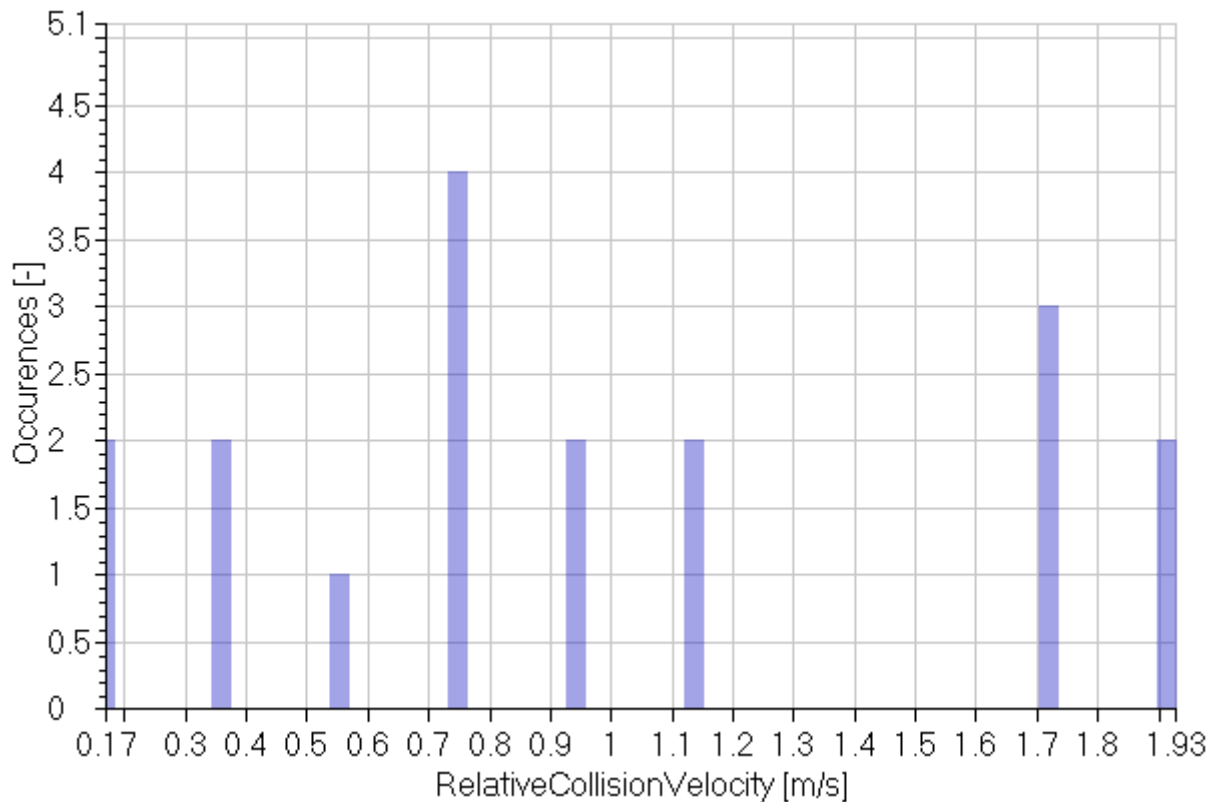


Figure 159: collision scenario number 23

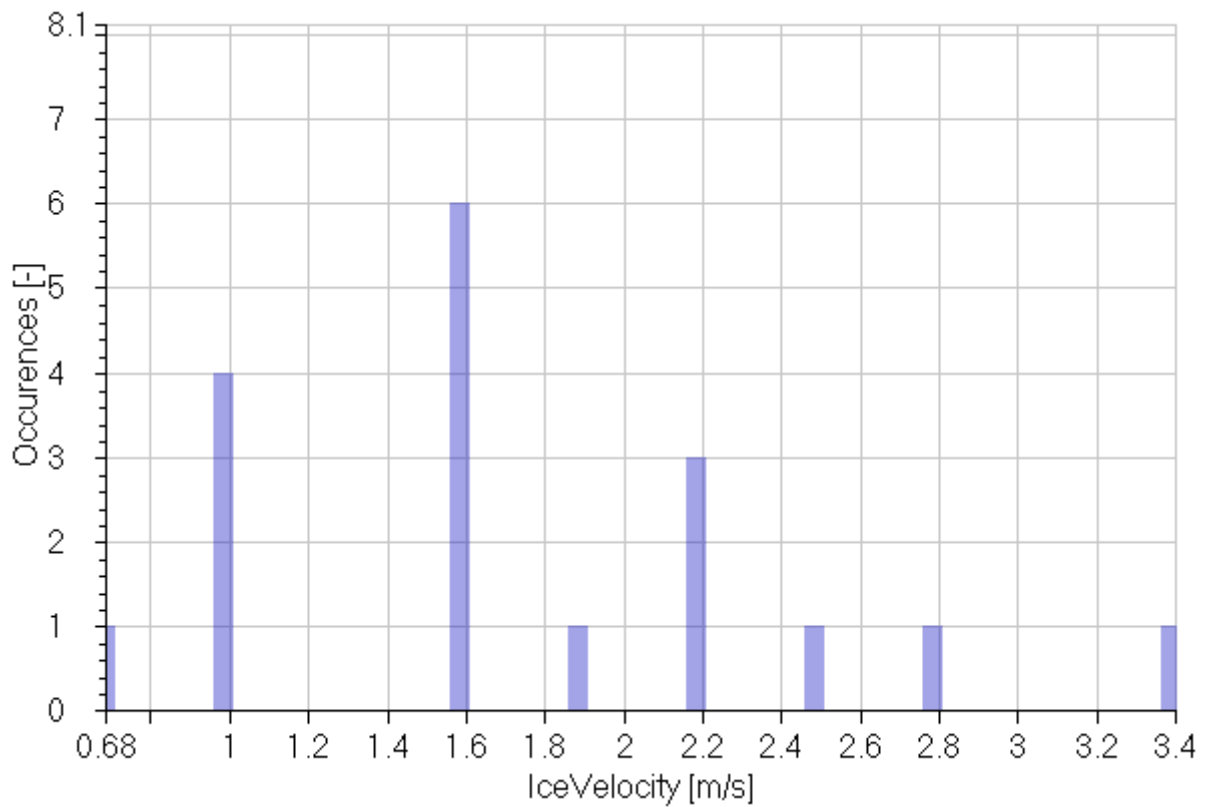


Figure 160: collision scenario number 23

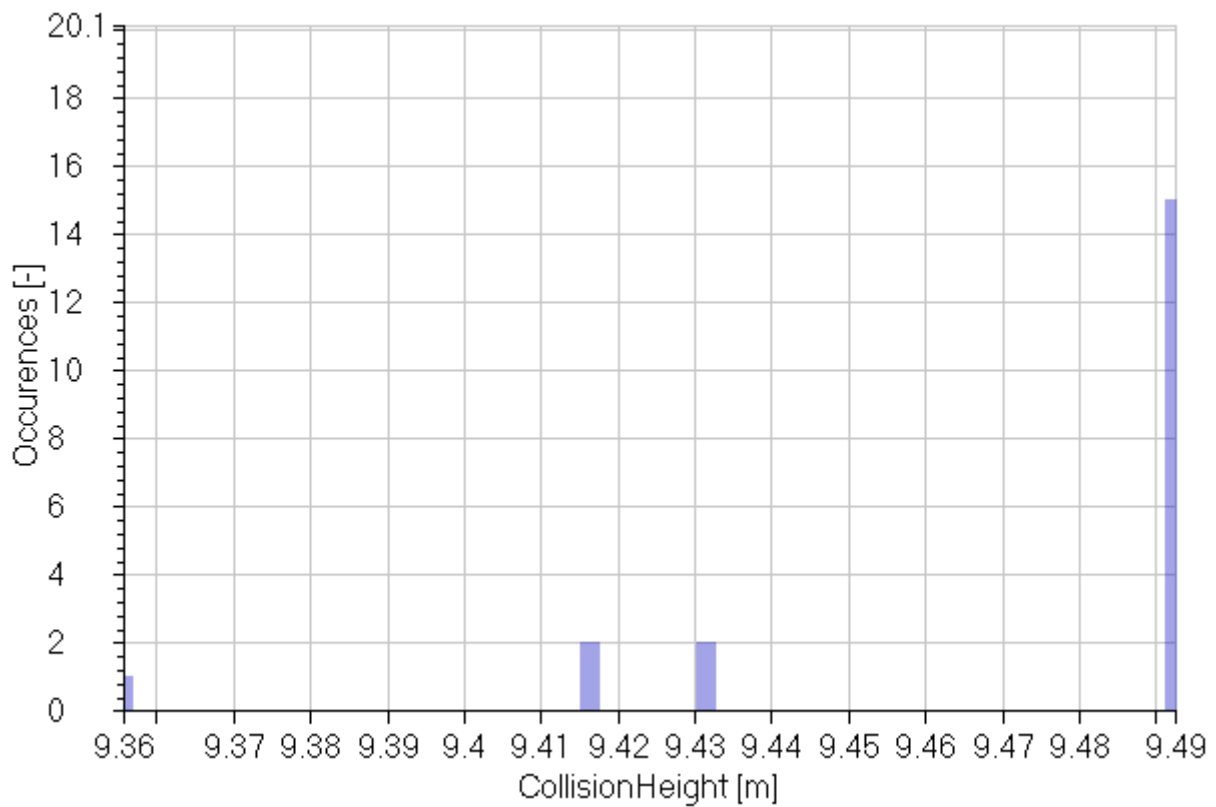


Figure 161: collision scenario number 23

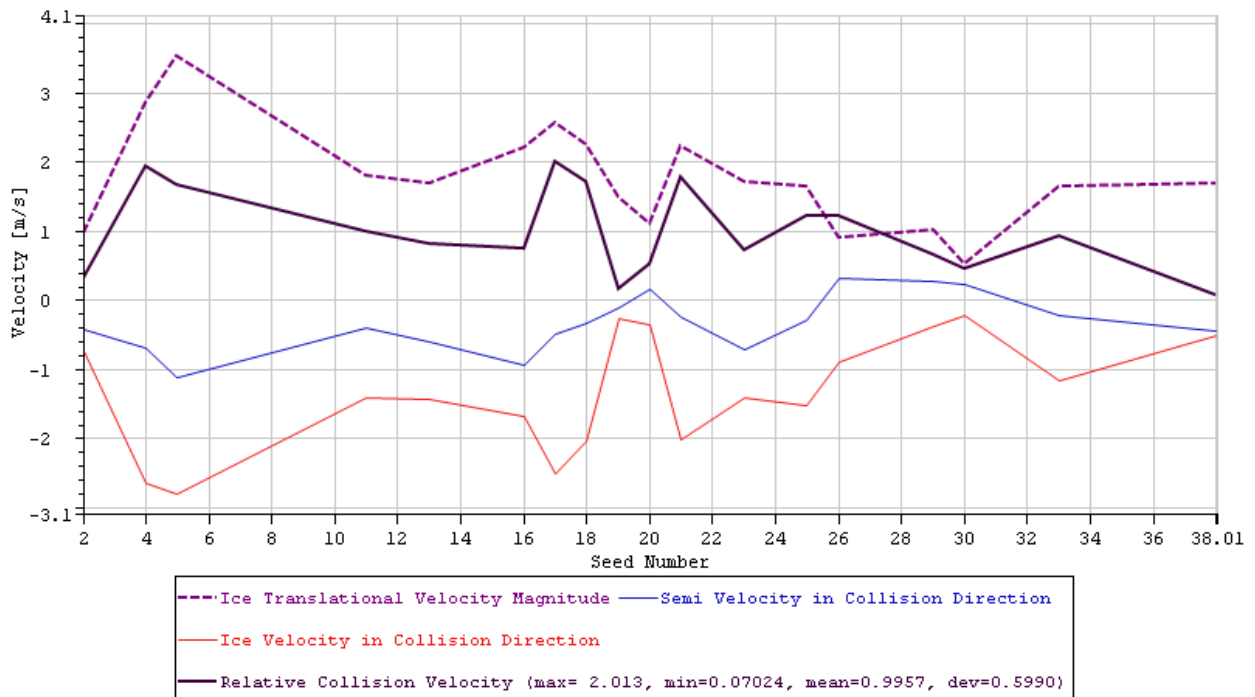


Figure 162: Total and relative collision velocities of ice and platform for different seeds, for case number 23.

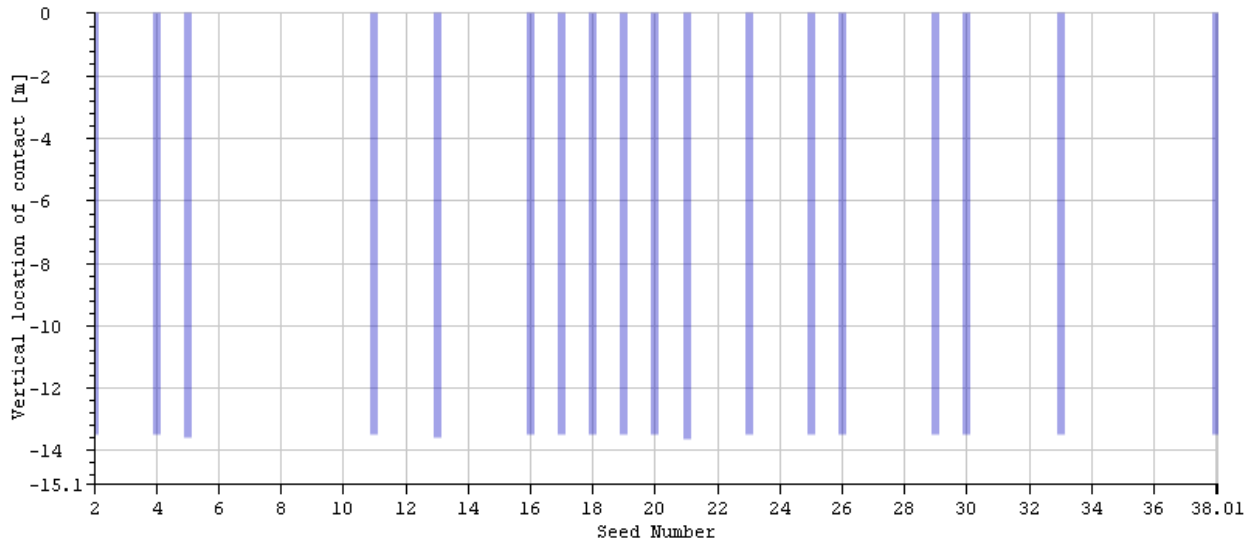


Figure 163: Vertical location of impact on the platform for different seeds, for case number 23.

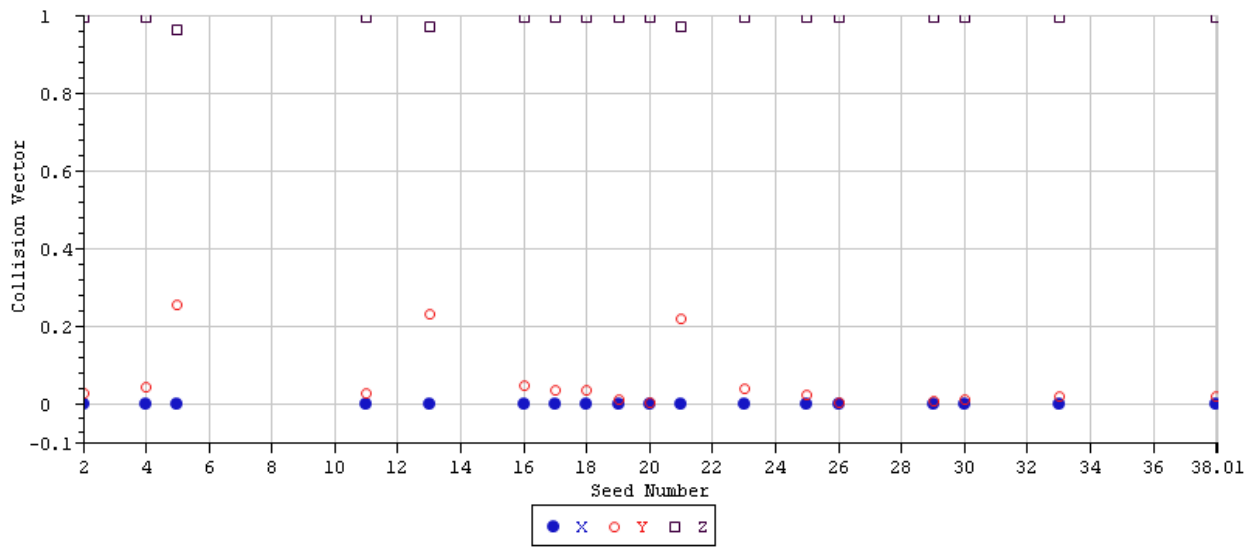


Figure 164: Collision vector components for different seeds, for case number 23.

Collision on the Brace

22 Collision Scenario Number 12

	1	2	3	4	5
Signals		Max	Min	Mean	St. Dev.
RelativeCollisionVelocity	[m/s]	2.49	0.18	1.23	0.64
IceVelocity	[m/s]	3.77	0.71	1.93	0.9
CollisionHeight	[m]	17.37	14.36	15.98	1.08

Table 68: Statistical values calculated for collision scenario number 12.

	1	2	3	4
Signals		MP	Exp	P90
RelativeCollisionVelocity	[m/s]	0.94	1.12	2.08
IceVelocity	[m/s]	1.52	1.78	3.14
CollisionHeight	[m]	15.49	15.8	17.43

Table 69: Statistical values calculated for collision scenario number 12.

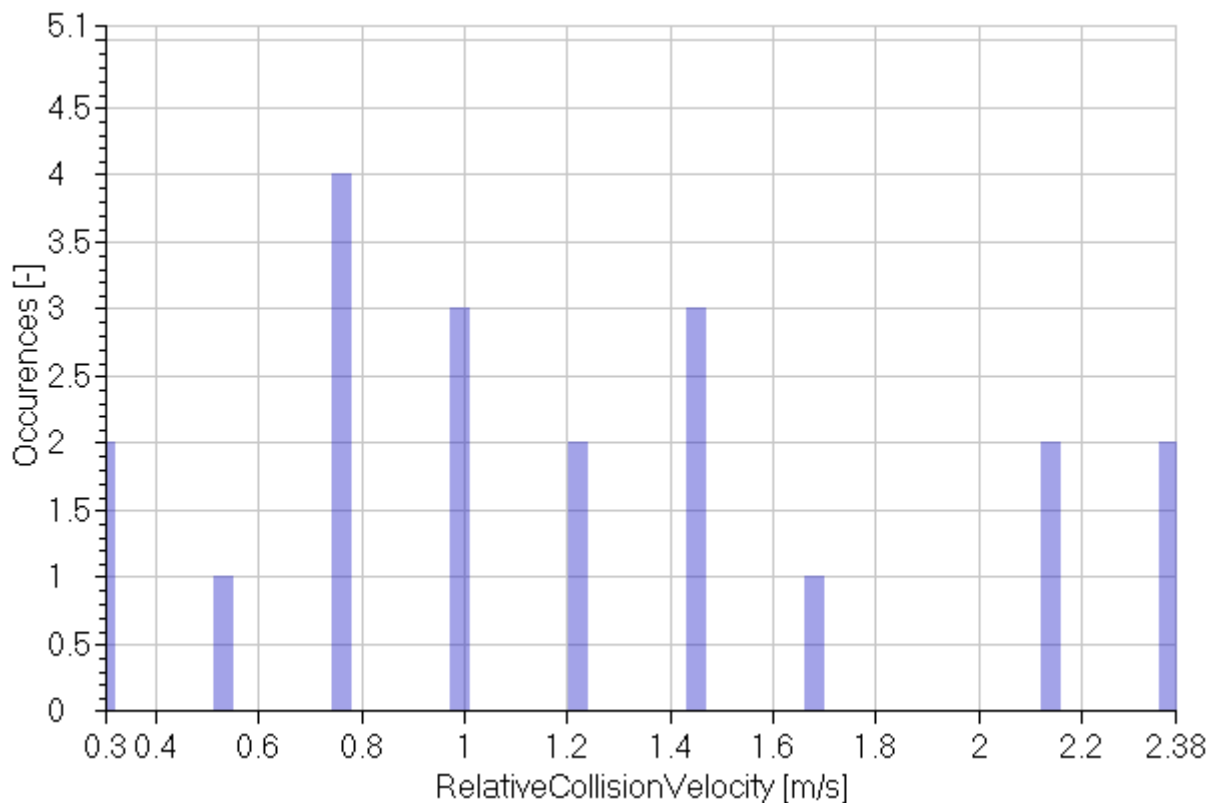


Figure 165: collision scenario number 12

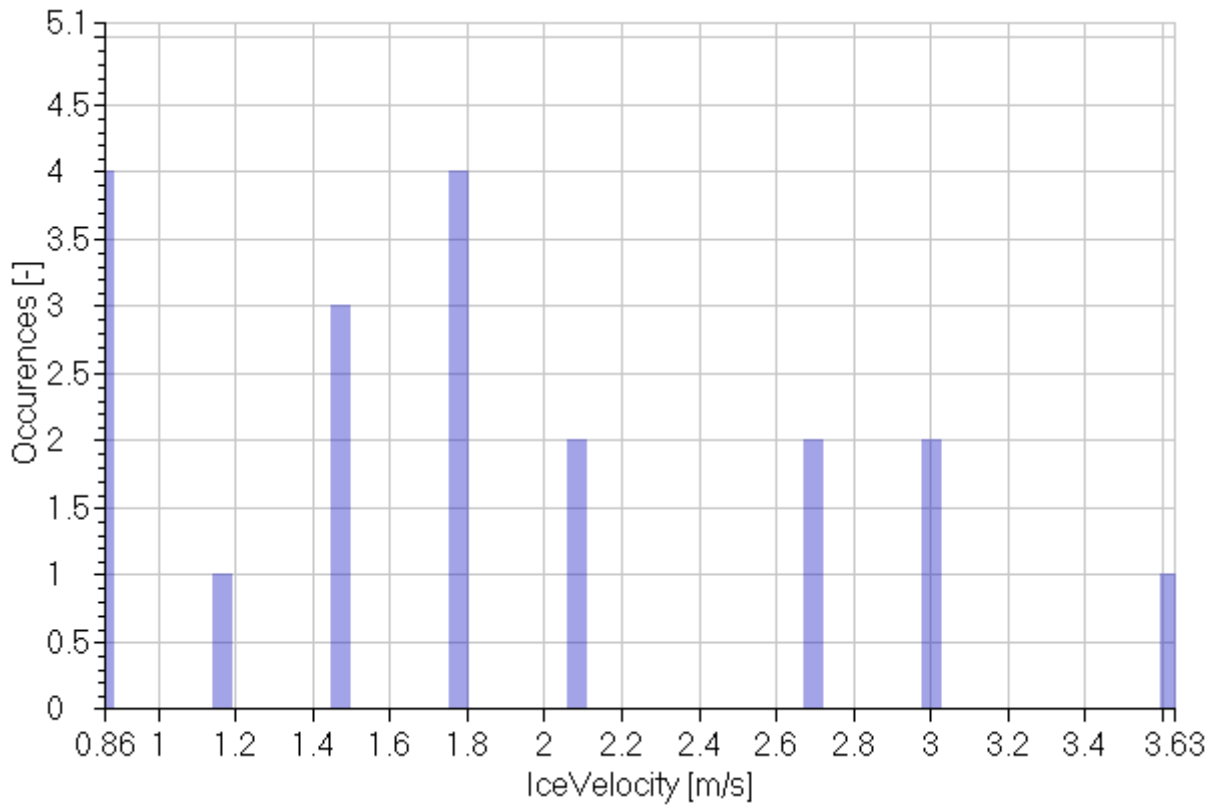


Figure 166: collision scenario number 12

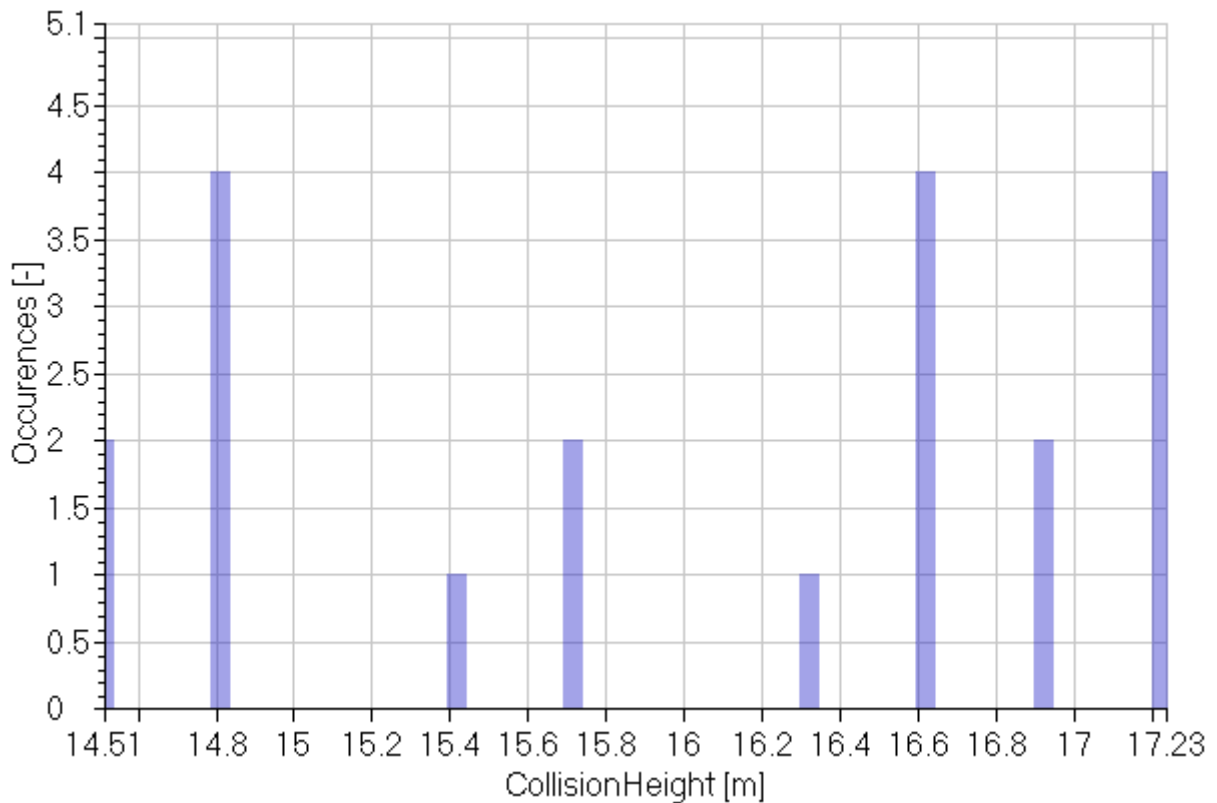


Figure 167: collision scenario number 12

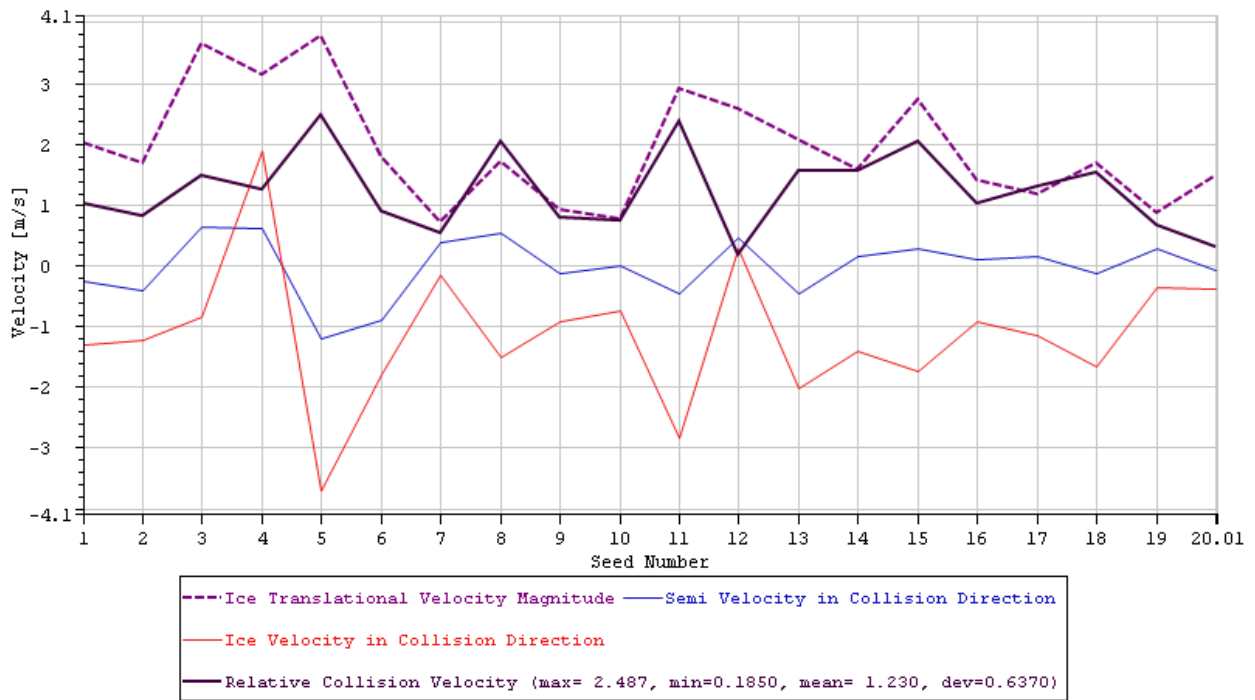


Figure 168: Total and relative collision velocities of ice and platform for different seeds, for case number 12.

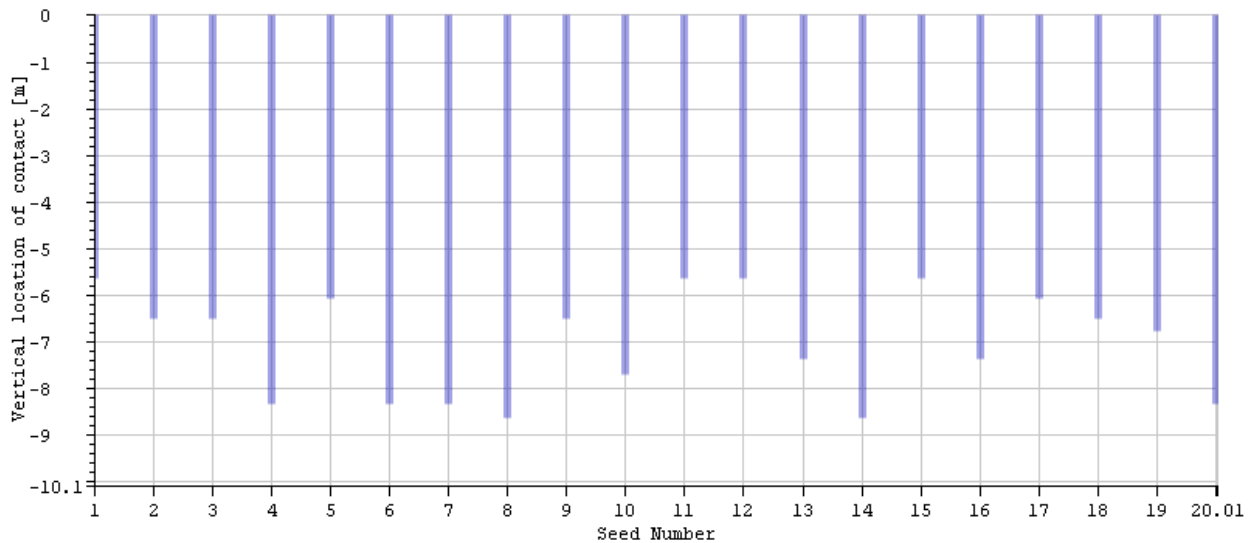


Figure 169: Vertical location of impact on the platform for different seeds, for case number 12.

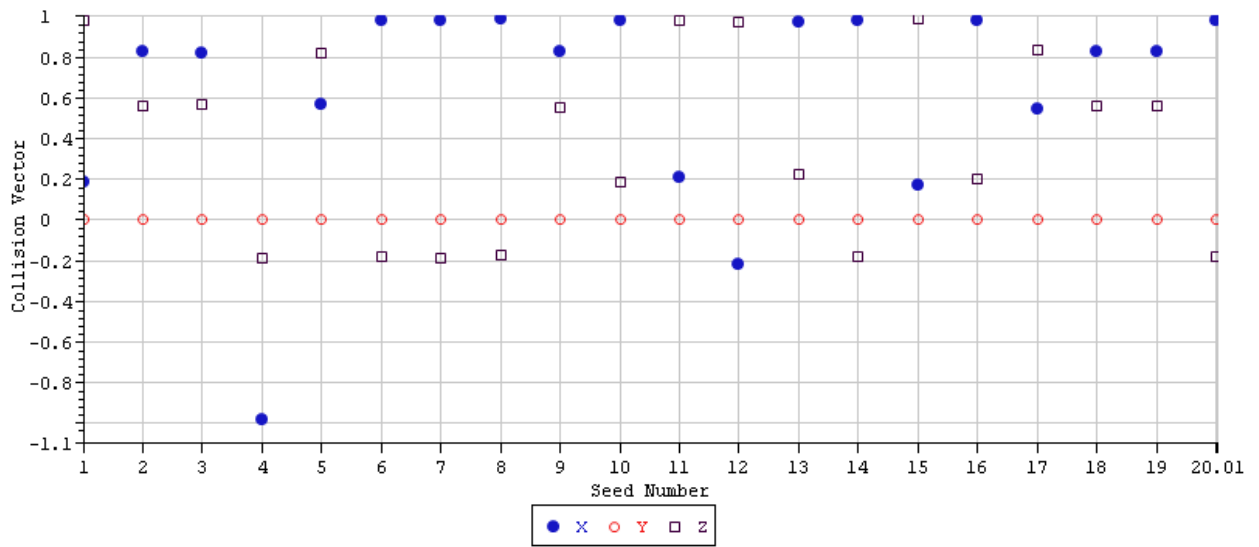


Figure 170: Collision vector components for different seeds, for case number 12.

23 Collision Scenario Number 13

	1	2	3	4	5
Signals		Max	Min	Mean	St. Dev.
RelativeCollisionVelocity	[m/s]	3.13	0.18	1.51	0.8
IceVelocity	[m/s]	4.47	0.48	2.29	1.02
CollisionHeight	[m]	17.44	14.36	16.49	0.9

Table 70: Statistical values calculated for collision scenario number 13.

	1	2	3	4
Signals		MP	Exp	P90
RelativeCollisionVelocity	[m/s]	1.14	1.38	2.59
IceVelocity	[m/s]	1.82	2.12	3.65
CollisionHeight	[m]	16.07	16.33	17.7

Table 71: Statistical values calculated for collision scenario number 13.

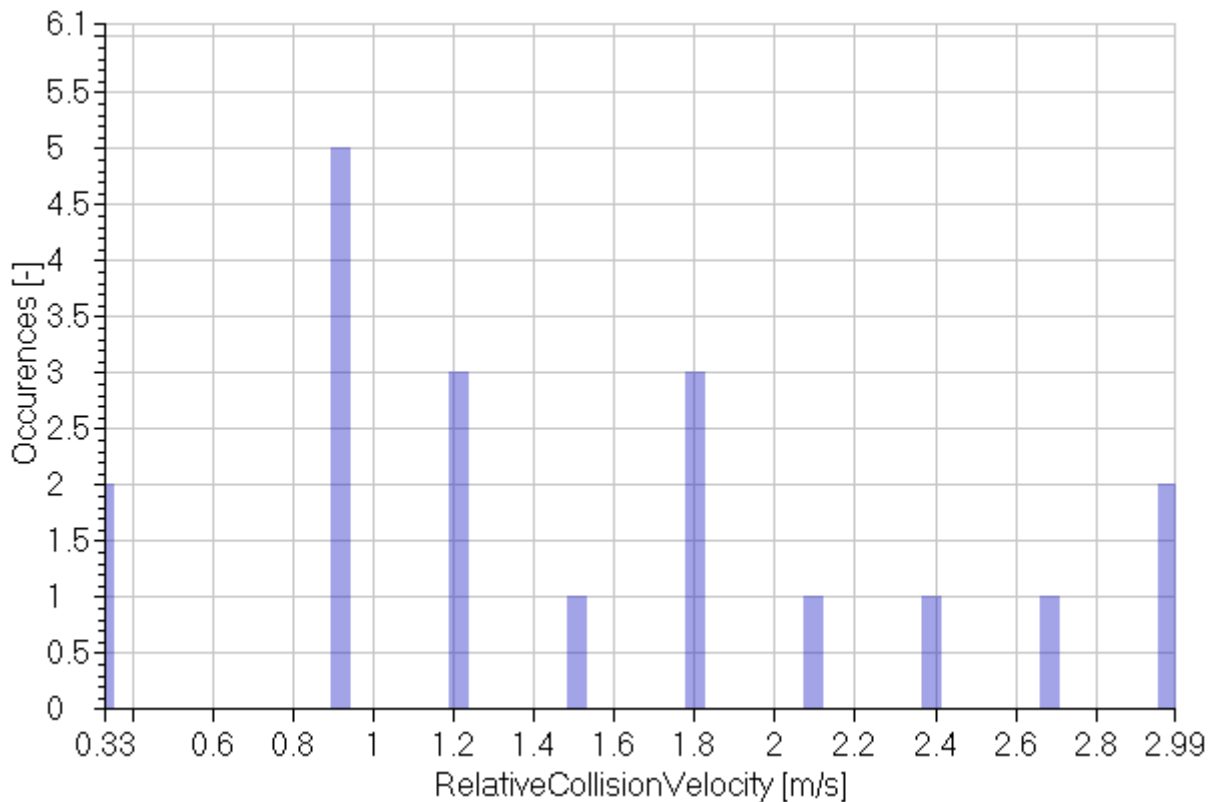


Figure 171: collision scenario number 13

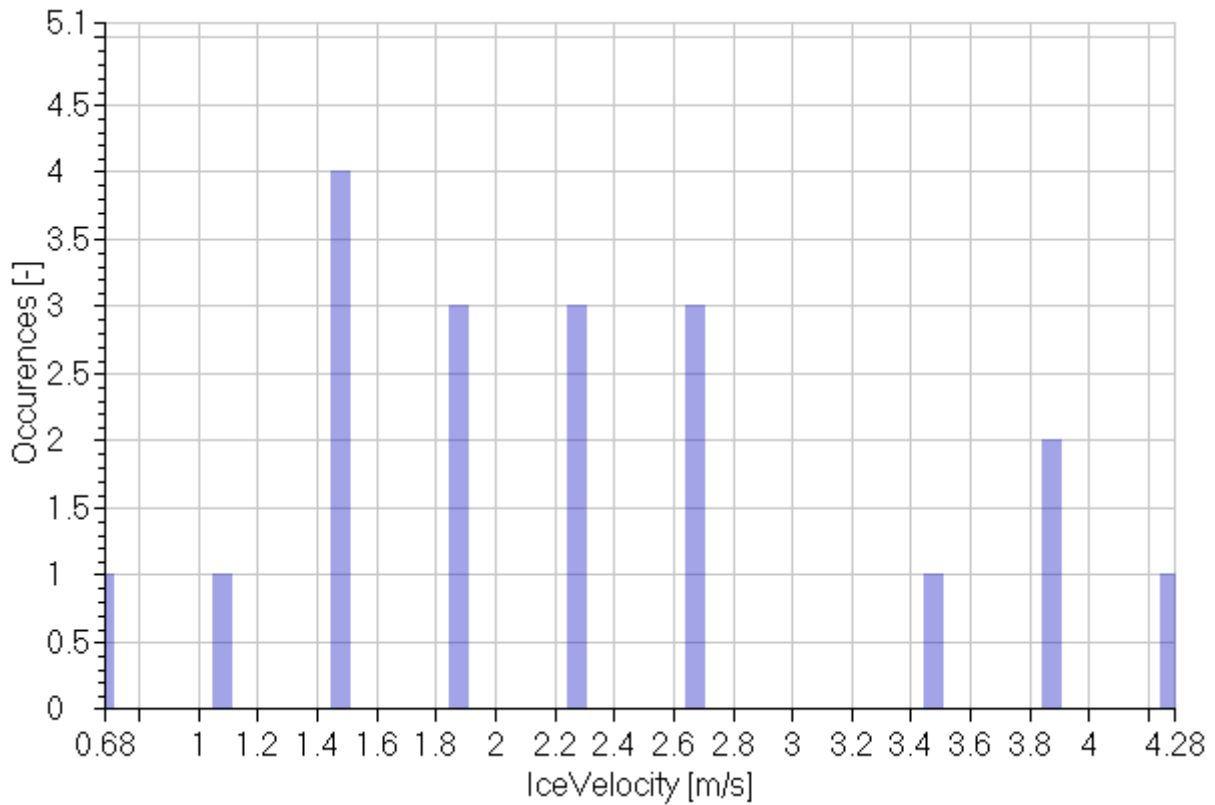


Figure 172: collision scenario number 13

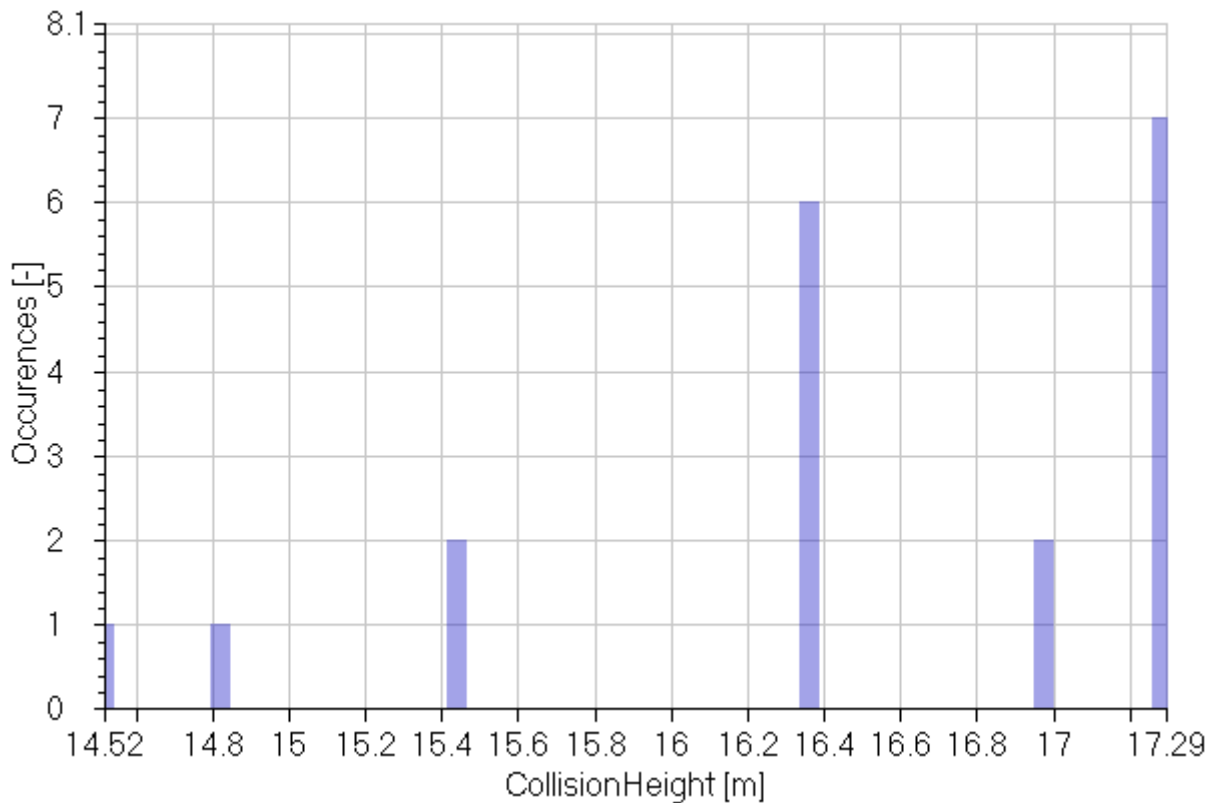


Figure 173: collision scenario number 13

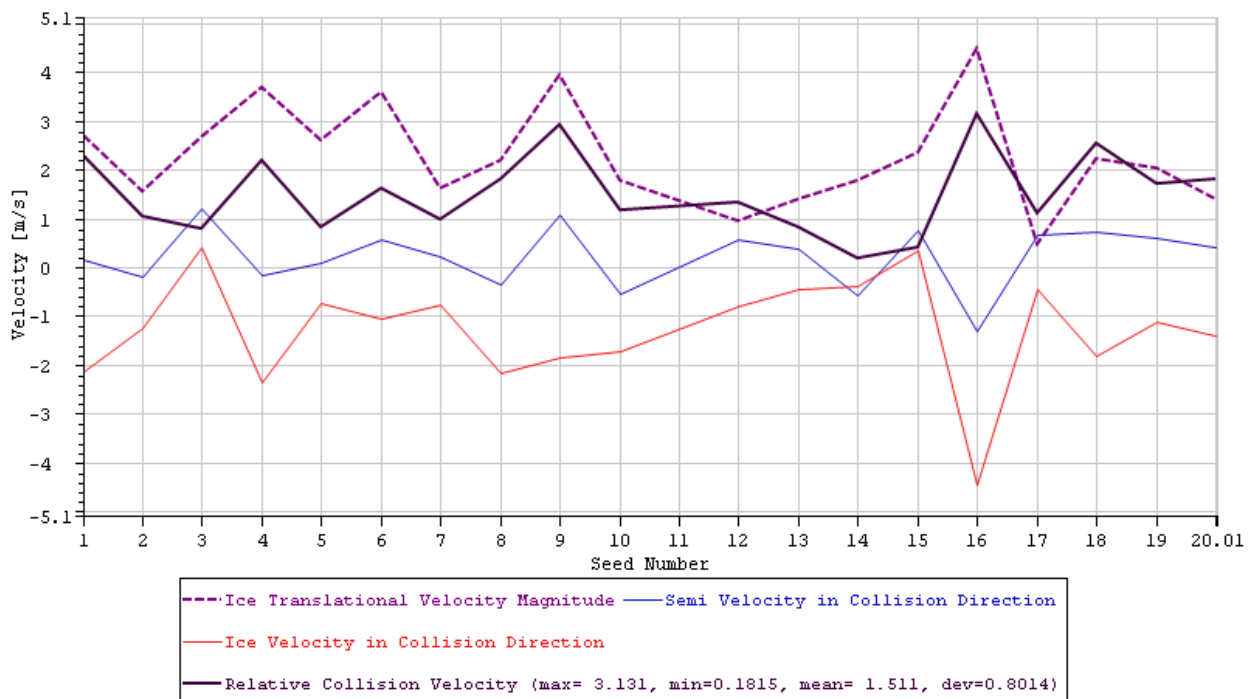


Figure 174: Total and relative collision velocities of ice and platform for different seeds, for case number 13.

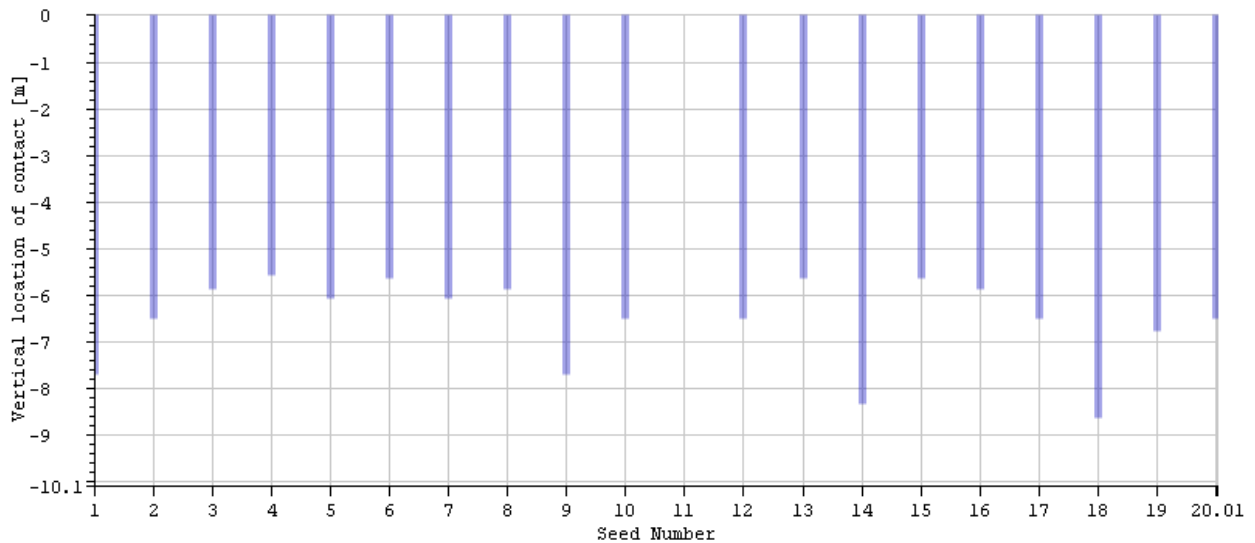


Figure 175: Vertical location of impact on the platform for different seeds, for case number 13.

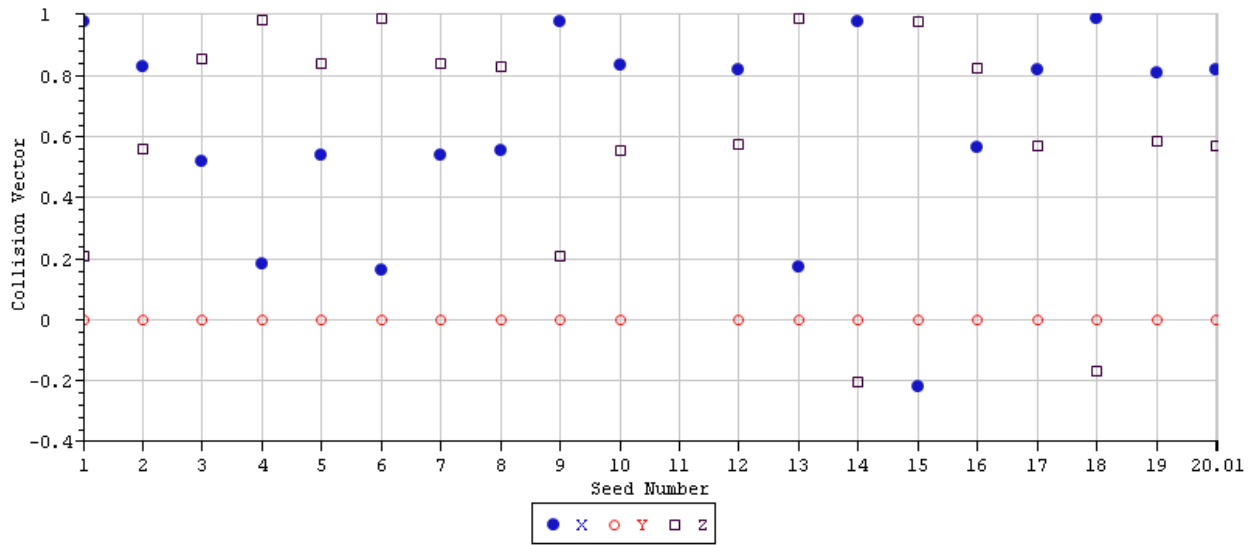


Figure 176: Collision vector components for different seeds, for case number 13.

Collision on the Riser

24 Collision Scenario Number 16

	1	2	3	4	5
Signals		Max	Min	Mean	St. Dev.
RelativeCollisionVelocity	[m/s]	2.46	0.21	1.27	0.49
IceVelocity	[m/s]	4.46	0.47	2.2	0.95
CollisionHeight	[m]	26.33	14.33	21.21	3.09

Table 72: Statistical values calculated for collision scenario number 16.

	1	2	3	4
Signals		MP	Exp	P90
RelativeCollisionVelocity	[m/s]	1.04	1.18	1.92
IceVelocity	[m/s]	1.77	2.04	3.47
CollisionHeight	[m]	19.81	20.7	25.32

Table 73: Statistical values calculated for collision scenario number 16.

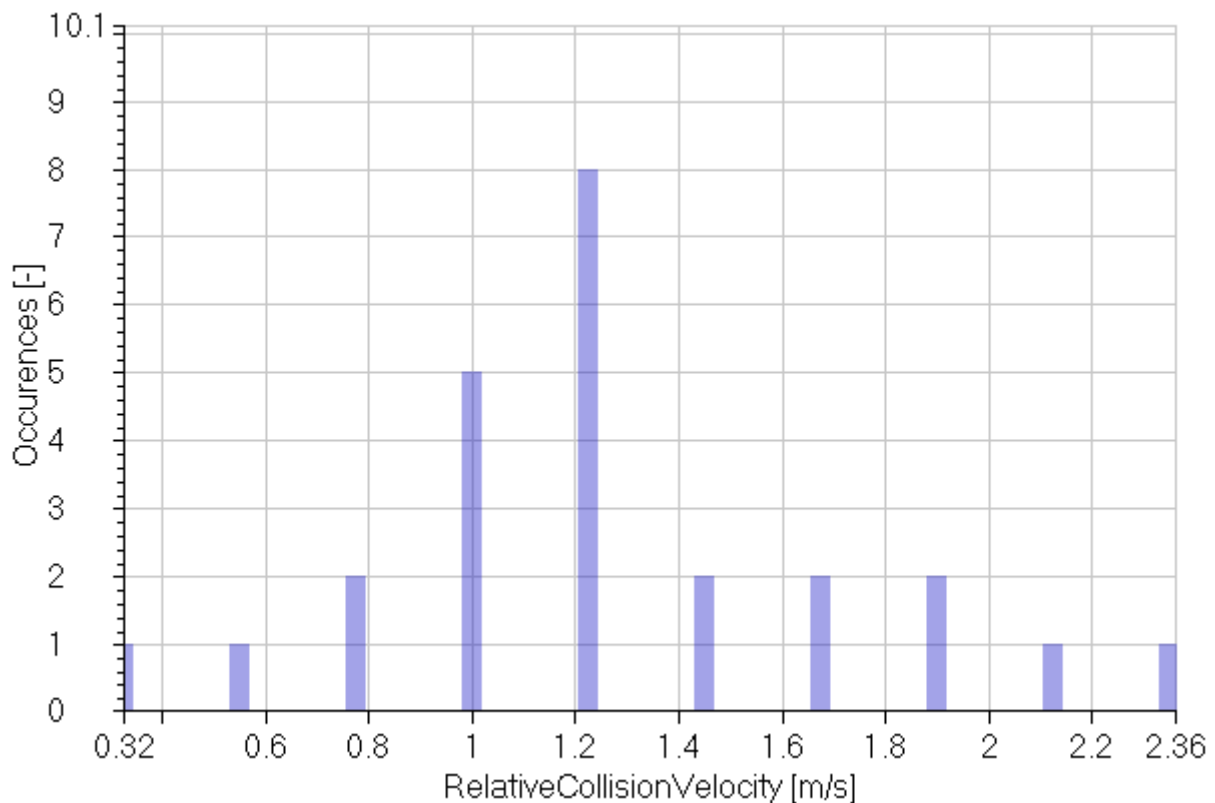


Figure 177: collision scenario number 16

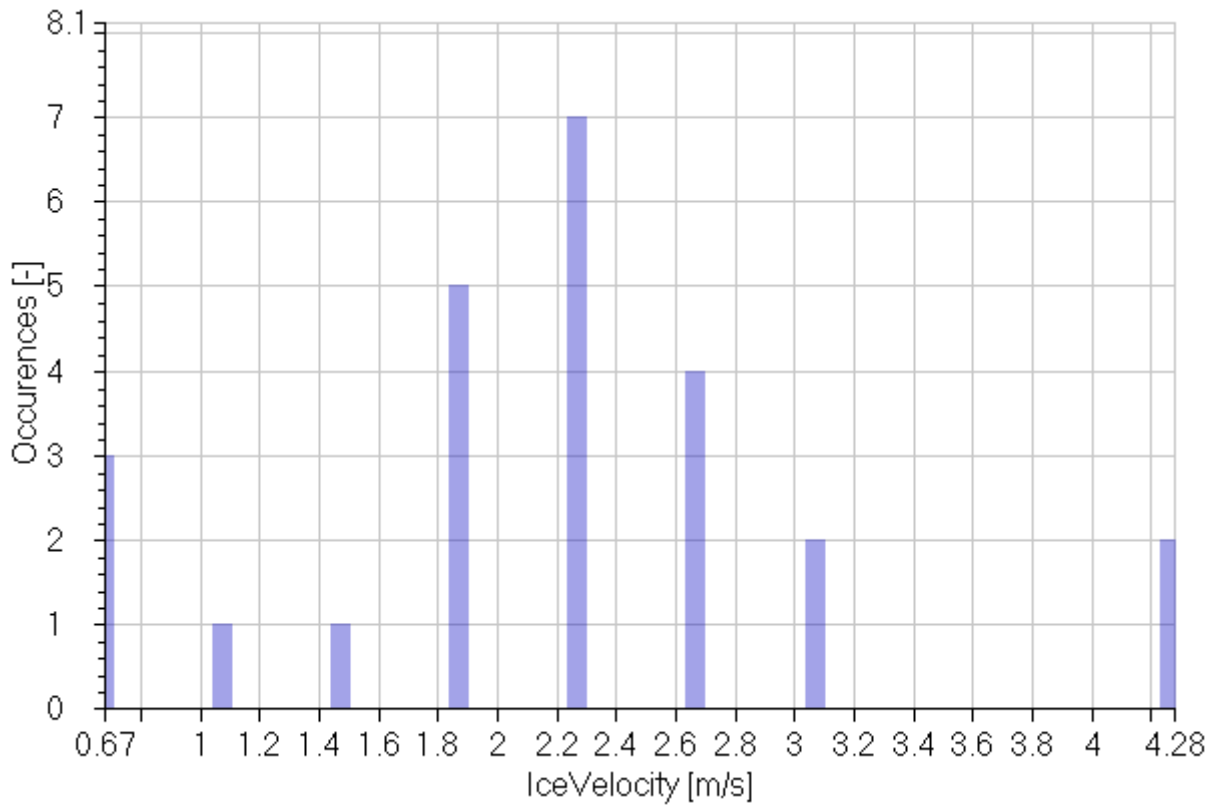


Figure 178: collision scenario number 16

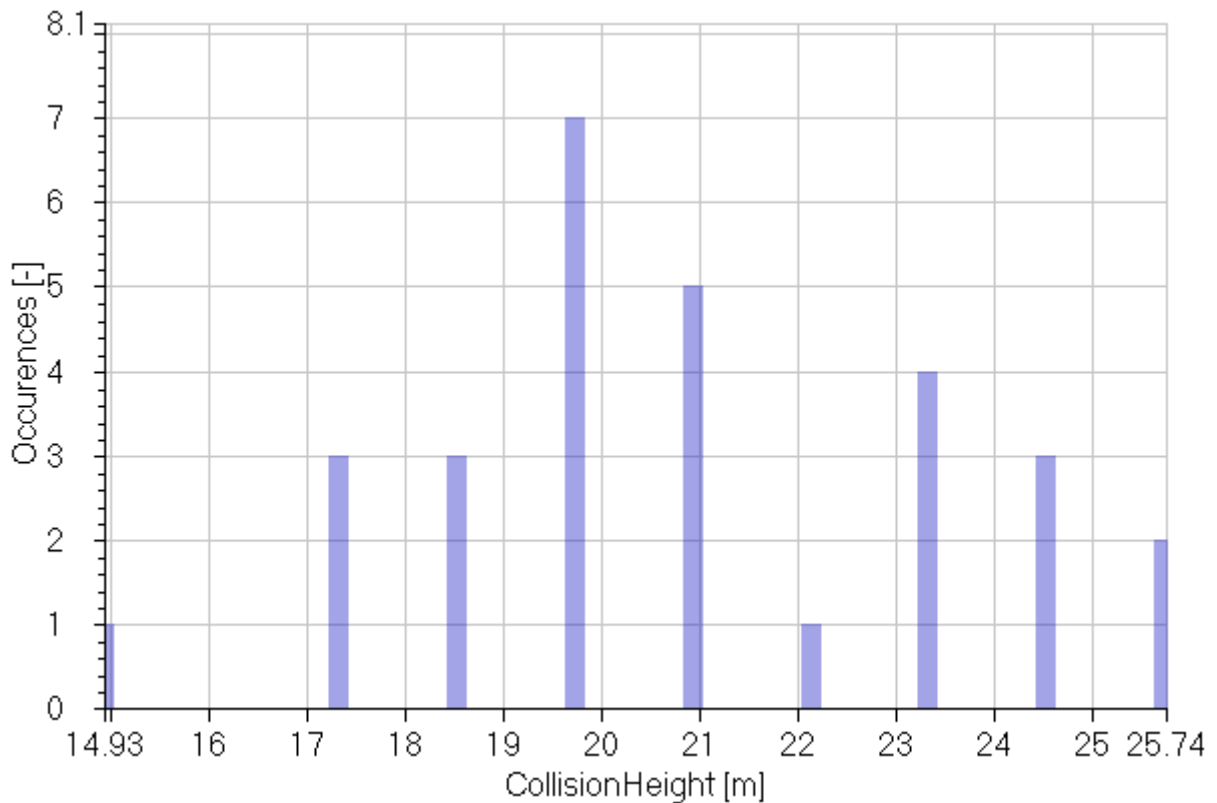


Figure 179: collision scenario number 16

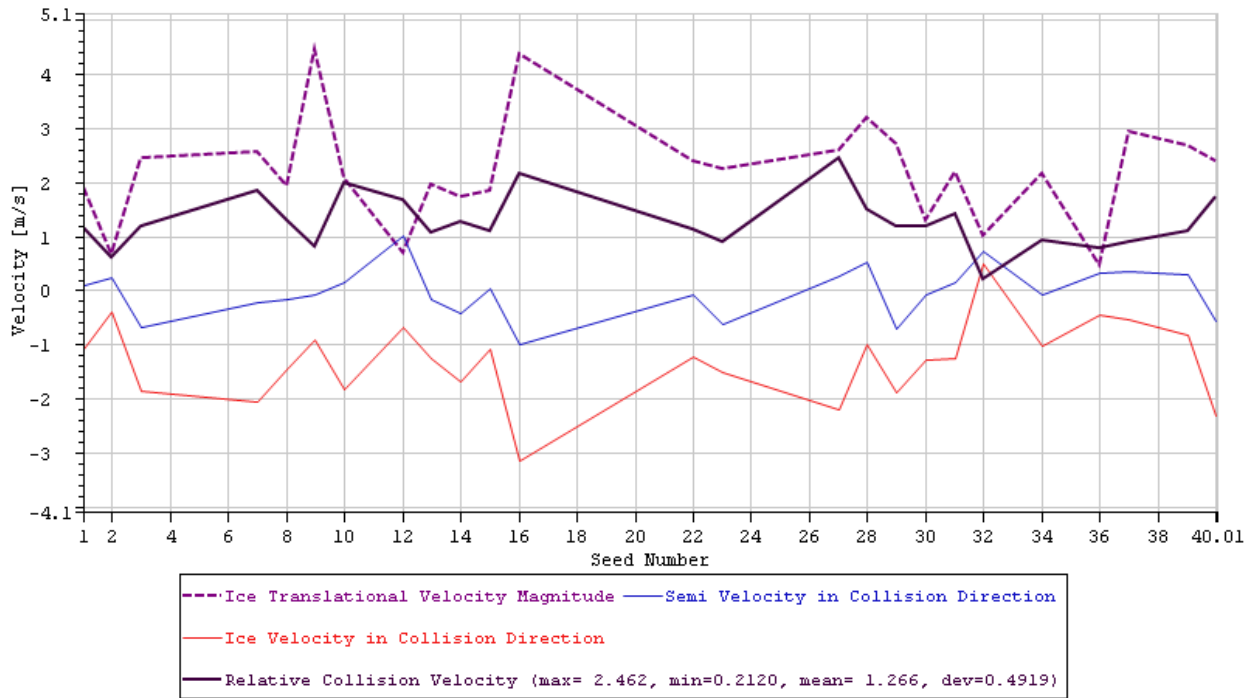


Figure 180: Total and relative collision velocities of ice and platform for different seeds, for case number 16.

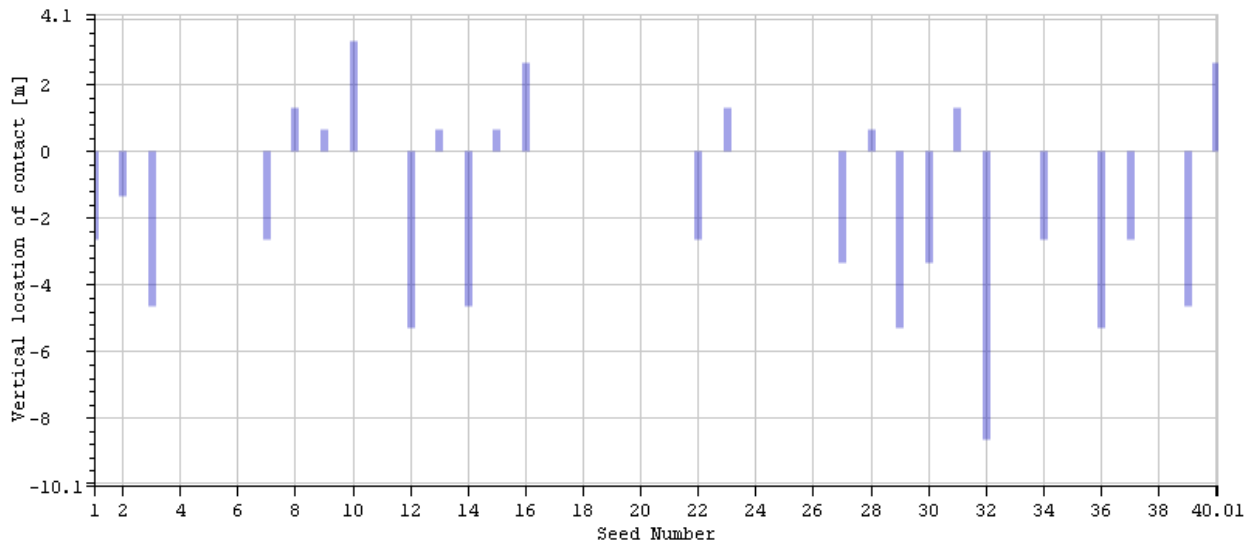


Figure 181: Vertical location of impact on the platform for different seeds, for case number 16.

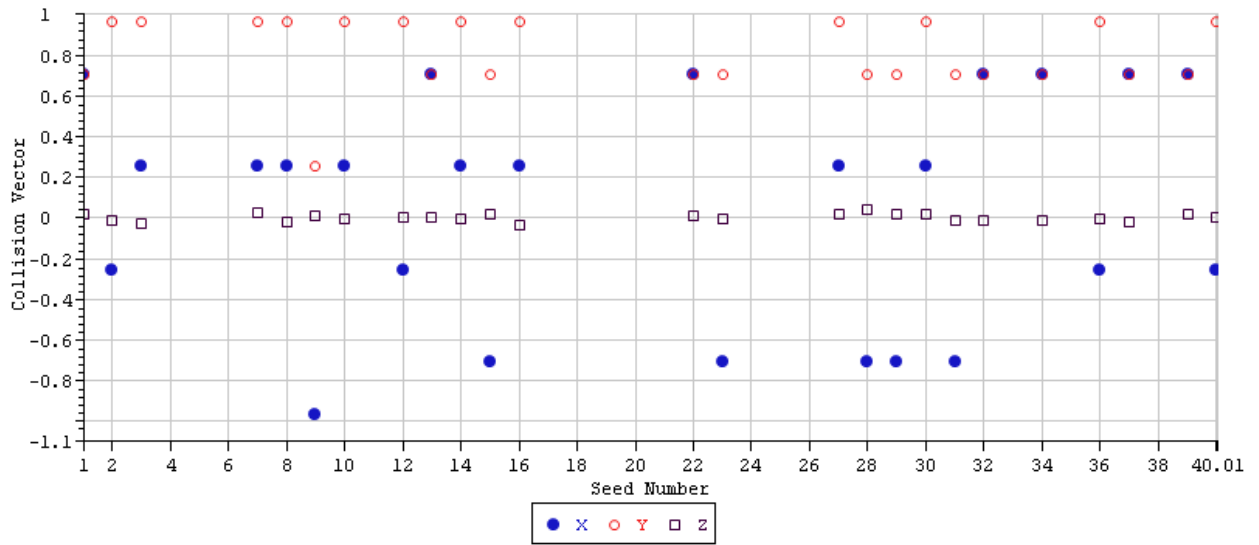


Figure 182: Collision vector components for different seeds, for case number 16.

25 Collision Scenario Number 22

	1	2	3	4	5
Signals		Max	Min	Mean	St. Dev.
RelativeCollisionVelocity	[m/s]	3.54	0.24	1.53	0.71
IceVelocity	[m/s]	5.79	0.66	2.55	1.07
CollisionHeight	[m]	25.67	16.33	21.11	2.47

Table 74: Statistical values calculated for collision scenario number 22.

	1	2	3	4
Signals		MP	Exp	P90
RelativeCollisionVelocity	[m/s]	1.21	1.41	2.46
IceVelocity	[m/s]	2.07	2.37	3.95
CollisionHeight	[m]	19.99	20.7	24.36

Table 75: Statistical values calculated for collision scenario number 22.

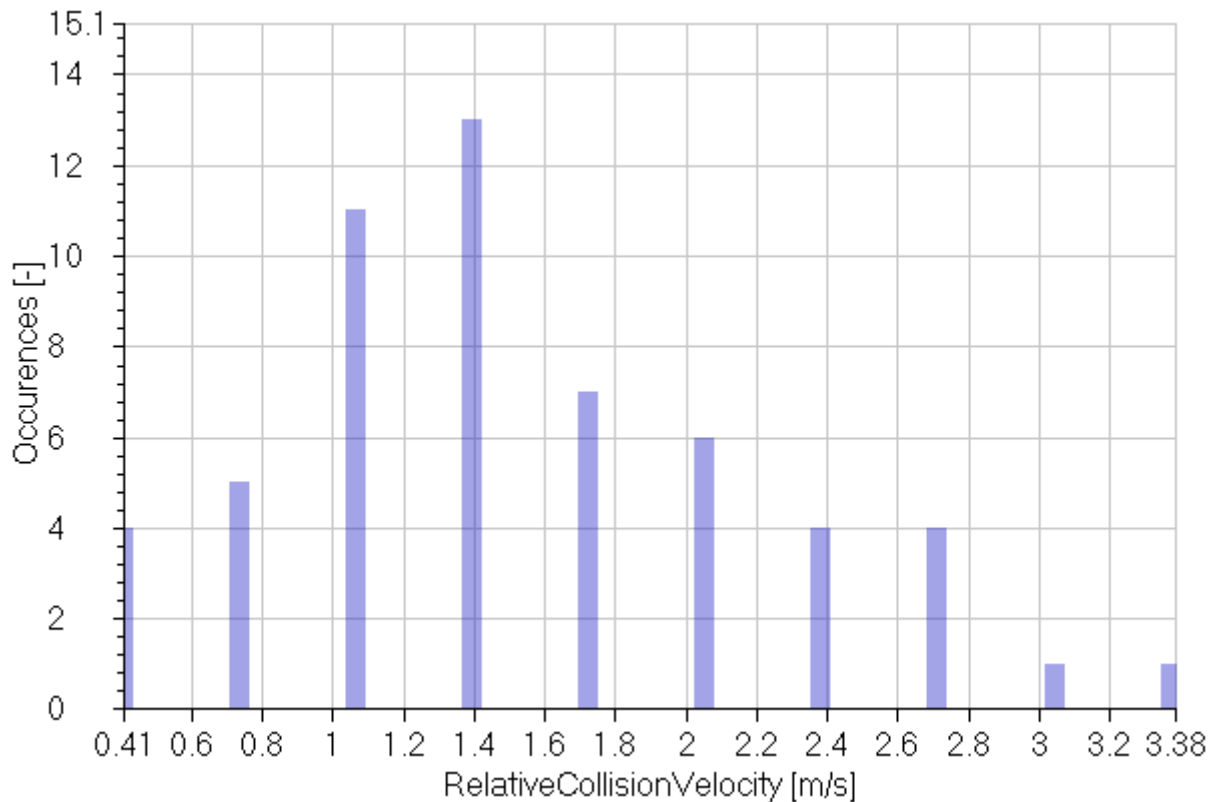


Figure 183: collision scenario number 22

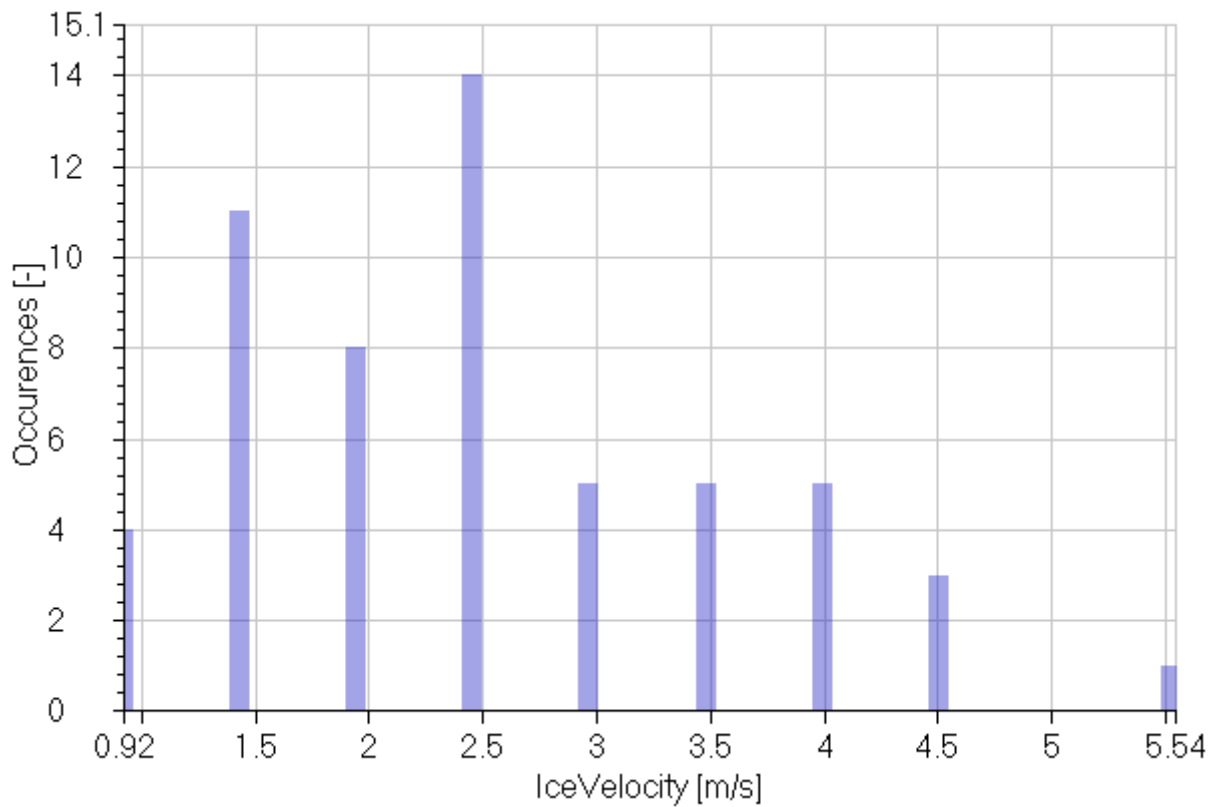


Figure 184: collision scenario number 22

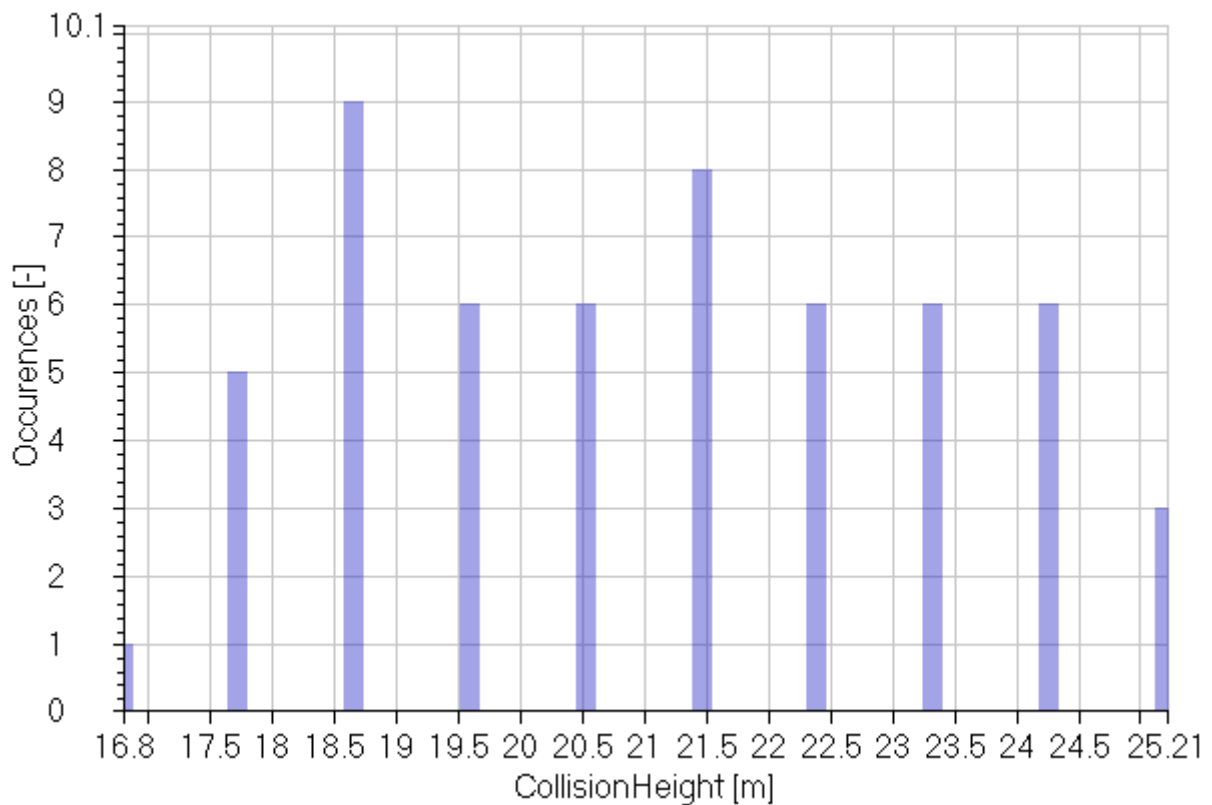


Figure 185: collision scenario number 22

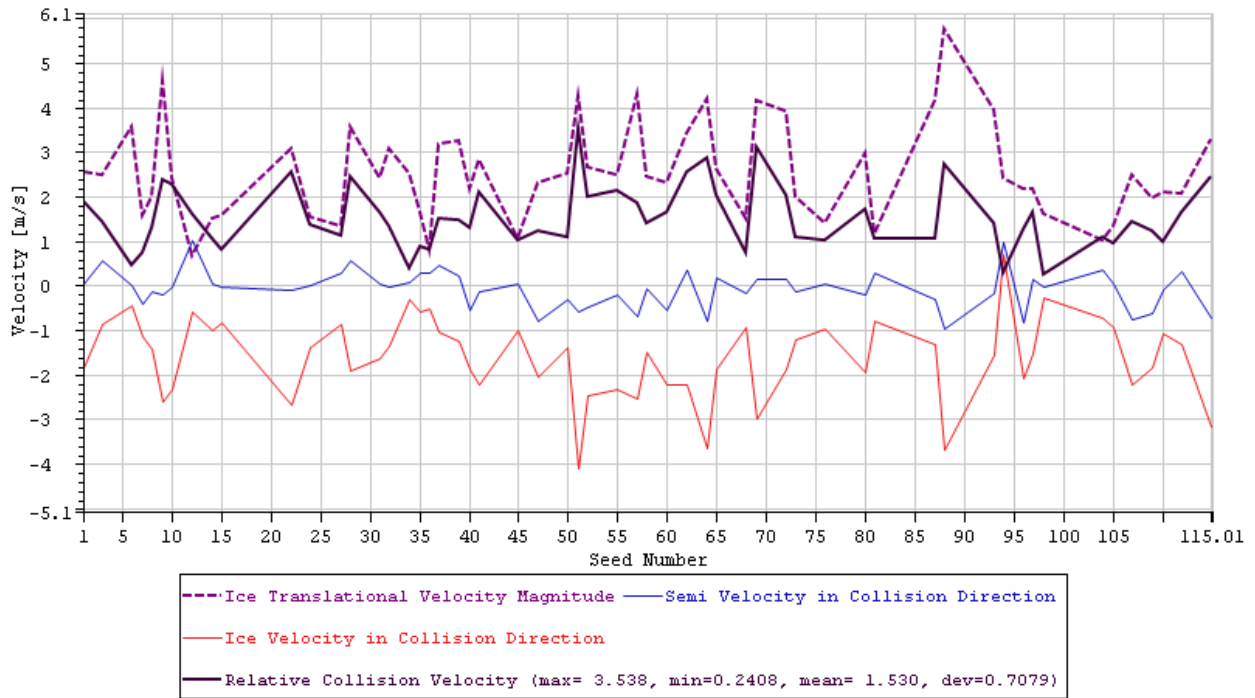


Figure 186: Total and relative collision velocities of ice and platform for different seeds, for case number 22.

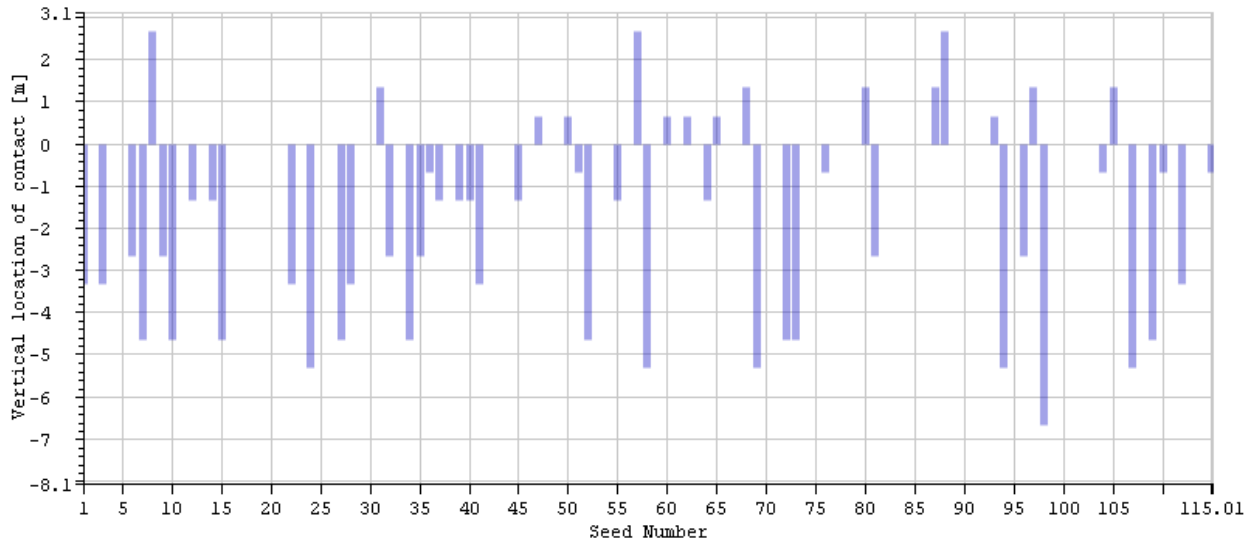


Figure 187: Vertical location of impact on the platform for different seeds, for case number 22.

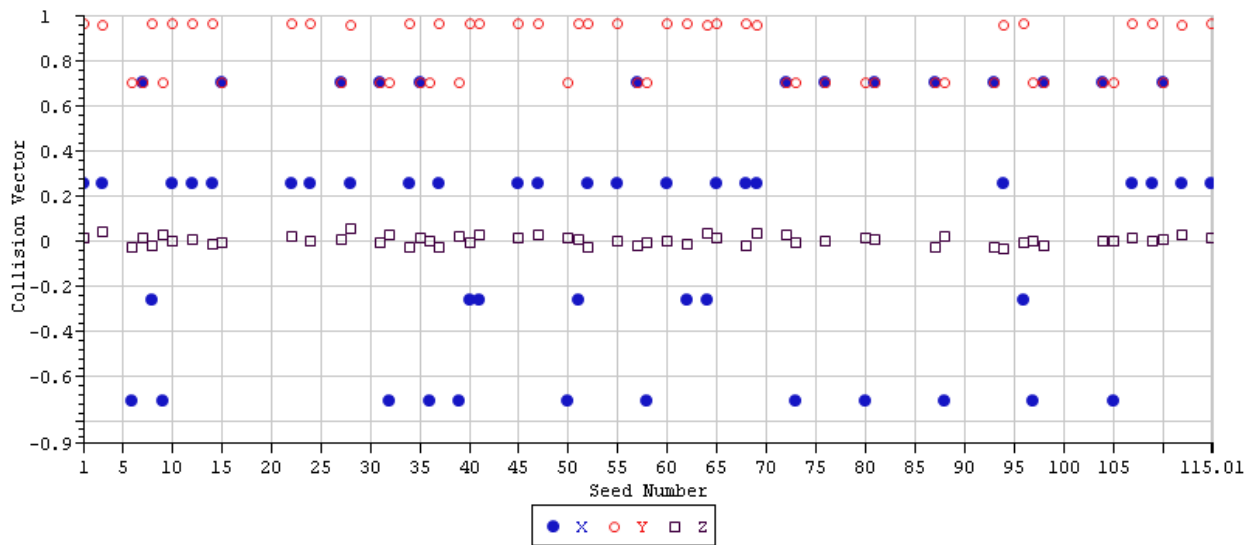


Figure 188: Collision vector components for different seeds, for case number 22.

26 Collision Scenario Number 23

	1	2	3	4	5
Signals		Max	Min	Mean	St. Dev.
RelativeCollisionVelocity	[m/s]	2.57	0.4	1.4	0.61
IceVelocity	[m/s]	4.63	0.66	2.35	0.96
CollisionHeight	[m]	25.67	17.67	20.45	1.98

Table 76: Statistical values calculated for collision scenario number 23.

	1	2	3	4
Signals		MP	Exp	P90
RelativeCollisionVelocity	[m/s]	1.13	1.3	2.21
IceVelocity	[m/s]	1.91	2.19	3.63
CollisionHeight	[m]	19.55	20.12	23.09

Table 77: Statistical values calculated for collision scenario number 23.

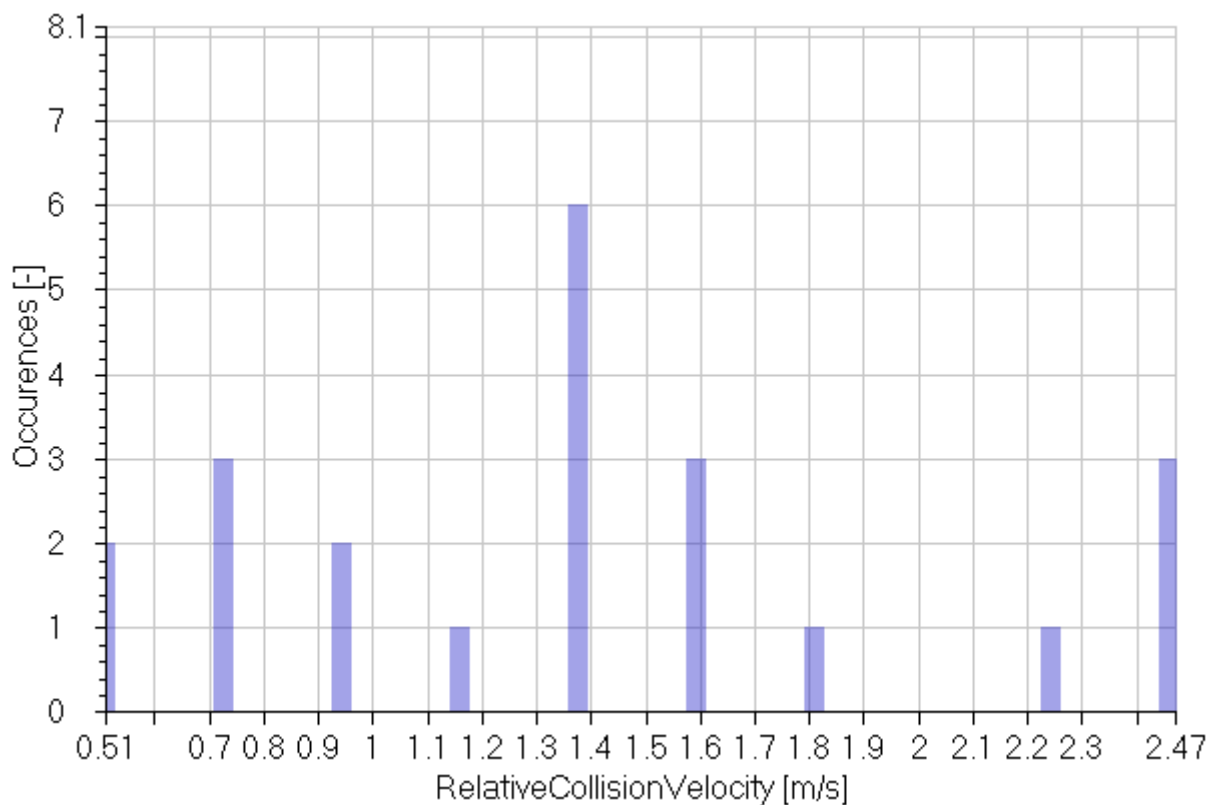


Figure 189: collision scenario number 23

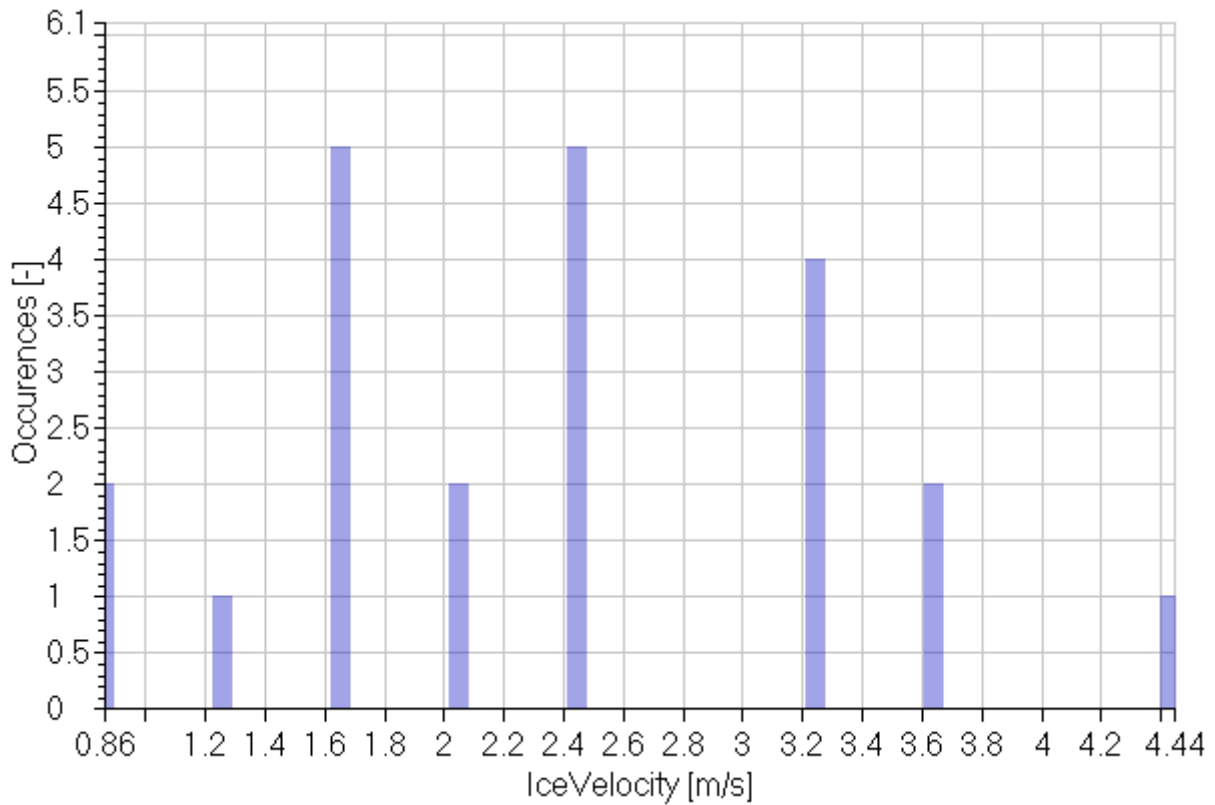


Figure 190: collision scenario number 23

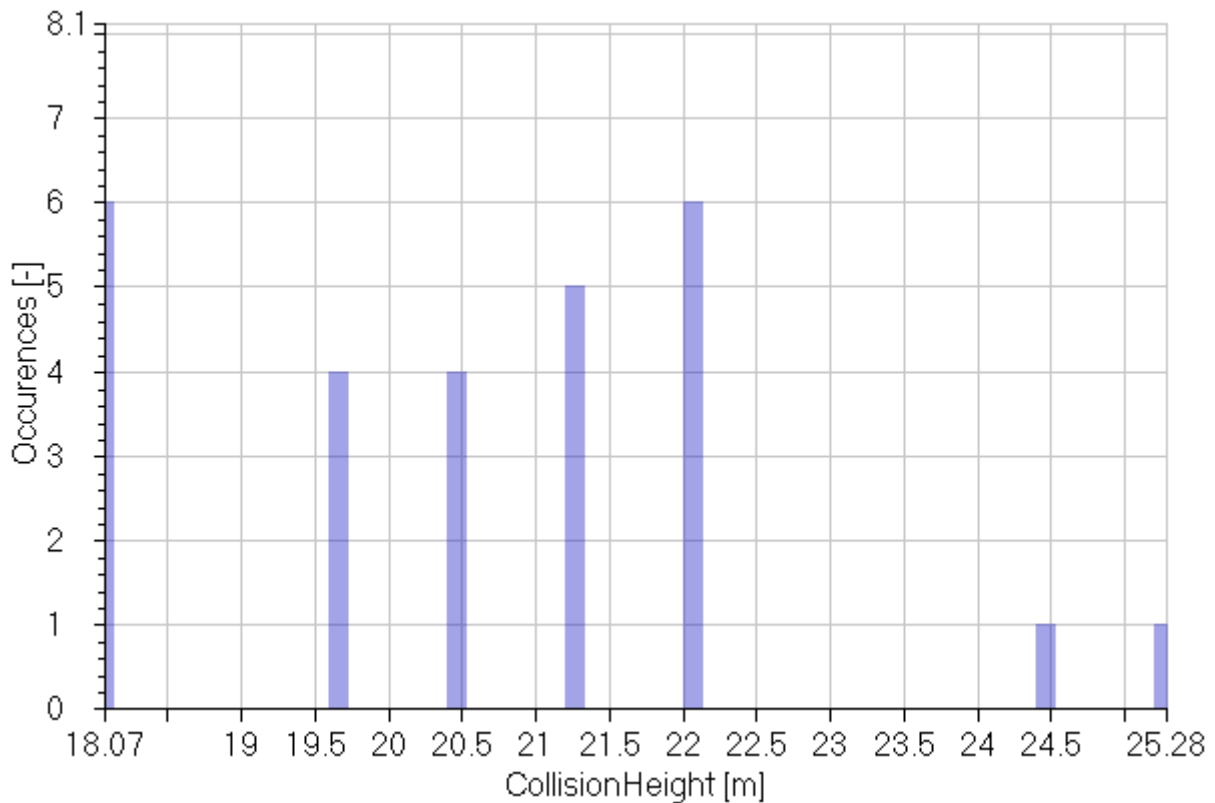


Figure 191: collision scenario number 23

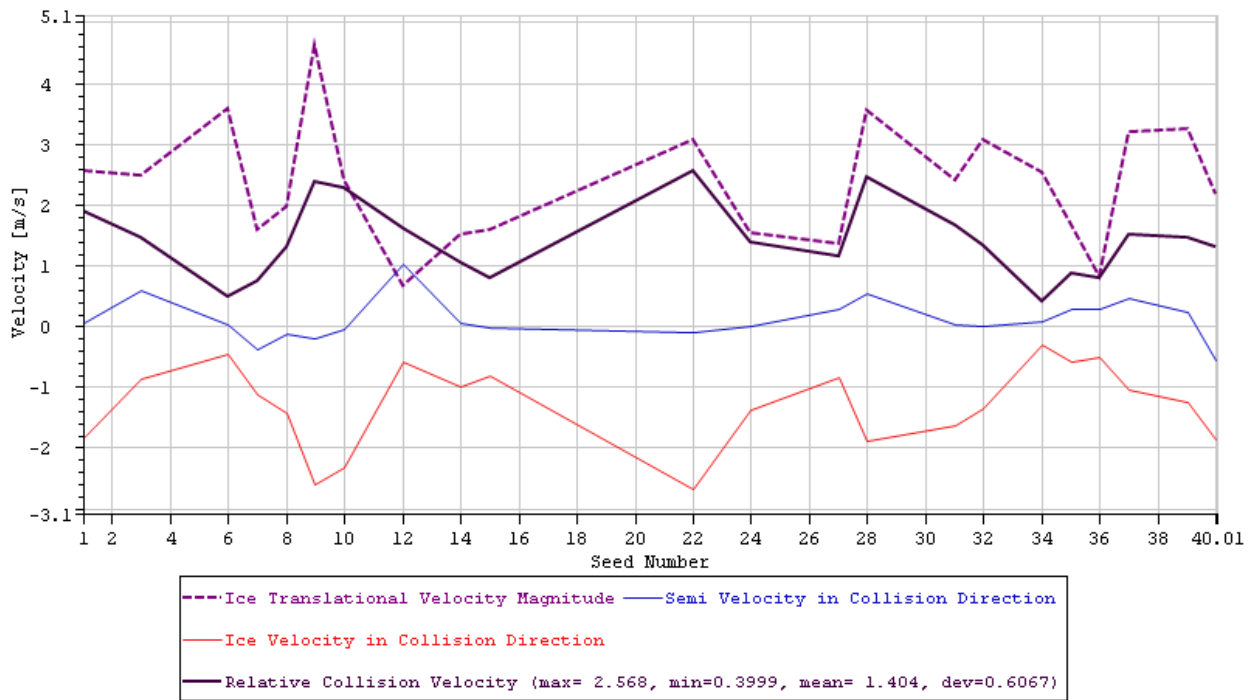


Figure 192: Total and relative collision velocities of ice and platform for different seeds, for case number 23.

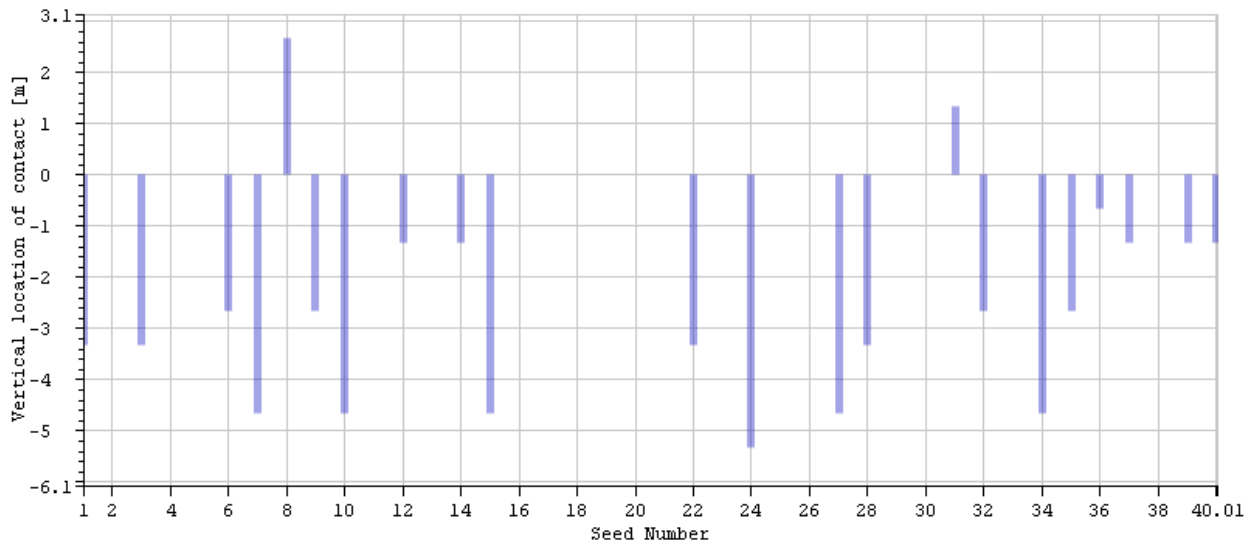


Figure 193: Vertical location of impact on the platform for different seeds, for case number 23.

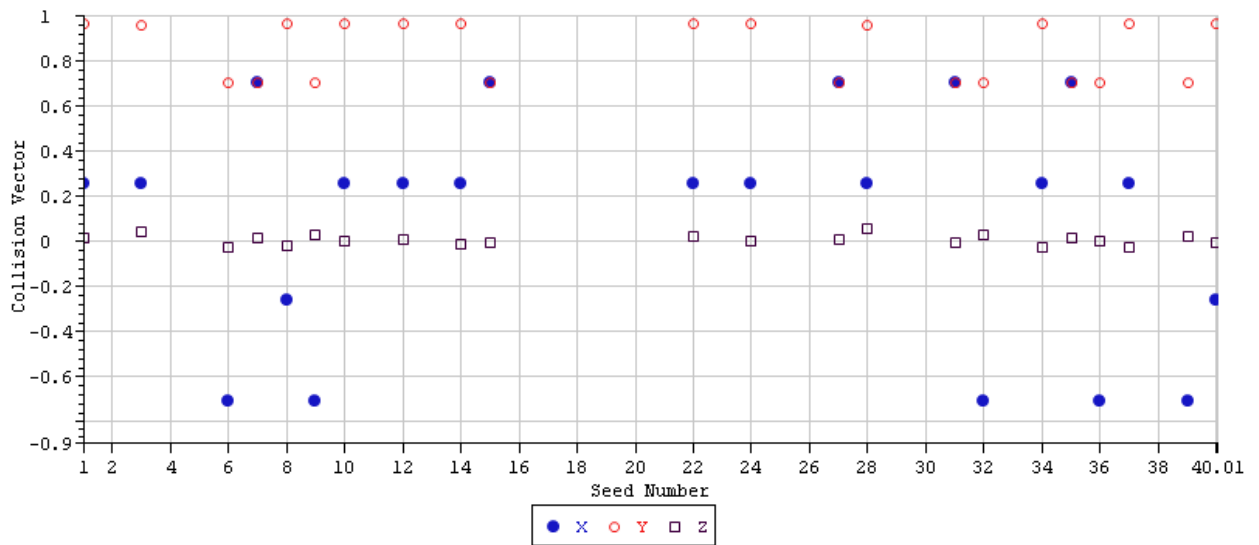


Figure 194: Collision vector components for different seeds, for case number 23.